Development and Applications of the Frequency-Dependent Polarizable Force Field ACKS2ω

Ontwikkeling en Toepassingen van het Frequentie-Afhankelijke Polarizeerbare Krachtveld ACKS2ω

YingXing Cheng

Supervisors: prof. dr. ir. T. Verstraelen
Dissertation submitted in fulfillment of the requirements for the degree of Doctor (Ph.D.) of Science: Physics

Department of Physics and Astronomy
Department chair: prof. dr. Jan Ryckebusch
Ghent University
Academic year 2023–2024

GHENT UNIVERSITY

Members of the Examination Committee

Chair

prof. dr. Natalie Jachowicz (Ghent University)

Reading Committee

dr. Igor Poltavskyi (University of Luxembourg, Luxembourg)
prof. dr. Frank Jensen (Aarhus University, Denmark)
prof. Dimitri Van Neck (Ghent University)
prof. dr. ir. Louis Vanduyfhuys (Ghent University, secretary)

Supervisors

prof. dr. ir. Toon Verstraelen (Ghent University)

This research has been conducted at the **Center for Molecular Modeling**.

Preface

New land is harsh, and vigorous, and sturdy. It scorns evidence of weakness. There is nothing of sham or hypocrisy in it. It is what it is, without apology.
J. E. Lawrence

I am delighted to present my doctoral thesis entitled "Development and Applications of the Frequency-Dependent Polarizable Force Field ACKS2ω". This study is the culmination of several years of research, dedicated efforts, and in-depth exploration, undertaken at Ghent University, under the exceptional guidance of my promotor, Prof. Toon Verstraelen.

This thesis represents not only my academic journey but also the personal growth and transformation I have undergone during its completion. It seeks to explore a general framework for frequency-dependent polarizable force fields, drawing from a variety of perspectives and methodologies. The intent is to contribute to a deeper understanding and, where possible, to propose potential solutions.

The journey of compiling this thesis was not a solitary effort, and this preface is an opportunity to express my deepest gratitude to those who have accompanied me on this journey.

To my promotor, Toon, I am truly thankful. You always believed in me, gave me support, and taught me so much, not just about our research, but lessons that will help me in life. Your way of doing science is something I really look up to and I have learned a lot from it during my PhD. Thank you for everything.

I am indebted to all colleagues and friends at CMM who offered their expertise, shared their wisdom, and fostered an environment of intellectual stimulation. Your guidance has been instrumental in the completion of this research.

I would like to extend my sincerest gratitude to Leen, Wim, Samuel, and Mieke, who, as exceptional office managers, ensured the smooth functioning of our daily operations. I also want to express my heartfelt thanks to Ruben, Martin, and Massimo, whose warmth and welcoming nature eased my transition into the CMM community.

My office neighbors, Martin, Farnaz, David (Kim), Michael (Gustavo), Leo, Michael (Sluydts), Jelle (Vekeman), Loïc, Lukas, and Gözde deserve special recognition. Your stimulating discussions, constant curiosity, and shared laughter made the long hours at the office both engaging and enjoyable. In particular, I would like to extend my deepest gratitude to Jelle (Vekeman) for your invaluable assistance in revising my papers.

My time with the CMM football team, filled with camaraderie and sportsmanship, was unforgettable. Thank you, Alen, Alexander, David (Devoogdt), Jelle (Wieme), Jenna, Jonas, Juul, Kuber, Louis, Loïc, Lukas, Reza, Ruben, Sander (Borgmans), Sander (Vandenhaute), Siddharth, Tom, for the games, the teamwork, game-after drinks and the much-needed breaks from research.

My heartfelt appreciation goes to my Chinese friends, who provided a comforting and supportive environment during times of stress and uncertainty. Your unwavering support, endless patience, and constant encouragement kept me motivated and focused on my goals.

To the members of the basketball team, XiaoZhou, WangHao, Chang (Liu), XiaoYu, YaXin, YuHuang, ShengJie, MingYe, ZhiWei, Tie (Guo), YaoWei, LinFeng, WeiXi, XingZhen, YanQi, XiangTian, PengFei, Tao (Fang), RenJie, Ting (Feng), Hui (Xiang), HongChao, Le (Zhang), Ke (Xu), Qi (Zhao), and YiHang, YuFei, I owe a debt of gratitude. Your competitive spirit, the friendly games, and the shared joy of victory have been a source of motivation and inspiration.

To my volleyball friends, Cheng (Wang), Xin (Wang), Chao (Song), WenJing, Chen (Yang), thank you for your companionship on and off the court. Your supportive cheers and genuine camaraderie have made every match a memory to cherish.

A special note of gratitude to my cycling team, WenJing, XiaoYu, ShiWei, LinNan. Our shared journeys, the thrill of speed, and the breathless conversations have been an integral part of this journey.

To my board game team, WenJing, XiaoYu, ShiWei, LinNan, Qian, QiQiong, JunHua, ShanShan, YuJie, MengMeng, LinLong, RenJie, ShengPu, Ye (Gu), ZengYuan, WenQiong, SiYu, XiaoNa (Hu), XiaoDi, WeiXi, Miao (Li), Tian (Jin), YuXuan, YuLin, Qi (Si), your strategic minds and light-hearted banter have provided welcome distractions and memorable moments. I appreciate each game, each victory, and each moment of shared laughter.

To the social drinking group, Anna, Chiara, David (Kim), Massimo, Michael (Gustavo), Tomi, Ruben, Samuel (Neale), XiaoHui, WangHao, YuHuang, XiaoZhou, YiShan, Elei, YiPing, JiaMin, JinMing, Zhen (Li), Ye (Yuan), YangBo, XuQi, ManXian, Lin (Cao), Rong, WeiWei, ZhiWei (Wang), XianQi, Chao (Wang), ChengJin, Ya (Wang), YangFeng, HuiYu, Lei (Xie), PeiTao, YiPing, JinFeng, YuXiao, Hao (Wu), and Peng (Wang), your gatherings have been a source of relaxation and bonding. The light-hearted conversations and shared jokes played a vital role in maintaining my morale throughout this journey, particularly during the Covid period.

To YunHan, I extend my gratitude for the support and encouragement. Your belief in my capabilities provided strength at crucial moments.

To my good friend, Peng Qi, you are like a big brother in a family, and you always provide a new perspective on life and the world, which gives me many good suggestions for my life. Chatting with you always gives me more guidance and new knowledge. Your encouragement and support have been my rock on this journey, and I really appreciate the friendship between us.

And finally, to my family, words fall short to express my gratitude. Your constant support, endless love, and absolute belief in my abilities have been my guiding light in this journey. You have been my pillars of strength, and this achievement is as much yours as it is mine.

I also acknowledge the countless researchers and authors whose works I have consulted, each of whom has contributed to the shape and direction of this research. Their pioneering work has been the groundwork on which this study is built.

Lastly, this thesis is dedicated to all the researchers with a thirst for knowledge, a curiosity about the world, and the courage to ask questions. May you find this research beneficial in your pursuit of knowledge.

YingXing Cheng
Ghent, June 2023

Contents

Samenvatting

Van der Waals dispersie-interacties zijn zwakke maar universeel attractieve krachten tussen atomen in moleculaire systemen en materialen, en spelen een cruciale rol in verschillende toepassingen in de chemie en fysica. Dichtheidsfunctionaal Theorie (DFT), een gevestigde kwantummechanische methode voor het oplossen van elektronische grondtoestanden, wordt vaak gebruikt, vooral voor grote systemen, omdat het een gunstige balans biedt tussen nauwkeurigheid en computationele efficiëntie. DFT heeft echter moeite om het attractieve deel van van der Waals dispersie-interacties nauwkeurig te beschrijven, waardoor de ontwikkeling van gepaste dispersiecorrecties nodig is.

Er zijn verschillende correctieschema's voorgesteld die compenseren voor de ontbrekende langeafstandscorrelatie-energie in DFT. Deze correctieschema's werken goed in de meeste gevallen in de chemie en fysica. Echter, de type-C niet-additieve dispersie-interacties, zoals gedefinieerd door Dobson, kunnen niet nauwkeurig worden weergegeven door deze modellen. De belangrijkste reden hiervoor is dat type-C dispersie-energie gerelateerd is aan ladingsfluctuaties over lange afstanden, die in de meeste bekende dispersie modellen worden verwaarloosd.

Om type-C-dispersie-interacties aan te pakken is een algemenere aanpak nodig, die correlatie-energie kan beschrijven met behulp van de adiabatische connectie-fluctuatie-dissipatie (ACFD) stelling. Deze stelling kan zowel monopolen als hogere-orde multipolen aan tot alle ordes en wordt vaak gebruikt om de exacte correlatie-energie in tijdsafhankelijke dichtheidsfunctionaaltheorie (TDDFT) te berekenen. ACFD-berekeningen zijn echter rekenintensief, zelfs als de *random-phase approximation* (RPA) gebruikt wordt. Dit motiveert de auteur om een nieuw dispersiemodel te onderzoeken om de correlatie-energie over lange afstand met fluctuerende ladingen en dipolen te berekenen. Het basisidee is om grootheden gedefinieerd in ACFD te berekenen met behulp van frequentie-afhankelijke polariseerbare krachtvelden. Onlangs is er een nieuwe polariseerbare krachtveldmethode ontwikkeld, de

Atom-Condensed Kohn-Sham Density Functional Theory Approximated to 2nd order (ACKS2), om moleculaire lineaire responseigenschappen te reproduceren met alleen monopolen en dipolen. Het doel van dit proefschrift is het ontwikkelen van een frequentie-afhankelijke uitbreiding van het ACKS2 model, aangeduid als ACKS2ω.

In **Hoofdstuk 1**, wordt een algemene inleiding gegeven om licht te werpen op de achtergrond van deze scriptie.

In **Hoofdstuk 2**, worden de relevante computationele methoden in deze scriptie kort besproken. Dit omvat kwantummechanische methoden evenals moleculaire krachtvelden. Binnen de kwantummechanica worden zowel op golfunctie gebaseerde benaderingen als Dichtheidsfunctionaal Theorie theorie uitgewerkt. Vervolgens wordt een uitgebreid overzicht van moleculaire krachtvelden gepresenteerd. Er worden gedetailleerde discussies gegeven over conventionele krachtvelden, polariseerbare krachtvelden en reactieve krachtvelden.

In **Hoofdstuk 3**, wordt de afleiding van het ACKS2ω model gebaseerd op Floquet Tijdsafhankelijke DFT (TDDFT) geïntroduceerd. Floquet TDDFT, ook wel bekend als de quasi-energie formalisme, faciliteert de afleiding van frequentie-afhankelijke responsmethoden analoog aan statische methoden. Zo kan ACKS2ω direct worden afgeleid, op gelijkaardige wijze als het ACKS2 model.

In **Hoofdstuk 4**, wordt de toepassing van het ACKS2ω model besproken, met name zijn nut bij het onderzoeken van de impact van monopool-effecten op moleculaire responseigenschappen. Dit omvat de frequentie-afhankelijke dipoolpolariseerbaarheid en C_6 dispersiecoëfficiënten.

Tot slot, in **Hoofdstuk 5**, worden de conclusies en toekomstperspectieven van deze scriptie uiteengezet.

Summary

Van der Waals dispersion interactions are weak yet universally attractive forces between atoms in molecular systems and materials, and play a crucial role in various applications in chemistry and physics. Density functional theory (DFT), an established quantum-mechanical method for solving electronic ground states, is frequently employed, especially for large systems, as it provides a favorable balance between accuracy and computational efficiency. However, DFT struggles to accurately describe the attractive part of van der Waals dispersion interactions, necessitating the development of suitable dispersion corrections.

Several correction schemes have been proposed to compensate for the missing long-range correlation energy in DFT. These correction schemes work well in most cases in chemistry and physics. However, the type-C non-additive dispersion interactions defined by Dobson cannot be accurately captured by these models. The main reason is that type-C dispersion energy is related to long-range charge fluctuations, which are neglected in most well-known dispersion models.

To address type-C dispersion interactions, a more general approach is needed, which can describe correlation energy using the adiabatic connection fluctuation-dissipation (ACFD) theorem. This theorem is capable of handling both monopoles and higher-order multipoles to all orders and is frequently employed to compute the exact correlation energy in time-dependent density functional theory (TDDFT). However, ACFD calculations are computationally demanding, even when the random phase approximation (RPA) is employed. This motivates the author to explore a novel dispersion model to compute long-range correlation energy with fluctuating charges and dipoles. The basic idea is to compute quantities defined in ACFD using frequency-dependent polarizable force fields. Recently, a novel polarizable force-field method, atom-condensed Kohn-Sham density functional theory approximated to 2nd order (ACKS2), has been developed to reproduce molecular linear-response properties only using monopoles and dipoles. The

target of this thesis is to develop a frequency-dependent extension of the ACKS2 model, denoted as ACKS2ω.

In **Chapter 1**, a general introduction is provided to shed light on the background of this thesis.

In **Chapter 2**, the computational methods relevant to this thesis are briefly discussed. These include quantum-mechanical methods as well as molecular force fields. Within quantum mechanics, both wavefunction-based approaches and density functional theory are elaborated upon. Subsequently, a comprehensive overview of molecular force fields is presented. Detailed discussions on conventional force fields, polarizable force fields, and reactive force fields are provided.

In **Chapter 3**, the derivation of the ACKS2ω model based on Floquet TDDFT is introduced. Floquet Time-Dependent DFT (TDDFT), also referred to as the quasi-energy formalism, facilitates the derivation of frequency-dependent response methods analogous to static methods. Thus, ACKS2ω can be derived similarly to the ACKS2 model.

In **Chapter 4**, the application of the ACKS2ω model is discussed, particularly its utility in examining the impact of monopolar effects on molecular response properties. This encompasses the frequency-dependent dipole polarizability and C_6 dispersion coefficients.

Lastly, in **Chapter 5**, the conclusions and future perspectives of this thesis are elaborated upon.

List of Abbreviations

QM	Quantum Mechanics
GCP	Generalized Casimir-Polder equation
MBD	Many-body Disperson model
XDM	Exchange-hole Dipole moment model
DFT+Dn	Density Function Theory with n-th generation dispersion correlation method
BO	Born-Oppenheimer
HF	Hartree Fock
post-HF	Post Hartree Fock
CI	Configuration Interaction
CISD	Configuration Interaction with Singles and Doubles
CC	Coupled Cluster
CCSD	Coupled Cluster with Singles and Doubles
CCSD(T)	Coupled Cluster with Singles, Doubles, and a perturbative treatment of Triples
DFT	Density Functional Theory
XC	Exchange-Correlation functional
TDDFT	Time-Dependent Functional Theory
MM	Molecular Mechanics
FF	Force Fields
PFF	Polarizable Force Fields
ReaxFF	Reactive Force Fields
EEM	Electronegativity Equalization Method
ACKS2	Atom-Condensed Kohn-Sham density functional theory approximated to 2nd order
ACKS2ω	Frequency-dependent ACKS2 model
ACFD	Adiabatic Connection Fluctuation-Dissipation theorem

List of Figures

List of Tables

Part I

Development and Applications of the Frequency-Dependent Polarizable Force Field ACKS2ω

1

Introduction

The underlying physical laws necessary for the mathematical theory of a large part of physics and the whole of chemistry are thus completely known, and the difficulty is only that the exact application of these laws leads to equations much too complicated to be soluble.
Paul Dirac (1902-1984)

Molecular modeling is a computational technique that predicts the physical and chemical properties of molecules and materials, playing a crucial role in various scientific fields such as chemistry, materials science, and biophysics. This revolutionary technique has transformed the way scientists design new materials, drugs, and molecular systems by offering insights into the atomic-scale behavior of molecules. To accomplish this, molecular modeling employs a range of computational methods, including quantum chemical calculations and molecular dynamics simulations, which enable the prediction of molecular behavior under diverse conditions.

In practice, molecular modeling is complex, involving critical steps that determine the success of the simulation.

1. The initial stage is choosing an appropriate molecular model, which includes consideration of atomic arrangements, boundaries, and potential imperfections within the material. This decision determines the accuracy and relevance of the simulation. Algorithm efficiency and model reliability are fundamental. They must balance computational

demands with precision to ensure the simulations are both feasible and reflective of true physical phenomena. This balance influences every decision in the computational process.

2. Next, researchers must select a sampling scheme that fits the objectives of interest. Options include geometric optimization for energy states, Hessian analysis for vibrational properties, molecular dynamics for time-dependent phenomena, Monte Carlo simulations for statistical properties, etc. Each has its benefits and limitations.

3. In the end, the process involves using techniques to extract useful results from simulation results and analysis of properties.

This thesis focuses on the potential energy surface, a crucial concept that maps a system's potential energy across atomic configurations, offering deep insights into material behavior and aiding predictions of their properties.

Molecular simulation methods can be roughly classified into two main categories: quantum-mechanical (QM) electronic structure methods and molecular mechanics (MM) which are also known as force-field (FF) methods. QM methods, often referred to as *ab initio* or first-principle methods due to their independence from empirical parameters, boast high accuracy but come with significant computational expense. On the other hand, FF methods rely on empirical parameters derived from *ab initio* methods or experiments, making them suitable for large-scale systems because of their lower computational cost. By offering detailed information about molecular systems that is otherwise difficult to obtain through experiments alone, molecular modeling serves as an invaluable supplement to experimental studies. Figure 1.1 illustrates the relationship between QM and FF methods in terms of computational complexity and accuracy.

The van der Waals (vdW) interaction, named after Dutch physicist Johannes Diederik van der Waals, plays an important role in molecular interactions. This interaction can be split into two primary components: a repulsive segment and an attractive one. At short distances, repulsion dominates due to the superposition of electron densities. The canonical power laws governing vdW interactions are illustrated in Figure 1.2. These forces are ubiquitous non-bonded interactions in molecular systems and materials, playing a crucial role in various applications in chemistry and physics. Generally, these interactions are relatively weak compared to bonded forces, such as covalent and ion bonds. Moreover, they are always attractive at long range due to the instantaneous motion of electrons at different sites.

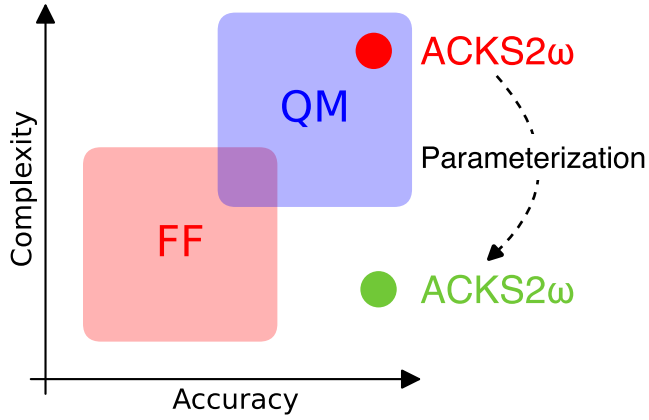

Figure 1.1: Comparision of force-field (FF) and quantum-mechanical (QM) methods in terms of computational complexity and accuracy. The ACKS2ω model is categorized as a QM method. After parameterization, it transforms into a method that combines high accuracy with the computational cost of a FF approach.

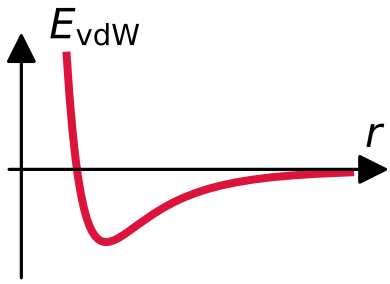

Figure 1.2: Conventional power laws employed in molecular force fields.

The vdW interactions also exist in the ground state of a system, i.e., at 0 K. Classical models fail to describe these interactions, and the only viable approach to studying them is by using quantum-mechanical models. [1]

The first quantum-mechanical model, by London, applied perturbation theory to the Coulomb interaction between electrons of two polarizable hydrogenic atoms.[2] Building on London's work, the generalized Casimir-Polder (GCP) expression describes dispersion interactions for any pair of molecules.[3] At long distances R, the dominant attractive term is proportional to R^{-6}. There are also additional attractive terms proportional to R^{-8}, R^{-10}, etc., which can be important in van der Waals contacts, but at long distances they

are generally less significant. Molecules with multiple atoms are typically decomposed using a distributed multipole expansion, treating each atom or group as a multipole polarizable site. Ignoring non-local and coupling terms, the total dispersion energy is approximated by a simple pairwise-additive form.

$$E_{\text{vdW}} = -\sum_{ab} \sum_{n=6,8,10,\cdots} f_n(R_{ab}) \frac{C_n^{ab}}{R_{ab}^n} \tag{1.1}$$

where R_{ab} is the distance between atoms a and b, and $f_n(R_{ab})$ is a damping function for short-range phenomena. C_n^{ab} are dispersion coefficients computed using frequency-dependent multipole polarizabilities of a and b.

The empirical expression given by Eq. (1.1) is frequently used in force field (FF) methods as well as in empirical dispersion corrections for density functional theory (DFT).[4] DFT is one of the most popular quantum mechanics (QM)-based methods in computational chemistry and physics, especially when examining larger systems. In Eq. 1.1, the C_6 dispersion coefficients always serve as the leading term, playing a critical role in determining the strength of dispersion interactions within molecular systems and materials. However, the straightforward pairwise-additive format of Eq. (1.1) can lead to inaccuracies if applied directly because identical C_n^{ab} coefficients are consistently utilized across varied atomic environments. Moreover, many-body effects are often overlooked.

Dobson initially categorized non-additive dispersion interactions into three distinct types: type-A, type-B, and type-C, as depicted in Figure 1.3.[5] Type-A non-additivity is observed when the atomic C_n coefficients within a molecule differ from those of isolated atoms. Type-B non-additivity arises when the interaction between two atoms is modified by the presence of a third atom, leading to a change in the dispersion interaction that does not exist in an isolated system. Recent research suggests that Type-B non-additivity might also represent an expression of electric many-body effects.[6] Type-C non-additivity becomes apparent in low-dimensional nanostructures or metallic systems. In these systems, long-range charge fluctuations give rise to notable dipoles, subsequently boosting the electronic polarizability and amplifying the dispersion interactions.

Semiclassical models that employ pairwise expressions, exemplified by Eq. (1.1), such as Grimme's DFT+Dn schemes ($n = 1, 2, 3, 4$),[7–11] the Tkatchenko and Scheffler (TS) method,[12] the exchange-hole dipole moment (XDM) method proposed by Becke and Johnson,[13–15] and the local-response dispersion (LRD) model introduced by Sato and Nakai,[16–18] all address type-A non-additive dispersion interactions.[5] However, only a handful of these mod-

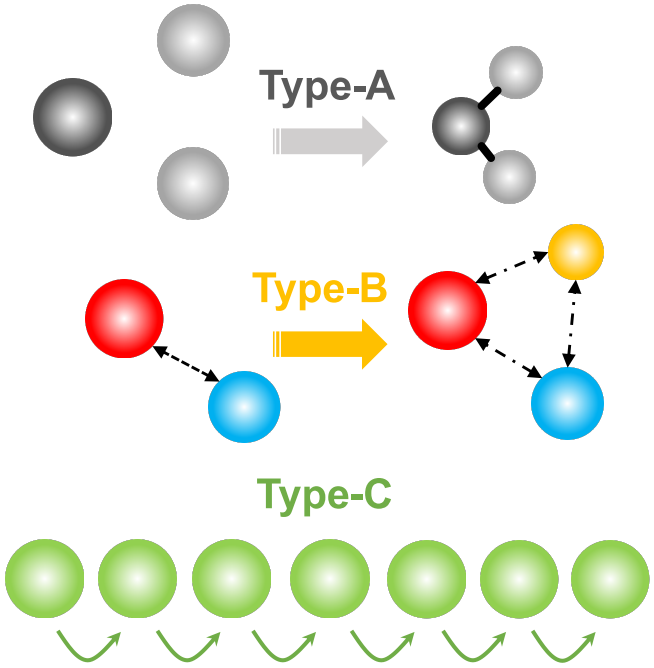

Figure 1.3: Dobson's classification of three types of non-additivity.

els take into account type-B non-additivity to some extent, since straightforward pairwise methods have challenges when handling many-body effects. The DFT+D3 and DFT+D4 methods integrate the three-body Axilrod-Teller-Muto (ATM) term,[19, 20], and the XDM can encompass type-B interactions via electronic many-body effects.[6, 21] Though the three-body ATM term can be incorporated into the XDM, its influence is often overshadowed by dominant higher-order two-body dispersion terms, implying that atomic many-body effects could be minimal.[22, 23] The many-body dispersion model (MBD), based on the dipolar coupling among atomic quantum harmonic oscillators,[24–26] stands out as a prominent method adept at comprehensively addressing both type-A and type-B non-additive dispersion energies. MBD techniques accurately represent many-body interactions and predict considerable departures from conventional power laws. However, all the models discussed above are local models and overlook fluctuating charges, the leading terms of the distributed multipole expansion, also referred to as monopoles.

Fluctuating charges can contribute significantly to the dispersion energy in many systems,[27] including carbon nanomaterials,[28–30] traditional semiconductors,[31, 32] and low-dimensional materials,[28, 33] where the GCP equation is insufficient. For chemical systems with delocalized bonds,

Table 1.1: Expected performance of dispersion theories based on their physical content

Method	Type-A	Type-B	Type-C
TS, LRD, DFT+Dn ($n = 1, 2$)	Y	N	N
DFT+Dn ($n = 3, 4$)	Y	Partial	N
XDM	Y	Partial	N
MBD	Y	Y	N
dRPA + extensions	Y	Y	Y
High-level QM methods, e.g., TDDFT+ACFD, DMC, CI and CC	Y	Y	Y

monopolar fluctuations have complex non-local resonance features.[34] The contribution of charge fluctuations to dispersion interactions have been studied in some specialized systems, e.g., between infite wires and slabs,[28, 35, 36] and in fullerenes and aromatic systems.[37, 38] A recent study by Dobson demonstrates that local models cannot accurately capture type-C non-additive dispersion interactions properly, because long-range charge fluctuations are not considered in these models.[30]

Alternatively, a more general approach is using adiabatic connection fluctuation-dissipation (ACFD) theorem, which treats both monopolar and higher-order multipolar fluctuations to infinite orders and is often used to compute the exact correlation energy in time-dependent density functinoal theory (TDDFT). The random phase approximation (RPA) is often used to reduce computational costs. RPA variants have been shown to handle all three types of non-additive dispersion interactions correctly.[30] Nonetheless, they are still computationally demanding for large-scale systems. Table 1.1 summarizes the relationship between different dispersion models and their expected performance.

The long-term goal of this thesis is to develop a new dispersion model that incorporates both monopole and dipole effects. To reduce the computational costs, molecular force field methods are considered. A novel polarizable force field, named atom-condensed Kohn-Sham density functional theory approximated to second order (ACKS2), is utilized in this thesis because it is rigorously derived from DFT, and all parameters can be directly derived from the underlying wavefunction. The molecular linear interacting response properties can be reproduced exactly. Moreover, this model can also treat monopoles and dipoles on the same footing.

However, the ACFD theorem necessitates a frequency-dependent interacting response function, which motivates the development of a frequency-

dependent generalization of the ACKS2 model, referred to as ACKS2ω. The primary goal of this thesis is to develop the ACKS2ω model and explore its applications in frequency-dependent properties. The categorization of ACKS2ω is depicted in Figure 1.1, where the ACKS2ω model is classified as a QM method. However, after parameterization, it transforms into a method that combines high accuracy with the computational cost of a FF approach.

To ensure the self-consistency of this thesis, general computational methods are introduced in **Chapter** 2. Readers who already know these methods can skip it. It should be noted that these methods are extensively described in any standard computational chemistry book. All methods mentioned in this thesis were employed during my PhD period, even if they may not be used in the studies presented within this thesis. **Chapter** 3 and **Chapter** 4 are papers that were published in the Journal of Chemical Physics. In these works, I led the conceptualization of the study, data curation and analysis, methodology development, and the writing of the original draft. My contributions also included software development, validation, and visualization of the findings. TV provided invaluable assistance in these areas and also spearheaded the project administration and supervision. Specifically, the derivation of the ACKS2ω model is discussed in **Chapter** 3. An application of the ACKS2ω model is studied, i.e., the impact of fluctuating charges on molecular response properties, as addressed in **Chapter** 4. A conclusion and perspective of this thesis are discussed in **Chapter** 5.

2

Review of computational methods

It doesn't matter how beautiful your theory is; it doesn't matter how smart you are. If it doesn't agree with experiment, it's wrong.
Richard Feynman (1918-1988)

Before we begin discussing the development and applications of ACKS2ω model, it is an essential prerequisite to review the basis concepts of computational methods in the field of computational chemistry.

2.1 Wavefunction-based methods

This section will focus on wavefunction-based methods, starting from the Schrödinger equation and moving to the Born-Oppenheimer approximation. Next, mean-field methods are introduced, including Hartree and Hartree-Fock, followed by several post-Hartree-Fock methods, such as configuration interaction and coupled cluster methods. These methods are usually employed to obtain a more accurate correlation energy that is missed entirely in the Hartree-Fock method.

2.1.1 Schrödinger equation

In quantum mechanics, the energy and state of a system, e.g., atoms, moleucles, or clusters, can be determined using the time-independent

Schrödinger's equation:

$$\hat{H}|\Psi\rangle = E|\Psi\rangle, \tag{2.1}$$

where $\hat{H}$ is the Hamiltonian operator, $|\Psi\rangle$ is the wavefunction, and E is the total energy of the system. In addition, operator and ket notation are commonly used to represent physical quantities and states of a system, respectively. The use of operator and ket notation provides a compact and consistent mathematical framework for expressing quantum mechanical concepts and calculations, enabling the efficient manipulation and interpretation of complex quantum systems.

The non-relativistic molecular Hamiltonian without external fields can be expressed as:

$$\hat{H} = \hat{T}_e + \hat{V}_{ee} + \hat{V}_{en} + \hat{V}_{nn} + \hat{T}_n, \tag{2.2}$$

where $\hat{T}_e$, $\hat{V}_{ee}$, $\hat{V}_{en}$, $\hat{V}_{nn}$, and $\hat{T}_n$ are operators representing the kinetic energy of electrons, electron-electron Coulomb interaction, electron-nuclei Coulomb interaction, nuclei-nuclei Coulomb interaction, and kinetic energy of nuclei, respectively.

The individual operators are defined as:

$$\begin{aligned}
\hat{T}_e &= -\frac{1}{2}\sum_{i=1}^{N_e}\nabla_i^2 & \hat{V}_{en} &= -\sum_{J=1}^{N_n}\sum_{i=1}^{N_e}\frac{Z_J}{|\boldsymbol{r}_i - \boldsymbol{R}_J|} \\
\hat{V}_{ee} &= \sum_{i=1}^{N_e}\sum_{j>i}^{N_e}\frac{1}{|\boldsymbol{r}_i - \boldsymbol{r}_j|} & \hat{V}_{nn} &= \sum_{I=1}^{N_n}\sum_{I<J}^{N_n}\frac{Z_I Z_J}{|\boldsymbol{R}_I - \boldsymbol{R}_J|} \\
\hat{T}_n &= -\frac{1}{2}\sum_{I=1}^{N_n}\nabla_I^2. &&
\end{aligned} \tag{2.3}$$

Here, $\boldsymbol{r}_i$ and $\boldsymbol{r}_j$ are the coordinates of electrons i and j, respectively, while $\boldsymbol{R}_I$ and $\boldsymbol{R}_J$ are the coordinates of nuclei I and J, respectively. Z_I and Z_J represent the atomic charge of nuclei I and J, respectively, and N_e and N_n represent the number of electrons and nuclei in the system, respectively. The kinetic energy operator is defined as:

$$\nabla_i^2 = \frac{\partial^2}{\partial x_i^2} + \frac{\partial^2}{\partial y_i^2} + \frac{\partial^2}{\partial z_i^2} \tag{2.4}$$

where x_i, y_i, and z_i are the Cartesian coordinates of particle i. It represents the energy associated with the motion of the particle.

Generally, the nuclei in a molecule are much heavier than the electrons and move much more slowly. Therefore, the electronic structure of the molecule can be determined by assuming that the nuclei are stationary at their equilibrium positions. This approximation, known as the Born-Oppenheimer approximation, is widely used in quantum chemistry calculations. In this approximation, the nuclei are treated as classical particles, i.e., having exact positions and velocities at the same time. As a result, solving Eq. (2.1) is reduced to a set of equations for the electronic part and the nuclei part separately:

$$(\hat{T}_e + \hat{V}_{ee} + \hat{V}_{en} + \hat{V}_{nn})|\Psi_e\rangle = E_e|\Psi_e\rangle \tag{2.5}$$

$$(\hat{T}_n + E_e)|\Psi_n\rangle = E_{\text{tot}}|\Psi_n\rangle \tag{2.6}$$

where Ψ_e and Ψ_n are wavefunctions of electrons and nuclei, respectively. The electronic energy $E_e = E_e(\boldsymbol{R})$ obtained contributes a potential term to the motion of nuclei, where $\boldsymbol{R}$ are the Cartesian coordinates of nuclei. It often referred to as the potential energy surface (PES), which includes the electronic energy and nuclear-nuclear interactions, as a function of nuclear coordinates. The PES encapsulates the intricate interactions between electrons and nuclei, dictating the overall potential energy experienced by the system at different nuclear configurations. By analyzing this PES, one can study the stable configurations, transition states, and reactive pathways of molecules, shedding light on chemical reactions and molecular behavior in the realm of quantum mechanics.

The total wavefunction can then be constructed as the product of electronic and nuclear parts:

$$|\Psi\rangle = |\Psi_e\rangle \otimes |\Psi_n\rangle. \tag{2.7}$$

Here, $\otimes$ is the tensor product symbol, which denotes the mathematical operation of taking the product of two vector spaces to form a new, larger vector space. Solving Eq. (2.5) yields the molecular electronic wavefunction, from which various electronic properties can be derived. In this thesis, the focus is solely on the electronic part, i.e., $|\Psi_e\rangle$.

In practice, obtaining the exact wavefunction for systems with more than two electrons is challenging. To simplify calculations, mean-field methods are usually employed. These methods treat electrons as independent particles moving in an effective mean field contributed by all electrons.

2.1.2 Hartree method

The Hartree method, named after the physicist Hartree, is an early example of a mean-field method. In this method, the total wavefunction, Φ_{Hartree}, is

obtained as the product of all N single-electron wavefunctions:

$$\Phi_{\text{Hartree}}(\boldsymbol{r}_1, \boldsymbol{r}_2, \ldots, \boldsymbol{r}_N) = \phi_1(\boldsymbol{r}_1) \times \phi_2(\boldsymbol{r}_2) \times \cdots \times \phi_i(\boldsymbol{r}_i) \cdots \times \phi_n(\boldsymbol{r}_N) \tag{2.8}$$

where $\phi_i(\boldsymbol{r}_i)$ represents the spatial one-electron wavefunction, i.e., the electron orbital of electron i. However, the Hartree method has a significant shortcoming, namely the neglect of electron exchange effects. This limitation motivated the development of the Hartree-Fock method.

2.1.3 Hartree-Fock method

The Hartree-Fock (HF) method treats the many-electron wavefunction as a single Slater determinant, $\Phi(\boldsymbol{r}_1, \boldsymbol{r}_2, \ldots, \boldsymbol{r}_N)$, which can be written as a sum of a series of product of one-electron orbitals, $\phi(\boldsymbol{r}_i)$:

$$\Phi_{\text{HF}}(\boldsymbol{r}_1, \boldsymbol{r}_2, \ldots, \boldsymbol{r}_N) = \frac{1}{\sqrt{N!}} \begin{vmatrix} \phi_1(\boldsymbol{r}_1) & \phi_2(\boldsymbol{r}_1) & \cdots & \phi_N(\boldsymbol{r}_1) \\ \phi_1(\boldsymbol{r}_2) & \phi_2(\boldsymbol{r}_2) & \cdots & \phi_N(\boldsymbol{r}_2) \\ \vdots & \vdots & \ddots & \vdots \\ \phi_1(\boldsymbol{r}_N) & \phi_2(\boldsymbol{r}_N) & \cdots & \phi_N(\boldsymbol{r}_N) \end{vmatrix}. \tag{2.9}$$

The one-electron orbitals in the HF method are optimized to minimize the total energy of the system, subject to the constraint that they are orthogonal to each other. These electron orbitals can be used to construct the total wavefunction. Since electrons are fermions, each spatial orbital can only be occupied by two electrons with different spin states, i.e., spin up and spin down. Occupied orbitals are those occupied by electrons, while unoccupied orbitals are called virtual orbitals. The highest energy occupied orbital and the lowest energy unoccupied orbital are denoted as HOMO and LUMO, respectively, and are very important in determining molecular properties, such as reactivity, ionization potential, and electron affinity. Figure 2.1 summarizes these typical electron orbitals obtained by a HF calculation.

Although the HF method accurately accounts for electron exchange effects, it does not capture electron correlation effects. Nonetheless, the simplicity of the HF method makes it an important tool in quantum chemistry, providing a starting point for more accurate post-HF methods, e.g., configuration interactions and coupled cluster methods.

2.1.4 Configuration interaction

Configuration interaction (CI) is a quantum mechanical method that accounts for electronic correlation effects in molecules. This is done by expanding the wavefunction as a linear combination of Slater determinants, which

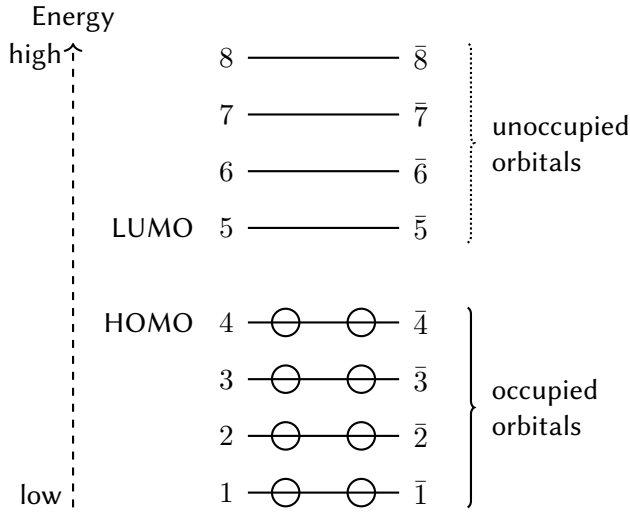

Figure 2.1: A typical molecular orbitals diagram obtained by mean-field methods, e.g., Hartree and HF methods. The numbers without bar index spin-up orbitals, while numbers with bar index spin-down orbitals.

are constructed by exciting electrons from occupied to virtual orbitals. The single-determinant HF wavefunction is typically employed as the starting point for CI. Excited determinants are obtained by applying a series of excitation operators to the HF wavefunction.

Consider the single excitation operator $\hat{T}_i^a$, which creates an electron in a virtual orbital a and removes one from an occupied orbital i,

$$\hat{T}_1 = \sum_{i}^{\text{occ.}} \sum_{a}^{\text{vir.}} c_i^a \hat{T}_i^a. \tag{2.10}$$

Here, c_i^a is the coefficient that determines the contribution of each determinant generated by T_i^a. An example of a single excitation operator, $\hat{T}_4^7$, is shown in Figure 2.2.

The double excitation operator $\hat{T}_{ij}^{ab}$ creates two electrons in virtual orbitals (a, b) and removes two from occupied orbitals (i, j),

$$\hat{T}_2 = \sum_{i,j}^{\text{occ.}} \sum_{a,b}^{\text{vir.}} c_{ij}^{ab} \hat{T}_{ij}^{ab}, \tag{2.11}$$

where c_{ij}^{ab} is the coefficient that determines the contribution of each determinant generated by T_{ij}^{ab}. An example of a double excitation operator, $\hat{T}_{4\bar{4}}^{5\bar{6}}$, is shown in Figure 2.3.

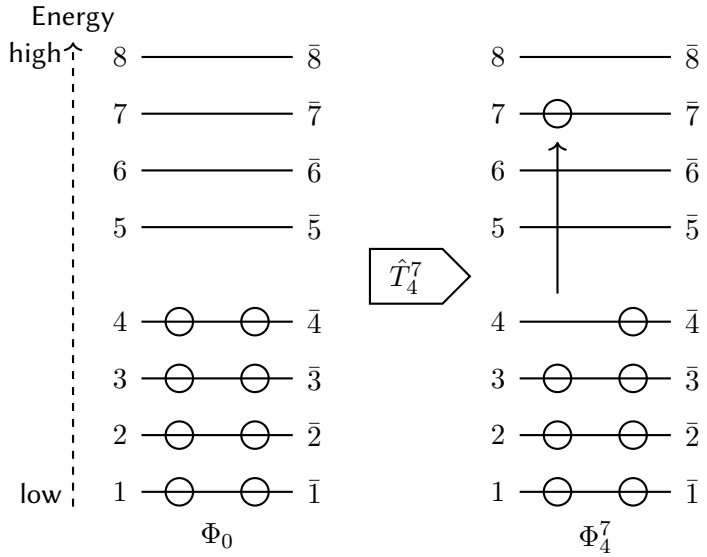

Figure 2.2: An example moleuclar orbitals diagram generated by applying $\hat{T}_4^7$ single excitation operator.

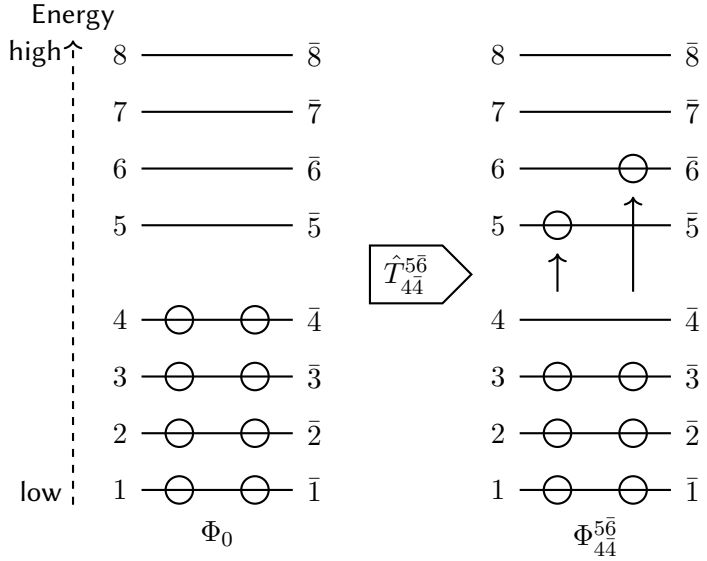

Figure 2.3: An example molecular orbitals diagram generated by applying $\hat{T}_{4\bar{4}}^{5\bar{6}}$ double excitation operator.

Higher excitation operators act on a determinant by exciting multiple electrons between occupied and virtual orbitals. The CI wavefunction is expressed as a linear combination of the excited determinants, with the coefficients determined variationally and iteratively.

$$|\Psi_{\mathsf{CI}}\rangle = c_0|\Phi_{\mathsf{HF}}\rangle + \sum_{ia} c_i^a \hat{T}_i^a |\Phi_{\mathsf{HF}}\rangle + \sum_{ijab} c_{ij}^{ab} \hat{T}_{ij}^{ab} |\Phi_{\mathsf{HF}}\rangle + \cdots . \tag{2.12}$$

Here, c_0 is the coefficient for the HF determinant. The CI method offers a systematic approach to include electron correlation effects beyond the mean-field approximation and is widely used in computational chemistry for electronic structure calculations.

The method that includes all excitations is termed "full CI", which accounts for complete electron correlation but is computationally expensive and only practical for systems with a few atoms. In practice, excitation operators are truncated and higher-order excitation operators are neglected. For instance, CIS refers to CI where only single excitations are accounted for, while CISD refers to CI with both single and double excitations. These methods are feasible for systems where higher-order excitation is negligible. However, for systems with significant multi-reference character, these higher-order excitations cannot be ignored.

2.1.5 Coupled cluster

The coupled cluster (CC) method builds upon the HF method by providing improvements analogous to CI approximations. Unlike the CI method, which constructs the wavefunction as a linear combination of excitation operators acting on the HF reference wavefunction, the CC method uses an exponential ansatz for the combination of these operators:

$$|\Psi_{\mathsf{CC}}\rangle = e^{\hat{T}} |\Phi_{\mathsf{HF}}\rangle. \tag{2.13}$$

Here, $e^{\hat{T}}$ denotes a complex excitation operator constructed using the exponential of the cluster operator. This is typically expressed as a Taylor series expansion:

$$e^{\hat{T}} = \sum_{n=0}^{\infty} \frac{1}{n!} \hat{T}^n. \tag{2.14}$$

The cluster operator, $\hat{T}$, represents a sum of all excitation operators:

$$\hat{T} = \hat{T}_1 + \hat{T}_2 + \cdots , \tag{2.15}$$

where $\hat{T}_1$ (defined in Eq. (2.10)) stands for all single excitations, $\hat{T}_2$ (defined in Eq. (2.11)) denotes all double excitations, and so on. Therefore, the CC wavefunction is expressed as a truncated series expansion of the exponential ansatz:

$$|\Psi_{\mathrm{CC}}\rangle = e^{\hat{T}}|\Phi_{\mathrm{HF}}\rangle \approx (1 + \hat{T} + \frac{1}{2!}\hat{T}^2 + \cdots + \frac{1}{n!}\hat{T}^n)|\Phi_{\mathrm{HF}}\rangle. \tag{2.16}$$

In the above equation, only a finite number of excitation operators are utilized in the calculation because the number of molecular orbitals is finite. CCSD, where "SD" signifies singles and doubles excitations, is often considered superior to CISD because it exhibits size-consistency. This implies that the energy of a system composed of non-interacting parts should equal the sum of the energies of individual parts. Furthermore, the CCSD method implicitly includes certain effects of higher-order correlation, such as triple and quadruple excitations, which are neglected in the CISD method. This can be attributed to the exponential ansatz of the wavefunction in CCSD, which integrates combinations of single and double excitations to emulate the effects of higher-order excitations.

An extension of CCSD, known as CCSD(T), where "T" denotes a correction originating from perturbative triples excitations, is deemed the gold standard in computational chemistry owing to its computational precision and efficiency. While CCSD(T) can be computationally demanding for large molecules, it has consistently demonstrated the capability to provide highly accurate results across a diverse range of chemical systems.

2.2 Density Functional Theory

This section introduces the development of AKCS2ω. Before delving into ACKS2ω, it is essential to provide some theoretical methods. This section begins with a discussion of DFT, a widely-used mean-field method in materials science and computational chemistry. The fundamental ideas behind this theory and its applications will be introduced. Subsequently, the focus shifts to molecular mechanics force fields, specifically polarizable force fields. Additional mathematical details on two specific polarizable force fields, namely the EEM and ACKS2 methods, will be provided, as they are fundamental to the research presented in this thesis.

2.2.1 Hohenberg-Kohn theorems

DFT is based on the Hohenberg-Kohn theorems,[39] which states that the ground-state energy and wavefunction of a many-electron system are

uniquely determined by the system's electron density alone. The electronic energy can be obtained from Eq. (2.5):

$$E = E[\rho] = \langle \Psi | \hat{H} | \Psi \rangle \tag{2.17}$$

where the subscript "e" is omitted, also in the text below for brevity.

The total electronic energy can be expressed by

$$E[\rho] = F[\rho] + V_{\text{ext}}[\rho] = F[\rho] + \langle \Psi | \hat{V}_{\text{ext}} | \Psi \rangle \tag{2.18}$$

where $F[\rho]$ is a universal functional of electron density, and $V_{\text{ext}}[\rho]$ is potential energy. The term "universal" means that this functional is the same for all systems, i.e., independent of $V_{\text{ext}}[\rho]$. The universal functional consists of two parts: the kinetic energy of electrons ($T[\rho]$) and the electron-electron interaction energy ($U[\rho]$):

$$F[\rho] = T[\rho] + U[\rho] \tag{2.19}$$

$$T[\rho] = \langle \Psi | \hat{T} | \Psi \rangle \tag{2.20}$$

$$U[\rho] = \langle \Psi | \hat{V}_{ee} | \Psi \rangle. \tag{2.21}$$

The functional $U[\rho]$ contains electron-electron Coulomb interaction, exchange, and correlation effects.

2.2.2 Kohn-Sham DFT

Although the Hohenberg-Kohn theorem shows that the state of a system is determined by the density of the system, it does not provide a practical approach to compute the density. In 1965, Kohn and Sham demonstrated that the properties of an interacting system can be described using a non-interacting reference system.[40] The universal functional in Kohn-Sham DFT can be expressed as:

$$F[\rho] = T_s[\rho] + \iint d\boldsymbol{r} d\boldsymbol{r}' \frac{\rho(\boldsymbol{r})\rho(\boldsymbol{r}')}{|\boldsymbol{r} - \boldsymbol{r}'|} + E_{xc}[\rho] \tag{2.22}$$

$$T_s[\rho] = \langle \Phi | \hat{T} | \Phi \rangle \tag{2.23}$$

where T_s and E_{xc} denote the kinetic and XC energy of electrons in the non-interacting system, i.e., the Kohn-Sham system. The term with the integrals represents the Hartree interaction, accounting for the classical electron-electron repulsion. Central to the Kohn-Sham scheme is the introduction

of the Kohn-Sham effective potential ($V_{\text{eff}}[\rho]$), which contains the external potential along with the Hartree and XC potential contributions:

$$V_{\text{eff}}[\rho] = \iint d\boldsymbol{r} d\boldsymbol{r}' \frac{\rho(\boldsymbol{r})\rho(\boldsymbol{r}')}{|\boldsymbol{r} - \boldsymbol{r}'|} + E_{xc}[\rho] + V_{\text{ext}}[\rho] \tag{2.24}$$

This effective potential drives the behavior of non-interacting electrons in the Kohn-Sham system such that they reproduce the electron density of the true interacting system. This elegant framework circumvents the complexities of many-body interactions by recasting the problem in terms of an equivalent non-interacting system governed by the Kohn-Sham effective potential.

The XC functional can be expressed as:

$$E_{xc}[\rho] = (T[\rho] - T_s[\rho]) + U[\rho] - \iint d\boldsymbol{r} d\boldsymbol{r}' \frac{\rho(\boldsymbol{r})\rho(\boldsymbol{r}')}{|\boldsymbol{r} - \boldsymbol{r}'|}. \tag{2.25}$$

However, the exact expression of the XC functional is still not known, and one has to choose approximate XC functionals in practice.

XC functionals are crucial in DFT calculations and can be classified according to the level of approximation used to describe the XC energy density. Jacob's ladder, introduced by Perdew and Schmidt in 2001, is a widely-used hierarchy for these functionals, consisting of five rungs with increasing levels of sophistication and accuracy: (1) Local Density Approximation (LDA), (2) Generalized Gradient Approximation (GGA), (3) Meta-GGA, (4) Hyper-GGA or hybrid functionals, and (5) Double hybrid. Each rung incorporates additional terms or corrections to improve the accuracy of the XC energy density calculation. The first tree rungs are also called semi-local XC functionals, which offer a balance between computational efficiency and accuracy, making them widely used in electronic structure calculations for various materials and chemical systems.

2.3 Time-Dependent Density Functional Theory (TDDFT)

Time-Dependent Density Functional Theory (TDDFT) is an extension of DFT to describe time-dependent quantum systems, primarily focusing on electron dynamics under the influence of external perturbations. It is anchored on the Runge-Gross (RG) theorem (1984), [41] which states that for a given initial wavefunction, there is a unique mapping between the time-dependent external potential of a system and its time-dependent density. In principle, TDDFT is an exact theory when the correct time-dependent exchange-correlation functional is employed. In addition, there is no general energy

minimization principle in TDDFT. In analogy to Kohn-Sham DFT, there is also a fictitious non-interacting system, i.e., time-dependent Kohn-Sham system, which shares the same density as the interacting system of interest.

TDDFT provides a means to access excited-state properties of molecules without directly solving the full many-body Schrödinger equation. This feature is instrumental in studying electronic excitations, as encountered in photochemistry and spectroscopy.[42, 43] In addition, TDDFT allows for the simulation of real-time evolution of electronic systems, offering insights into phenomena like electron transfer, plasmonic responses, and photon-induced processes in various materials.[42, 43] In this thesis, our focus is solely on weak perturbations, namely, the linear-response regime. Linear-response TDDFT is instrumental in calculating electronic excitation energies and oscillator strengths, which are crucial for simulating spectra such as UV-Vis and other electronic absorption spectra.[42, 43] Moreover, the linear-response regime typically validates Floquet TDDFT. Consequently, this section will provide a straightforward introduction to Floquet TDDFT, a methodology extensively utilized in this thesis.

2.3.1 Linear-response TDDFT

Linear-response TDDFT is a powerful approach for studying the response of a system to small linear-dependent perturbations, usually expressed in the frequency domain. Within the linear-response regime, the change in electron density, $\delta\rho(\boldsymbol{r},\omega)$, due to a small perturbation in the external potential, $\delta V_{\text{ext}}(\boldsymbol{r},\omega)$, can be related through the system's response function, $\chi(\boldsymbol{r},\boldsymbol{r}',\omega)$:[42]

$$\delta\rho(\boldsymbol{r},\omega) = \int d\boldsymbol{r}'\chi(\boldsymbol{r},\boldsymbol{r}',\omega)\delta V_{\text{ext}}(\boldsymbol{r}',\omega). \tag{2.26}$$

In TDDFT, the response function contains all the information about the system's excited states. The poles of the response function correspond to the excitation energies of the system.

In the non-interacting Kohn-Sham system, we have [42]

$$\begin{aligned}\delta\rho(\boldsymbol{r},\omega) &= \int d\boldsymbol{r}'\chi_{\text{KS}}(\boldsymbol{r},\boldsymbol{r}',\omega)\delta V_{\text{eff}}[\rho](\boldsymbol{r}',\omega)\\ \delta V_{\text{eff}}[\rho](\boldsymbol{r}',\omega) &= \delta V_{\text{ext}}(\omega) + \frac{\delta\rho(\boldsymbol{r}',\omega)}{|\boldsymbol{r}-\boldsymbol{r}'|} + f_{\text{xc}}(\boldsymbol{r},\boldsymbol{r}',\omega)\delta\rho(\boldsymbol{r},\omega).\end{aligned} \tag{2.27}$$

where $f_{\text{xc}}(\boldsymbol{r},\boldsymbol{r}',\omega)$ is the exchange-correlation kernel, which is the functional derivative of the exchange-correlation potential with respect to the density.

Importantly, to obtain accurate excitation energies and response properties, an appropriate exchange-correlation kernel must be employed. When the adiabatic approximation is employed, $f_{\text{xc}}(\boldsymbol{r}, \boldsymbol{r}', \omega) \approx f_{\text{xc}}(\boldsymbol{r}, \boldsymbol{r}', 0)$, i.e., it is frequency-independent.

From Eqs. (2.26)-(2.27), one can compute the interacting response function from the Kohn-Sham non-interacting response function via the Dyson-like equation:[42]

$$\chi(\boldsymbol{r}, \boldsymbol{r}', \omega) = \chi_{\text{KS}}(\boldsymbol{r}, \boldsymbol{r}', \omega) + \iint d\boldsymbol{r}_1 d\boldsymbol{r}_2 \chi_{\text{KS}}(\boldsymbol{r}_1, \boldsymbol{r}, \omega) \left[\frac{1}{|\boldsymbol{r}_1 - \boldsymbol{r}_2|} + f_{\text{xc}}(\boldsymbol{r}_1, \boldsymbol{r}_2, \omega) \right] \chi(\boldsymbol{r}_2, \boldsymbol{r}', \omega) \tag{2.28}$$

In practice, the Dyson-like equation is usually solved with a matrix format, also known as Casida's equations,[44] of which solution gives the excitation energies of the system.

2.3.2 Floquet TDDFT

Floquet states correspond to the steady-state solutions of the time-dependent Schrödinger equation when we have a time-periodic Hamiltonian, $\hat{H}(t+T) = \hat{H}(t)$. A comprehensive set of Floquet solutions can be expressed as,[45, 46]

$$\psi_n(t) = \exp^{-i\epsilon_n t} u_n(t) \quad u_n(t+T) = u_n(t). \tag{2.29}$$

These time-periodic functions $u_n(t)$ are defined as quasi-energy eigenstates (QES), while ϵ_n is referred to as the quasi-energy. The QESs adhere to

$$\left[\hat{H}(t) - i\frac{\partial}{\partial t} \right] u_n(t) = \epsilon_n u_n(t) \tag{2.30}$$

and are analogous to the stationary states found in a time-independent Hamiltonian.

The merits of the quasi-energy approach have been extensively discussed in the literature.[47] A notable benefit of quasi-energy TDDFT is the elimination of the initial state dependence mandated by the Runge-Gross theorem, replacing it with periodic boundary conditions for external perturbations. Additionally, the quasi-energy ansatz provides a cohesive framework for calculating dynamic linear-response properties using both wavefunction and DFT methods, as it is universally applicable to both variational and non-variational approaches.[47] This unified framework enables the derivation of

dynamic response properties through the energy derivative approach within the quasi-energy formalism. However, the validity of Floquet theory has been subject to debate,[46, 48–50] and its application necessitates the following approximations: (i) utilization of a finite basis; [49, 50] (ii) the assumption that the external driving perturbation is weak and off-resonant.[49–51] The first condition guarantees the existence of an adiabatic limit for the "Floquet ground state", upon which the energy minimum principle is valid, while the second condition ensures a one-to-one density-potential mapping. The second condition also implies that Floquet theory serves as a suitable approximate method for addressing linear-response problems. Despite these limitations, for the purpose of developing molecular force-field methods, these conditions are typically met, allowing the utilization of Floquet theory in the development of frequency-dependent force-field methodologies.

2.4 Force-fields methods

QM methods can provide highly accurate results, close to experimental results, but they are often computationally expensive for large-scale systems. For example, the Kohn-Sham DFT with density fitting has a computational complexity of O(N^3), where N is the number of basis functions. This hinders its application to large-scale systems, especially for molecular dynamics (MD) simulations. In contrast, FF methods, have been developed and applied to large-scale MD simulations. FF methods play a crucial role in computational chemistry, modeling the behavior of molecules and materials. These force fields, grounded in classical mechanics, employ empirical functions to represent interatomic interactions within a molecule or system. By using force fields, researchers can simulate the behavior of complex molecules, biomolecules, and materials, which is essential for understanding their properties and designing new drugs or materials.

Over the years, various categories of molecular mechanics force fields have been developed, each with its unique strengths and weaknesses. These force fields differ in functional forms, parameterization methods, and level of detail. They are typically chosen based on the specific research question and the properties of the system being studied.

The general force-field methods can be summarized as follows:

- (1) Conventional Force Fields: The conventional FF methods can be divided into two categories, Class I and Class II force fields. They describe interatomic interactions differently, with Class I being computationally efficient but less accurate, while Class II uses higher-

order contributions and cross terms, offering more accuracy but being computationally expensive.

- (2) Polarizable Force Fields:[52–70] These force fields explicitly include electronic polarization, allowing for a more nuanced representation of interatomic interactions.

- (3) Reactive Force Fields:[68, 71–73] These force fields are designed to handle complex chemical reactions with dynamically changing bond topologies, making it suitable for studying reactions and dynamics in chemically reactive systems. One of the famous ones is ReaxFF, which has been extensively parameterized for a wide range of materials and conditions. Unlike traditional force fields that rely on fixed bond parameters, ReaxFF uses a more flexible approach where bond energies and forces are calculated on-the-fly as a function of atomic positions. Therefore, ReaxFF is especially well-suited for studying processes like combustion, catalysis, and polymerization, where bond breaking and formation are essential.

Additional information regarding these three categories will be introduced in the subsequent sections.

Furthermore, additional force field models have been proposed in the literature. Nevertheless, these concepts are often overlaped with each other and with the general force-field methods.

- QM-derived Force Fields:[74, 75] These force fields utilize quantum mechanics and empirical expressions for energy calculations. QM data is typically used to fit parameters and incorporate physically-motivated terms, resulting in a more accurate representation of molecular interactions.

- *Ab initio* force fields:[76] These force fields also use QM data but mainly investigate intermolecular force fields. Generally, only a few empirical parameters need to be fitted, while other parameters are computed by *ab initio* calculations. This makes them computationally expensive, even when density-fitting approximations or semi-empirical methods, such as tight-binding methods, are employed.

- Machine-Learning Force Fields:[77–88] These force fields, also known as machine-learning potentials (MLPs), are used in computational chemistry and materials science to predict the forces between atoms in simulations. Unlike traditional hand-tuned models, a machine learning algorithm can learn the model directly from data, usually from

quantum mechanical calculations or experimental measurements. This approach tends to provide more accurate and versatile models, while also being faster and cheaper than performing quantum mechanical calculations directly. Various machine learning models, including neural networks, Gaussian processes, and decision tree models, can be utilized depending on the specific application and available resources.

Interested readers can refer to the provided references for more information.

2.4.1 Class-I force fields

Class I force fields include AMBER,[67, 89, 90] CHARMM,[53, 64, 69, 70, 91, 92] OPLS,[93, 94] GROMACS,[95–97] NAMD,[98] and ECEPP.[99] The total potential energy (E_{pot}) in this group can be divided into two parts: the bonded (E_{bonded}) and non-bonded terms ($E_{\text{nonbonded}}$):

$$E_{\text{pot}} = E_{\text{bonded}} + E_{\text{nonbonded}} \tag{2.31}$$

which is an empirical approximation to the potential energy, defined in Eq. (2.5).

The bonded term, also known as intramolecular or internal terms, is concerned with the connectivity of atoms within a molecule. It is usually composed of several contributions, for instance in the CHARMM force field as shown in Figure 2.4,[69] bond stretching (E_{bonds}), bond angle deformation (E_{angles}), improper dihedral angle deformation (E_{improper}), and dihedral angle deformation ($E_{\text{dihedrals}}$):[53, 69, 70, 91]

$$E_{\text{bonded}} = E_{\text{bonds}} + E_{\text{angles}} + E_{\text{improper}} + E_{\text{dihedrals}} \tag{2.32}$$

with

$$E_{\text{bonds}} = \sum_{\text{bonds}} K_b(b - b_0)^2 \tag{2.33}$$

$$E_{\text{angles}} = \sum_{\text{angles}} K_\theta(\theta - \theta_0)^2 \tag{2.34}$$

$$E_{\text{improper}} = \sum_{\text{improper}} K_\psi(\psi - \psi_0)^2 \tag{2.35}$$

$$E_{\text{dihedrals}} = \sum_{\text{dihedrals}} \sum_{n=1}^{6} K_{\phi,n}(1 + \cos(n\phi - \delta_n)) \tag{2.36}$$

where b, θ, ψ, and ϕ represent the bond lengths, valence angles, improper dihedral angles, and dihedral angles, determined from the molecular geometry. For the first three terms, b_0, θ_0, and ψ_0 respectively represent the

corresponding bond, angle, and improper equilibrium values, and parameters K_b, K_θ, and K_ψ denote the force constants fitted to experimental or *ab initio* data. As for the dihedral term, parameter $K_{\phi,n}$ represents the amplitude and δ_n is the phase for each multiplicity n.

The non-bonded term usually consists of an electrostatic term and a vdW term:

$$E_{\text{nonbonded}} = E_{\text{electrostatic}} + E_{\text{vdW}} \tag{2.37}$$

with

$$E_{\text{electrostatic}} = \sum_{i<j}^{\text{non-bonded pairs}} \frac{q_i q_j}{r_{ij}} \tag{2.38}$$

$$E_{\text{vdW}} = \sum_{i<j}^{\text{non-bonded pairs}} \epsilon_{ij} \left[\left(\frac{\sigma_{ij}}{r_{ij}} \right)^{12} - 2 \left(\frac{\sigma_{ij}}{r_{ij}} \right)^{6} \right] \tag{2.39}$$

where q_i and q_j are the respective partial atomic charges on atom i and j, and the atoms in the model are usually treated as point charges. The vdW term is treated by the Lennard-Jones (LJ) 6–12 potential in which ϵ_{ij} is the well depth and parameters σ_{ij} is the sum of atomic vdW radius σ_i and σ_j of atoms i and j, respectively, and r_{ij} is the distance between atom i and j.

Apart from the LJ potential, other forms are also employed to treat nonbonded vdW interaction, such as buffered 14–7 potential,[65, 100] 9–6 potential,[101, 102] and Buckingham exp-6 potential.[103–106]

2.4.2 Class-II force fields

Generally, Class I force fields are diagonal quadratic functional forms, while Class II force fields usually employ more complex functional forms involving higher-order bonded terms to calculate bond and valence angle terms. The Class II force fields include AMOEBA,[65, 107] MM3,[108] MM4,[109] MMFF,[110, 111] CFF,[101, 112–116], UFF,[106, 117] and CVFF.[118–120]

For instance, in CFF,[101] the bond stretching term becomes:

$$E_{\text{bonds}} = \sum_{\text{bonds}} K_{2,b}(b - b_0)^2 + K_{3,b}(b - b_0)^3 + K_{4,b}(b - b_0)^4 \tag{2.40}$$

where $K_{n,b}$ represents the parameter to be determined for the n-th order bonds term. An extra cross term for bond terms is defined as:

$$E_{b,b'} = K_{b,b'}(b - b_0)(b' - b'_0). \tag{2.41}$$

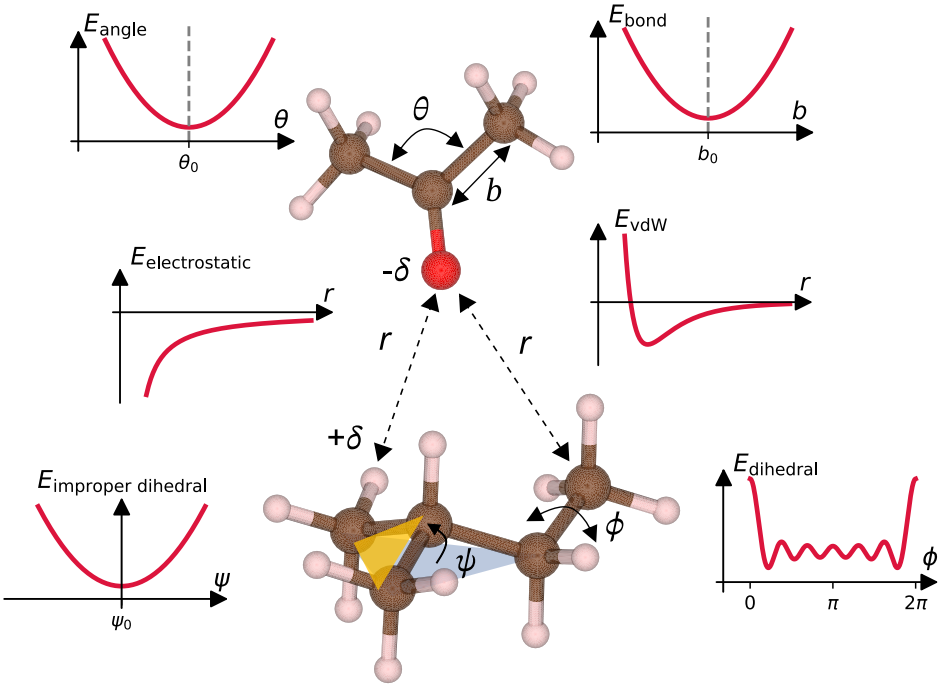

Figure 2.4: Different energy potential in molecular force fields.

These additional terms increase the accuracy of the force field when calculating relative energies and geometries, as well as performing vibrational analyses. By accurately capturing the intricate interactions between atoms and molecules, force fields can lead to more reliable simulations and predictions.

However, determining parameter sets for these functions can be challenging due to the lack of suitable target data. This is particularly true when it comes to quantitative data, as the larger number of parameters in these more refined functions can make the optimization process much more difficult.

As a result, scientists working in this area must often rely on a combination of experimental data, computational simulations, and theoretical models to develop potential energy functions that accurately capture the behavior of molecular systems.[54, 69] The Class II force fields also use more sophisticated methods to compute non-bonded interactions, including multipole expansion,[108] polarization, and charge penetration effects, which can lead to more accurate results.

2.4.3 Polarizable force fields

A significant drawback of traditional FF methods is the lack of electronic polarization, which refers to the response of the electron distribution to the surrounding environment. This is because classical force fields typically use a fixed-charge model for electrostatic interaction, as shown in Figure 2.5, where a water molecule is used, and fixed charges are assigned to oxygen and hydrogen atoms independently of the electric field generated by an atom with positive charge q.

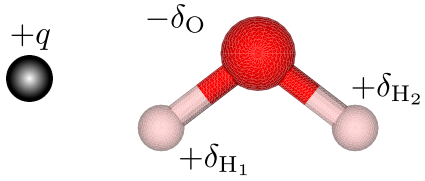

Figure 2.5: The fixed-charge model of a water molecule, where fixed charges are assigned to oxygen and hydrogen atoms independently of the electric field generated by an atom with positive charge q.

To address this limitation, the molecular modeling community has developed PFFs that explicitly incorporate polarization effects, thus improving the predictive accuracy of long-range interactions. In general, the energy associated with electronic polarization is given by:

$$E_{\text{pol}} = E_{\text{self}} + E_{\text{multipole-multipole}} \tag{2.42}$$

where the total polarization energy consists of two parts: the self-energy term E_{self} and the multipole-multipole term $E_{\text{multipole-multipole}}$. The self-energy term corresponds to the work needed to change the charge distribution, while the multipole-multipole term is an extension of Coulomb interaction usually used in FFs by including multipole-multipole interactions, such as (induced) charge-dipole and (induced) dipole-dipole interactions, etc.

There are four major categories of PFFs in literature: induced dipoles or multipoles,[107, 121–124] Drude oscillator,[62, 125–127] Electronegativity Equalization Method (EEM),[128, 129] and the explicit electron model.[80, 130–133] The explicit electron model treats electrons as separate classical particles in the system.[80, 130–133] These particles can freely move from one atom to another within a molecule due to a perturbation. By explicitly modeling the electrons, the model can account for electronic polarization in a detailed and accurate manner.

As an example, the LEWIS model is a computational approach designed to simulate important characteristics of molecular behavior, such as reactivity, polarizability, and flexibility. It strives for a balance between chemical

intuitiveness and computational simplicity, enabling it to model complex molecular interactions and geometrical rearrangements that signal the onset of chemical reactions. Although it offers several advantages in terms of computational efficiency and certain predictive capabilities, the model has limitations due to simplifications like treating electrons in pairs and excluding multi-body interactions. Despite these constraints, the LEWIS model contributes valuable insights into the behavior of molecular systems, especially in situations where traditional computational methods like DFT are too computationally expensive.

This thesis focuses on the other three categories of PFFs, which have been widely implemented in PFF frameworks.

I. Induced dipole model

Induced dipole or multipole models are based on the concept that each atom is represented by a set of electronic dipoles and/or higher order multipoles. For simplicity, this thesis only focus on the induced dipole model. In the linear response regime, the induced dipole moment $\boldsymbol{\mu}$ is

$$\boldsymbol{\mu} = \boldsymbol{\alpha} \cdot \boldsymbol{E}_{\text{ext}}(\boldsymbol{r}) \tag{2.43}$$

where $\boldsymbol{\alpha}$ is the 3×3 dipole polarizability tensor and $\boldsymbol{E}_{\text{ext}}(\boldsymbol{r})$ is the external electric field strength at position $\boldsymbol{r}$.

For a system consisting of multiple atoms, the induced dipole moment of atom i is given by:

$$\boldsymbol{\mu}_i = \boldsymbol{\alpha}_i \cdot \left[\boldsymbol{E}_{\text{ext}}(\boldsymbol{r}_i) - \sum_{j \neq i}^{N} \boldsymbol{E}_j(\boldsymbol{r}_i) \right] = \boldsymbol{\alpha}_i \cdot \left[\boldsymbol{E}_{\text{ext}}(\boldsymbol{r}_i) - \sum_{j \neq i}^{N} \boldsymbol{T}_{ij} \boldsymbol{\mu}_j \right], \tag{2.44}$$

where $\boldsymbol{\mu}_i$ is the dipole moment of atom i, $\boldsymbol{\alpha}_i$ is the polarizability tensor of atom i, $\boldsymbol{E}_{\text{ext}}(\boldsymbol{r}_i)$ is the external electric field at the position of atom i, and $\boldsymbol{E}_j(\boldsymbol{r}_i)$ is the electric field generated by the dipole moment of atom j at the position of atom i. The sum is taken over all atoms j other than i.

In the induced dipole model, each atom is treated as a rigid particle, but its induced dipole moment is allowed to vary during simulation. Figure 2.6 shows an example of the induced dipole model in a water molecule, where the arrows represent the induced dipole moments.

The total polarization energy for the induced dipole model is:

$$E_{\text{pol}} = \frac{1}{2} \sum_{i=1}^{N} \boldsymbol{\mu}_i^T \boldsymbol{\alpha}^{-1} \boldsymbol{\mu}_i - \sum_{i=1}^{N} \boldsymbol{\mu}_i \cdot \boldsymbol{E}^0(\boldsymbol{r}_i) + \frac{1}{2} \sum_{i \neq j}^{N} \boldsymbol{\mu}_i^T \boldsymbol{T}_{ij} \boldsymbol{\mu}_j \tag{2.45}$$

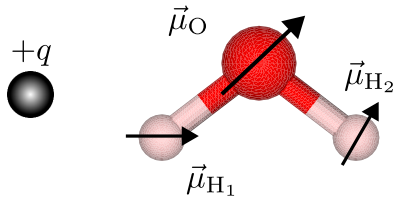

Figure 2.6: The induced dipole model of a water molecule in an electric field generated by an atom with positive charge q. The arrows represent the induced dipole momments.

where the first term is the self-energy, the second term represents the interaction of the induced dipole with the external field $E^0(\boldsymbol{r}_i)$, and the last term describes the mutual interaction of induced dipoles.

When atomic isotropic dipole polarizability is used, the self-energy term can be written as follows:

$$E_{\text{self}}^{\text{ind}} = \frac{1}{2} \sum_i \alpha_i^{-1} \|\boldsymbol{\mu}_i\|^2 \tag{2.46}$$

where α_i is the atomic isotropic dipole polarizability for atom i and μ_i is the induced dipole moment. The total potential energy is then given for induced dipole PFFs:

$$E_{\text{pot}} = E_{\text{bonded}} + E_{\text{non-bonded}} + E_{\text{pol}} \tag{2.47}$$

II. Drude oscillator model

The Drude oscillator model, also known as shell model, is another well-known method used to represent electronic polarization in molecules. This is achieved by placing (usually negative) auxiliary particles, referred to as Drude particles, near the location of each atom within the molecule. Each particle is tethered to its parent atom by a harmonic spring with a force constant denoted as k. These particles interact with their corresponding parent atoms and other particles within the system, thereby simulating the effects of polarization. The white circles represent negative Drude particles, and the black circles represent positive cores.

The total charge of a parent atom $\tilde{Q}_i$ is the sum of the nuclear charge Q_i and the auxiliary particle charge $q_{s,i}$. The total polarization energy of the

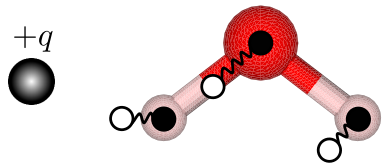

Figure 2.7: The Drude model of a water molecule in the electric field generated by an atom with a positive charge of q.

molecule with Drude particles is given by:

$$E_{\text{pol}} = \frac{1}{2}\sum_{i=1}^{N} k_i \|\Delta \boldsymbol{r}_i\|^2 + \sum_{i=1}^{N-1}\sum_{j>i}^{N}\left[\frac{\tilde{Q}_i\tilde{Q}_j}{\|\boldsymbol{r}_{ij}\|} + \frac{\tilde{Q}_i q_{s,j}}{\|\boldsymbol{r}_{ij} + \Delta\boldsymbol{r}_j\|} + \frac{q_{s,i}\tilde{Q}_j}{\|\boldsymbol{r}_{ij} - \Delta\boldsymbol{r}_i\|} + \frac{q_{s,i}q_{s,j}}{\|\boldsymbol{r}_{ij} - \Delta\boldsymbol{r}_i + \Delta\boldsymbol{r}_j\|}\right], \tag{2.48}$$

where $\|\boldsymbol{r}_{ij}\|$ is the distance between two atoms. The first term in the equation represents the self-energy E_{self}, which is associated with separating the parent atom and auxiliary particle by a distance $\|\Delta\boldsymbol{r}_i\|$. This term also corresponds to the mechanical energy of the associated harmonic spring. The rest of the terms represent the Coulomb interaction between particles with charges Q and q as parent and auxiliary particles, respectively.

Compared to Eq. (2.45), there is a relationship between the parameters q_s, k, and the atomic isotropic polarizability α given by:

$$\alpha = \frac{q_s^2}{k}. \tag{2.49}$$

III. EEM model

The EEM was developed by Mortier *et al.* by applying Sanderson's principle of electronegativity equalization to basic DFT equations.[129] The EEM has several variants, including fluctuating charges (FQ or FlucQ), charge equilibration (QE, QEq, or CHEQ), and chemical potential equalization (CPE).[64, 92, 134–139] Compared to the induced dipole model and Drude model, the EEM model does not employ induced dipoles directly. Instead, it introduces variable charges, which are fixed in the induced dipole and Drude oscillator models.

The energy required to create a charge Q on a neutral atom can be expressed as a Taylor series,[140]

$$E_{\text{pol}}(Q) = E_0 + Q\left(\frac{\partial E_{\text{pol}}}{\partial Q}\right)_{Q=0} + \frac{1}{2}Q^2\left(\frac{\partial E_{\text{pol}}}{\partial Q^2}\right)_{Q=0} + O(Q^3) \quad (2.50)$$

where E_0 is the reference energy, such as the ground-state energy of Kohn-Sham DFT. The first-order partial derivatives of energy, usually denoted as χ^0, in the series represent the atomic (absolute) electronegativity. The second-order partial derivatives of energy, usually denoted as η^0, correspond to the atomic hardness, determining resistance to the flow of electrons. The high order contributions are usually neglected.

Figure 2.8 shows an example of the fluctuating-charge model for a water molecule in an electric field generated by an atom with a positive charge q. The partial charges, i.e., Q_{O}, Q_{H1} and Q_{H2}, are a function of the charge q, and it is therefore possible for the partial charges of atoms to be redistributed due to external environmental factors during molecular simulations.

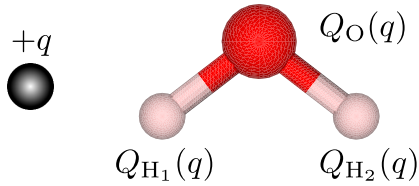

Figure 2.8: The fluctuating-charge model of a water molecule in the electric field generated by an atom with a positive charge q.

For a system consisting of N atoms, the total electrostatic energy becomes

$$E_{\text{pol}} = \sum_i^N (E_i^0 + \chi_i^0 Q_i) + \sum_{i,j}^N \eta_{ij}(r_{ij}) Q_i Q_j \quad (2.51)$$

where η_{ij} are coupling terms dependent on the distance between the interacting atoms i and j, and the diagonal element, i.e., when $i = j$, $\eta_{ij}(r_{ij}) = \eta_{ii}(0) = \eta_i^0$ is just the atomic hardness defined above. For long distances between atoms i and j, the η_{ij} reduces to $1/r_{ij}$, corresponding to the Coulomb interactions often used in force fields. The self-energy is given by:

$$E_{\text{self}} = \sum_i (\chi_i^0 Q_i + \eta_i^0 Q_i^2). \quad (2.52)$$

In practice, the net charge of a system is conserved, i.e.,

$$Q_{\text{tot}} = \sum_i Q_i. \quad (2.53)$$

As a result, the Lagrangian of the system can be expressed as the total polarization energy with an additional Lagrange multiplier to account for the boundary condition.

$$L_{\text{pol}}(Q) = E_{\text{pol}}(Q) - \lambda \left(Q_{\text{tot}} - \sum_i Q_i \right). \tag{2.54}$$

Minimizing the equations with respect to Q_i results in a set of Euler-Lagrange equations:

$$\left. \frac{\partial E_{\text{pol}}}{\partial Q_i} \right|_{Q_i=0} - \lambda = 0. \tag{2.55}$$

It should be noted that λ, i.e., the multiplier, is a constant, which means for any atom pairs i and j one has

$$\left. \frac{\partial E_{\text{pol}}}{\partial Q_i} \right|_{Q_i=0} = \left. \frac{\partial E_{\text{pol}}}{\partial Q_j} \right|_{Q_j=0}. \tag{2.56}$$

This first partial derivative of energy is none other than atomic electronegativity for atoms in molecules:

$$\chi_i = \left. \frac{\partial E_{\text{pol}}}{\partial Q_i} \right|_{Q_i=0} = \chi_i^0 + 2\eta_{ii} Q_i + \sum_{i \neq j} \eta_{ij} Q_j. \tag{2.57}$$

The atom-specific values of electronegativity χ^0 and atomic hardness η^0 can either be determined from experimental data or *ab initio* calculations. In practice, these quantities are often treated simply as adjustable parameters. The reason is that EEM is highly approximate, usually making it a useful model only through error compensation.

In original EEM paper,[128, 129] Hohenberg-Kohn DFT is employed as shown in Eq. (2.18):

$$E^{\text{HK}}[\rho] = F[\rho] + \int \rho(\boldsymbol{r}) v(\boldsymbol{r}) d\boldsymbol{r}. \tag{2.58}$$

The electron density and potential of the ground state are ρ_0 and v_0, and the ground-state energy is E_0^{HK}. The chemical potential is given by

$$\mu_0 = \left. \frac{\delta E[\rho]}{\delta \rho(\boldsymbol{r})} \right|_{\rho=\rho_0} = \left. \frac{\delta F[\rho]}{\delta \rho[\boldsymbol{r}]} \right|_{\rho=\rho_0} + v_0(\boldsymbol{r}). \tag{2.59}$$

Consider a perturbation $\delta v(\boldsymbol{r})$ on the ground-state system, the second-order perturbed energy can be expressed by:[139]

$$\begin{aligned} E^{\mathrm{HK}}[\rho_0+\delta\rho, v(\boldsymbol{r})+\delta v(\boldsymbol{r})] =& E_0^{\mathrm{HK}} + \mu_0 \int \delta\rho(\boldsymbol{r}) d\boldsymbol{r} \\ &+ \int (\rho_0(\boldsymbol{r}) + \delta\rho(\boldsymbol{r}))\delta v(\boldsymbol{r}) d\boldsymbol{r} \\ &+ \frac{1}{2} \iint \delta\rho(\boldsymbol{r}) \left.\frac{\delta^2 F[\rho]}{\delta\rho(\boldsymbol{r})\delta\rho(\boldsymbol{r}')}\right|_{\rho=\rho_0} \delta\rho(\boldsymbol{r}') d\boldsymbol{r} d\boldsymbol{r}'. \end{aligned} \tag{2.60}$$

According to Kohn-Sham DFT, the general functional can be written in three parts as shown in Eq. (2.22), and we have an analytic expression for the hardness kernel:

$$\begin{aligned} \eta(\boldsymbol{r}, \boldsymbol{r}') =& \left.\frac{\delta^2 F[\rho]}{\delta\rho(\boldsymbol{r})\delta\rho(\boldsymbol{r}')}\right|_{\rho=\rho_0} \\ =& \frac{1}{|\boldsymbol{r}-\boldsymbol{r}'|} + \left.\frac{\delta^2 T_s[\rho]}{\delta\rho(\boldsymbol{r})\delta\rho(\boldsymbol{r}')}\right|_{\rho=\rho_0} + \left.\frac{\delta^2 E_{\mathrm{xc}}[\rho]}{\delta\rho(\boldsymbol{r})\delta\rho(\boldsymbol{r}')}\right|_{\rho=\rho_0}. \end{aligned} \tag{2.61}$$

On the right-hand side, the first term is the Coulomb interaction contribution, the second is the contribution from (non-interacting) electron kinetic energy, and the third one is the contribution from the XC functional. In EEM, only the Coulomb interaction is considered, leading to the well-known limitations in simulations of extended systems or charge transfer during chemical reactions: (i) it always predicts a cubic scaling of the dipole polarizability with system size, which is incorrect for dielectric systems where a linear scaling exists in the macroscopic limit; and (ii) it obtains fractional molecular charges even when two molecules are well separated and gives a slowly decaying intermolecular charge transfer.

IV. ACKS2 model

Various approaches have been developed to improve the accuracy and applicability of the EEM model, such as incorporating higher-order multipoles, implementing distance-dependent scaling factors, or combining EEM with other polarizable force field methods.[141–144] In addition, *ad hoc* improvements have been proposed, such as applying artificial constraints to molecular charges or dipoles, or introducing a distance-dependent function to penalize long-range charge transfer. Improved models, such as the split-charge equilibration (SQE) model,[145–150], the Charge Response Kernel (CRK) model,[151, 152],

the Bond Capacity model,[153, 154] have also been developed. In the SQE model, charge can only be transferred between topologically connected atoms, and atomic charges are expressed as a sum of split-charge parameters, giving rise to the name SQE.[145–150]. In the CRK model,[151, 152] the molecular energy is expanded to the second order in the external potential produced by another molecule. As a result, the atomic charges are parameterized in terms of linear response, as the second-order derivative of energy with respect to the external potential corresponds to the response function of the system. Charge flow between fragments is prohibited due to the model's design, which distinctly separates intramolecular interactions (within a molecule or fragment) from intermolecular interactions (between different molecules or fragments). This distinction simplifies calculations, making the model more tractable. The BC model conceptualizes the capacity of chemical bonds to transport charge within molecules.[153, 154] It links charge conduction to bond order and differences in atomic potentials, with adjustments based on bond length. In essence, it provides a theoretical framework to quantify charge dynamics in molecular structures. Bond dissociation into integer charged fragments is enforced by the bond capacity decaying to zero. The similarities and differences between these models have been extensively discussed in Ref. 155.

ACKS2 can be shown as a generalization of EEM, similar to SQE and CRK models, that impedes long-range charge transfer. However, ACKS2 is rigorously derived from Kohn-Sham DFT. Two terms missed in EEM are fully considered in ACKS2: the electronic kinetic energy and exchange-correlation energy. The electronic kinetic energy term is added via the Legendre transform of the Kohn-Sham kinetic energy. It has been shown that this new kinetic energy term is equivalent to the bond-hardness energy in the SQE model.[156] Later, a generalization of the ACKS2 model for arbitrary variational wavefunctions was proposed.[157] All parameters defined in ACKS2 can be derived directly from the underlying wavefunction, enabling it to reproduce linear response properties exactly within the limit of a complete basis set.

The basic idea of ACKS2 is to split the general function defined in Eq. (2.18) into two parts: the explicit functional (E^{exp}), which explicitly depends on the electronic density, and the implicit functional (E^{imp}), which implicitly depends on the electronic density. In this way, the Hohenberg-Kohn functional becomes

$$E^{\text{HK}}[\rho] = E^{\text{exp}}[\rho] + E^{\text{imp}}[\rho] + \int \rho(\boldsymbol{r}) v(\boldsymbol{r}) d\boldsymbol{r}. \tag{2.62}$$

The implicit functional uses an auxiliary N-fermion wavefunction through a

constrained-search formulation

$$E^{\text{imp}}[\rho] = \min_{\Psi \to \rho} W[\Psi]. \tag{2.63}$$

where W can be regarded as the 'kinetic energy' functional of the new system.

As a special case, the Kohn-Sham ground-state wavefunction can be used. With the method of Lagrange multipliers, it can also be written out explicitly

$$E^{\text{imp}}[\rho] = \sup_{u} \left(E^{\text{KS}}[u, N] - \int \rho(\boldsymbol{r}) u(\boldsymbol{r}) d\boldsymbol{r} \right) \tag{2.64}$$

$$E^{\text{KS}}[u, N] = \min_{\Psi} \left(W[\Psi] + \int \rho[\Psi](\boldsymbol{r}) u(\boldsymbol{r}) d\boldsymbol{r} \right) \tag{2.65}$$

where $u(\boldsymbol{r})$ is a function that specifies a Lagrange multiplier at every point in space, and $\rho[\Psi](\boldsymbol{r})$ is the electron density of the auxiliary wavefunction. All terms that are dependent on the auxiliary wavefunction are collected in $E^{\text{KS}}[u, N]$. This energy can be interpreted as the ground-state energy of $W[\Psi]$ in the Kohn-Sham potential, $u(\boldsymbol{r})$.

For a given external potential, $v(\boldsymbol{r})$, the N-electron ground state is solved by minimizing the following Lagrangian with respect to $\rho(\boldsymbol{r})$ and maximizing it with respect to $u(\boldsymbol{r})$ and μ:

$$L[\rho, u, \mu] = E^{\text{HK}}[\rho, u] - \mu \left(\int \rho(\boldsymbol{r}) d\boldsymbol{r} - N \right) \tag{2.66}$$

where the energy is now a functional of the density and auxiliary potential

$$E^{\text{HK}}[\rho, u] = E^{\text{exp}}[\rho] + E^{\text{KS}}[u, N] + \int \rho(\boldsymbol{r})[v(\boldsymbol{r}) - u(\boldsymbol{r})] d\boldsymbol{r}. \tag{2.67}$$

Finally, the stationary point is defined by the following sets of Euler-Lagrange equations,

$$\frac{\delta E^{\text{exp}}[\rho]}{\delta \rho(\boldsymbol{r})} + v(\boldsymbol{r}) - u(\boldsymbol{r}) = \mu \tag{2.68}$$

$$\frac{\delta E^{\text{KS}}[u, N]}{\delta u(\boldsymbol{r})} = \rho(\boldsymbol{r}) \tag{2.69}$$

$$\int \rho(\boldsymbol{r}) d\boldsymbol{r} = N. \tag{2.70}$$

where the ground-state density ($\rho(\boldsymbol{r})$), the optimal auxiliary potential ($u(\boldsymbol{r})$) and the Lagrange multiplier (μ), also known as the chemical potential, are

defined. These functions constitute the central equations for deriving the ACKS2 model with finite basis sets.[157] With the linear response approximation and finite basis sets, the second derivative of electronic kinetic energy concerning density can be estimated approximately. This is achieved by computing the second derivative of Kohn-Sham energy with respect to the auxiliary potential, known as the non-interacting response functions. In practical applications, the construction of two basis sets is necessary: one for the auxiliary potential and another for the response density. To simplify the process, biorthogonal basis sets are commonly employed.[157]

Both the CRK and ACKS2 models employ a "charge response kernel matrix" connecting all atom pairs and offer a definition for an atom within a molecule. Additionally, they emphasize the linear scaling of polarizability with the system size and account for a portion of the bonded energy terms in force fields. However, the two models differ in several key aspects. In the CRK model, there are N_{atom} atomic charges as variables, and it seeks solutions for N_{atom} equations, while in the ACKS2 approach, $2N_{\text{atom}}$ atomic charges and potentials are treated as variables, aiming to solve $2N_{\text{atom}}$ equations. Furthermore, the CRK's bond dissociation cannot be encapsulated within a fixed partitioning of atoms into disjoint fragments, in contrast to the ACKS2's bond dissociation, which mandates a geometry-dependent charge response kernel matrix. Notably, while CRK prohibits charge transfer between fragments, ACKS2 allows for charge transfers between molecules, provided the intermolecular charge response kernel elements are non-zero.

It is worth noting that from Eq. (2.68) to Eq. (2.70), we can also derive a Dyson-like equation in the static case. To do so, we calculate the functional derivative with respect to $\rho(\boldsymbol{r})$ on both sides of Eq. (2.68), the functional derivative with respect to $u(\boldsymbol{r'})$ on both sides of Eq. (2.69), and apply the functional derivative on both sides of Eq. (2.70).

$$\frac{\delta^2 E^{\text{exp}}[\rho]}{\delta\rho(\boldsymbol{r})\delta\rho(\boldsymbol{r'})} + \frac{\delta v(\boldsymbol{r})}{\delta\rho(\boldsymbol{r'})} - \frac{\delta u(\boldsymbol{r})}{\delta\rho(\boldsymbol{r'})} = 0 \tag{2.71}$$

$$\frac{\delta^2 E^{\text{KS}}[u, N]}{\delta u(\boldsymbol{r})\delta u(\boldsymbol{r'})} = \frac{\delta\rho(\boldsymbol{r})}{\delta u(\boldsymbol{r'})} \tag{2.72}$$

$$\int \delta\rho(\boldsymbol{r}) d\boldsymbol{r} = 0. \tag{2.73}$$

Recall the following equations:

$$\chi(\boldsymbol{r},\boldsymbol{r}') = \frac{\delta\rho(\boldsymbol{r})}{\delta v(\boldsymbol{r}')} \tag{2.74}$$

$$\chi^{\mathrm{KS}}(\boldsymbol{r},\boldsymbol{r}') = \frac{\delta\rho(\boldsymbol{r})}{\delta u(\boldsymbol{r}')} \tag{2.75}$$

$$\eta^{\mathrm{exp}}(\boldsymbol{r},\boldsymbol{r}') = \frac{\delta^2 E^{\mathrm{exp}}[\rho]}{\delta\rho(\boldsymbol{r})\delta\rho(\boldsymbol{r}')}. \tag{2.76}$$

Combining Eq.(2.71) with Eq.(2.72) gives:

$$\eta^{\mathrm{exp}}(\boldsymbol{r},\boldsymbol{r}') + \chi^{-1}(\boldsymbol{r},\boldsymbol{r}') - \chi_{\mathrm{KS}}^{-1}(\boldsymbol{r},\boldsymbol{r}') = 0 \tag{2.77}$$

with

$$\chi^{-1}(\boldsymbol{r},\boldsymbol{r}') = \frac{\delta v(\boldsymbol{r})}{\delta\rho(\boldsymbol{r}')} \tag{2.78}$$

$$\chi_{\mathrm{KS}}^{-1}(\boldsymbol{r},\boldsymbol{r}') = \frac{\delta u(\boldsymbol{r})}{\delta\rho(\boldsymbol{r}')}. \tag{2.79}$$

By multiplying both sides by $\chi(\boldsymbol{r}_1,\boldsymbol{r})\chi^{\mathrm{KS}}(\boldsymbol{r}',\boldsymbol{r}_2)$ and integrating with respect to $\boldsymbol{r}$ and $\boldsymbol{r}'$, followed by some simple manipulations and reindexing of variables, we obtain:

$$\chi(\boldsymbol{r},\boldsymbol{r}') = \chi^{\mathrm{KS}}(\boldsymbol{r},\boldsymbol{r}') + \iint \chi^{\mathrm{KS}}(\boldsymbol{r},\boldsymbol{r}_1)\eta^{\mathrm{exp}}(\boldsymbol{r}_1,\boldsymbol{r}_2)\chi(\boldsymbol{r}_2,\boldsymbol{r}')d\boldsymbol{r}_1 d\boldsymbol{r}_2, \tag{2.80}$$

which corresponds to the Dyson-like equation in the static case with $\eta^{\mathrm{exp}}(\boldsymbol{r},\boldsymbol{r}')$ being the Hartree-exchange-correlation kernel.

This expression also works for the frequency-dependent case, i.e., the ACKS2ω model that will be discussed in the next chapter. However, a more rigorous derivation would be of interest because the ACSK2ω model is derived from Floquet TDDFT, which is an approximation of TDDFT.

So far, the parameters defined in ACKS2 have been computed as expectation values of the electric wavefunction, i.e., the computation of parameters still depends on ground-state calculations. However, the ACKS2 parameters are non-robust, e.g., they are sensitive to nuclear coordinates, due to the numerical limitations of the pseudo-inverse when using biorthogonal basis sets.[157] Although ACKS2 has been used in reactive force fields for induced charge computations, which will be discussed later, its application in polarizable force fields is still scarce. After obtaining a robust ACKS2ω model. Machine learning techniques may provide a new perspective. For example, the relationship between molecular coordinates and the Kohn-Sham response matrix, as well as the coordinates and atomic hardness, can be learned using machine learning techniques.

2.4.4 ReaxFF

One application of the ACKS2 model is to use it to calculate variable charges in ReaxFF, a type of reactive force field. ReaxFF models are a group of force fields that have been widely employed to investigate chemical reactions in various systems, including combustion, catalysis, fuel cells, and nanotubes.[71] In ReaxFF, interactions between bonded atoms depend on bond order instead of using fixed bond parameters, as seen in conventional force fields for chemical systems. Consequently, atomic interactions become bond-order dependent, allowing for a dynamic description of atomic or molecular interactions.

The total potential energy expression used in ReaxFF is analogous to conventional force fields and polarizable force fields. It consists of bonded and nonbonded terms, as shown in Eq. (2.31):[68, 158, 159]

$$E_{\text{pot}} = E_{\text{bonded}} + E_{\text{nonbonded}} + E_{\text{Specific}} \tag{2.81}$$

with an additional "Specific" term included to account for certain interactions or effects not explicitly captured by the bonded and nonbonded terms, such as lone pairs, conjugation, hydrogen bonding, etc.

For the bonded terms, ReaxFF employs a different expression:[68, 158]

$$E_{\text{bonded}} = E_{\text{bonds}} + E_{\text{angles}} + E_{\text{tors}} + E_{\text{over}} \tag{2.82}$$

where the first three terms on the right-hand side correspond to energy terms related to bond stretching, three-bond valence angle strain, and four-body torsional angle strain in conventional and polarizable force fields. However, these terms are all bond-order dependent in ReaxFF methods . For example, the carbon-carbon bond term differs between σ and π bonds. The term E_{over} represents an energy penalty that prevents atoms from being overcoordinated based on atomic valence rules. For instance, a carbon atom should have no more than four bonds in a stable chemical system. Therefore, the bond order is then adjusted for overcoordination.[68, 158]

The nonbonded terms in ReaxFF are quite similar to those in standard force fields and include electrostatic and polarization energies, as well as vdW energies. The primary difference is the application of so-called shielding parameters to prevent excessive repulsive or attractive non-bonded interactions at short distances.[158] In its early stages, polarization energies were estimated by computing charge polarization using the EEM model. However, EEM always allows long-range charge transfer, even when two molecules are well separated. This motivation led researchers to develop a new version of ReaxFF in collaboration with the ACKS2 model, known as ACKS2-ReaxFF.[68, 73, 159]

This framework has been employed to investigate the charge transfer of water in the presence of an external electric field.[159] Furthermore, through cooperation with the explicit electron model, ACKS2-ReaxFF has proven successful in capturing the electron affinities of hydrocarbon radicals.[73]

3

The development of the ACKS2ω model

Everything should be made as simple as possible, but not simpler.
Albert Einstein (1879-1955)

The Journal of Chemical Physics ARTICLE scitation.org/journal/jcp

A new framework for frequency-dependent polarizable force fields

Cite as: J. Chem. Phys. **157**, 124106 (2022); doi: 10.1063/5.0115151
Submitted: 27 July 2022 • Accepted: 29 August 2022 •
Published Online: 26 September 2022

View Online Export Citation CrossMark

YingXing Cheng and Toon Verstraelen[a)]

AFFILIATIONS

Center for Molecular Modeling (CMM), Ghent University, Technologiepark-Zwijnaarde 46, B-9052 Gent, Belgium

[a)]**Author to whom correspondence should be addressed:** toon.verstraelen@ugent.be

ABSTRACT

A frequency-dependent extension of the polarizable force field "Atom-Condensed Kohn–Sham density functional theory approximated to the second-order" (ACKS2) [Verstraelen et al., J. Chem. Phys. **141**, 194114 (2014)] is proposed, referred to as ACKS2ω. The method enables theoretical predictions of dynamical response properties of finite systems after partitioning of the frequency-dependent molecular response function. Parameters in this model are computed simply as expectation values of an electronic wavefunction, and the hardness matrix is entirely reused from ACKS2 as an adiabatic approximation is used. A numerical validation shows that accurate models can already be obtained with atomic monopoles and dipoles. Absorption spectra of 42 organic and inorganic molecular monomers are evaluated using ACKS2ω, and our results agree well with the time-dependent DFT calculations. Also for the calculation of C_6 dispersion coefficients, ACKS2ω closely reproduces its TDDFT reference. When parameters for ACKS2ω are derived from a PBE/aug-cc-pVDZ ground state, it reproduces experimental values for 903 organic and inorganic intermolecular pairs with an MAPE of 3.84%. Our results confirm that ACKS2ω offers a solid connection between the quantum-mechanical description of frequency-dependent response and computationally efficient force-field models.

Published under an exclusive license by AIP Publishing. https://doi.org/10.1063/5.0115151

I. INTRODUCTION

Molecular simulation is a powerful tool to investigate and predict the properties and dynamics of a wide range of finite and condensed-phase systems. Different levels of theory for such simulations can be roughly divided into two categories: quantum-mechanical (QM) electric structure methods and force-field (FF) methods. Kohn–Sham Density Functional Theory (DFT) offers a good trade-off between computational efficiency and accuracy, which has been successfully applied to study both ground and excited state properties of inorganic and organic molecular systems. However, Kohn–Sham DFT (with density fitting) has an $O(N^3)$ computational complexity, where N is the number of basis functions, which impedes its application to large-scale systems, especially for molecular dynamics (MD) simulations. On the other hand, FF methods, only using a set of functions of molecular geometry with several empirical parameters to determine molecular energy, have been developed and applied to large-scale MD simulations. In general, FF methods have a much lower computational cost than QM methods, at the expense of a reduced, yet acceptable, computational accuracy. One significant problem in traditional FF methods is the lack of electronic polarization, i.e., the response of the electron distribution to the environment, which led the molecular modeling community to develop polarizable force fields (PFFs)[1–12] to improve the predictive accuracy of long-range interactions by adding explicit polarization effects.

Classical PFF models can be classified into four broad categories: induced dipoles or multipoles,[1–5] the Drude oscillator[6–8] (also known as "core–shell"[13] or "charge-on-spring"[14]), Electronegativity Equalization Method (EEM),[9,10] and the explicit electron model.[11,12] It should be noted that several models similar to the EEM exist, such as fluctuating charges (FQ or FlucQ),[15–19] charge equilibration (QE, QEq,[20] or CHEQ[21]), and chemical potential equalization (CPE).[22] Note that EEM is often not considered to be a proper PFF: because it only uses variable atomic charges, it cannot describe out-of-plane polarization of planar molecules.[22] One can represent these effects in EEM by including additional off-nuclear sites.[23–25] This leads to slightly more expensive models and additional model choices, such as the location of the extra sites and the associated parameters. Here, we will treat EEM on the same footing as other PFFs because its mathematical structure is completely analogous.

The EEM was first developed by Mortier *et al.* from basic DFT equations according to Sanderson's principle of electronegativity

Published under an exclusive license by AIP Publishing

The Journal of Chemical Physics ARTICLE scitation.org/journal/jcp

equalization,[26] i.e., electrons flow until all electronegativities are equalized during the formation of a molecule. The ability of EEM (or one of its close relatives) to predict ground-state charge distributions has been validated extensively, e.g., for inorganic liquids,[16] inorganic solids,[27–29] organic molecules,[18,30–32] and biomolecular systems.[19,33–35] One appealing aspect of the EEM is that atomic monopolar fluctuations are included, and that one may systematically extend it with higher atomic multipoles, as in CPE.[22] However, the EEM also has two fundamental issues in simulations of extended systems or charge transfer during chemical reactions as follows:[36–40] (1) the EEM always predicts a cubic scaling of the dipole polarizability with system size, which is not correct for dielectric systems where a linear scaling exists in the macroscopic limit; (2) EEM obtains fractional molecular charges even when two molecules are well separated and gives a slowly decaying intermolecular charge transfer. The main reason for both problems is that long-range charge flow is always allowed in EEM, which is only realistic in metallic systems. Shortly after these shortcomings were first discussed in the literature, several *ad hoc* improvements were proposed, for instance, by applying artificial constraints to molecular charges[18,38] or dipoles,[41] or introducing a distance-dependent function to penalize long-range charge transfer.[42] Later, more consistent models were proposed, such as the split-charge equilibration (SQE): by adding a bond-hardness term to EEM, SQE becomes capable of modeling dielectric materials.[37,39]

Recently, Verstraelen *et al.* developed a new polarizable force field (PFF), namely Atom-Condensed Kohn–Sham DFT approximated to second-order (ACKS2),[40] which has been validated and applied to molecular systems and which addresses both fundamental issues of the EEM. ACKS2 improves upon the EEM by adding an electronic kinetic energy term via the Legendre transform of the Kohn–Sham kinetic energy, enabling one to expand the kinetic energy to second-order in the atomic populations and atomic Kohn–Sham potentials. It was shown that this new kinetic energy term is equivalent to the bond-hardness energy in the SQE. Later, a generalization of the ACKS2 model for arbitrary variational wavefunctions was proposed.[43] The ACKS2 formalism was numerically validated by a direct computation of the ACKS2 parameters from a reference Kohn–Sham DFT calculation. With these parameters, the static linear response properties of molecules obtained with an underlying theory, e.g., Kohn–Sham DFT, can be reproduced precisely in the limit of a complete basis sets for density and potential fluctuations.

To use ACKS2 for approximate polarization energy calculations, a tailored empirical parameterization was incorporated into ReaxFF, as an alternative to the EEM, which turned out to be essential in the development of eReaxFF.[44] Later, Gütlein *et al.* developed a new PFF using Gaussian basis sets, based on the ACKS2 model,[45] where generic parameters were proposed for elements C and H, such as widths of Gaussian basis functions. This parameterization can predict DFT data, such as response properties and interaction energies, of a series of hydrocarbons. Later, they proposed two ACKS2 variants, f-ACKS2 and scf-ACKS2, to handle condensed phases by dividing them into molecular fragments, which are coupled by Coulomb interactions.[46]

This work extends ACKS2 to the time- and frequency-dependent domain to compute the dynamical response properties of finite molecules, e.g., frequency-dependent polarizabilities, C_6 dispersion coefficients, and molecular absorption spectra. The resulting ACKS2ω model, through its use of atomic multipole expansions, allows one to investigate the contribution of charge-flow effects on dynamic response properties, which is a topic of ongoing research. One of the future applications envisioned for ACKS2ω is an efficient approximation of the non-local dispersion energy, i.e., for which interatomic charge fluctuations become important,[47–54] such as carbon nanomaterials,[48,49] traditional semiconductors,[50,51] and low-dimensional materials.[48,52–54] To the best of our knowledge, the time-dependent or frequency-dependent extension of ACKS2 has not been investigated yet.

The derivation of ACKS2ω relies on time-dependent DFT (TDDFT). TDDFT has received much attention in recent decades because of its good trade-off between numerical efficiency and accuracy compared to wavefunction-based methods. The standard formalism of TDDFT builds on the Runge–Gross theorem,[55] stating that there exists a one-to-one correspondence between densities and potentials for any fixed initial many-body state. TDDFT uses many DFT concepts, e.g., the whole interacting many-body system is replaced by a non-interacting Kohn–Sham system that shares the same density. However, it also has unique requirements, such as the initial state dependence and time-dependent exchange–correlation functional. Readers are referred to recent books[56,57] and review articles[58–61] for further details about TDDFT. Within the TDDFT regime, the linear response of the electron density can be calculated precisely, assuming one disposes of the exact exchange–correlation functional. In practice, TDDFT is a useful and relatively simple scheme to compute molecular linear-response properties.[62–66]

To derive the ACKS2ω model, we use a quasi-energy formalism, also known as the Floquet theory, which is often used in time-dependent response model development[66–72] and can be seen as a special case of TDDFT.[55,73] The benefits of the quasi-energy language have been discussed elsewhere.[72] One of the advantages of quasi-energy DFT is that the initial state dependence of the Runge–Gross theorem is not necessary anymore, and instead a periodic boundary condition is applied to an external perturbation. Moreover, the quasi-energy ansatz enables a unified framework for dynamic linear-response property calculations based on wavefunction and DFT methods, as it is generally valid for both variational and non-variational methods.[72] This allows dynamical response properties to be derived by the virtues of the energy derivative approach using the quasi-energy formalism. However, the validity of Floquet theory has been a point of discussion elsewhere,[74–77] and principle requires the following approximations: (i) a finite basis is employed;[76,77] (ii) the driving external perturbation is weak and off-resonant.[76–78] Point (i) ensures an adiabatic limit exists for the "Floquet ground state," on which the energy minimum principle is valid, and the latter determines the one-to-one density-potential mapping. Point (ii) suggests that Floquet theory is only a proper approximate method to treat linear-response problems. Nonetheless, for molecular force-field development, these two conditions are generally satisfied; thus, one can still use Floquet theory to develop frequency-dependent force-field methods.

The goal of this paper is to introduce ACKS2ω as a model with a structure reminiscent of conventional PFFs, yet with all parameters defined in terms of an underlying electronic structure theory. This direct connection to electronic structure theory

Published under an exclusive license by AIP Publishing

The Journal of Chemical Physics ARTICLE scitation.org/journal/jcp

assures a solid foundation for more pragmatic parameterizations of frequency-dependent PFFs.[79–84] The main distinction with the work of Misquitta and Stone, e.g., ISA-Pol,[85] is that ACKS2ω explicitly describes the transformation from non-interacting to interacting response functions through electron–electron interactions, whereas ISA-Pol directly models the interacting response relying on time-dependent Hartree–Fock or TDDFT results. Potential applications of frequency-dependent PFFs include modeling of optical spectra of complex systems at a force-field cost,[79–81] approximations of dispersion in force fields,[85] computationally efficient non-local dispersion corrections, including many-body effects for DFT calculations[82,83] or frequency-dependent polarizable embedding.[84] In this paper, ACKS2ω parameters are always computed from a Kohn–Sham DFT calculation for any given molecular geometry. This leads to relatively accurate and expensive parameterizations of test systems, primarily intended to validate the ACKS2ω equations. Obviously, for large-scale simulations, more efficient parameterizations should be developed, not involving a prior Kohn–Sham DFT calculation, for which machine-learning approaches have shown promising results.[86]

A benchmark database, including 42 inorganic and organic molecules from Ref. 87, referred to as TS42, is used for a numerical validation of the ACKS2ω model. First, the absorption spectra of the 42 molecules are investigated using ACKS2ω in comparison to TDDFT calculations. Then, the C_6 dispersion coefficients are compared against experimental data and Tkatchenko–Scheffler van der Waals method (called TS in what follows). More specifically, the accuracy of the ACKS2ω model is tested by checking the C_6 coefficients of 903 molecular pairs constructed from the database. Furthermore, we also compare the performance of ACKS2ω to the range-separated calculations of Toulouse *et al.* on 27 homodimers from a subset of TS42, hereafter referred to as the TS27 database.[88]

The remainder of this paper is organized as follows: the basic theory of the ACKS2ω model is introduced in Sec. II, followed by computational details of the numerical validation in Sec. III. Results and discussion are presented in Sec. IV. A summary is given in Sec. V. Atomic units are used, unless noted otherwise.

II. THEORY

This section derives the ACKS2ω formalism from TDDFT, using the quasi-energy formalism. Hence, a brief review of the quasi-energy method is first presented in Sec. II A. The quasi-energy expressions have been employed in response theory because of their straightforward definition.[70,89] The theory of ACKS2ω within quasi-energy ansatz is presented in Sec. II B, where a set of equations is derived in analogy with ACKS2.[43] A dynamic linear-response theory is then provided in the frequency domain in Sec. II C. As a result, a set of linear-response equations are generated when two finite basis sets are applied (Sec. II D). Finally, in Sec. II E, we apply ACKS2ω in Kohn–Sham DFT with a semi-local exchange–correlation (xc) functional.

A. Quasi-energy formalism

The quasi-energy formalism or Floquet theory is employed in the original TDDFT derivation.[55] The definitions of time-dependent exchange–correlation potentials and kernels are much more accessible using the quasi-energy notation. In this section, we use the notation of Salek *et al.*[72] and Christiansen *et al.*[70] From the time-dependent Schrödinger equation, we have

$$\left(\hat{H} - i\frac{\partial}{\partial t}\right)|\bar{0}(t)\rangle = 0, \tag{1}$$

$$\hat{H} = \hat{H}_0 + \hat{V}_1(t), \tag{2}$$

where $\hat{H}_0$ and $\hat{V}_1(t)$ are the time-independent zeroth-order Hamiltonian and time-dependent perturbation operator, respectively. The exact solution of $\hat{H}_0$ is given by a ground-state calculation and perturbation theory can be developed through a generalization of the Rayleigh–Schrödinger theory.[72] We consider the time-dependent perturbation theory[70,78]

$$|\bar{0}(t)\rangle = e^{-iF(t)}|\tilde{0}(t)\rangle, \tag{3}$$

where $F(t)$ is a purely time-dependent function. The vector $|\bar{0}\rangle$ represents the complete wavefunction whose phase-isolated part is denoted by $|\tilde{0}\rangle$, where time dependence of the vectors is understood. The time-dependent Schrödinger equation is then rewritten as

$$\left(\hat{H} - i\frac{\partial}{\partial t}\right)|\tilde{0}\rangle = L(t)|\tilde{0}\rangle \tag{4}$$

in which $L(t) = \dot{F}(t)$ is the time-dependent quasi-energy. Langhoff *et al.* showed that $|\tilde{0}\rangle$ can be normalized at all times.[78] Consequently, the time-dependent quasi-energy can be expressed as

$$L(t) = \langle\tilde{0}|\hat{H} - i\frac{\partial}{\partial t}|\tilde{0}\rangle. \tag{5}$$

In order to use Hellmann–Feynman theorem, in analogy to the static case, the external time-dependent perturbation is assumed to be periodic, i.e., $\hat{V}_1(t) = \hat{V}_1(t + \mathcal{T})$.[72] Here, we use the symbol $\mathcal{T}$, referred to as the time period, instead of T used in Ref. 72 to avoid ambiguity with kinetic energy functional T, which is well-known in DFT or TDDFT. Using curly brackets for time-averaging,

$$\{f(t)\}_{\mathcal{T}} = \frac{1}{\mathcal{T}}\int_{-\mathcal{T}/2}^{+\mathcal{T}/2} f(t)dt, \tag{6}$$

the quasi-energy is defined as

$$Q = \{L(t)\}_{\mathcal{T}}. \tag{7}$$

Techniques for time-independent problems, such as the variational principle[70] as well as the Hellman–Feynman theorem,[72] can be applied to the quasi-energy, to obtain a solution or a response to a perturbation for the time-dependent case. The quasi-energy formalism is also generally applicable to wavefunction methods and DFT,[71,72] at least for weak and off-resonant perturbation and when using finite basis sets approximations.[76,77]

In the context of TDDFT, the quasi-energy can be written a functional of the time-dependent density, $\rho(\boldsymbol{r}, t)$,[64,72]

$$Q[\rho] = \left\{\langle\tilde{0}|\hat{H} - i\frac{\partial}{\partial t}|\tilde{0}\rangle\right\}_{\mathcal{T}} = T[\rho] + V[\rho] + J[\rho] + Q_{\mathrm{ncl}}[\rho] - S[\rho], \tag{8}$$

Published under an exclusive license by AIP Publishing

The Journal of Chemical Physics ARTICLE scitation.org/journal/jcp

where $T[\rho]$ and $V[\rho]$ are the kinetic energy and the interaction with the external potential, respectively. The non-classical quasi-energy $Q_{\mathrm{ncl}}[\rho]$ includes the effects of exchange and correlation, whereas $J[\rho]$ and $S[\rho]$ are formally defined by

$$J[\rho] = \frac{1}{2}\left\{ \iint \frac{\rho(\boldsymbol{r},t)\rho(\boldsymbol{r}',t)}{|\boldsymbol{r}-\boldsymbol{r}'|} d\boldsymbol{r}d\boldsymbol{r}' \right\}_{\mathcal{T}}, \tag{9}$$

$$S[\rho] = \left\{ \langle \tilde{0}|i\frac{\partial}{\partial t}|\tilde{0}\rangle \right\}_{\mathcal{T}}. \tag{10}$$

A more extensive discussion of the quasi-energy formalism in DFT can be found in Refs. 72, 76, and 77.

B. Decomposition of the quasi-energy into explicit and implicit terms

The functional in DFT can be written as the sum of a universal functional and the interaction of the electrons with external potential. The universal functional is a general term for all systems, which can be divided into two parts suggested by the ACKS2 model: the explicit functional (E^{exp}), which is a known functional of the density, and the implicit functional (E^{imp}). Similarly, in quasi-energy TDDFT the corresponding explicit functional Q^{exp} and implicit functional Q^{imp} are given as

$$Q_v[\rho] = Q^{\mathrm{exp}}[\rho] + Q^{\mathrm{imp}}[\rho] + \left\{ \int \rho(\boldsymbol{r},t)v(\boldsymbol{r},t)d\boldsymbol{r} \right\}_{\mathcal{T}}. \tag{11}$$

The implicit functional uses an auxiliary N-fermion wavefunction through a constrained-search formulation

$$Q^{\mathrm{imp}}[\rho] = \min_{\Psi\to\rho} W[\Psi]. \tag{12}$$

With the method of Lagrange multipliers, it can also be written out explicitly

$$Q^{\mathrm{imp}}[\rho] = \sup_{u}\left(Q^{\mathrm{o}}[u,N] - \left\{ \int \rho(\boldsymbol{r},t)u(\boldsymbol{r},t)d\boldsymbol{r} \right\}_{\mathcal{T}} \right), \tag{13}$$

$$Q^{\mathrm{o}}[u,N] = \min_{\Psi}\left(W[\Psi] + \left\{ \int \rho[\Psi](\boldsymbol{r},t)u(\boldsymbol{r},t)d\boldsymbol{r} \right\}_{\mathcal{T}} \right), \tag{14}$$

where $u(\boldsymbol{r},t)$ is a function that specifies a Lagrange multiplier at every point in terms of both space and time, and $\rho[\Psi](\boldsymbol{r},t)$ is the electron density of the auxiliary wavefunction. All terms that are dependent on the auxiliary wavefunction are collected in $Q^{\mathrm{o}}[u,N]$. This quasi-energy can be interpreted as the ground-state energy of $W[\Psi]$ in a specified auxiliary potential, $u(\boldsymbol{r},t)$.

For a given external potential, $v(\boldsymbol{r},t)$, the N-electron ground state is solved by minimizing the following Lagrangian with respect to $\rho(\boldsymbol{r},t)$ and maximizing it with respect to $u(\boldsymbol{r},t)$ and $\mu(t)$:

$$L_v[\rho,u,\mu] = Q_v[\rho,u] - \left\{ \mu(t)\left(\int \rho(\boldsymbol{r},t)d\boldsymbol{r} - N \right) \right\}_{\mathcal{T}}, \tag{15}$$

where the quasi-energy is now a functional of the density and auxiliary potential

$$Q_v[\rho,u] = Q^{\mathrm{exp}}[\rho] + Q^{\mathrm{o}}[u,N] + \left\{ \int \rho(\boldsymbol{r},t)[v(\boldsymbol{r},t) - u(\boldsymbol{r},t)]d\boldsymbol{r} \right\}_{\mathcal{T}}. \tag{16}$$

Finally, the stationary point is defined by the following sets of Euler–Lagrange equations:[64]

$$\frac{\delta Q^{\mathrm{exp}}[\rho]}{\delta\rho(\boldsymbol{r},t)} + v(\boldsymbol{r},t) - u(\boldsymbol{r},t) = \mu(t), \tag{17}$$

$$\frac{\delta Q^{\mathrm{o}}[u,N]}{\delta u(\boldsymbol{r},t)} - \rho(\boldsymbol{r},t) = 0, \tag{18}$$

$$\int \rho(\boldsymbol{r},t)d\boldsymbol{r} = N. \tag{19}$$

C. Linear response

In linear-response theory, it is more convenient to first apply a Fourier-transform to all time-dependent functions,[56] which yields formally similar Euler–Lagrange equations

$$\frac{\delta Q^{\mathrm{exp}}[\rho]}{\delta\rho(\boldsymbol{r},\omega)} + v(\boldsymbol{r},\omega) - u(\boldsymbol{r},\omega) = \mu(\omega), \tag{20}$$

$$\frac{\delta Q^{\mathrm{o}}[u,N]}{\delta u(\boldsymbol{r},\omega)} - \rho(\boldsymbol{r},\omega) = 0, \tag{21}$$

$$\int \rho(\boldsymbol{r},\omega)d\boldsymbol{r} = N. \tag{22}$$

In analogy with the ACKS2 method, a static DFT ground state is taken as the reference to which fluctuations are considered, including the external potential $v_0(\boldsymbol{r})$, density $\rho_0(\boldsymbol{r})$, auxiliary potential $u_0(\boldsymbol{r})$, and equalized chemical potential μ_0. The main difference with the original ACKS2 method is that we now consider frequency-dependent fluctuations

$$v(\boldsymbol{r},\omega) = v_0(\boldsymbol{r}) + \Delta v(\boldsymbol{r},\omega), \qquad \rho(\boldsymbol{r},\omega) = \rho_0(\boldsymbol{r}) + \Delta\rho(\boldsymbol{r},\omega),$$
$$u(\boldsymbol{r},\omega) = u_0(\boldsymbol{r}) + \Delta u(\boldsymbol{r},\omega), \qquad \mu(\omega) = \mu_0 + \Delta\mu(\omega),$$

where $\Delta v(\boldsymbol{r},\omega)$ is a frequency-dependent perturbation and $\Delta\rho(\boldsymbol{r},\omega)$, $\Delta u(\boldsymbol{r},\omega)$, and $\Delta\mu(\omega)$ are corresponding frequency-dependent responses to the perturbation. After substitution in the Euler–Lagrange equations, one obtains

$$\left.\frac{\delta Q^{\mathrm{exp}}[\rho]}{\delta\rho(\boldsymbol{r},\omega)}\right|_{\rho=\rho_0+\Delta\rho} - \left.\frac{\delta Q^{\mathrm{exp}}[\rho]}{\delta\rho(\boldsymbol{r},\omega)}\right|_{\rho=\rho_0} + \Delta v(\boldsymbol{r},\omega) - \Delta u(\boldsymbol{r},\omega) = \Delta\mu(\omega), \tag{23}$$

$$\left.\frac{\delta Q^{\mathrm{o}}[u,N]}{\delta u(\boldsymbol{r},\omega)}\right|_{u=u_0+\Delta u} - \left.\frac{\delta Q^{\mathrm{o}}[u,N]}{\delta u(\boldsymbol{r},\omega)}\right|_{u=u_0} - \Delta\rho(\boldsymbol{r},\omega) = 0, \tag{24}$$

$$\int \Delta\rho(\boldsymbol{r},\omega)d\boldsymbol{r} = 0. \tag{25}$$

In the limit of a small perturbation, the first two equations can be linearized,

$$\int \left.\frac{\delta^2 Q^{\mathrm{exp}}[\rho]}{\delta\rho(\boldsymbol{r},\omega)\delta\rho(\boldsymbol{r}',\omega)}\right|_{\rho=\rho_0} \Delta\rho(\boldsymbol{r}',\omega)d\boldsymbol{r}' + \Delta v(\boldsymbol{r},\omega) - \Delta u(\boldsymbol{r},\omega) \approx \Delta\mu(\omega), \tag{26}$$

Published under an exclusive license by AIP Publishing

The Journal of Chemical Physics ARTICLE scitation.org/journal/jcp

$$\int \left.\frac{\delta^2 Q^{\mathrm{o}}[u,N]}{\delta u(\boldsymbol{r},\omega)\delta u(\boldsymbol{r}',\omega)}\right|_{u=u_0} \Delta u(\boldsymbol{r}',\omega)d\boldsymbol{r}' - \Delta\rho(\boldsymbol{r},\omega) \approx 0. \quad (27)$$

The second order functional derivatives in Eqs. (26) and (27) are the hardness kernel of the explicit functional and response kernel of implicit functional, referred to as $\eta^{\mathrm{exp}}(\boldsymbol{r},\boldsymbol{r}',\omega)$ and $\chi^{\mathrm{imp}}(\boldsymbol{r},\boldsymbol{r}',\omega)$, respectively.

D. Expansion in a finite basis

In a practical simulation, one must expand the density and the auxiliary potential fluctuations in a finite basis,

$$\Delta\rho(\boldsymbol{r},\omega) = \sum_m^M C_m(\omega) f_m(\boldsymbol{r}), \quad (28)$$

$$\Delta u(\boldsymbol{r},\omega) = \sum_n^N U_n(\omega) g_n(\boldsymbol{r}), \quad (29)$$

where f_m (g_n) denote density (potential) basis functions, while $C_m(\omega)$ ($U_n(\omega)$) denote the expansion coefficients of the induced density (potential) changes $\Delta\rho$ (Δu). It is worth mentioning that both basis sets are time-independent, and only the corresponding coefficients are dynamic, suggesting that the basis sets used in the ACKS2 model can also be employed herein.

Substitution of the basis-set expansion in Eq. (26), followed by a multiplication with $f_k(\boldsymbol{r})$ and integration over $\boldsymbol{r}$, leads to

$$\sum_m^M \eta^{\mathrm{exp}}_{km}(\omega) C_m(\omega) + V_k(\omega) - \sum_n^N O_{kn} U_n(\omega) = \Delta\mu(\omega) D_k \quad \forall k \in \{1 \ldots M\} \quad (30)$$

with

$$\eta^{\mathrm{exp}}_{km}(\omega) = \iint \eta^{\mathrm{exp}}(\boldsymbol{r},\boldsymbol{r}',\omega) f_k(\boldsymbol{r}) f_m(\boldsymbol{r}') d\boldsymbol{r} d\boldsymbol{r}', \quad (31)$$

$$O_{kn} = \int f_k(\boldsymbol{r}) g_n(\boldsymbol{r}) d\boldsymbol{r}, \quad (32)$$

$$V_k(\omega) = \int f_k(\boldsymbol{r}) \Delta v(\boldsymbol{r},\omega) d\boldsymbol{r}, \quad (33)$$

$$D_k = \int f_k(\boldsymbol{r}) d\boldsymbol{r}. \quad (34)$$

Similar manipulations of Eqs. (27) and (25) lead to algebraic equations as follows:

$$\sum_n^N \chi^{\mathrm{imp}}_{kn}(\omega) U_n(\omega) - \sum_m^M O_{km} C_m(\omega) = 0 \quad \forall k \in \{1 \ldots N\}, \quad (35)$$

$$\sum_m^M D_m C_m(\omega) = 0, \quad (36)$$

with

$$\chi^{\mathrm{imp}}_{kn}(\omega) = \iint \chi^{\mathrm{imp}}(\boldsymbol{r},\boldsymbol{r}',\omega) g_k(\boldsymbol{r}) g_n(\boldsymbol{r}') d\boldsymbol{r} d\boldsymbol{r}'. \quad (37)$$

The linear system can be written in block matrix notation as follows:

$$\begin{bmatrix} -\boldsymbol{\eta}^{\mathrm{exp}}_{M,M} & \boldsymbol{O}_{M,N} & \boldsymbol{D}_{M,1} \\ \boldsymbol{O}^T_{N,M} & -\boldsymbol{\chi}^{\mathrm{imp}}_{N,N} & \boldsymbol{0}_{N,1} \\ \boldsymbol{D}^T_{1,M} & \boldsymbol{0}_{1,N} & 0 \end{bmatrix} \begin{bmatrix} \boldsymbol{C}_{M,1}(\omega) \\ \boldsymbol{U}_{N,1}(\omega) \\ \Delta\mu(\omega) \end{bmatrix} = \begin{bmatrix} \boldsymbol{V}_{M,1}(\omega) \\ \boldsymbol{0}_{N,1} \\ 0 \end{bmatrix}, \quad (38)$$

where a bold letter denotes a block matrix and the subscript gives its dimension. For example, $\boldsymbol{\eta}^{\mathrm{exp}}_{M,M}$ represents the $M \times M$ hardness submatrix, $\boldsymbol{O}_{M,N}$ is the $M \times N$ overlap submatrix, and the $\boldsymbol{0}_{N,1}$ ($\boldsymbol{0}_{1,N}$) is a column (row) vector with all elements equal 0. Solving this block matrix equation gives the expansion coefficients for the induced density, i.e., $\boldsymbol{C}_{M,1}(\omega)$, which is also known as the response vector. The subscript will be omitted below for the sake of visual clarity.

According to linear response theory, the induced density can be expressed through an *interacting* response function, χ,

$$\Delta\rho(\boldsymbol{r},\omega) = \int d\boldsymbol{r}' \chi(\boldsymbol{r},\boldsymbol{r}',\omega) V(\boldsymbol{r}',\omega), \quad (39)$$

where $V(\boldsymbol{r},\omega)$ is the frequency-dependent external perturbation. ACKS2ω can be used to approximate the interacting response, for which two strategies can be followed. The first and most straightforward option is to invert the block matrix in Eq. (38) directly. The top-left block of the inverse transforms the input $\boldsymbol{V}(\omega)$ into the output $\boldsymbol{C}(\omega)$ and is therefore the ACKS2ω approximation of the interacting response.

One may also derive a useful closed expression for the interacting response matrix. This derivation starts by solving the second row of Eq. (38) to obtain $\boldsymbol{U}(\omega) = (\boldsymbol{\chi}^{\mathrm{imp}})^* \boldsymbol{O}^T \boldsymbol{C}(\omega)$. A pseudo-inverse of the implicit response matrix is needed, because it contains at least one zero eigenvalue, due to the charge distribution not being sensitive to a constant shift in Kohn–Sham potential. Next, one uses this solution to eliminate $\boldsymbol{U}(\omega)$ from the first row of Eq. (38), yielding

$$\boldsymbol{A}\boldsymbol{C}(\omega) = \boldsymbol{V}(\omega) - \boldsymbol{D}\Delta\mu(\omega), \quad (40)$$

where we introduced a shorthand $\boldsymbol{A} = -\boldsymbol{\eta} + \boldsymbol{O}(\boldsymbol{\chi}^{\mathrm{imp}})^* \boldsymbol{O}^T$ to facilitate the derivation. This equation can be solved, assuming $\boldsymbol{A}$ is non-singular,

$$\boldsymbol{C}(\omega) = \boldsymbol{A}^{-1}(\boldsymbol{V}(\omega) - \boldsymbol{D}\Delta\mu(\omega)). \quad (41)$$

When $\boldsymbol{A}$ is singular, the density response is not well-defined. While we cannot exclude this possibility of $\boldsymbol{A}$ being singular, we never encountered this issue in our numerical results. The Lagrange multiplier is found by substituting this result in the third row of Eq. (38),

$$\Delta\mu(\omega) = \frac{\boldsymbol{D}^T\boldsymbol{A}^{-1}\boldsymbol{V}(\omega)}{\boldsymbol{D}^T\boldsymbol{A}^{-1}\boldsymbol{D}}. \quad (42)$$

The final expression for the interacting response is

$$\boldsymbol{C}(\omega) = \boldsymbol{\chi}\boldsymbol{V}(\omega) = \left(\boldsymbol{A}^{-1} - \frac{\boldsymbol{A}^{-1}\boldsymbol{D}\boldsymbol{D}^T\boldsymbol{A}^{-1}}{\boldsymbol{D}^T\boldsymbol{A}^{-1}\boldsymbol{D}}\right)\boldsymbol{V}(\omega). \quad (43)$$

The second term in $\boldsymbol{\chi}$ (due to normalization) is responsible for a proper zero eigenvalue in the interacting response, which also guarantees the constraint of particle conservation, i.e., $\boldsymbol{D}^T\boldsymbol{\chi} = \boldsymbol{0}$.

Published under an exclusive license by AIP Publishing

The Journal of Chemical Physics ARTICLE scitation.org/journal/jcp

Note that $\boldsymbol{C}(\omega) = \boldsymbol{\chi}\boldsymbol{V}(\omega)$ does not contain an overlap matrix, unlike $\boldsymbol{O}^T\boldsymbol{C}(\omega) = \boldsymbol{\chi}^{\text{imp}}\boldsymbol{U}(\omega)$, because $\boldsymbol{V}(\omega)$ is defined with respect to the density basis f_m, whereas $\boldsymbol{U}(\omega)$ is expanded in terms of g_n. Hence, $\boldsymbol{\chi}$ is the interacting response expanded in the density basis. If desired, one may also express it in the potential basis by assuming that perturbations in the external potential have the following form:

$$\Delta v(\boldsymbol{r},\omega) = \sum_n^N V'_n(\omega) g_n(\boldsymbol{r}). \tag{44}$$

The new expansion coefficients, $V'_n(\omega)$, can always be transformed to those from Eq. (33),

$$V_k(\omega) = \sum_n^N O_{kn} V'_n(\omega). \tag{45}$$

With that, one can left-multiply Eq. (43) with $\boldsymbol{O}^T$ and substitute $\boldsymbol{V}(\omega)$ with $\boldsymbol{O}\boldsymbol{V}'(\omega)$,

$$\begin{aligned}\boldsymbol{O}^T\boldsymbol{C}(\omega) &= \boldsymbol{O}^T\boldsymbol{\chi}\boldsymbol{O}\boldsymbol{V}'(\omega)\\ &= \boldsymbol{O}^T\left(\boldsymbol{A}^{-1} - \frac{\boldsymbol{A}^{-1}\boldsymbol{D}\boldsymbol{D}^T\boldsymbol{A}^{-1}}{\boldsymbol{D}^T\boldsymbol{A}^{-1}\boldsymbol{D}}\right)\boldsymbol{O}\boldsymbol{V}'(\omega) = \boldsymbol{\chi}'\boldsymbol{V}'(\omega),\end{aligned} \tag{46}$$

where $\boldsymbol{\chi}'$ is finally identified as the interacting response matrix in the potential basis.

E. ACKS2ω matrix elements

So far, the precise forms of the implicit and explicit functionals were not specified, and one may use, in principle, any definition whose sum equals (or approximates) the total quasi-energy. In this section, we show that for Kohn–Sham DFT, a convenient choice can be made, leading to straightforward equations for all coefficients in the ACKS2ω equations.

The Kohn–Sham DFT expression of the quasi-energy is

$$Q^{\text{o}}[\rho] = T_s[\rho] + V[\rho] + J[\rho] + Q_{xc}[\rho] - S_s[\rho], \tag{47}$$

where $T_s[\rho]$ and $S_s[\rho]$ are defined using the determinant of the non-interacting system ($|\tilde{0}_s\rangle$),

$$T_s[\rho] = \left\{\langle\tilde{0}_s|\hat{T}|\tilde{0}_s\rangle\right\}_{\mathcal{F}}, \tag{48}$$

$$S_s[\rho] = \left\{\langle\tilde{0}_s|i\frac{\partial}{\partial t}|\tilde{0}_s\rangle\right\}_{\mathcal{F}}. \tag{49}$$

The quasi-energy xc functional is thereby defined as

$$Q_{xc}[\rho] = Q_{ncl}[\rho] + (T[\rho] - T_s[\rho]) + (S[\rho] - S_s[\rho]). \tag{50}$$

Within the quasi-energy formalism, we employ the adiabatic approximation by replacing $Q_{xc}[\rho]$ with a time-independent counterpart $\{E_{xc}[\rho]\}_{\mathcal{F}}$.

With a semi-local xc functional, the explicit part of the energy functional in Kohn–Sham DFT takes the following form:

$$Q^{\text{exp}}[\rho] = \left\{\frac{1}{2}\iint\frac{\rho(\boldsymbol{r},t)\rho(\boldsymbol{r}',t)}{|\boldsymbol{r}-\boldsymbol{r}'|}d\boldsymbol{r}d\boldsymbol{r}' + E_{xc}[\rho]\right\}_{\mathcal{F}}, \tag{51}$$

where the first term is the Hartree quasi-energy, $J[\rho]$, while the second is the xc functional. The auxiliary wavefunction Φ is a single Slater determinant of Kohn–Sham orbitals, and $W[\Phi]$ is the Kohn–Sham kinetic energy minus functional $S_s[\rho]$,

$$W[\Phi] = \left\{\sum_{i\in\text{Occ.}}\int\phi_i^*(\boldsymbol{r},t)\left(-\frac{1}{2}\nabla^2\right)\phi_i(\boldsymbol{r},t)d\boldsymbol{r}\right\}_{\mathcal{F}} - S_s[\rho], \tag{52}$$

where ϕ_i is the ith occupied (Occ.) molecular spatial orbital.

The expressions for the explicit hardness matrix and implicit response matrix with the Lehmann representation[56,57] take the following forms in frequency space, respectively:

$$\eta^{\text{exp}}_{km} = \iint\left(\frac{1}{|\boldsymbol{r}-\boldsymbol{r}'|} + \frac{\delta^2E_{xc}[\rho]}{\delta\rho(\boldsymbol{r})\delta\rho(\boldsymbol{r}')}\right)f_k(\boldsymbol{r})f_m(\boldsymbol{r}')d\boldsymbol{r}d\boldsymbol{r}', \tag{53}$$

$$\begin{aligned}\chi^{\text{imp}}_{kn}(\omega) = \lim_{\eta\to0^+}\sum_{\substack{i\in\text{Occ.}\\ a\in\text{Vir.}}}(n_i - n_a)\\ \times\left[\frac{\int\phi_i^*(\boldsymbol{r})g_k(\boldsymbol{r})\phi_a(\boldsymbol{r})d\boldsymbol{r}\int\phi_i(\boldsymbol{r}')g_n(\boldsymbol{r}')\phi_a^*(\boldsymbol{r}')d\boldsymbol{r}'}{\omega - (\varepsilon_a - \varepsilon_i) + i\eta}\right.\\ \left. - \frac{\int\phi_i(\boldsymbol{r})g_n(\boldsymbol{r})\phi_a^*(\boldsymbol{r})d\boldsymbol{r}\int\phi_i^*(\boldsymbol{r}')g_k(\boldsymbol{r}')\phi_a(\boldsymbol{r}')d\boldsymbol{r}'}{\omega + (\varepsilon_a - \varepsilon_i) + i\eta}\right],\end{aligned} \tag{54}$$

where n_i and n_a are 1 and 0 for occupied and virtual (Vir.) molecular spatial orbitals, respectively. After simple manipulations, the matrix elements of χ^{imp} have a simplified form

$$\chi^{\text{imp}}_{kn}(\omega) = \lim_{\eta\to0^+}\sum_{\substack{i\in\text{Occ.}\\ a\in\text{Vir.}}}\frac{2\Omega_{ia}}{(\omega+i\eta)^2 - \Omega_{ia}^2}\langle\phi_i|g_k|\phi_a\rangle\langle\phi_a|g_n|\phi_i\rangle, \tag{55}$$

where $\Omega_{ia} = \varepsilon_a - \varepsilon_i$ and the Dirac notation is used. For closed-shell molecules, a factor four is applied instead of two in Eq. (55) and the sum is restricted to spin-up orbitals only.

F. Dynamic polarizability and related properties

The dynamic linear-response properties, such as dipole polarizabilities, can be derived from the frequency-dependent response matrix. Moreover, with a proper choice of density and potential basis functions, distributed polarizabilities[90] are also available.

The potential basis set is constructed as

$$g_{n(a,\ell,m)}(\boldsymbol{r}) = w_a(\boldsymbol{r})R^m_\ell(\boldsymbol{r}-\boldsymbol{R}_a), \tag{56}$$

where $R^m_\ell(\boldsymbol{r}-\boldsymbol{R}_a)$ is a real solid harmonic with angular quantum number ℓ and magnetic quantum number m, using the position of nucleus a as origin. The functions $w_a(\boldsymbol{r})$ $(0 \le w_a(\boldsymbol{r}) \le 1)$ are so-called atom-in-molecule (AIM) weights functions, determining which proportion of the molecular ground-state density is assigned to atom a.[91] The rationale is that the integral of the product of such a potential basis function and a (response) density can be interpreted as distributed multipole moment.

Published under an exclusive license by AIP Publishing

The Journal of Chemical Physics ARTICLE scitation.org/journal/jcp

The density basis set can be organized similarly, using atom-centered functions with unit monopole, dipole, etc., moments. One may use Gaussian basis sets,[45] or construct a basis that is bi-orthogonal to the potential basis set,[43] which is also the approach followed in this work.

Both basis sets are truncated by discarding all solid harmonics for which $\ell > \ell_{\max}$, where $\ell_{\max}$ is a user-specified threshold. For instance, $\ell_{\max} = 0$ and $\ell_{\max} = 1$ corresponds to fluctuating charges only and charges + dipoles, respectively. The total basis size is therefore $2(\ell_{\max}+1)^2$ times the number of atoms.

For the remainder of this section, it is convenient to change the index notation and introduce a compound index t (or u) for the components of multipole moments, instead of separate indices ℓ and m. With these, we can define a distributed polarizability as

$$\alpha_{tu}^{ab} = -\chi_{k(a,t)\,n(b,u)}, \tag{57}$$

where $\chi_{k(a,t)\,n(b,u)}$ are elements of the response matrix defined in Eq. (43). When considering the case $\ell_{\max} = 1$, distributed polarizability comprises several physically distinct blocks: the distributed charge-flow, α_{qq}^{ab}, charge–dipole, $\alpha_{q\beta}^{ab}$, dipole–charge, $\alpha_{\alpha q}^{ab}$, and dipole–dipole, $\alpha_{\alpha\beta}^{ab}$, components. The subscript q is used to denote the monopole block and $\alpha(\beta)$ refers to dipole blocks, whereby both α and β could be x, y, or z. The total molecular dipole polarizability can be recovered as follows:[91]

$$\alpha_{\alpha\beta} = \sum_{a,b} r_\alpha^a \alpha_{qq}^{ab} r_\beta^b + r_\alpha^a \alpha_{q\beta}^{ab} + \alpha_{\alpha q}^{ab} r_\beta^b + \alpha_{\alpha\beta}^{ab}, \tag{58}$$

where r_α^a and r_β^b are corresponding atomic coordinates. The isotropic dipole polarizability of molecules is formally given as

$$\bar{\alpha} = \frac{1}{3}(\alpha_{xx} + \alpha_{yy} + \alpha_{zz}). \tag{59}$$

Equations (58) and (59) remain valid for frequency-dependent polarizabilities. When a real frequency is used, $\bar{\alpha}$ becomes complex (when $i\eta \neq 0$). The dipole strength function $S(\omega)$ can be computed using the imaginary part of $\bar{\alpha}$ with[92]

$$S(\omega) = \frac{2\omega}{\pi\hbar^2}\Im[\bar{\alpha}(\omega)]. \tag{60}$$

The excitation energies are thus determined from the positions of the peaks, and the area under the peaks represents the oscillator strength of the corresponding transition. In addition, the isotropic C_6 dispersion coefficient can be computed with imaginary frequencies ($\omega = iu$) using the Casimir–Polder equation[93]

$$C_6 = \frac{3}{\pi}\int_0^\infty \bar{\alpha}^A(iu)\bar{\alpha}^B(iu)du, \tag{61}$$

where superscripts A and B denote different molecules.

G. Two-site ACKS2ω model

Before studying the absorption spectra of molecular systems, it is instructive to start with a simple model system to illustrate the workings of the ACKS2ω approach in analogy to the TDDFT method. We consider a two-site system of an electric dipole along x-axis with coordinates of -1 and 1, and only s-type density and potential functions are considered. The two-site ACKS2ω problem can be solved analytically after making the following assumptions:

1. The hardness matrix η is $\begin{bmatrix} a & b \\ b & a \end{bmatrix}$, where non-negative numbers a and b denotes atomic hardness and the classical Coulomb interaction between the density functions, respectively. The xc contribution to the hardness is neglected entirely, i.e., the RPA is used.
2. The overlap matrix is $\begin{bmatrix} c & 0 \\ 0 & c \end{bmatrix}$, where c is the overlap between the potential and density functions on the same site. Any overlap between functions on different sites is neglected for simplicity. Furthermore, we assume that the density basis functions are normalized, i.e., $D_k = 1$ for all k in Eq. (34).
3. The non-interacting response matrix is $\begin{bmatrix} f & -f \\ -f & f \end{bmatrix}$ with

$$f = \frac{2\Omega d}{(\omega + i\eta)^2 - \Omega^2}, \tag{62}$$

where Ω_{12} is the excitation energy between the ground state and the first excited state, determining the pole position of the non-interacting response function. In addition, an arbitrary amplifier d is added to create a more general non-interacting response matrix.

One may solve the interacting response of this model analytically, by working out Eq. (43). Doing so leads to an interacting response matrix of the form $\begin{bmatrix} g & -g \\ -g & g \end{bmatrix}$ with

$$g = \frac{2\Omega d}{[(\omega + i\eta)^2 - \Omega^2]c^2 - 4\Omega(a-b)d}. \tag{63}$$

Therefore, the pole of the interacting response function is

$$\omega = \sqrt{\Omega^2 + \frac{4\Omega(a-b)d}{c^2}} > \Omega, \tag{64}$$

where the condition $a > b$ is generally satisfied with the RPA approximation because the Hartree kernel is positive definite. This inequality implies that the pole of the interacting response is shifted to higher frequencies compared to the non-interacting response, when using RPA.

Figure 1 gives the absorption spectra computed by both non-interacting and interacting response functions, where the parameters a, b, c, d, Ω, and η are assigned 1.0, 0.2, 3.0, 1.2, 1.2, and 0.05 (all in atomic units), respectively. The position of the pole is depicted with dotted (dashed) lines for the interacting (non-interacting) response function, overlapping with the peak position in the corresponding absorption spectrum. It can be seen that the pole of the interacting response function shifts to a higher frequency compared to the non-interacting case.

Published under an exclusive license by AIP Publishing

The Journal of Chemical Physics ARTICLE scitation.org/journal/jcp

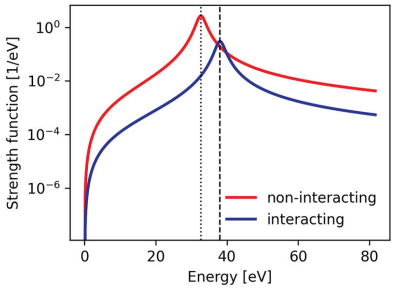

FIG. 1. Spectra of a finite dipole along *x*-axis with a single excited state. The pole of the non-interacting (interacting) system is indicated by a dotted (dashed) line. Numerical parameters are given in the main text.

III. COMPUTATIONAL DETAILS

This section presents the details of the numerical validation of ACKS2ω using the TS42 database and its TS27 subset. As discussed in Sec. II D, both potential and density basis functions are frequency-independent. Here, the basis sets are constructed in the same way as in one of our previous studies on ACKS2.[43] The MBIS method[94] was used to define the AIM weight functions, $w_a(\boldsymbol{r})$. Using the same procedure as in Ref. 43, the density basis set consists of non-interacting responses to each potential basis function, when used as a perturbation. This set is augmented with one Fukui function, to have at least one basis function that is not norm-preserving. Later, a linear transformation is applied to the density basis functions, such that they become bi-orthogonal to the potential basis, enabling one to label them as s-type, p-type, etc. This definition of the density basis set is relatively expensive and is geared toward an accurate description of linear response functions. The goal of this work is to test the validity of the ACKS2ω theory, justifying the use of carefully constructed basis functions. The bi-orthogonality of the density and potential basis functions also simplifies the elements of ACKS2ω working matrix in Eq. (38). More specifically, the overlap matrix $\boldsymbol{O}$ becomes an identity matrix, and all non-zero elements of the vector $\boldsymbol{D}$ are equal to 1, corresponding to integrals from s-type density functions. Moreover, when the adiabatic approximation is used, the hardness matrix becomes frequency-independent and takes the same form as in the ACKS2 paper.[43] More specifically, integrals including the hardness kernel of the explicit functional were evaluated numerically using a pruned Becke–Lebedev integration grid.[95] Integrals over the Hartree kernel were implemented with a Becke–Poisson solver.[96] Although the analytic expressions for LDA and PBE kernels are already provided in LibXC, integrals involving the exchange–correlation kernel were evaluated with the finite difference method used to be consistent with the previous work.[43] The only frequency-dependent parameters of ACKS2ω are found in the non-interacting response tensor, which can be evaluated using Eq. (54) on the same numerical grids.

The workflow of the ACKS2ω parameterization in this work is analogous to our earlier assessment of the ACKS2 theory:[43]

(1) The molecular structures listed in the T42 dataset are optimized using DFT at B3LYP/aug-cc-pVDZ level. (The optimized geometries are available in the supplementary material.)
(2) A new DFT calculation with LDA or PBE functional is employed to obtain ground-state information used in ACKS2ω parameter evaluations, e.g., unperturbed electron density and Kohn–Sham orbitals. All DFT calculations were performed in the quantum chemistry program GAUSSIAN 16.[97]
(3) The Kohn–Sham density and orbitals are then imported into ACKS2ω implemented in the Horton library,[98] where the MIBS partitioning scheme[94] is applied to generate the weight function $w_a(\boldsymbol{r})$ for each atom. In ACKS2ω, all parameters are evaluated on numerical Becke–Lebedev grids[95,99] implemented in Horton,[98] providing six user options from cheap to expensive: `coarse`, `medium`, `fine`, `veryfine`, `ultrafine`, and `insane`. `Medium` grids are employed for all ACKS2ω calculations, unless noted elsewhere.
(4) Frequency-dependent distributed polarizabilities are evaluated up to charges ($\ell_{max} = 0$) and charges + dipoles ($\ell_{max} = 1$), respectively. An LDA or PBE hardness kernel is used, consistently with the functional in step (2).
(5) Consequently, dynamic dipole polarizabilities can be constructed using the distributed polarizabilities from Eq. (58).

To demonstrate the accuracy of ACKS2ω on dynamic linear-response properties, we first studied absorption spectra of 42 molecules from the TS42 dataset. We only estimate the absorption spectra at the PBE/aug-cc-pVDZ level to save computational resources. 300 real frequencies ranging from 0.2 to 0.5 a.u. (i.e., 5.4 ~ 13.6 eV) are selected for absorption spectra, and the parameter η in Eq. (54) is set to 0.001. Then, the isotropic C_6 coefficients (in a.u.) are investigated for 903 molecular pairs constructed from the 42 molecules. The effect of xc functional is investigated on the C_6 coefficient by comparing two types of functional, i.e., LDA and PBE. The Slater exchange functional[100–102] and the VWN5 correlation functional[103] are used for the LDA functional in this work. Moreover, four different Dunning basis sets, aug-cc-pVDZ, aug-cc-pVTZ, d-aug-cc-pVDZ, and d-aug-cc-pVTZ, are utilized to study the impact of the basis size. The integral in Eq. (61) is evaluated using the Gaussian–Legendre quadrature with 12 imaginary frequencies. Furthermore, for comparison, we also evaluated the linear-response properties using linear-response TDDFT (LrTDDFT) with the LDA (PBE) functional, referred to as LrTDLDA (LrTDPBE). All LrTDDFT calculations are carried out in the quantum chemistry program Dalton.[104–106]

In the following context, we use the notation ACKS2ω@X to specify the ACKS2ω model with parameters estimated using functional X, for instance ACKS2ω@LDA indicates that LDA functional is used. The ACKS2ω@X evaluated with both $\ell_{max} = 0$ and $\ell_{max} = 1$ are called s-type and sp-type ACKS2ω@X, respectively. As an exception to this nomenclature, ACKS2ω@LDAx means that the ground-state DFT uses full LDA xc functional, just as ACKS2ω@LDA, but that the correlation contribution to the hardness kernel is neglected. (Only Hartree and exchange are included.)

In this work, all parameters in ACKS2ω are computed as expectation values of an electronic wavefunction, which is the most

Published under an exclusive license by AIP Publishing

The Journal of Chemical Physics ARTICLE scitation.org/journal/jcp

time-consuming step. For applications of ACKS2ω to larger systems, this step should be replaced by a simpler empirical model for the ACKS2ω, analogous to general PFFs, such that the calculation of all matrix elements becomes fast, with a quadratic complexity with the number of atoms in the system. In the long run, we hope that screening approximations and advanced Poisson solvers may further reduce the scaling of setting up and solving the relevant part of the equations to $O(N_{\text{atom}} \log N_{\text{atom}})$.

In comparison, the bottleneck of TDDFT is the transformation of electron repulsion integrals (ERI) from atomic orbitals (AO) to molecular orbitals (MO), which cannot be applied in large-scale systems due to its significantly expensive $O(N_{\text{occ}} N_{\text{AO}}^4)$ complexity from the conventional transformation or $O(N_{\text{occ}}^2 N_{\text{vir}}^2 N_{\text{aux}})$ from density fitting procedures, where N_{AO} is the size of the basis set and N_{occ}, N_{vir}, and $N_{\text{aux}} \approx 3N_{\text{AO}}$ are the number of occupied, virtual orbitals and the size of auxiliary basis sets, respectively.[107–110]

Finally, for the matrix inversion to calculate the interacting response matrix, a similar linear-algebra technology can be employed for both ACKS2ω and TDDFT with a semi-local exchange–correlation functional. However, the dimension of ACKS2ω working matrix with $l_{max} = 1$ is $4N_{\text{atom}}$, in practice, much less than the TDDFT counterpart, i.e., $N_{\text{nocc}} \times N_{\text{nvir}}$.

Because our current implementation is merely a prototype, we only illustrate timings of the different steps in the computational workflow, for the case of benzene with an Aug-cc-pVTZ basis set, on a 4-core AMD EPYC 7552 processor (AMD Zen2 microarchitecture). The following numbers may change with future software and hardware improvements. The calculation of the hardness matrix and 13 (12 frequency-dependent and one static) Kohn–Sham response matrices take 101 s in this case. Once the matrix elements are available, the ACKS2ω@LDA response calculation is trivial and has a much lower runtime (1.97 ms) compared to the corresponding LrTDLDA calculation (290 s), excluding the walltime of ground-state DFT and ERI transformation.

IV. RESULTS AND DISCUSSION

A. Absorption spectra of molecules in the TS42 set

Figure 2 shows the results computed by sp-type ACKS2ω for four example molecules, i.e., C_2H_2, C_2H_4, C_2H_5OH, and C_2H_6, while the other spectra can be found in Figs. S1–S5 of the supplementary material. From the figures, we can see that the position of peaks obtained by the ACKS2ω model overlaps almost perfectly with the LrTDPBE data, suggesting that the ACKS2ω model is a faithful approximation of its TDDFT reference. At higher excitation energies, beyond 13.6 eV, we observe a similar correspondence of the spectra, which is not included in the figures for the sake of visual clarity. It should be noted that a near-quantitative reproduction of the reference can be achieved with the sp-type basis functions only, i.e., charges + dipoles functions, which agrees well with the ACKS2 model.[43] The small deviation between ACKS2ω and TDDFT is potentially due to the atom-condensed basis functions and the numerical integration errors in the calculation of the parameters.

B. Comparison of ACKS2ω and TDDFT C_6 coefficients

This section presents a comparison of C_6 coefficients obtained with ACKS2ω and TDDFT to validate the ACKS2ω formalism.

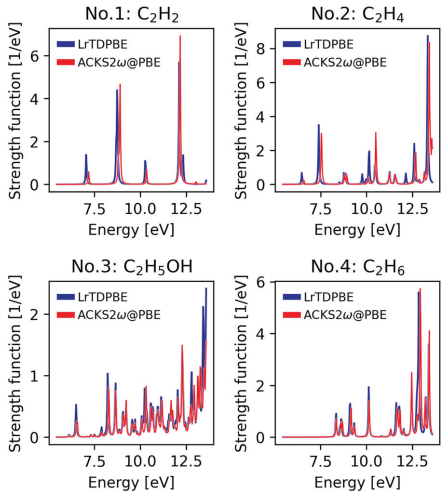

FIG. 2. Comparison of optical absorption spectra, computed with sp-type ACKS2ω@PBE and LrTDPBE methods for C_2H_2, C_6H_4, C_2H_5OH, and C_2H_6 molecules, using the aug-cc-pVDZ basis set in the DFT calculations.

Figure 3 shows a parity plot of C_6 dispersion coefficients for 903 molecular pairs, based on the TS42 dataset, computed with s-type and sp-type ACKS2ω models. The ACKS2ω parameters are derived from LDA/aug-cc-pVDZ calculations and LrTDLDA/aug-cc-pVDZ C_6 coefficients are used as a reference. All s-type ACKS2ω parametrizations significantly underestimate C_6 coefficients, averaging around 93% with respect to the reference values. The reason for this large error is that the dipole polarizability is significantly underestimated due to less complete basis sets in s-type ACKS2.[43] This effect is amplified in the isotropic C_6 coefficient, because it scales quadratically with the dipole polarizability. In contrast, very small errors can already be obtained with the sp-type ACKS2ω model, i.e., just considering fluctuating atomic charges and dipoles.

Table I presents the mean percentage errors (MPE) and mean absolute percentage errors (MAPE) over all molecule pairs, between LrTDLDA reference values and sp-type ACKS2ω@LDA models, for different orbital basis sets. For all tested basis sets, the sp-type ACKS2ω@LDA has a negative MPE, indicating that ACKS2ω@LDA slightly underestimates C_6 with respect to the TDDFT reference. Moreover, in all cases, sp-type ACKS2ω@LDA has a MAPE below 3%, which numerically confirms the validity of ACKS2ω and its ability to construct faithful approximations of its TDDFT reference. The absolute value of the MPE is clearly smaller than the MAPE, suggesting that the underestimation of C_6 by ACKS2ω is not systematic. Overall, the MPE and MAPE are not sensitive to the orbital basis, safe for a slight increase in error for larger orbital basis sets. This is to be expected, since the TDDFT calculations with larger basis sets have richer response functions, which are harder to reproduce with a simple sp-type ACKS2ω model.

Published under an exclusive license by AIP Publishing

The Journal of Chemical Physics ARTICLE scitation.org/journal/jcp

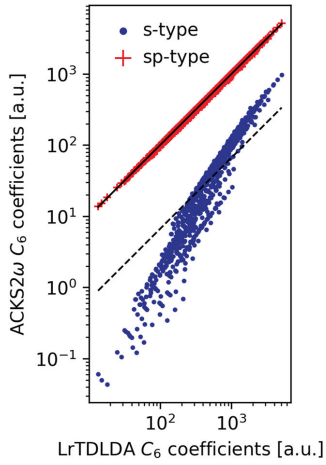

FIG. 3. Parity plot of the C_6 coefficients (in a.u.) of all 903 molecular dimers computed by ACKS2ω@LDA compared to the LrTDLDA reference values. Two datasets are included: the lowest set (blue) is generated by s-type ACKS2ω@LDA (see text), while the higher set (red) is generated by sp-type ACKS2ω@LDA. The first bisector is plotted as a solid black line, and a dashed line parallel to the bisector (factor 0.07 lower) is representative of the MAPE of the s-type ACKS2ω model.

The non-zero MPEs and MAPEs in Table I are due to the finite sp basis used in ACKS2ω. This is unavoidably a smaller basis compared to the TDDFT reference calculations, in which the Casida equations are solved in the product space of the occupied and virtual Kohn–Sham orbitals.[111] One may reduce the error of ACKS2ω by systematically including higher-order atomic multipoles, shown in Table II. It should be noted that veryfine numerical grids were needed to obtain numerically stable results for higher values of ℓ_{max}. This also results in a small deviation from $\ell_{max} = 1$ compared to Table I, for which medium grids were used. Increasing ℓ_{max} beyond 4 is expected to lower the MAPE even further, provided that even larger integration grids are used, and in the limit of a complete basis set, we expect the MAPE to vanish. The near zero (-4.88×10^{-4}%)

TABLE I. Comparison of the performance of sp-type ACKS2ω@LDA with different basis sets used in ground-state DFT calculations. MPE and MAPE stand for the mean percentage error and mean absolute percentage error between C_6 coefficients of LrTDLDA references and the corresponding ACKS2ω results for the 903 intermolecular pairs from the TS42 dataset.

Basis sets	MPE (%)	MAPE (%)
aug-cc-pVDZ	−1.62	2.35
aug-cc-pVTZ	−1.94	2.60
d-aug-cc-pVDZ	−1.41	2.31
d-aug-cc-pVTZ	−1.81	2.55

TABLE II. Comparison of the performance of ACKS2ω@LDA with the aug-cc-pVDZ basis set derived using the different bi-orthogonal basis sets (defined by ℓ_{max}, see text). MAPE (MPE) stand for the mean absolute percentage error (mean percentage error) between C_6 coefficients of LrTDLDA references and the corresponding ACKS2ω results for the 903 intermolecular pairs from the TS42 dataset.

ℓ_{max}	MAPE (%)	MPE (%)
0	93.35	2.18×10^{-1}
1	2.39	-4.88×10^{-4}
2	2.12	1.32×10^{-3}
3	1.79	1.27×10^{-3}
4	1.59	3.63×10^{-4}

MPE obtained with monopoles and dipoles is likely coincidental, as the MPE is higher for $\ell_{max} > 1$.

C. Comparison to experimental C_6 coefficients

Figure 4 shows the MPE and MAPE of C_6 coefficients computed by ACKS2ω and LrTDLDA from experimentally derived reference taken from Ref. 87. We only consider results computed by sp-type ACKS2ω due to the large errors made by s-type ACKS2ω discussed in Sec. IV B. ACKS2ω parameters were derived using different xc functionals to study the impact of the functional. Some interesting observations can be made:

(1) The positive MPE implies that all computational models in this work slightly overestimate C_6 values to some extent.
(2) For LrTDLDA, the MPE almost equals MAPE, except when using the aug-cc-pVDZ basis. This suggests LrTDLDA systematically overestimates C_6 values when extensive basis sets

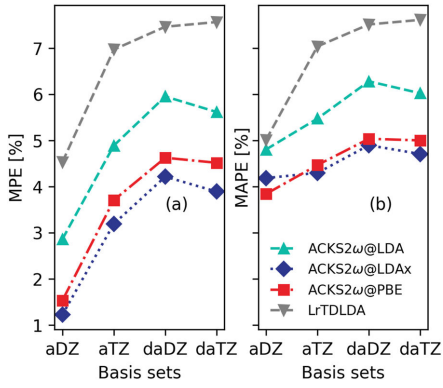

FIG. 4. The impact of the size of the basis set on the error of different methods with respect to experimental reference data: (a) MPE and (b) MAPE, where "aDZ," "aTZ," "daDZ," and "daTZ" denote aug-cc-pVDZ, aug-cc-pVTZ, d-aug-cc-pVDZ, and d-aug-cc-pVTZ basis sets, respectively.

Published under an exclusive license by AIP Publishing

The Journal of Chemical Physics ARTICLE scitation.org/journal/jcp

TABLE III. Isotropic C_6 coefficients (in a.u.) for the TS27 dataset obtained by the ACKS2ω model with bare LDA, RPA@LDA, LDAx, LDA, PBE, RPA@PBE, and PBE kernels, with d-aug-cc-pVTZ basis sets. Computational values of TDRSHLDA[88] are presented, as well as the experimental reference data compiled from Ref. 87. The geometry was optimized at the B3LYP/aug-cc-pVDZ level. Mean percentage error (MPE) and mean absolute percentage errors (MAPE) over all molecules with respect to reference values are given.

	ACKS2ω								
	Bare LDA	RPA@LDA	LDAx	LDA	Bare PBE	RPA@PBE	PBE	TDRSHLDA[a]	Exp.[b]
H_2	20.11	11.01	14.03	14.45	18.88	10.41	13.65	12.70	12.10
HF	32.94	19.14	22.20	22.58	33.17	19.29	22.65	19.20	19.00
H_2O	84.09	43.17	51.07	52.09	83.95	43.17	51.92	43.40	45.30
N_2	179.25	63.11	72.21	73.16	178.47	63.16	73.22	72.70	73.30
CO	182.42	65.87	76.60	77.73	180.90	65.88	77.91	77.10	81.40
NH_3	166.17	79.17	94.82	96.88	163.92	78.34	95.78	80.80	89.00
CH_4	241.97	111.97	134.34	137.05	234.09	109.11	134.05	121.20	129.70
HCl	295.43	107.80	127.46	129.76	290.76	106.49	128.33	122.90	130.40
CO_2	392.45	137.70	155.13	156.97	390.03	138.01	157.54	150.90	158.70
H_2CO	314.90	128.76	150.73	153.25	311.55	128.13	152.87	138.40	165.20
N_2O	581.17	156.22	175.71	177.72	578.60	156.75	178.37	179.80	184.90
C_2H_2	497.75	180.45	212.02	216.01	494.75	180.27	216.33	198.90	204.10
HBr	524.77	182.43	216.97	221.24	520.74	181.76	221.56	205.50	216.60
H_2S	543.41	182.32	219.14	223.72	529.72	178.96	220.21	209.00	216.80
CH_3OH	426.69	196.89	231.62	235.60	418.51	194.35	233.70	205.00	222.00
SO_2	961.52	263.01	298.19	301.89	960.93	264.22	304.05	295.30	294.00
C_2H_4	651.83	259.34	307.48	313.29	640.10	256.29	311.24	287.30	300.20
CH_3NH_2	601.55	271.57	320.30	326.20	588.09	267.27	322.48	279.60	303.80
SiH_4	777.20	302.19	369.60	378.07	725.68	288.91	364.81	329.60	343.90
C_2H_6	750.74	332.35	392.56	399.72	727.40	324.66	392.87	352.70	381.90
Cl_2	1095.68	315.22	366.12	371.26	1077.08	312.46	369.93	385.40	389.20
CH_3CHO	923.40	375.91	434.97	441.78	904.54	371.51	438.12	386.60	401.70
COS	1415.93	358.36	409.47	415.10	1399.21	357.42	415.24	425.40	402.20
CH_3OCH_3	1091.09	485.48	566.65	576.14	1061.04	476.27	568.58	496.10	534.10
C_3H_6	1461.23	583.62	683.18	694.79	1423.72	573.31	686.75	622.00	662.10
CS_2	3759.03	733.53	841.33	852.85	3710.36	730.39	852.50	923.00	871.10
CCl_4	5918.94	1723.00	1949.94	1971.80	5787.63	1703.58	1962.53	1924.90	2024.10
MPE	138.96	−12.64	2.42	4.20	134.92	−13.59	3.32	−3.83	
MAPE	138.96	12.69	5.29	6.18	134.92	13.70	5.38	5.17	

[a]From Ref. 88, computed by range-separated hybrid TDDFT at the LDA/d-aug-cc-pVTZ level.
[b]From Ref. 87, obtained from experimental dipole oscillator strength distribution data.

are used. The MAPE (and MPE) increases with the size of the basis, and it is found to be converged at around 7%.

(3) The MAPE (MPE) of ACKS2ω has a similar trend as LrTDLDA, but two significant differences should be pointed out. First, the ACKS2ω model has a larger MAPE than MPE, indicating that the overestimation is not systematic in the ACKS2 model, i.e., for some molecules, ACKS2ω underestimates C_6 coefficients. Second, ACKS2ω@LDA has a lower MAPE (MPE) than the corresponding LrTDLDA for all cases, implying that the improvement compared to LrTDDFT is somewhat systematic. One possible expansion is that TDDFT always gives an overestimated C_6 with LDA functional, and the incomplete basis in ACKS2ω compensates for the overestimation of TDDFT to some extent, leading to a lower MAPE. This type of error compensation is obviously fortuitous and should therefore not be relied upon blindly.

(4) The comparison between ACKS2ω@LDA and ACKS2ω@PBE shows a systematic improvement when using PBE instead of LDA. One possible reason could be that the contribution of correlation functional can be described more precisely with PBE than LDA. This inspired us to also test the ACKS2ω@LDAx model, which entirely ignores the correlation contribution in the hardness kernel, compared to ACKS2ω@LDA. As expected, it shows a significant deviation from the ACKS2ω@LDA model. Interestingly, ACKS2ω@LDAx performs slightly better than ACKS2ω@PBE, except for the aug-cc-pVDZ basis, where the latter has a lower MAPE (3.84%). Besides the potentially beneficial error compensation, these results also show that

Published under an exclusive license by AIP Publishing

The Journal of Chemical Physics ARTICLE scitation.org/journal/jcp

ACKS2ω is quite sensitive to the choice of functional because the TDDFT reference also exhibits this sensitivity.

D. Comparison of ACKS2ω and range-separated TDDFT C_6 coefficients

Toulouse *et al.* calculated C_6 coefficients using range-separated hybrid TDDFT at the LDA/d-aug-cc-pVTZ level (TDRSHLDA) for 27 homodimers from the TS27 dataset.[88] The spirit of the TDRSHLDA method is to improve the quality of exchange kernel in TDDFT, by incorporating Hartree–Fock exchange at longer ranges, thereby suppressing systematic errors of pure exchange functionals. Table III reports the results of C_6 coefficients computed by the ACKS2ω model for the TS27 dataset, where effects of different Hartree-exchange–correlation kernels are also presented. The literature results for TDRSHLDA[88] and experimental data[87] are also presented. We use a similar notation as in Ref. 88, e.g., the bare LDA indicates no hardness kernel is applied, while RPA@LDA, TDLDAx, and TDLDA mean that the response kernel is evaluated considering only Hartree, Hartree + LDA exchange, and whole LDA Hartree-exchange–correlation kernel, respectively. Corresponding results with PBE functional are also reported.

As we can see from Table III, bare LDA and PBE largely overestimate the C_6 coefficients by as much as 138.96% and 134.92%, respectively, as one could expect.[88] However, RPA@LDA and RPA@PBE, by making use of the Hartree kernel only, underestimate the coefficients by 12.64% and 13.59%, respectively. LDAx, LDA, and PBE give C_6 coefficients with overall comparable accuracy, LDAx having a slightly smaller MAPE of 5.29% in comparison to the MAPE of LDA and PBE, 6.18% and 5.38%, respectively. The MAPE of ACKS2ω@LDAx is lower than LrTDLDA (6.3%),[88] but greater than TDRSHLDA (5.17%),[88] demonstrating that when correlation is entirely ignored in response calculations, ACKS2ω@LDAx gives a better performance, close to the TDRSHLDA method. Note that ACKS2ω@LDAx has a positive MPE but TDRSHLDA negative, indicating that C_6 coefficients obtained by ACKS2ω@LDAx and TDRSHLDA are in general overestimated and underestimated, respectively. As discussed above, LrTDLDA overestimates C_6 coefficients and ACKS2ω@LDA slightly compensates for the overestimation due to the less complete bio-orthogonal basis sets. However, the compensation is too small to offer a significant improvement compared to TDRSHLDA. Interestingly, the results are improved and even better than PBE by removing the electron correlation contribution in response calculations, which again demonstrates that the effects of xc functional on C_6 coefficients with ACKS2ω are of significant importance.

V. CONCLUSIONS AND OUTLOOK

A frequency-dependent ACKS2 model, referred to as ACKS2ω, is proposed using the quasi-energy formalism. This allows us to approach ACKS2ω directly using the variational principle, in the same way as the time-independent ACKS2 derivation. For the xc contribution to the hardness, an adiabatic approximation is applied, and the hardness is thereby frequency-independent, just as in the ACKS2 model. For the frequency-dependent non-interacting response matrix, a similar Lehmann representation is employed as in the static case. Given the hardness and non-interacting response matrix, the interacting response matrix can be reproduced in analogy to the procedure used in the ACKS2 model.

The ACKS2ω equations are validated with several numerical assessments. Absorption spectra obtained from the strength function are evaluated for all 42 molecular monomers from the TS42 dataset. The results agree well with the LrTDDFT reference data, indicating that the ACKS2ω model is reasonably accurate for linear-response property calculations of finite systems. Furthermore, we test C_6 coefficients for the TS42 dataset to validate the new model, including 903 organic and inorganic molecule pairs. These tests confirm that ACKS2ω can reproduce TDDFT C_6 coefficients with only a small systematic error, when at least fluctuating atomic charges and dipoles are used.

A comparison of ACKS2ω, using the LDA and PBE kernels, to experimental data and results obtained with range-separated calculations, provides some additional insights. The deviation of the ACKS2ω C_6 coefficients from the experiment is quite sensitive to the choice of the functional, with PBE and LDAx (correlation omitted from the hardness kernel), being favorable choices. The best ACKS2ω model, ACKS2ω@PBE with the aug-cc-pVDZ basis, gives C_6 coefficients of molecules with an MAPE of 3.84%, a slight improvement over the TS method (6.3%). This improvement is significant because it potentially provides a better way to describe non-local dispersion energy between molecular dimers, which is a topic of ongoing research. In addition, the ACKS2ω@LDAx model has only a slightly inferior accuracy of C_6 coefficients than TDRSHLDA response calculations, with MAPEs of 5.29% and 5.17%, respectively, for 27 homodimers from the TS27 database.

The strength of the ACKS2ω model is that, once parameterized, calculations involving response kernels have a low computational cost, comparable in complexity to conventional polarizable force fields. In this work, the parametrization is relatively expensive to obtain accurate predictions, thereby showing that ACKS2ω is capable of reproducing its LrTDDFT reference. In future work, simpler force-field like parameterizations could be used instead to overcome the computational bottleneck of the current parametrization. We anticipate that this approach will be beneficial, e.g., for calculations of long-range correlation energies or optical properties of extended systems, for which DFT would be infeasible.

SUPPLEMENTARY MATERIAL

Additional display items showing spectra for the remaining molecules of the TS42 set, not included in Fig. 2 are included in the supplementary material. Optimized geometries for the TS42 molecules are stored in XYZ format in a supplementary ZIP file.

ACKNOWLEDGMENTS

Y.C. and T.V. acknowledge the Foundation of Scientific Research – Flanders (FWO, File No. G0A9717N) and the Research Board of Ghent University (BOF) for their financial support. The resources and services used in this work were provided by the VSC (Flemish Supercomputer Center), funded by the Research Foundation – Flanders (FWO) and the Flemish Government. We thank Dr. Jelle Vekeman for helpful comments on the manuscript.

Published under an exclusive license by AIP Publishing

The Journal of Chemical Physics ARTICLE scitation.org/journal/jcp

AUTHOR DECLARATIONS

Conflict of Interest

The authors have no conflicts to disclose.

Author Contributions

YingXing Cheng: Data curation (lead); Formal analysis (equal); Investigation (equal); Methodology (equal); Software (lead); Validation (equal); Visualization (lead); Writing – original draft (equal); Writing – review & editing (equal). **Toon Verstraelen**: Conceptualization (equal); Data curation (supporting); Formal analysis (equal); Funding acquisition (lead); Investigation (equal); Methodology (equal); Software (supporting); Supervision (lead); Visualization (supporting); Writing – original draft (equal); Writing – review & editing (equal).

DATA AVAILABILITY STATEMENT

The data that support the findings of this study are available within the article and its supplementary material.

REFERENCES

[1] A. Warshel and M. Levitt, J. Mol. Biol. **103**, 227 (1976).
[2] G. A. Kaminski, H. A. Stern, B. J. Berne, R. A. Friesner, Y. X. Cao, R. B. Murphy, R. Zhou, and T. A. Halgren, J. Comput. Chem. **23**, 1515 (2002).
[3] P. Ren and J. W. Ponder, J. Comput. Chem. **23**, 1497 (2002).
[4] W. L. Jorgensen, K. P. Jensen, and A. N. Alexandrova, J. Chem. Theory Comput. **3**, 1987 (2007).
[5] Y. Shi, Z. Xia, J. Zhang, R. Best, C. Wu, J. W. Ponder, and P. Ren, J. Chem. Theory Comput. **9**, 4046 (2013).
[6] G. Lamoureux, A. D. MacKerell, and B. Roux, J. Chem. Phys. **119**, 5185 (2003).
[7] H. Yu, T. Hansson, and W. F. Van Gunsteren, J. Chem. Phys. **118**, 221 (2003).
[8] J. A. Lemkul, J. Huang, B. Roux, and A. D. Mackerell, Chem. Rev. **116**, 4983 (2016).
[9] W. J. Mortier, K. Van Genechten, and J. Gasteiger, J. Am. Chem. Soc. **107**, 829 (1985).
[10] W. J. Mortier, S. K. Ghosh, and S. Shankar, J. Am. Chem. Soc. **108**, 4315 (1986).
[11] C. Bai, S. Kale, and J. Herzfeld, Chem. Sci. **8**, 4203 (2017).
[12] M. Cools-Ceuppens, J. Dambre, and T. Verstraelen, J. Chem. Theory Comput. **18**, 1672 (2022).
[13] P. J. Van Maaren and D. van der Spoel, J. Phys. Chem. B **105**, 2618 (2001).
[14] A.-P. E. Kunz and W. F. Van Gunsteren, J. Phys. Chem. A **113**, 11570 (2009).
[15] S. W. Rick, S. J. Stuart, and B. J. Berne, J. Chem. Phys. **101**, 6141 (1994).
[16] S. W. Rick and B. J. Berne, J. Am. Chem. Soc. **118**, 672 (1996).
[17] H. A. Stern, F. Rittner, B. J. Berne, and R. A. Friesner, J. Chem. Phys. **115**, 2237 (2001).
[18] S. Patel and C. L. Brooks, J. Comput. Chem. **25**, 1 (2004).
[19] S. Patel, A. D. Mackerell, and C. L. Brooks, J. Comput. Chem. **25**, 1504 (2004).
[20] A. K. Rappé and W. A. Goddard, J. Phys. Chem. **95**, 3358 (1991).
[21] Y. Zhong and S. Patel, J. Phys. Chem. B **114**, 11076 (2010).
[22] D. M. York and W. Yang, J. Chem. Phys. **104**, 159 (1996).
[23] M. Devereux, S. Raghunathan, D. G. Fedorov, and M. Meuwly, J. Chem. Theory Comput. **10**, 4229 (2014).
[24] O. T. Unke, M. Devereux, and M. Meuwly, J. Chem. Phys. **147**, 161712 (2017).
[25] M. Devereux, M. Pezzella, S. Raghunathan, and M. Meuwly, J. Chem. Theory Comput. **16**, 7267 (2020).
[26] R. T. Sanderson, Science **114**, 670 (1951).
[27] A. C. T. Van Duin, A. Strachan, S. Stewman, Q. Zhang, X. Xu, and W. A. Goddard, J. Phys. Chem. A **107**, 3803 (2003).
[28] K. S. Smirnov and D. Bougeard, Chem. Phys. **292**, 53 (2003).
[29] A. Hallil, R. Tétot, F. Berthier, I. Braems, and J. Creuze, Phys. Rev. B. **73**, 165406 (2006).
[30] P. Bultinck, W. Langenaeker, P. Lahorte, F. De Proft, P. Geerlings, M. Waroquier, and J. P. Tollenaere, J. Phys. Chem. A **106**, 7887 (2002).
[31] A. C. T. Van Duin, S. Dasgupta, F. Lorant, and W. A. Goddard, J. Phys. Chem. A **105**, 9396 (2001).
[32] P. Bultinck, R. Vanholme, P. L. A. Popelier, F. De Proft, and P. Geerlings, J. Phys. Chem. A **108**, 10359 (2004).
[33] Q. Yang and K. A. Sharp, J. Chem. Theory Comput. **2**, 1152 (2006).
[34] T. Verstraelen, E. Pauwels, F. De Proft, V. Van Speybroeck, P. Geerlings, and M. Waroquier, J. Chem. Theory Comput. **8**, 661 (2012).
[35] C.-M. Ionescu, S. Geidl, R. Svobodová Vařeková, and J. Koča, J. Chem. Inf. Model. **53**, 2548 (2013).
[36] R. Chelli, P. Procacci, R. Righini, and S. Califano, J. Chem. Phys. **111**, 8569 (1999).
[37] R. a. Nistor, J. G. Polihronov, M. H. Müser, and N. J. Mosey, J. Chem. Phys. **125**, 094108 (2006).
[38] G. Lee Warren, J. E. Davis, and S. Patel, J. Chem. Phys. **128**, 144110 (2008).
[39] R. A. Nistor and M. H. Müser, Phys. Rev. B **79**, 104303 (2009).
[40] T. Verstraelen, P. W. Ayers, V. Van Speybroeck, and M. Waroquier, J. Chem. Phys. **138**, 074108 (2013).
[41] R. Chelli, M. Pagliai, P. Procacci, G. Cardini, and V. Schettino, J. Chem. Phys. **122**, 074504 (2005).
[42] J. Chen and T. J. Martínez, Chem. Phys. Lett. **438**, 315 (2007).
[43] T. Verstraelen, S. Vandenbrande, and P. W. Ayers, J. Chem. Phys. **141**, 194114 (2014).
[44] M. M. Islam, G. Kolesov, T. Verstraelen, E. Kaxiras, and A. C. T. van Duin, J. Chem. Theory Comput. **12**, 3463 (2016).
[45] P. Gütlein, L. Lang, K. Reuter, J. Blumberger, and H. Oberhofer, J. Chem. Theory Comput. **15**, 4516 (2019).
[46] P. Gütlein, J. Blumberger, and H. Oberhofer, J. Chem. Theory Comput. **16**, 5723 (2020).
[47] A. J. Stone and C.-S. Tong, Chem. Phys. **137**, 121 (1989).
[48] J. F. Dobson, A. White, and A. Rubio, Phys. Rev. Lett. **96**, 073201 (2006).
[49] J. Hermann, D. Alfè, and A. Tkatchenko, Nat. Commun. **8**, 14052 (2017).
[50] K. Jackson, M. Yang, and J. Jellinek, J. Phys. Chem. C **111**, 17952 (2007).
[51] K. Jackson and J. Jellinek, J. Chem. Phys. **145**, 244302 (2016).
[52] A. J. Misquitta, J. Spencer, A. J. Stone, and A. Alavi, Phys Rev. B **82**, 075312 (2010).
[53] J. F. Dobson and T. Gould, J. Phys.: Condens. Matter **24**, 073201 (2012).
[54] A. J. Misquitta, R. Maezono, N. D. Drummond, A. J. Stone, and R. J. Needs, Phys. Rev. B **89**, 045140 (2014).
[55] E. Runge and E. K. U. Gross, Phys. Rev. Lett. **52**, 997 (1984).
[56] C. A. Ullrich, *Time-dependent Density-Functional Theory: Concepts and Applications* (OUP Oxford, 2011).
[57] M. A. Marques, N. T. Maitra, F. M. Nogueira, E. K. Gross, and A. Rubio, *Fundamentals of Time-dependent Density Functional Theory* (Springer, 2012), Vol. 837.
[58] K. Burke, J. Werschnik, and E. K. U. Gross, J. Chem. Phys. **123**, 062206 (2005).
[59] M. E. Casida and M. Huix-Rotllant, Annu. Rev. Phys. Chem. **63**, 287 (2012).
[60] M. A. L. Marques and E. K. U. Gross, Annu. Rev. Phys. Chem. **55**, 427 (2004).
[61] A. D. Laurent and D. Jacquemin, Int. J. Quantum Chem. **113**, 2019 (2013).
[62] E. R. Kjellgren, E. D. Hedegård, and H. J. A. Jensen, J. Chem. Phys. **151**, 124113 (2019).
[63] V. P. Osinga, S. J. A. Van Gisbergen, J. G. Snijders, and E. J. Baerends, J. Chem. Phys. **106**, 5091 (1997).
[64] F. Aiga, T. Tada, and R. Yoshimura, J. Chem. Phys. **111**, 2878 (1999).
[65] A. Castro, M. A. L. Marques, J. A. Alonso, G. F. Bertsch, and A. Rubio, Eur. Phys. J. D **28**, 211 (2004).
[66] E. D. Hedegård, F. Heiden, S. Knecht, E. Fromager, and H. J. A. Jensen, J. Chem. Phys. **139**, 184308 (2013).
[67] E. Fromager, S. Knecht, and H. J. A. Jensen, J. Chem. Phys. **138**, 084101, (2013).

Published under an exclusive license by AIP Publishing

The Journal of Chemical Physics ARTICLE scitation.org/journal/jcp

[68]P. Salek, O. Vahtras, T. Helgaker, and H. Ågren, J. Chem. Phys. **117**, 9630 (2002).
[69]I. Tunell, Z. Rinkevicius, O. Vahtras, P. Salek, T. Helgaker, and H. Ågren, J. Chem. Phys. **119**, 11024 (2003).
[70]O. Christiansen, P. Jørgensen, and C. Hättig, Int. J. Quantum Chem. **68**, 1 (1998).
[71]D. A. Telnov and S.-I. Chu, Chem. Phys. Lett. **264**, 466 (1997).
[72]P. Salek, T. Helgaker, and T. Saue, Chem. Phys. **311**, 187 (2005).
[73]B. M. Deb and S. K. Ghosh, J. Chem. Phys. **77**, 342 (1982).
[74]N. T. Maitra and K. Burke, Chem. Phys. Lett. **359**, 237 (2002).
[75]P. Samal and M. K. Harbola, Chem. Phys. Lett. **433**, 204 (2006).
[76]N. T. Maitra and K. Burke, Chem. Phys. Lett. **441**, 167 (2007).
[77]V. Kapoor, M. Ruggenthaler, and D. Bauer, Phys. Rev. A **87**, 1 (2013).
[78]P. W. Langhoff, S. T. Epstein, and M. Karplus, Rev. Mod. Phys. **44**, 602 (1972).
[79]A. Mayer, P. Lambin, and P.-O. Åstrand, Nanotechnology **19**, 025203 (2008).
[80]H. S. Smalø, P.-O. Åstrand, and A. Mayer, Mol. Phys. **111**, 1470 (2013).
[81]S. Haghdani, N. Davari, R. Sandnes, and P.-O. Åstrand, J. Phys. Chem. A **118**, 11282 (2014).
[82]J. Hermann and A. Tkatchenko, Phys. Rev. Lett. **124**, 146401 (2020).
[83]A. Ambrosetti, A. M. Reilly, R. A. Distasio, and A. Tkatchenko, J. Chem. Phys. **140**, 18A508 (2014).
[84]A. Wildman, G. Donati, F. Lipparini, B. Mennucci, and X. Li, J. Chem. Theory Comput. **15**, 43 (2019).
[85]A. J. Misquitta and A. J. Stone, Theor. Chem. Acc. **137**, 153 (2018).
[86]J. B. Schriber, D. R. Nascimento, A. Koutsoukas, S. A. Spronk, D. L. Cheney, and C. D. Sherrill, J. Chem. Phys. **154**, 184110 (2021).
[87]A. Tkatchenko and M. Scheffler, Phys. Rev. Lett. **102**, 073005 (2009).
[88]J. Toulouse, E. Rebolini, T. Gould, J. F. Dobson, P. Seal, and J. G. Ángyán, J. Chem. Phys. **138**, 194106 (2013).
[89]J. E. Rice and N. C. Handy, J. Chem. Phys. **94**, 4959 (1991).
[90]A. J. Stone, Mol. Phys. **56**, 1065 (1985).
[91]J. G. Ángyán, G. Jansen, M. Loss, C. Hättig, and B. A. Heß, Chem. Phys. Lett. **219**, 267 (1994).
[92]R. M. Martin, *Electronic Structure: Basic Theory and Practical Methods* (Cambridge University Press, 2020).
[93]E. Zaremba and W. Kohn, Phys. Rev. B **13**, 2270 (1976).
[94]T. Verstraelen, S. Vandenbrande, F. Heidar-Zadeh, L. Vanduyfhuys, V. Van Speybroeck, M. Waroquier, and P. W. Ayers, J. Chem. Theory Comput. **12**, 3894 (2016).
[95]A. D. Becke, J. Chem. Phys. **88**, 2547 (1988).
[96]A. D. Becke and R. M. Dickson, J. Chem. Phys. **89**, 2993 (1988).
[97]M. J. Frisch, G. W. Trucks, H. B. Schlegel, G. E. Scuseria, M. A. Robb, J. R. Cheeseman, G. Scalmani, V. Barone, G. A. Petersson, H. Nakatsuji, X. Li, M. Caricato, A. V. Marenich, J. Bloino, B. G. Janesko, R. Gomperts, B. Mennucci, H. P. Hratchian, J. V. Ortiz, A. F. Izmaylov, J. L. Sonnenberg, D. Williams-Young, F. Ding, F. Lipparini, F. Egidi, J. Goings, B. Peng, A. Petrone, T. Henderson, D. Ranasinghe, V. G. Zakrzewski, J. Gao, N. Rega, G. Zheng, W. Liang, M. Hada, M. Ehara, K. Toyota, R. Fukuda, J. Hasegawa, M. Ishida, T. Nakajima, Y. Honda, O. Kitao, H. Nakai, T. Vreven, K. Throssell, J. A. Montgomery, Jr., J. E. Peralta, F. Ogliaro, M. J. Bearpark, J. J. Heyd, E. N. Brothers, K. N. Kudin, V. N. Staroverov, T. A. Keith, R. Kobayashi, J. Normand, K. Raghavachari, A. P. Rendell, J. C. Burant, S. S. Iyengar, J. Tomasi, M. Cossi, J. M. Millam, M. Klene, C. Adamo, R. Cammi, J. W. Ochterski, R. L. Martin, K. Morokuma, O. Farkas, J. B. Foresman, and D. J. Fox, GAUSSIAN 16, Revision C.01 (Gaussian Inc, Wallingford CT, 2016).
[98]T. Verstraelen, P. Tecmer, F. Heidar-Zadeh, C. E. González-Espinoza, M. Chan, T. D. Kim, K. Boguslawski, S. Fias, S. Vandenbrande, D. Berrocal, and P. W. Ayers, HORTON 2.1.0 (2017).
[99]V. I. Lebedev and D. N. Laikov, Dokl. Math. **59**, 477 (1999).
[100]P. Hohenberg and W. Kohn, Phys. Rev. **136**, B864 (1964).
[101]W. Kohn and L. J. Sham, Phys. Rev. **140**, A1133 (1965).
[102]J. C. Slater, *The Self-Consistent Field for Molecular and Solids* (1974), Vol. 4.
[103]S. H. Vosko, L. Wilk, and M. Nusair, Can. J. Phys. **58**, 1200 (1980).
[104]K. Aidas, C. Angeli, K. L. Bak, V. Bakken, R. Bast, L. Boman, O. Christiansen, R. Cimiraglia, S. Coriani, P. Dahle, E. K. Dalskov, U. Ekström, T. Enevoldsen, J. J. Eriksen, P. Ettenhuber, B. Fernández, L. Ferrighi, H. Fliegl, L. Frediani, K. Hald, A. Halkier, C. Hättig, H. Heiberg, T. Helgaker, A. C. Hennum, H. Hettema, E. Hjertenæs, S. Høst, I.-M. Høyvik, M. F. Iozzi, B. Jansík, H. J. A. Jensen, D. Jonsson, P. Jørgensen, J. Kauczor, S. Kirpekar, T. Kjærgaard, W. Klopper, S. Knecht, R. Kobayashi, H. Koch, J. Kongsted, A. Krapp, K. Kristensen, A. Ligabue, O. B. Lutnæs, J. I. Melo, K. V. Mikkelsen, R. H. Myhre, C. Neiss, C. B. Nielsen, P. Norman, J. Olsen, J. M. H. Olsen, A. Osted, M. J. Packer, F. Pawlowski, T. B. Pedersen, P. F. Provasi, S. Reine, Z. Rinkevicius, T. A. Ruden, K. Ruud, V. V. Rybkin, P. Sałek, C. C. M. Samson, A. S. de Merás, T. Saue, S. P. A. Sauer, B. Schimmelpfennig, K. Sneskov, A. H. Steindal, K. O. Sylvester-Hvid, P. R. Taylor, A. M. Teale, E. I. Tellgren, D. P. Tew, A. J. Thorvaldsen, L. Thøgersen, O. Vahtras, M. A. Watson, D. J. D. Wilson, M. Ziolkowski, and H. Ågren, Wiley Interdiscip. Rev.: Comput. Mol. Sci. **4**, 269 (2014).
[105]P. Jørgensen, H. J. A. Jensen, and J. Olsen, J. Chem. Phys. **89**, 3654 (1988).
[106]J. Olsen, D. L. Yeager, and P. Jørgensen, J. Chem. Phys. **91**, 381 (1989).
[107]A. C. Limaye and S. R. Gadre, J. Chem. Phys. **100**, 1303 (1994).
[108]K. C. Tang and C. Edmiston, J. Chem. Phys. **52**, 997 (1970).
[109]C. F. Bender, J. Comput. Phys. **9**, 547 (1972).
[110]C. D. Sherrill, "Density-fitting approximations to the electron repulsion integrals," Technical Note (Georgia Institute of Technology, 2010), (Last accessed, 09-15-2022); available at http://vergil.chemistry.gatech.edu/notes/df.pdf.
[111]M. E. Casida, in *Recent Advances in Density Functional Methods*, edited by D. P. Chong (World Scientific, 1995) pp. 155–192.

Published under an exclusive license by AIP Publishing

Supplementary Material for "A new framework for frequency-dependent polarizable force fields"

YingXing Cheng and Toon Verstraelen

Center for Molecular Modeling (CMM), Ghent University - Technologiepark-Zwijnaarde 46, B-9052 Gent, Belgium

(*Electronic mail: toon.verstraelen@ugent.be)

(Dated: 15 September 2022)

I. ADDITIONAL DISPLAY ITEMS

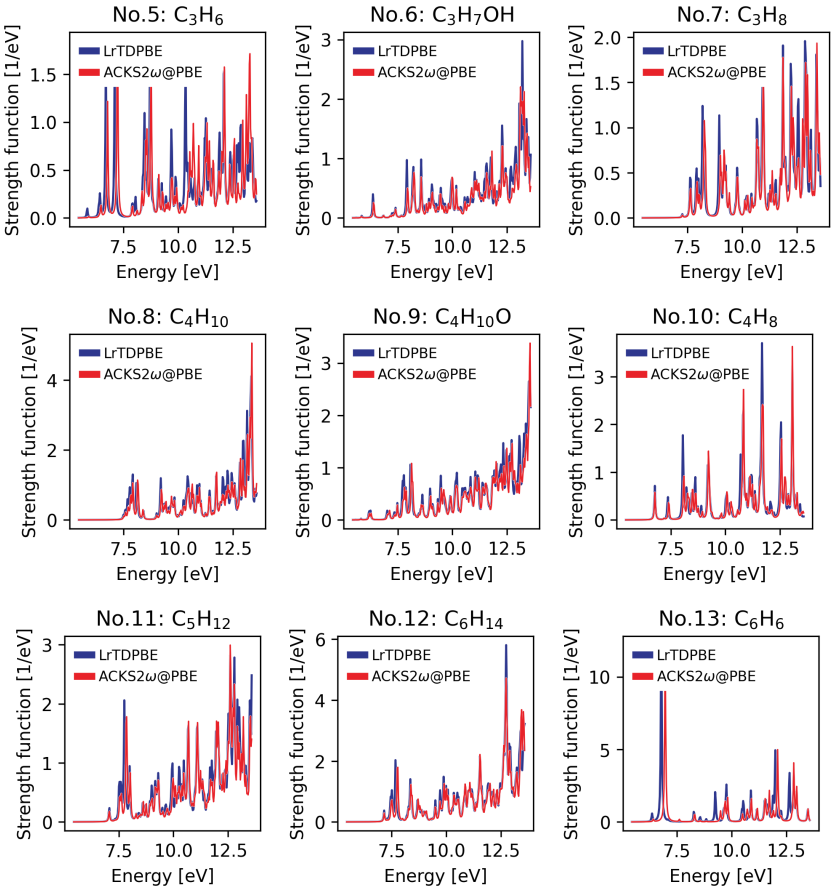

FIG. S1. Comparison of spectra calculated by ACKS2ω@PBE and LrTDPBE methods for C_3H_6, C_3H_7OH, C_3H_8, C_4H_{10}, $C_4H_{10}O$, C_4H_8, C_5H_{12}, C_6H_{14}, and C_6H_6.

REFERENCES

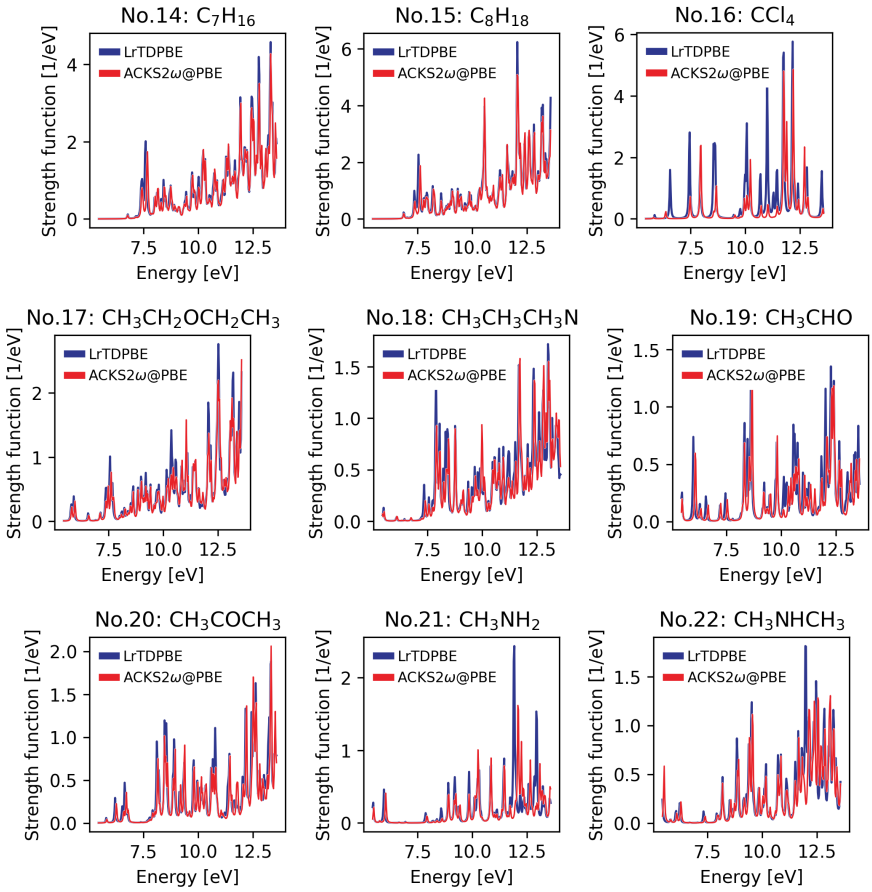

FIG. S2. Comparison of spectra calculated by ACKS2ω@PBE and LrTDPBE methods for C_7H_{16}, C_8H_{18}, CCl_4, $CH_3CH_2OCH_2CH_3$, $CH_3CH_3CH_3N$, CH_3CHO, CH_3COCH_3, CH_3NH_2, and CH_3NHCH_3.

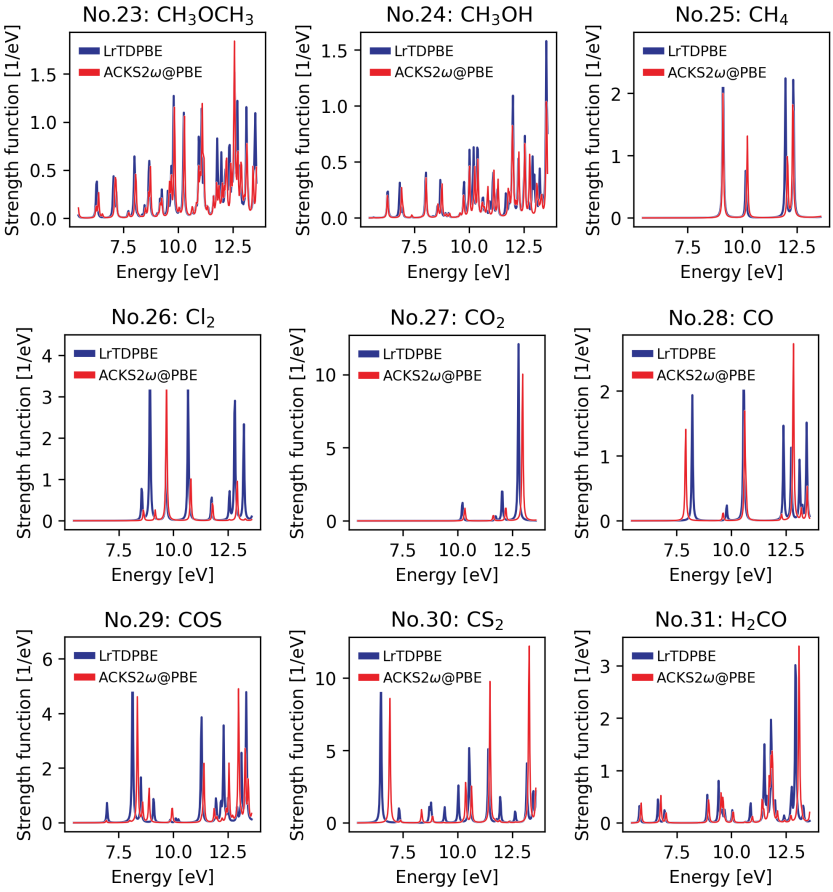

FIG. S3. Comparison of spectra calculated by ACKS2ω@PBE and LrTDPBE methods for CH_3OCH_3,CH_3OH, CH_4, Cl_2, CO_2, CO, COS, CS_2, and H_2CO.

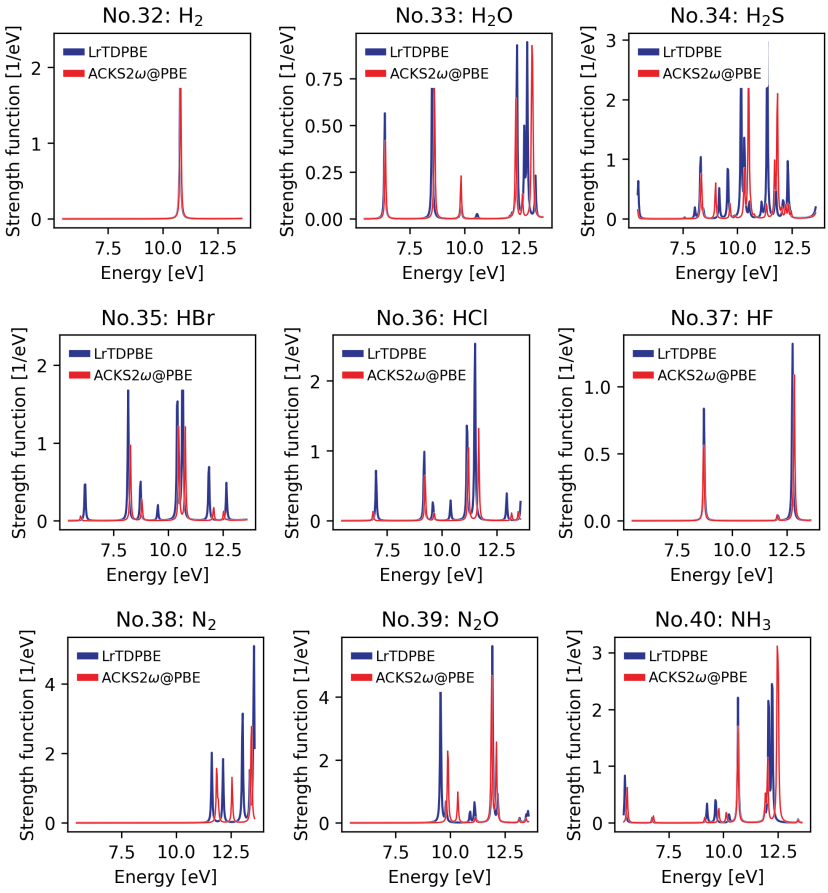

FIG. S4. Comparison of spectra calculated by ACKS2ω@PBE and LrTDPBE methods for H_2, H_2O, H_2S, HBr, HCl, HF, N_2, N_2O, and NH_3.

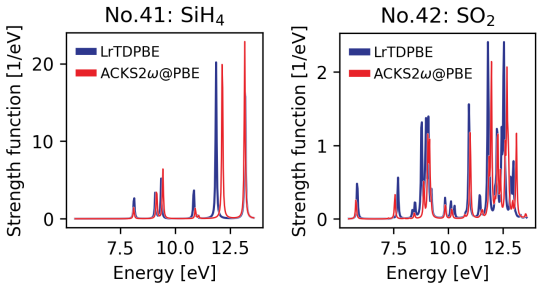

FIG. S5. Comparison of spectra calculated by ACKS2ω@PBE and LrTDPBE methods for SiH_4 and SO_2.

Table 3.1: Optimized coordinates for C_2H_2 at B3LYP/aug-cc-pVDZ level.

Element	x-coordinate	y-coordinate	z-coordinate
C	0.0000000000	0.0000000000	0.6048729969
C	0.0000000000	0.0000000000	-0.6048729969
H	0.0000000000	0.0000000000	1.6757349931
H	0.0000000000	0.0000000000	-1.6757349931

Table 3.2: Optimized coordinates for C_2H_4 at B3LYP/aug-cc-pVDZ level.

Element	x-coordinate	y-coordinate	z-coordinate
C	-0.0000000000	0.0000000000	0.6676689957
C	0.0000000000	0.0000000000	-0.6676689957
H	-0.0000000000	0.9287199973	1.2408559938
H	-0.0000000000	-0.9287199973	1.2408559938
H	0.0000000000	-0.9287199973	-1.2408559938
H	0.0000000000	0.9287199973	-1.2408559938

Table 3.3: Optimized coordinates for C_2H_5OH at B3LYP/aug-cc-pVDZ level.

Element	x-coordinate	y-coordinate	z-coordinate
C	1.1789489916	-0.4000409982	0.0000000000
C	0.0000000000	0.5567759958	0.0000000000
O	-1.2016479950	-0.2244839987	0.0000000000
H	-1.9618379899	0.3680309980	0.0000000000
H	2.1240969884	0.1611479995	0.0000000000
H	1.1537639930	-1.0423779958	0.8907539933
H	1.1537639930	-1.0423779958	-0.8907539933
H	0.0348519998	1.2055209954	0.8926449975
H	0.0348519998	1.2055209954	-0.8926449975

Table 3.4: Optimized coordinates for C_2H_6 at B3LYP/aug-cc-pVDZ level.

Element	x-coordinate	y-coordinate	z-coordinate
C	-0.0000000000	-0.0000000000	0.7655919945
C	-0.0000000000	-0.0000000000	-0.7655919945
H	0.0000000000	1.0244419947	1.1649439940
H	-0.8871927947	-0.5122209973	1.1649439940
H	0.8871927947	-0.5122209973	1.1649439940
H	-0.0000000000	-1.0244419947	-1.1649439940
H	-0.8871927947	0.5122209973	-1.1649439940
H	0.8871927947	0.5122209973	-1.1649439940

Table 3.5: Optimized coordinates for C_3H_6 at B3LYP/aug-cc-pVDZ level.

Element	x-coordinate	y-coordinate	z-coordinate
C	-1.1423439943	-0.5017299973	0.0000000000
C	0.0000000000	0.4728389977	0.0000000000
C	1.2967759910	0.1466479994	0.0000000000
H	1.6246559937	-0.8954739947	0.0000000000
H	2.0764699919	0.9089779938	0.0000000000
H	-0.2737089987	1.5334099942	0.0000000000
H	-0.7853269971	-1.5406549911	0.0000000000
H	-1.7843409897	-0.3563989982	0.8831849970
H	-1.7843409897	-0.3563989982	-0.8831849970

Table 3.6: Optimized coordinates for C_3H_7OH at B3LYP/aug-cc-pVDZ level.

Element	x-coordinate	y-coordinate	z-coordinate
C	-1.4476199915	1.2419109933	0.0000000000
C	0.0000000000	0.7416159965	0.0000000000
C	0.0918359993	-0.7771479971	0.0000000000
O	1.4770869915	-1.1416439934	0.0000000000
H	-1.4828449952	2.3396729879	0.0000000000
H	-1.9941989912	0.8919199982	0.8884419969
H	-1.9941989912	0.8919199982	-0.8884419969
H	0.5341709954	1.1231929971	0.8827949934
H	0.5341709954	1.1231929971	-0.8827949934
H	-0.4142699981	-1.1862519916	0.8927289938
H	-0.4142699981	-1.1862519916	-0.8927289938
H	1.5494439948	-2.1025139880	0.0000000000

Table 3.7: Optimized coordinates for C_3H_8 at B3LYP/aug-cc-pVDZ level.

Element	x-coordinate	y-coordinate	z-coordinate
C	0.0000000000	-0.0000000000	0.5853199996
C	0.0000000000	1.2777139960	-0.2596509987
C	-0.0000000000	-1.2777139960	-0.2596509987
H	0.8804569933	-0.0000000000	1.2469029918
H	-0.8804569933	0.0000000000	1.2469029918
H	0.0000000000	2.1773989872	0.3719059981
H	-0.0000000000	-2.1773989872	0.3719059981
H	0.8877429961	1.3233959911	-0.9084319940
H	-0.8877429961	1.3233959911	-0.9084319940
H	-0.8877429961	-1.3233959911	-0.9084319940
H	0.8877429961	-1.3233959911	-0.9084319940

Table 3.8: Optimized coordinates for $C_4H_{10}O$ at B3LYP/aug-cc-pVDZ level.

Element	x-coordinate	y-coordinate	z-coordinate
C	1.3556259947	-0.3499939981	0.0000000000
C	0.0000000000	0.3407309982	0.0000000000
C	-1.1733489950	-0.6452999978	0.0000000000
C	-2.5374839898	0.0515779998	0.0000000000
O	2.3721809894	0.6601459956	0.0000000000
H	1.4531959953	-0.9929159926	0.8927859967
H	1.4531959953	-0.9929159926	-0.8927859967
H	-0.0589119995	0.9957689933	0.8830409973
H	-0.0589119995	0.9957689933	-0.8830409973
H	-1.1005779952	-1.3029149917	0.8812419959
H	-1.1005779952	-1.3029149917	-0.8812419959
H	-3.3587379812	-0.6787619946	0.0000000000
H	-2.6560219864	0.6901209951	0.8877949931
H	-2.6560219864	0.6901209951	-0.8877949931
H	3.2371579829	0.2353819990	0.0000000000

Table 3.9: Optimized coordinates for C_4H_{10} at B3LYP/aug-cc-pVDZ level.

Element	x-coordinate	y-coordinate	z-coordinate
C	-0.4210589978	0.6404719966	0.0000000000
C	0.4210589978	-0.6404719966	0.0000000000
C	0.4210589978	1.9196579890	0.0000000000
C	-0.4210589978	-1.9196579890	0.0000000000
H	-1.0837009941	0.6366129983	0.8807639954
H	-1.0837009941	0.6366129983	-0.8807639954
H	1.0837009941	-0.6366129983	0.8807639954
H	1.0837009941	-0.6366129983	-0.8807639954
H	-0.2127359990	2.8176149837	0.0000000000
H	1.0693179947	1.9674319909	0.8877939982
H	1.0693179947	1.9674319909	-0.8877939982
H	0.2127359990	-2.8176149837	0.0000000000
H	-1.0693179947	-1.9674319909	0.8877939982
H	-1.0693179947	-1.9674319909	-0.8877939982

Table 3.10: Optimized coordinates for C_4H_8 at B3LYP/aug-cc-pVDZ level.

Element	x-coordinate	y-coordinate	z-coordinate
C	0.0000000000	1.0866088600	0.1212186120
C	-0.0000000000	-1.0866088600	0.1212186120
C	-1.0866088600	0.0000000000	-0.1212186120
C	1.0866088600	-0.0000000000	-0.1212186120
H	0.0000000000	1.4334046354	1.1635024359
H	0.0000000000	1.9635926092	-0.5390544596
H	-0.0000000000	-1.4334046354	1.1635024359
H	-0.0000000000	-1.9635926092	-0.5390544596
H	-1.4334046354	0.0000000000	-1.1635024359
H	-1.9635926092	0.0000000000	0.5390544596
H	1.4334046354	-0.0000000000	-1.1635024359
H	1.9635926092	-0.0000000000	0.5390544596

Table 3.11: Optimized coordinates for C_5H_{12} at B3LYP/aug-cc-pVDZ level.

Element	x-coordinate	y-coordinate	z-coordinate
C	0.0000000000	-0.0000000000	0.3170917326
C	0.0000000000	1.2825312973	-0.5219735407
C	-0.0000000000	-1.2825312973	-0.5219735407
C	0.0000000000	2.5603529227	0.3227369374
C	-0.0000000000	-2.5603529227	0.3227369374
H	0.8811656356	-0.0000000000	0.9807119808
H	-0.8811656356	0.0000000000	0.9807119808
H	0.8808406573	1.2810527232	-1.1841728544
H	-0.8808406573	1.2810527232	-1.1841728544
H	-0.8808406573	-1.2810527232	-1.1841728544
H	0.8808406573	-1.2810527232	-1.1841728544
H	0.0000000000	3.4590719378	-0.3100559592
H	-0.0000000000	-3.4590719378	-0.3100559592
H	-0.8878288446	2.6072475062	0.9709170536
H	0.8878288446	2.6072475062	0.9709170536
H	0.8878288446	-2.6072475062	0.9709170536
H	-0.8878288446	-2.6072475062	0.9709170536

Table 3.12: Optimized coordinates for C_6H_{14} at B3LYP/aug-cc-pVDZ level.

Element	x-coordinate	y-coordinate	z-coordinate
C	1.4117418932	2.9044089307	0.0000000000
C	-1.4117418932	-2.9044089307	0.0000000000
C	0.0041799984	0.7660565116	0.0000000000
C	-0.0041799984	-0.7660565116	0.0000000000
C	-1.4117418932	-1.3727737070	0.0000000000
C	1.4117418932	1.3727737070	0.0000000000
H	-2.4351796789	-3.3052121616	0.0000000000
H	2.4351796789	3.3052121616	0.0000000000
H	0.8969015349	3.3010651374	0.8877933526
H	0.8969015349	3.3010651374	-0.8877933526
H	-0.8969015349	-3.3010651374	-0.8877933526
H	-0.8969015349	-3.3010651374	0.8877933526
H	1.9633034086	1.0061954512	-0.8807148772
H	1.9633034086	1.0061954512	0.8807148772
H	-1.9633034086	-1.0061954512	-0.8807148772
H	-1.9633034086	-1.0061954512	0.8807148772
H	-0.5486281961	1.1329167712	0.8810845287
H	-0.5486281961	1.1329167712	-0.8810845287
H	0.5486281961	-1.1329167712	-0.8810845287
H	0.5486281961	-1.1329167712	0.8810845287

Table 3.13: Optimized coordinates for C_6H_6 at B3LYP/aug-cc-pVDZ level.

Element	x-coordinate	y-coordinate	z-coordinate
C	0.0000000000	1.3991649914	0.0000000000
C	1.2117124269	0.6995824984	0.0000000000
C	1.2117124269	-0.6995824984	0.0000000000
C	-0.0000000000	-1.3991649914	0.0000000000
C	-1.2117124269	-0.6995824984	0.0000000000
C	-1.2117124269	0.6995824984	0.0000000000
H	0.0000000000	2.4899709887	0.0000000000
H	2.1563781317	1.2449854917	0.0000000000
H	2.1563781317	-1.2449854917	0.0000000000
H	-0.0000000000	-2.4899709887	0.0000000000
H	-2.1563781317	-1.2449854917	0.0000000000
H	-2.1563781317	1.2449854917	0.0000000000

Table 3.14: Optimized coordinates for C_7H_{16} at B3LYP/aug-cc-pVDZ level.

Element	x-coordinate	y-coordinate	z-coordinate
C	-0.0000000000	0.0000000000	0.4933639977
C	0.0000000000	1.2824539951	-0.3450589984
C	-0.0000000000	-1.2824539951	-0.3450589984
C	0.0000000000	2.5651919889	0.4937529975
C	-0.0000000000	-2.5651919889	0.4937529975
C	0.0000000000	3.8422809791	-0.3510539983
C	-0.0000000000	-3.8422809791	-0.3510539983
H	-0.8808449966	0.0000000000	1.1569059933
H	0.8808449966	-0.0000000000	1.1569059933
H	-0.8807809979	1.2832959954	-1.0088579958
H	0.8807809979	1.2832959954	-1.0088579958
H	0.8807809979	-1.2832959954	-1.0088579958
H	-0.8807809979	-1.2832959954	-1.0088579958
H	0.8804729956	2.5635029876	1.1564209918
H	-0.8804729956	2.5635029876	1.1564209918
H	-0.8804729956	-2.5635029876	1.1564209918
H	0.8804729956	-2.5635029876	1.1564209918
H	0.0000000000	4.7415379769	0.2809759988
H	0.8876709963	3.8891939832	-0.9994719955
H	-0.8876709963	3.8891939832	-0.9994719955
H	-0.0000000000	-4.7415379769	0.2809759988
H	-0.8876709963	-3.8891939832	-0.9994719955
H	0.8876709963	-3.8891939832	-0.9994719955

Table 3.15: Optimized coordinates for C_8H_{18} at B3LYP/aug-cc-pVDZ level.

Element	x-coordinate	y-coordinate	z-coordinate
C	0.0001443998	0.7663204334	0.0000000000
C	-0.0001443998	-0.7663204334	0.0000000000
C	-1.4034994132	1.3810182244	0.0000000000
C	1.4034994132	-1.3810182244	0.0000000000
C	-1.4034994132	2.9137216876	0.0000000000
C	1.4034994132	-2.9137216876	0.0000000000
C	-2.8096769075	3.5204696599	0.0000000000
C	2.8096769075	-3.5204696599	0.0000000000
H	0.5554072842	1.1291635448	0.8808825788
H	0.5554072842	1.1291635448	-0.8808825788
H	-0.5554072842	-1.1291635448	0.8808825788
H	-0.5554072842	-1.1291635448	-0.8808825788
H	-1.9593386066	1.0184721190	-0.8809047830
H	-1.9593386066	1.0184721190	0.8809047830
H	1.9593386066	-1.0184721190	-0.8809047830
H	1.9593386066	-1.0184721190	0.8809047830
H	-0.8482570523	3.2750214536	0.8806192231
H	-0.8482570523	3.2750214536	-0.8806192231
H	0.8482570523	-3.2750214536	0.8806192231
H	0.8482570523	-3.2750214536	-0.8806192231
H	-2.7724959855	4.6189389316	0.0000000000
H	-3.3780506209	3.2050558392	-0.8877248454
H	-3.3780506209	3.2050558392	0.8877248454
H	2.7724959855	-4.6189389316	0.0000000000
H	3.3780506209	-3.2050558392	-0.8877248454
H	3.3780506209	-3.2050558392	0.8877248454

Table 3.16: Optimized coordinates for CCl_4 at B3LYP/aug-cc-pVDZ level.

Element	x-coordinate	y-coordinate	z-coordinate
C	0.0000000000	0.0000000000	-0.0000000000
Cl	1.0350569931	1.0350569931	1.0350569931
Cl	-1.0350569931	-1.0350569931	1.0350569931
Cl	-1.0350569931	1.0350569931	-1.0350569931
Cl	1.0350569931	-1.0350569931	-1.0350569931

Table 3.17: Optimized coordinates for $CH_3CH_2OCH_2CH_3$ at B3LYP/aug-cc-pVDZ level.

Element	x-coordinate	y-coordinate	z-coordinate
O	0.0000000000	-0.0000000000	0.2642227051
C	0.0000000000	1.1865515747	-0.5184397180
C	-0.0000000000	-1.1865515747	-0.5184397180
C	0.0000000000	2.3874391950	0.4113255540
C	-0.0000000000	-2.3874391950	0.4113255540
H	0.8914431778	1.2004385235	-1.1740771746
H	-0.8914431778	1.2004385235	-1.1740771746
H	0.8914431778	-1.2004385235	-1.1740771746
H	-0.8914431778	-1.2004385235	-1.1740771746
H	0.0000000000	3.3182084522	-0.1732810052
H	-0.0000000000	-3.3182084522	-0.1732810052
H	-0.8908176533	2.3799537241	1.0536147616
H	0.8908176533	2.3799537241	1.0536147616
H	0.8908176533	-2.3799537241	1.0536147616
H	-0.8908176533	-2.3799537241	1.0536147616

Table 3.18: Optimized coordinates for $CH_3CH_3CH_3N$ at B3LYP/aug-cc-pVDZ level.

Element	x-coordinate	y-coordinate	z-coordinate
C	1.4301584825	1.3015310027	0.0000000000
C	0.0000000000	0.7522020808	0.0000000000
C	-0.0523547839	-0.7828055470	0.0000000000
N	-1.3888931856	-1.3863855100	0.0000000000
H	1.4375099869	2.4002663606	0.0000000000
H	1.9855498702	0.9640298598	0.8878295695
H	1.9855498702	0.9640298598	-0.8878295695
H	-0.5430549600	1.1284852930	0.8825899584
H	-0.5430549600	1.1284852930	-0.8825899584
H	0.4857962577	-1.1672723578	-0.8807717056
H	0.4857962577	-1.1672723578	0.8807717056
H	-1.9193311109	-1.0858092944	-0.8156212862
H	-1.9193311109	-1.0858092944	0.8156212862

Table 3.19: Optimized coordinates for CH_3CHO at B3LYP/aug-cc-pVDZ level.

Element	x-coordinate	y-coordinate	z-coordinate
C	0.0000000000	0.4614089975	0.0000000000
C	-0.9363189979	-0.7159059960	0.0000000000
O	1.2090379918	0.3802709981	0.0000000000
H	-0.4919089975	1.4651219932	0.0000000000
H	-0.3781419980	-1.6590919942	0.0000000000
H	-1.5921699901	-0.6606059987	0.8832849957
H	-1.5921699901	-0.6606059987	-0.8832849957

Table 3.20: Optimized coordinates for CH_3COCH_3 at B3LYP/aug-cc-pVDZ level.

Element	x-coordinate	y-coordinate	z-coordinate
C	-0.0000000000	-0.0000000000	0.1819499989
O	0.0000000000	-0.0000000000	1.3993029956
C	0.0000000000	1.2921539932	-0.6125879985
C	-0.0000000000	-1.2921539932	-0.6125879985
H	0.0686079997	2.1495969903	0.0645899995
H	-0.0686079997	-2.1495969903	0.0645899995
H	0.8387819968	1.3063689948	-1.3246599944
H	-0.9235669967	1.3642589917	-1.2074639965
H	-0.8387819968	-1.3063689948	-1.3246599944
H	0.9235669967	-1.3642589917	-1.2074639965

Table 3.21: Optimized coordinates for CH_3NH_2 at B3LYP/aug-cc-pVDZ level.

Element	x-coordinate	y-coordinate	z-coordinate
C	0.0494859998	0.7074659952	0.0000000000
N	0.0494859998	-0.7591359956	-0.0000000000
H	-0.9512839970	1.1775919960	-0.0000000000
H	0.5931959980	1.0670229955	0.8843329941
H	0.5931959980	1.0670229955	-0.8843329941
H	-0.4392149979	-1.1212419948	-0.8151109954
H	-0.4392149979	-1.1212419948	0.8151109954

Table 3.22: Optimized coordinates for CH_3NHCH_3 at B3LYP/aug-cc-pVDZ level.

Element	x-coordinate	y-coordinate	z-coordinate
N	0.0268779999	0.5812749955	0.0000000000
H	-0.7781969956	1.2015759952	0.0000000000
C	0.0268779999	-0.2219989989	1.2175869925
C	0.0268779999	-0.2219989989	-1.2175869925
H	-0.8034729968	-0.9564209954	1.2711279941
H	-0.8034729968	-0.9564209954	-1.2711279941
H	0.9712669932	-0.7822899961	1.2835669923
H	0.9712669932	-0.7822899961	-1.2835669923
H	-0.0340369998	0.4354559977	2.0949189880
H	-0.0340369998	0.4354559977	-2.0949189880

Table 3.23: Optimized coordinates for CH_3OCH_3 at B3LYP/aug-cc-pVDZ level.

Element	x-coordinate	y-coordinate	z-coordinate
O	-0.0000000000	-0.0000000000	0.5901339988
C	0.0000000000	1.1770739950	-0.1959789989
C	-0.0000000000	-1.1770739950	-0.1959789989
H	0.0000000000	2.0293289917	0.4936159977
H	-0.0000000000	-2.0293289917	0.4936159977
H	0.8973669939	1.2313169926	-0.8391389956
H	-0.8973669939	1.2313169926	-0.8391389956
H	-0.8973669939	-1.2313169926	-0.8391389956
H	0.8973669939	-1.2313169926	-0.8391389956

Table 3.24: Optimized coordinates for CH_3OH at B3LYP/aug-cc-pVDZ level.

Element	x-coordinate	y-coordinate	z-coordinate
C	-0.0465179998	0.6672779973	0.0000000000
O	-0.0465179998	-0.7592479959	0.0000000000
H	-1.0973839927	0.9804009940	0.0000000000
H	0.4416149975	1.0806519968	0.8981439953
H	0.4416149975	1.0806519968	-0.8981439953
H	0.8654099981	-1.0713929938	0.0000000000

Table 3.25: Optimized coordinates for CH_4 at B3LYP/aug-cc-pVDZ level.

Element	x-coordinate	y-coordinate	z-coordinate
C	0.0000000000	0.0000000000	0.0000000000
H	0.6333279984	0.6333279984	0.6333279984
H	-0.6333279984	-0.6333279984	0.6333279984
H	-0.6333279984	0.6333279984	-0.6333279984
H	0.6333279984	-0.6333279984	-0.6333279984

Table 3.26: Optimized coordinates for CO_2 at B3LYP/aug-cc-pVDZ level.

Element	x-coordinate	y-coordinate	z-coordinate
C	0.0000000000	0.0000000000	0.0000000000
O	0.0000000000	0.0000000000	1.1673619952
O	0.0000000000	0.0000000000	-1.1673619952

Table 3.27: Optimized coordinates for COS at B3LYP/aug-cc-pVDZ level.

Element	x-coordinate	y-coordinate	z-coordinate
C	0.0000000000	0.0000000000	-0.5320149952
O	0.0000000000	0.0000000000	-1.6954519930
S	0.0000000000	0.0000000000	1.0472319954

Table 3.28: Optimized coordinates for CO at B3LYP/aug-cc-pVDZ level.

Element	x-coordinate	y-coordinate	z-coordinate
C	0.0000000000	0.0000000000	-0.6480558151
O	0.0000000000	0.0000000000	0.4860418600

Table 3.29: Optimized coordinates for CS_2 at B3LYP/aug-cc-pVDZ level.

Element	x-coordinate	y-coordinate	z-coordinate
C	0.0000000000	0.0000000000	0.0000000000
S	0.0000000000	0.0000000000	1.5701009933
S	0.0000000000	0.0000000000	-1.5701009933

Table 3.30: Optimized coordinates for Cl_2 at B3LYP/aug-cc-pVDZ level.

Element	x-coordinate	y-coordinate	z-coordinate
Cl	0.0000000000	0.0000000000	1.0228319836
Cl	0.0000000000	0.0000000000	-1.0228319836

Table 3.31: Optimized coordinates for H_2CO at B3LYP/aug-cc-pVDZ level.

Element	x-coordinate	y-coordinate	z-coordinate
O	-0.0000000000	-0.0000000000	0.6771249955
C	0.0000000000	0.0000000000	-0.5302049974
H	0.0000000000	0.9463269930	-1.1178839950
H	-0.0000000000	-0.9463269930	-1.1178839950

Table 3.32: Optimized coordinates for H_2O at B3LYP/aug-cc-pVDZ level.

Element	x-coordinate	y-coordinate	z-coordinate
O	0.0000000000	0.0000000000	0.1177929992
H	0.0000000000	0.7642109955	-0.4711729975
H	-0.0000000000	-0.7642109955	-0.4711729975

Table 3.33: Optimized coordinates for H_2S at B3LYP/aug-cc-pVDZ level.

Element	x-coordinate	y-coordinate	z-coordinate
S	0.0000000000	0.0000000000	0.1042529997
H	-0.0000000000	0.9794449930	-0.8340229950
H	-0.0000000000	-0.9794449930	-0.8340229950

Table 3.34: Optimized coordinates for H_2 at B3LYP/aug-cc-pVDZ level.

Element	x-coordinate	y-coordinate	z-coordinate
H	0.0000000000	0.0000000000	0.3806317270
H	0.0000000000	0.0000000000	-0.3806317270

Table 3.35: Optimized coordinates for HBr at B3LYP/aug-cc-pVDZ level.

Element	x-coordinate	y-coordinate	z-coordinate
H	0.0000000000	0.0000000000	-1.3918319924
Br	0.0000000000	0.0000000000	0.0397669998

Table 3.36: Optimized coordinates for HCl at B3LYP/aug-cc-pVDZ level.

Element	x-coordinate	y-coordinate	z-coordinate
Cl	0.0000000000	0.0000000000	0.0719459998
H	0.0000000000	0.0000000000	-1.2230759942

Table 3.37: Optimized coordinates for HF at B3LYP/aug-cc-pVDZ level.

Element	x-coordinate	y-coordinate	z-coordinate
H	0.0000000000	0.0000000000	-0.8331105559
F	0.0000000000	0.0000000000	0.0925678398

Table 3.38: Optimized coordinates for N_2O at B3LYP/aug-cc-pVDZ level.

Element	x-coordinate	y-coordinate	z-coordinate
N	0.0000000000	0.0000000000	-1.2059439932
N	0.0000000000	0.0000000000	-0.0725659997
O	0.0000000000	0.0000000000	1.1186959962

Table 3.39: Optimized coordinates for N_2 at B3LYP/aug-cc-pVDZ level.

Element	x-coordinate	y-coordinate	z-coordinate
N	0.0000000000	0.0000000000	0.5522039682
N	0.0000000000	0.0000000000	-0.5522039682

Table 3.40: Optimized coordinates for NH_3 at B3LYP/aug-cc-pVDZ level.

Element	x-coordinate	y-coordinate	z-coordinate
N	-0.0000000000	-0.0000001000	0.1148519995
H	0.0000000000	0.9439289948	-0.2679869987
H	0.8174665748	-0.4719646477	-0.2679869987
H	-0.8174665748	-0.4719646477	-0.2679869987

Table 3.41: Optimized coordinates for SO_2 at B3LYP/aug-cc-pVDZ level.

Element	x-coordinate	y-coordinate	z-coordinate
S	0.0000000000	-0.0000000000	0.3852949980
O	0.0000000000	1.2684379958	-0.3852949980
O	-0.0000000000	-1.2684379958	-0.3852949980

Table 3.42: Optimized coordinates for SiH_4 at B3LYP/aug-cc-pVDZ level.

Element	x-coordinate	y-coordinate	z-coordinate
Si	0.0000000000	0.0000000000	0.0000000000
H	0.8619639961	0.8619639961	0.8619639961
H	-0.8619639961	-0.8619639961	0.8619639961
H	-0.8619639961	0.8619639961	-0.8619639961
H	0.8619639961	-0.8619639961	-0.8619639961

4

The applications of the ACKS2ω model

Reality is very complex, and our theories are just working models that are designed to understand a certain range of phenomena.

Gerard't Hooft (1946-)

The Journal of Chemical Physics ARTICLE pubs.aip.org/aip/jcp

The significance of fluctuating charges for molecular polarizability and dispersion coefficients

Cite as: J. Chem. Phys. 159, 094111 (2023); doi: 10.1063/5.0163842
Submitted: 19 June 2023 • Accepted: 14 August 2023 •
Published Online: 6 September 2023

View Online Export Citation CrossMark

YingXing Cheng and Toon Verstraelen[a]

AFFILIATIONS

Center for Molecular Modeling (CMM), Ghent University, Technologiepark-Zwijnaarde 46, B-9052 Ghent, Belgium

[a]Author to whom correspondence should be addressed: toon.verstraelen@ugent.be

ABSTRACT

The influence of fluctuating charges or charge flow on the dynamic linear response properties of isolated molecules from the TS42 database is evaluated, with particular emphasis on dipole polarizability and C_6 dispersion coefficients. Two new descriptors are defined to quantify the charge-flow contribution to response properties, making use of the recoupled dipole polarizability to separate isotropic and anisotropic components. Molecular polarizabilities are calculated using the "frequency-dependent atom-condensed Kohn–Sham density functional theory approximated to second order," i.e., the ACKS2ω model. With ACKS2ω, the charge-flow contribution can be constructed in two conceptually distinct ways that appear to yield compatible results. The charge-flow contribution is significantly affected by molecular geometry and the presence of polarizable bonds, in line with previous studies. We show that the charge-flow contribution qualitatively reproduces the polarizability anisotropy. The contribution to the anisotropic C_6 coefficients is less pronounced but cannot be neglected. The effect of fluctuating charges is only negligible for small molecules with at most one non-hydrogen atom. They become important and sometimes dominant for larger molecules or when highly polarizable bonds are present, such as conjugated, double, or triple bonds. Charge flow contributions cannot be explained in terms of individual atomic properties because they are affected by non-local features such as chemical bonding and geometry. Therefore, polarizable force fields and dispersion models can benefit from the explicit modeling of charge flow.

Published under an exclusive license by AIP Publishing. https://doi.org/10.1063/5.0163842

I. INTRODUCTION

Van der Waals (vdW) dispersion interactions are ubiquitous non-bonded forces in molecular systems and materials, playing a crucial role in various applications in chemistry and physics. These interactions are relatively weak compared to bonded forces, yet universally attractive between all atoms due to the coupled motion of electrons at different sites. While classical models for the coupled electronic vibrations exist, only the zero-point oscillations in quantum-mechanical models can explain the persistence of vdW interactions at 0 K.[1] Density functional theory (DFT) is extensively employed in chemistry and physics, particularly for large systems, as it provides a favorable balance between computational accuracy and efficiency compared to more accurate wavefunction methods such as configuration interaction (CI) and coupled cluster (CC). However, one of the main challenges with DFT is its struggle to accurately describe the attractive part of vdW dispersion interactions, also known as long-range correlation energy, necessitating the development of appropriate dispersion corrections.

To address the lack of long-range correlation energy in DFT approximations, several correction terms have been proposed. Prominent correction schemes can be classified into three categories:[2] (i) semiclassical schemes, which apply corrections mainly to the total energy E, (ii) nonlocal, density-based functionals, which incorporate corrections to the electronic potential V, and (iii) one-electron effective potential methods, which rely on a single electron's potential for corrections. This study focuses on the first category, semiclassical schemes, as methods in this group explicitly use C_6 or higher-order dispersion coefficients, which play a significant role in determining the interaction strengths in molecular systems and materials. For more details about methods in other categories, refer to a recent review.[3] In addition, dispersion energy

The Journal of Chemical Physics ARTICLE pubs.aip.org/aip/jcp

calculations have been extensively covered in numerous review articles.[2,4–9]

The first quantum-mechanical dispersion model, by London, applied perturbation theory to the Coulomb interaction between electrons in two polarizable hydrogenic atoms.[10] Building on London's work, the generalized Casimir–Polder (GCP) expression describes dispersion interactions for any pair of molecules A and B.[11] At long distances R, the leading attractive terms are proportional to R^{-6}, R^{-8}, R^{-10}, etc. Molecules are typically treated with a distributed multipole expansion, i.e., they are decomposed into sites, $a \in A$ and $b \in B$, treating each atom or group as a multipole polarizable site. Ignoring intra-molecular coupling and non-local effects, the total dispersion energy is approximated by a simple pairwise-additive form.

$$E = -\sum_{ab} \sum_{n=6,8,10,\cdots} f_n(R_{ab}) \frac{C_n^{ab}}{R_{ab}^n}, \tag{1}$$

where R_{ab} is the distance between atoms a and b, and $f_n(R_{ab})$ is a damping function accounting for short-range phenomena. C_n^{ab} are dispersion coefficients, which can be expressed in terms of the frequency-dependent multipole polarizabilities of sites a and b. As the leading term in Eq. (1), the C_6 dispersion coefficients play a crucial role in determining the strengths of the dispersion interactions in molecular systems and materials. The conventional power laws are employed in most molecular force fields and in empirical dispersion corrections for DFT.[12–14]

The basic pairwise-additive form in Eq. (1) is only an approximation of the complete dispersion interaction between molecules A and B. The errors made by Eq. (1) were classified as different types of non-additivity.[15] Type-A non-additivity arises when atomic C_n coefficients in a molecule deviate from those of isolated atoms.[16] Type-B non-additivity emerges when the presence of a third atom or molecule screens the electrostatic interaction, modifying the dispersion interaction compared to just having molecules A and B in a vacuum. Recent studies have suggested that type-B non-additivity can also be interpreted as a manifestation of electric many-body effects.[17] Type-C non-additivity is observed in low-dimensional nanostructures or metallic systems, where long-range charge fluctuations result in dispersion interactions with non-standard power laws, with a smaller magnitude of the exponent of R.[18]

Semiclassical models with pairwise expressions, such as Eq. (1), including Grimme's DFT + Dn ($n = 1, 2, 3, 4$) schemes,[19–23] the Tkatchenko and Scheffler (TS) method,[13] the exchange-hole dipole moment (XDM) method by Becke and Johnson,[12,24,25] and the local-response dispersion (LRD) model by Sato and Nakai,[26–28] consider type-A non-additive dispersion interactions.[15] However, only a few models partially account for type-B non-additivity, as simple pairwise methods struggle with many-body effects. DFT + D3 and DFT + D4 methods include the three-body Axilrod–Teller–Muto (ATM) term,[29,30] and XDM can describe type-B interactions through electronic many-body effects.[17,31] Although the atomic three-body ATM term can be added in XDM, its contribution is typically small compared to higher-order two-body dispersion terms, suggesting that atomic many-body effects might be negligible.[32,33] A well-known method for fully treating both type-A and type-B non-additive dispersion energy is the many-body dispersion model (MBD),[34–36] based on dipolar coupling between atomic quantum harmonic oscillators. In addition, MBD also exhibits significant deviations from common power laws, which is normally associated with charge flow in type-C dispersion.[37] However, all models mentioned so far treat atoms as local (dipole and optionally higher multipole) polarizable sites, neglecting fluctuating charges or monopoles, which are the leading term of distributed multipole expansion.

Fluctuating charges can contribute significantly to the dispersion energy,[38] and they become essential in systems where the GCP equation is insufficient. For example, dispersion interactions are critically affected by monopolar effects in carbon nanomaterials,[7,39,40] traditional semiconductors,[41,42] and low-dimensional materials.[39,43] In the presence of delocalized bonds, monopolar fluctuations exhibit complex non-local features related to resonance.[44] Charge fluctuations have been used to model specific dispersion interactions, e.g., between infinite wires and slabs,[39,45,46] and in fullerenes and aromatic systems.[47,48] A recent study by Dobson shows that local models, e.g., MBD, cannot capture type-C non-additive dispersion interactions, which are related to long-range charge fluctuations.[40] To further explore the relevance of charge fluctuations, this work focuses on their impact on the polarizability and dispersion interaction of a more general set of molecules or molecular dimers. Understanding the contribution of fluctuating charges to polarizability and C_6 dispersion coefficients is crucial for developing more accurate polarizable force fields and dispersion models that can better describe the behavior of molecular systems and materials.

Previous studies have examined the significant contributions of charge-flow effects on static dipole polarizabilities in various systems, such as silicon clusters,[41,42] water and water-ion clusters,[49,50] hydrated methane sulfonic acid (MSA) clusters,[51] and stoichiometric aluminum phosphide clusters.[52] Recent work has also revealed that these effects can strongly influence the polarizability anisotropy, with the specific partitioning scheme employed further influencing the magnitude of their contribution.[53] Anisotropic polarization naturally leads to dispersion anisotropy, which was recently identified as a driving force for the conformational stability of macromolecules.[54] However, the influence of charge fluctuations on the anisotropy of frequency-dependent polarizabilities and dispersion coefficients has not been fully explored. This paper aims to address this knowledge gap by investigating the impact of charge fluctuations on the anisotropy of frequency-dependent dipole polarizabilities and C_6 dispersion coefficients in a more general set of molecules or molecular dimers.

To accurately investigate the contribution of charge flow to linear-response properties, non-local distributed polarizabilities must be computed. These polarizabilities can be determined using various methods, broadly categorized into two groups. The first group involves numerical partitioning of molecular properties in Hilbert space, such as distributed multipole analysis (DMA),[55] LoProp,[56,57] MoProp,[58] QUAMBO,[59] IAO/QUAO,[60–62] and also methods based on constrained density fitting.[63] While successful in developing useful models for polarization energies and dispersion models, these methods go beyond the scope of the current work. The second category of methods operates in real space by defining distributed multipole operators as products of atom-in-molecule (AIM) weight functions and regular multipole operators. The AIM weight functions determine the proportion of molecular

Published under an exclusive license by AIP Publishing

The Journal of Chemical Physics ARTICLE pubs.aip.org/aip/jcp

density attributed to each atom, using partitioning schemes such as QTAIM,[64,65] (Iterative) Hirshfeld,[66,67] Iterative Stockholder,[68,69] and so on. AIM weight functions directly partition the electron density, which also makes them trivially applicable to the partitioning of density response kernels. In any case, all methods in the two categories can be employed to derive distributed polarizabilities from the interacting linear-response kernel, which can be computationally demanding for large-scale systems.

In this paper, we present an alternative approach to studying the impact of charge flow effects on the frequency-dependent linear-response properties of molecules. Specifically, we utilize a novel polarizable force field called "frequency-dependent atom-condensed Kohn–Sham density functional theory approximated to second order" (ACKS2ω), which was introduced in previous studies.[70–72] This approach partitions both the hardness and non-interacting response kernels and can reproduce response properties with high accuracy. It even captures the correct trends with fluctuating charges alone. We employ ACKS2ω to compute the frequency-dependent response properties, including isotropic and anisotropic dipole polarizabilities and C_6 dispersion coefficients, of all molecules in the TS42 database, which is a diverse selection of organic and inorganic molecules.[13] We then investigate the significance of charge-flow using two descriptors, for isotropic and anisotropic response properties, respectively. Our methodology yields valuable insights into the dominant contributors to the molecular polarizability and C_6 coefficients, shedding light on the role of fluctuating atomic charges in the dynamic linear-response properties of finite systems. Our results can inform the development of more accurate polarizable force fields and dispersion models in the future.

For the definition of response basis functions in the ACKS2ω model, an atoms-in-molecules method is used, analogous to our previous publications.[71,72] Practically, multiple definitions of atoms in molecules exist, each having specific advantages, e.g., in terms of interpretability and robustness. We employ one of these methods in this work, namely Minimal Basis Iterative Stockholder,[73] and slightly different results may be obtained when using another AIM scheme. Still, we believe the general trends will hold across different AIM definitions, as they did in previous studies.[53]

The remainder of this paper is structured as follows: In Section II, we describe the relevant methodology for this study. We begin by defining charge-flow distributed polarizabilities and then introduce the concept of recoupled dipole polarizability, which we use to define the anisotropy of the (frequency-dependent) dipole polarizability. Moreover, we show that anisotropic C_6 coefficients can also be defined using recoupled dipole polarizability. Furthermore, we introduce two descriptors to compute the ratio of charge-flow contribution to various linear-response properties. In Sec. III, we provide computational details on the ACKS2ω model, the reference TD-DFT calculations, and introduce notation to describe the charge flow and other contributions. The results and discussion are presented in Secs. IV and V, respectively. Finally, a summary is given in Sec. VI. Atomic units are used throughout.

II. METHODS

In this section, we introduce the theory used in this work. First, we describe charge-flow distributed polarizabilities, as defined in Ref. 74. Next, we introduce recoupled dipole polarizabilities to define the anisotropy of dipole polarizability and C_6 dispersion coefficients. Finally, we introduce two descriptors to study the charge-flow contribution to dipole polarizability and C_6 coefficients.

A. Charge-flow contribution to the polarizability

The response of a molecule's charge density $\Delta\rho(\boldsymbol{r}',\omega)$ to an external field $V(\boldsymbol{r},\omega)$ at position $\boldsymbol{r}$ can be described by the density response function $\chi(\boldsymbol{r},\boldsymbol{r}',\omega)$, which quantifies the change in charge density at position $\boldsymbol{r}'$. This relationship can be expressed by the following equation:

$$\Delta\rho(\boldsymbol{r}',\omega) = -\int d\boldsymbol{r} V(\boldsymbol{r},\omega)\chi(\boldsymbol{r},\boldsymbol{r}',\omega). \tag{2}$$

One way to represent an external potential is through real spherical harmonics $R_{\ell\kappa}(\boldsymbol{r})$ and their corresponding fields $V_{\ell\kappa}(\omega)$ as $\sum_{\ell\kappa} R_{\ell\kappa}(\boldsymbol{r})V_{\ell\kappa}(\omega)$, following Stone's notation.[38] With this representation, the change in charge density can be expressed as

$$\Delta\rho(\boldsymbol{r}',\omega) = -\int \chi(\boldsymbol{r},\boldsymbol{r}',\omega)\sum_{\ell\kappa} R_{\ell\kappa}(\boldsymbol{r})V_{\ell\kappa}(\omega)d\boldsymbol{r}, \tag{3}$$

and the response multipole moments related to $R_{\ell'\kappa'}(\boldsymbol{r}')$ are

$$\Delta\mu_{\ell'\kappa'}(\omega) = \int d\boldsymbol{r}'\Delta\rho(\boldsymbol{r}',\omega)R_{\ell'\kappa'}(\boldsymbol{r}'). \tag{4}$$

As a result, the spherical-tensor polarizability $\alpha_{\ell\kappa,\ell'\kappa'}(\omega)$ can be determined through the following equation:

$$\alpha_{\ell\kappa,\ell'\kappa'}(\omega) = \int R_{\ell\kappa}(\boldsymbol{r})\chi(\boldsymbol{r},\boldsymbol{r}',\omega)R_{\ell'\kappa'}(\boldsymbol{r}')d\boldsymbol{r}d\boldsymbol{r}'. \tag{5}$$

The molecular dipole polarizability, represented as a 3×3 matrix, can be obtained with $\ell=\ell'=1$.

The radius of convergence of single-site molecular polarizability is limited by the largest distance between the molecular center and a point inside the molecule.[74] To overcome this limitation, distributed polarizabilities have been proposed, where a molecule is divided into atomic regions, and the potential is expanded using multipoles or Taylor series about each local center. The external potential can then be expressed as the sum of the potentials of the regions. The spherical-tensor form, similar to Eq. (5), is used, and the external potential can be written as follows:

$$V(\boldsymbol{r},\omega) = \sum_a w_a(\boldsymbol{r})\sum_{\ell\kappa} R_{\ell\kappa}(\boldsymbol{r}-\boldsymbol{R}^a)V^a_{\ell\kappa}(\omega), \tag{6}$$

where $w_a(\boldsymbol{r})$ is the AIM weight function $[0\le w_a(\boldsymbol{r})\le 1]$ that determines which portion of the total electron density is attributed to atom a. Within each atom a, a standard multipole expansion is used with fields $V^a_{\ell\kappa}(\omega)$ and spherical harmonics $R_{\ell\kappa}$, which use $\boldsymbol{R}^a$, the nucleus of atom a, as origin.[38]

The distributed polarizability is defined by the following expression:[75]

$$\alpha^{aa'}_{\ell\kappa,\ell'\kappa'}(\omega) = \iint d\boldsymbol{r}d\boldsymbol{r}' Q^a_{\ell\kappa}(\boldsymbol{r})\chi(\boldsymbol{r},\boldsymbol{r}',\omega)Q^b_{\ell'\kappa'}(\boldsymbol{r}'), \tag{7}$$

where $Q^a_{\ell\kappa}(\boldsymbol{r}) = w_a(\boldsymbol{r})R_{\ell\kappa}(\boldsymbol{r}-\boldsymbol{R}^a)$ is the distributed multipole operator with rank $\ell\kappa$ of atom a.

Published under an exclusive license by AIP Publishing

The Journal of Chemical Physics ARTICLE pubs.aip.org/aip/jcp

For a homogeneous electric field along the x axis, the multipole expansion is given by

$$x = \sum_a w_a(\boldsymbol{r}) X^a + \sum_a w_a(\boldsymbol{r})(x - X^a), \tag{8}$$

where X^a is the x-component of atomic coordinate $\boldsymbol{R}^a$. With this decomposition of a homogeneous field, distributed contributions to the dipole polarizability can be defined, for which a more convenient notation than that of Eq. (7) can be used. The frequency-dependent charge-flow, charge-dipole, and dipole-only distributed polarizabilities are defined, respectively, as

$$\alpha_{00}^{ab}(\omega) = \int d\boldsymbol{r} d\boldsymbol{r}' w_a(\boldsymbol{r}) \chi(\boldsymbol{r}, \boldsymbol{r}', \omega) w_b(\boldsymbol{r}') \tag{9}$$

$$\alpha_{0j}^{ab}(\omega) = \int d\boldsymbol{r} d\boldsymbol{r}' w_a(\boldsymbol{r}) \chi(\boldsymbol{r}, \boldsymbol{r}', \omega) w_b(\boldsymbol{r}') (\boldsymbol{r}_j - \boldsymbol{R}_j^b) \tag{10}$$

$$\alpha_{ij}^{ab}(\omega) = \int d\boldsymbol{r} d\boldsymbol{r}' w_a(\boldsymbol{r}) (\boldsymbol{r}_i - \boldsymbol{R}_i^a) \chi(\boldsymbol{r}, \boldsymbol{r}', \omega) w_b(\boldsymbol{r}') (\boldsymbol{r}_j - \boldsymbol{R}_j^b), \tag{11}$$

where i or j represents x, y, or z. The total molecular polarizability $\alpha_{ij}(\omega)$ is reconstructed from these contributions with[38]

$$\alpha_{ij}(\omega) = \sum_{ab} (\boldsymbol{R}_i^a \boldsymbol{R}_j^b \alpha_{00}^{ab}(\omega) + \boldsymbol{R}_i^a \alpha_{0j}^{ab}(\omega) + \boldsymbol{R}_j^b \alpha_{i0}^{ab}(\omega) + \alpha_{ij}^{ab}(\omega)). \tag{12}$$

In this study, we investigate the charge-flow contribution to the distributed polarizability of molecules, specifically the α_{00}^{ab} term. We define the charge-flow (CF) contribution to the molecular dipole polarizability as follows:[49–52,76–79]

$$\alpha_{ij}^{\mathrm{CF}} = \sum_{ab} \boldsymbol{R}_i^a \boldsymbol{R}_j^b \alpha_{00}^{ab} \tag{13}$$

This definition differs from that used in previous work by Jackson and co-workers,[41,42,53] where the CF contribution is defined as

$$\alpha_{ij}^{\mathrm{CF}} = \sum_a R_i^a \int w_a(\boldsymbol{r}) \Delta\rho_j(\boldsymbol{r}) d\boldsymbol{r} = \sum_{ab} (\boldsymbol{R}_i^a \boldsymbol{R}_j^b \alpha_{00}^{ab} + \boldsymbol{R}_i^a \alpha_{0j}^{ab}). \tag{14}$$

In the above-mentioned equation, $\Delta\rho_j(\boldsymbol{r})$ is the response density resulting from a homogeneous electric field applied along the j axis. Our focus, however, is solely on the charge-flow contribution described by Eq. (13).

B. Recoupled dipole polarizability

The definition of dipole polarizability in Eq. (5) uses two spherical harmonics, which can be expressed more elegantly using single harmonics, as has been extensively covered in previous studies.[38,80] We provide a brief summary of this concept here for the sake of clarity, and the frequency is omitted in this subsection for simplicity.

The components α_{LK} of the recoupled dipole polarizability are defined as

$$\begin{bmatrix} \alpha_{00} \\ \alpha_{20} \\ \alpha_{21c} \\ \alpha_{21s} \\ \alpha_{22c} \\ \alpha_{22s} \end{bmatrix} = \sqrt{\frac{2}{3}} \begin{bmatrix} -\frac{\sqrt{2}}{2} & 0 & 0 & -\frac{\sqrt{2}}{2} & 0 & -\frac{\sqrt{2}}{2} \\ -\frac{1}{2} & 0 & 0 & -\frac{1}{2} & 0 & 1 \\ 0 & 0 & \sqrt{3} & 0 & 0 & 0 \\ 0 & 0 & 0 & 0 & \sqrt{3} & 0 \\ \frac{\sqrt{3}}{2} & 0 & 0 & -\frac{\sqrt{3}}{2} & 0 & 0 \\ 0 & \sqrt{3} & 0 & 0 & 0 & 0 \end{bmatrix} \begin{bmatrix} \alpha_{xx} \\ \alpha_{xy} \\ \alpha_{xz} \\ \alpha_{yy} \\ \alpha_{yz} \\ \alpha_{zz} \end{bmatrix}, \tag{15}$$

where L can be either 0 or 2 and K can be 0, 1c, 1s, 2c, or 2s. (See Ref. 38 for more details.).

The isotropic dipole polarizability, denoted as α^{iso} or $\bar{\alpha}$, can be expressed in terms of the component α_{00} as

$$\alpha^{\mathrm{iso}} = \frac{1}{3}(\alpha_{xx} + \alpha_{yy} + \alpha_{zz}) = -\sqrt{\frac{1}{3}} \alpha_{00}. \tag{16}$$

The anisotropic dipole polarizability, denoted as $\vec{\alpha}$, is a vector composed of all elements α_{LK} with $L = 2$. It can be written as

$$\vec{\alpha} = \sqrt{\frac{1}{3}} (\alpha_{20}, \alpha_{21c}, \alpha_{21s}, \alpha_{22c}, \alpha_{22s}), \tag{17}$$

where $\sqrt{\frac{1}{3}}$ is a new prefactor instead of $\sqrt{\frac{3}{2}}$ in Ref. 38, in order to maintain consistency with the definition of isotropic dipole polarizability using recoupled polarizability. The anisotropy of the dipole polarizability, denoted as $\|\vec{\alpha}\|$, is defined as[38]

$$\begin{aligned} \|\vec{\alpha}\|^2 &= \frac{1}{3} \sum_q |\alpha_{2q}|^2 \\ &= \frac{2}{3}(\alpha_{xy}^2 + \alpha_{xz}^2 + \alpha_{yz}^2) + \frac{1}{9}\big[(\alpha_{xx} - \alpha_{yy})^2 \\ &\quad + (\alpha_{xx} - \alpha_{zz})^2 + (\alpha_{yy} - \alpha_{zz})^2\big], \end{aligned} \tag{18}$$

where the summation is taken over all K values associated with $L = 2$ in Eq. (15). It should be noted that anisotropy can be defined in terms of the tensor eigenvalues, which have the same form as Eq. (18) without the off-diagonal elements.[53,81,82] However, both definitions are equivalent, and Eq. (18) can be systematically extended to define the anisotropy of higher-multipole polarizabilities. Thus, we use Eq. (18) as the definition of anisotropy in this work.

C. C_6 dispersion coefficients

The C_6 dispersion coefficients of a pair of molecules are expressed in terms of the frequency-dependent polarizabilities of the individual molecules, as shown in Ref. 80,

$$C_6(L_A L_B J; K_A K_B) = N(L_A, L_B, J) \int_0^\infty \alpha_{L_A K_A}^A(iv) \alpha_{L_B K_B}^B(iv) dv, \tag{19}$$

where $|L_A - L_B| \le J \le L_A + L_B$, and A and B refer to the molecules. According to previous work,[38,80,83] C_6 with an odd J is negligible, so

Published under an exclusive license by AIP Publishing

The Journal of Chemical Physics ARTICLE pubs.aip.org/aip/jcp

we only consider C_6 with an even J. The prefactor N depends on L_A, L_B, and J, and its values are shown in Table I.

The isotropic C_6 coefficient, denoted as C_6^{iso}, can be expressed as $C_6(000;00)$,

$$C_6^{\text{iso}} = C_6(000;00) = \frac{3}{\pi}\int_0^\infty \tilde{\alpha}^A(iv)\tilde{\alpha}^B(iv)\,dv. \tag{20}$$

In analogy to the dipole polarizability in Sec. II B, the anisotropic C_6 coefficients are collected in a vector $\vec{C}_6$, which comprises all elements $C_6(L_AL_BJ;L_AL_B)$ that satisfy the condition $L_A + L_B + J \neq 0$. When $L_A = 0$ ($L_B = 0$), the K_A (K_B) is restricted to 0, whereas for $L_A = 2$ ($L_B = 2$), the possible values for K_A (K_B) include 00, 20, 21c, 21s, 22c, and 22s. Consequently, $\vec{C}_6$ encompasses 85 distinct components. The anisotropy of C_6, denoted as $\|\vec{C}_6\|$, is defined analogously to $\|\vec{\alpha}\|$,

$$\|\vec{C}_6\|^2 = \sum_{L_A+L_B+J\neq 0} |C_6(L_AL_BJ;K_AK_B)|^2. \tag{21}$$

Using the definition in Eq. (19), the long-range dispersion energy, which accounts for molecular polarizability anisotropy, is given by

$$E = -\sum_{n=6,8,10,\cdots}\frac{1}{R_{AB}^n}\sum_{L_AL_BJ}\sum_{K_AK_B} C_n^{AB}(L_AL_BJ;K_AK_B)\tilde{S}^{K_AK_B}_{L_AL_BJ} \tag{22}$$

where $\tilde{S}^{K_AK_B}_{L_AL_BJ}$ depends on the relative orientation between molecules A and B.[80]

D. Descriptors to quantify different contributions to polarizability and dispersion

In this study, the dipole polarizability or dispersion coefficients will be computed with different forms of the ACKS2 model. As explained below in Sec. III, ACKS2 allows us to isolate specific contributions, such as charge flow, to these quantities. The importance of a contribution, for any given molecule, will be quantified with the descriptors defined in this section. For the definition of these descriptors, the generic symbols X^{iso}, $\vec{X}$ and $\|\vec{X}\|^2$ are used, where X could refer to polarizability or dispersion coefficients, presented in Secs. II B and II C, respectively. The subscript c is added to denote a contribution of interest: X_c^{iso}, $\vec{X}_c$ and $\|\vec{X}_c\|^2$. The absence of a subscript in X, or the subscript "ref," will be used to refer to the reference result computed directly with TD-DFT. Plots and statistical properties of the descriptors will used to summarize the detailed results for the entire TS42 database.[13] The relevant dimensionless descriptors are defined as follows:

TABLE I. The factor $N(L_A, L_B, J)$.

L_A	L_B	J	$N(L_A, L_B, J)$
0	0	0	$1/\pi$
0	2	2	$-\sqrt{2}/2\pi$
2	0	2	$-\sqrt{2}/2\pi$
2	2	0	$1/10\pi$
2	2	2	$1/7\pi$
2	2	4	$54/35\pi$

- The descriptor s quantifies the isotropic part of contribution c relative to its reference value

$$s_c[X] = \frac{X_c^{\text{iso}}}{X^{\text{iso}}}. \tag{23}$$

  Because the isotropic property in the denominator of $s_c[X]$ is always non-zero in practice, this ratio is well-defined.
- The fractional anisotropy of a property X, which is independent of the contribution being considered:

$$u[X] = \frac{\|\vec{X}\|^2}{\|\vec{X}\|^2 + (X^{\text{iso}})^2}. \tag{24}$$

  For symmetric molecules, $u[X]$ may become zero. This descriptor will be analyzed as such to illustrate the overall anisotropy of the molecular properties under study.
- The scalar product of $\vec{X}$ and a contribution c to $\vec{X}$, normalized in the same way as $u[X]$,

$$u_c^{\parallel}[X] = \frac{\vec{X}\cdot\vec{X}_c}{\|\vec{X}\|^2 + (X^{\text{iso}})^2}. \tag{25}$$

  The term $(X^{\text{iso}})^2$ is included in the denominator to avoid divisions by zero for molecules lacking anisotropy. The superscript $\parallel$ indicates that this descriptor only considers the contribution of vector $\vec{X}_c$ along the vector $\vec{X}$. This descriptor is ideally close to $u[X]$.

Because $u[X]$ may become zero for symmetric molecules, the descriptor $u_c^{\parallel}[X]$ cannot be safely normalized on $u[X]$. Moreover, $u[X]$ can be interpreted as $u_c^{\parallel}[X]$ when $\vec{X}_c = \vec{X}$. The notation $u_{\text{ref}}^{\parallel}[X]$ is used to represent $u[X]$ in the remainder of the text, to emphasize that it is the reference value that includes all contributions.

Note that the descriptor $u[X]$ is guaranteed to lie in the interval $[0,1]$. The two other descriptors, $s_c[X]$ and $u_c^{\parallel}[X]$, can be interpreted on the same scale but are not guaranteed to remain within the $[0,1]$ interval, of which some examples can be found in the results.

III. COMPUTATIONAL DETAILS

In this study, we investigated the impact of charge flow on dipole polarizabilities and C_6 coefficients, including their anisotropies, for all molecules in the TS42 database. The LDA/aug-cc-pVDZ level of theory[84,85] was used for all response calculations, as it resulted in a good correspondence with experimental data in our previous work.[72]

The frequency-dependent dipole polarizabilities were computed using the ACKS2ω model with bi-orthogonal atomic potential and density basis sets, as described in Ref. 72: The potential basis set consists of distributed multipole operators defined with MBIS partitioning,[73] and the density basis set is derived from a Fukui function and the non-interacting response to the distributed multipole operators. To isolate the contribution of charge flow to the molecular dipole polarizability, $\ell_{\max}$ was set to 0 in the construction of the basis functions for ACKS2, which is denoted as contribution $c = 0$. The charge and dipole contributions to the molecular dipole polarizability were computed by setting $\ell_{\max} = 1$, which is denoted as contribution $c = 1$. Further exploration of $\ell_{\max} > 1$ is not expected

Published under an exclusive license by AIP Publishing

The Journal of Chemical Physics ARTICLE pubs.aip.org/aip/jcp

to yield qualitatively different results because the ACKS2 model with $\ell_{\max} = 1$ already quantitatively reproduces a frequency-dependent linear response, as shown in the results.[72] We defined more fine-grained contributions to the $\ell_{\max} = 1$ result by considering the four terms in Eq. (12): the first is due to charge flow, labeled $c = 1(0)$, the second and third terms are due to charge-dipole interactions, labeled $c = 1(1)$, and the last is due to dipole-only fluctuations, labeled $c = 1(2)$. One would not expect qualitative differences between $c = 0$ and $c = 1(0)$ *a priori* as they are two slightly different ways of modeling the charge-flow contribution to the polarizability.

TABLE II. Overview of all considered contributions c to the dipole polarizability and the dispersion coefficient. For the ACKS2ω model with $\ell_{\max} = 1$, the contributions to the response are further decomposed by grouping terms in Eq. (12): charge-flow (first term), charge-dipole (second and third term), and dipole–dipole (fourth term). For the dispersion coefficient, this classification of terms must be applied to both molecules A and B in the dimer. Symmetrically equivalent cases are combined into one contribution.

Quantity	Contribution c	Model	Molecule A	Molecule B
Polarizability α	Ref	TD-DFT reference		
	0	ACKS2ω $\ell_{\max} = 0$	All	⋯
	1	$\ell_{\max} = 1$	All	⋯
	1(0)	$\ell_{\max} = 1$	Charge-flow	⋯
	1(1)	$\ell_{\max} = 1$	Charge-dipole	⋯
	1(2)	$\ell_{\max} = 1$	Dipole-dipole	⋯
Dispersion C_6	Ref	TD-DFT reference		
	0	ACKS2ω $\ell_{\max} = 0$	All	All
	1	$\ell_{\max} = 1$	All	All
	1(00)	$\ell_{\max} = 1$	Charge-flow	Charge-flow
	1(01)	$\ell_{\max} = 1$	Charge-flow	Charge-dipole
	1(02)	$\ell_{\max} = 1$	Charge-flow	Dipole-dipole
	1(11)	$\ell_{\max} = 1$	Charge-dipole	Charge-dipole
	1(12)	$\ell_{\max} = 1$	Charge-dipole	Dipole-dipole
	1(22)	$\ell_{\max} = 1$	Dipole-dipole	Dipole-dipole

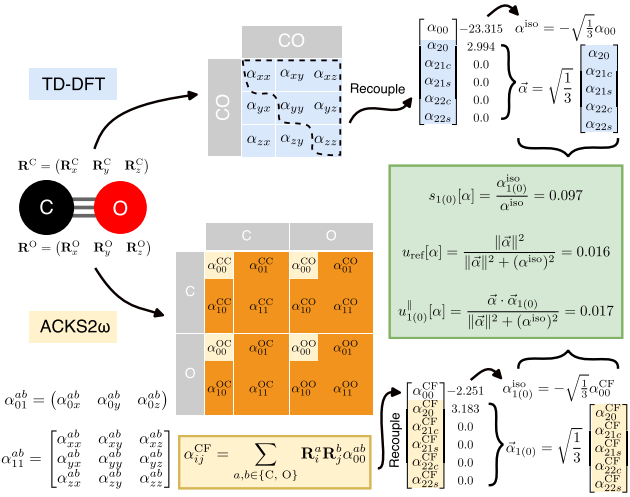

FIG. 1. The computational workflow to derive the polarizability descriptors from the TD-DFT and ACKS2ω ($\ell_{\max} = 1$) frequency-dependent polarizability tensors for the case of carbon monoxide. See the text for details.

Published under an exclusive license by AIP Publishing

The Journal of Chemical Physics ARTICLE pubs.aip.org/aip/jcp

The integral in Eq. (19) was evaluated using the Gaussian–Legendre quadrature with 12 imaginary frequencies to calculate C_6 coefficients. The same frequencies were also used to study the relative charge-flow contribution to the frequency-dependent dipole polarizabilities. Because C_6 is calculated from two molecular dipole polarizabilities, the integer indices 0, 1, and 2 to classify multipole contributions in Eq. (12) appear twice, once for molecule A and once for molecule B, leading to six

TABLE III. Isotropic descriptors $s_c[\alpha(0)]$ for all molecules in the TS42 database for each contribution c, as documented in Table II.

Molecule	$s_0[\alpha(0)]$	$s_1[\alpha(0)]$	$s_{1(0)}[\alpha(0)]$	$s_{1(1)}[\alpha(0)]$	$s_{1(2)}[\alpha(0)]$
C_8H_{18}	0.417	0.988	0.429	0.218	0.341
C_7H_{16}	0.404	0.988	0.415	0.224	0.349
C_6H_6	0.404	0.965	0.414	0.204	0.348
C_6H_{14}	0.387	0.987	0.398	0.230	0.359
C_5H_{12}	0.365	0.986	0.377	0.238	0.372
$CH_3CH_2OCH_2CH_3$	0.358	0.985	0.368	0.230	0.388
$C_4H_{10}O$	0.354	0.983	0.365	0.234	0.384
C_4H_{10}	0.337	0.986	0.348	0.248	0.391
C_4H_8	0.336	0.984	0.347	0.260	0.377
C_3H_7OH	0.322	0.982	0.332	0.242	0.408
$CH_3CH_3CH_3N$	0.318	0.981	0.329	0.244	0.408
CH_3COCH_3	0.312	0.974	0.329	0.222	0.422
C_3H_6	0.309	0.975	0.319	0.222	0.434
C_3H_8	0.299	0.985	0.308	0.258	0.419
CCl_4	0.299	0.905	0.303	0.126	0.475
CH_3OCH_3	0.284	0.982	0.292	0.254	0.437
CH_3CHO	0.273	0.970	0.291	0.224	0.456
CH_3NHCH_3	0.283	0.981	0.291	0.260	0.430
C_2H_5OH	0.278	0.980	0.286	0.248	0.447
CS_2	0.267	0.899	0.276	0.140	0.484
N_2O	0.235	0.934	0.270	0.162	0.504
CO_2	0.214	0.957	0.258	0.152	0.548
C_2H_6	0.249	0.984	0.257	0.264	0.463
C_2H_4	0.236	0.970	0.244	0.220	0.506
COS	0.218	0.922	0.242	0.128	0.552
SiH_4	0.235	0.975	0.242	0.194	0.540
SO_2	0.217	0.923	0.236	0.140	0.547
H_2CO	0.211	0.967	0.225	0.224	0.517
CH_3NH_2	0.215	0.978	0.222	0.254	0.503
CH_3OH	0.212	0.978	0.219	0.248	0.510
C_2H_2	0.183	0.966	0.190	0.176	0.600
Cl_2	0.156	0.894	0.156	0.108	0.631
CH_4	0.148	0.983	0.151	0.246	0.585
N_2	0.104	0.941	0.114	0.148	0.681
CO	0.090	0.932	0.097	0.120	0.715
H_2S	0.083	0.932	0.086	0.130	0.716
NH_3	0.078	0.972	0.080	0.190	0.703
H_2O	0.063	0.971	0.065	0.178	0.727
H_2	0.061	0.993	0.062	0.184	0.748
HBr	0.051	0.930	0.053	0.074	0.803
HCl	0.046	0.926	0.047	0.078	0.801
HF	0.045	0.973	0.047	0.134	0.791
Min.	0.045	0.894	0.047	0.074	0.341
Max.	0.417	0.993	0.429	0.264	0.803
Mean	0.237	0.964	0.247	0.197	0.520

Published under an exclusive license by AIP Publishing

The Journal of Chemical Physics ARTICLE pubs.aip.org/aip/jcp

categories of contributions to the dispersion coefficients, labeled as 1(00), 1(01), 1(02), 1(11), 1(12), or 1(22). There is no distinction between, e.g., 1(01) and 1(10), because all $N^2 = 1764$ molecular dimers were considered to collect the statistics, as opposed to only the unique $N(N+1)/2 = 903$ pairs in our previous work.[72] Table II provides an overview of all possible contributions to the polarizability and the dispersion coefficients.

All calculations were performed using the Horton package,[86] using the methodology described in Ref. 72. Reference TD-DFT calculations were performed with Dalton 2020.[87]

Figure 1 shows the computational workflow to obtain the above-mentioned descriptors, for the case of the static dipole polarizability of carbon monoxide. The upper part (blue boxes) represents the processing of TD-DFT reference results: by recoupling the Cartesian tensors, the isotropic and anisotropic components are separated, which are then used as input for the descriptors (the green box). The lower part (yellow and orange boxes) shows the ACKS2ω branch, whose main difference is the additional decomposition of the dipole polarizability to isolate different contributions, here charge flow [CF, $c = 1(0)$]. In addition, the recoupled ACKS2ω tensors are used as input for the descriptors (the green box). A similar workflow is used for dispersion coefficients, for which frequency-dependent polarizabilities at multiple imaginary frequencies are combined.

IV. RESULTS

A. Isotropic dipole polarizability

Table III presents the values of $s_c[\alpha(0)]$, i.e., the static case, for various contributions c. Supplementary material Tables S1–S12 show similar results at other imaginary frequencies. Figure 2 shows violin plots of $s_c[\alpha(0)]$ for different contributions c.

The charge-flow descriptors $s_0[\alpha(0)]$ (average 0.237) and $s_{1(0)}[\alpha(0)]$ (average 0.247) are very close. Except for slight differences, all results for $c = 0$ and $c = 1(0)$ are consistent, confirming that these are two comparable definitions of the charge-flow contribution. Any deviation between the two is due to the difference

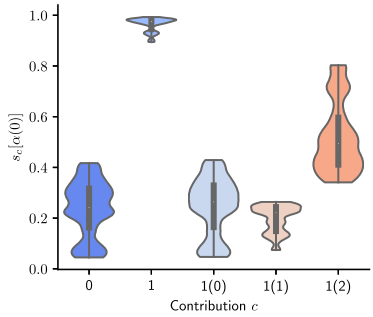

FIG. 2. Violin plots of the distribution of the isotropic descriptor for the static polarizability, $s_c[\alpha(0)]$, for all TS42 molecules, grouped by contribution c, as documented in Table II.

in ACSK2 basis set for $\ell_{max} = 0$ and $\ell_{max} = 1$. These values also show that the charge-flow contribution has an incomplete but non-negligible contribution to the isotropic polarizability. As mentioned above, the charge-flow contribution reported here is typically smaller than in some previous studies.[41,42,53] This difference arises from the distinct definitions of charge flow and the AIM schemes applied in prior studies, as detailed in Sec. II.

The average $s_1[\alpha(0)]$ value (0.964) approaches 1.0, indicating that the molecular dipole polarizability can be accurately predicted by considering both atomic fluctuating charges and dipoles. Such results are in accordance with previous research.[71,72] The charge-dipole contribution, $s_{1(1)}[\alpha(0)]$, is generally limited, yielding an average value of 0.197, while the dipole-only contribution has the main contribution with an average value of 0.520. Violin plots of $s_c[\alpha(\omega)]$ for other frequencies can be found in Fig. S1.

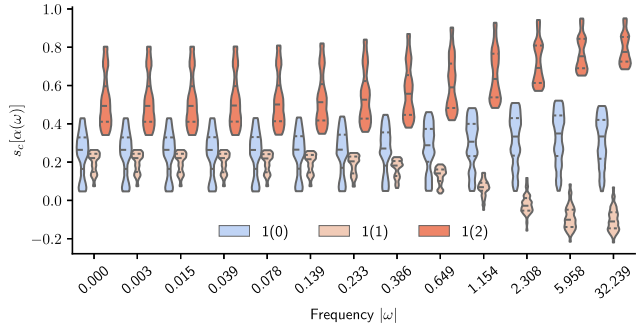

FIG. 3. The dependence on the frequency of the isotropic descriptor for the polarizability, $s_c[\alpha(\omega)]$, for the charge-flow [$c = 1(0)$], charge-dipole [$c = 1(1)$], and dipole-only [$c = 1(2)$], contributions.

Published under an exclusive license by AIP Publishing

The Journal of Chemical Physics ARTICLE pubs.aip.org/aip/jcp

Figure 3 further shows the dependence of $s_{1(0)}[\alpha(\omega)]$, $s_{1(1)}[\alpha(\omega)]$, and $s_{1(2)}[\alpha(\omega)]$ on the imaginary frequency. We observe a slight increase in the contribution of charge flow with increasing $|\omega|$, except for the highest frequency. Interestingly, a similar trend can be identified in the dipole-only contribution, where the increase is more pronounced than in the charge-flow case. Considering that the sum of charge-flow, dipole-only, and charge-dipole contributions nearly equals unity, the charge-dipole contribution, $s_{1(1)}[\alpha(\omega)]$, decreases with increasing $|\omega|$ as shown in Fig. 3, attaining a negative average value when $|\omega| \geq 2.308$. As $|\omega|$ increases, the difference between charge-flow and dipole-only contributions also increases, causing the contribution of charge-flow to fall below that of dipole-only in high-frequency cases for all molecules when $|\omega| \geq 1.154$. Overall, the frequency dependence is small, and the role of charge-flow remains comparable over the entire range of tested frequencies.

Figure 4 shows scatter plots of $s_{1(0)}[\alpha(0)]$ and $s_{1(2)}[\alpha(0)]$ as a function of the number of non-hydrogen atoms. We note that the contribution of charge flow increases with the number of non-hydrogen atoms, while that of the dipole only decreases. This trend also holds for nonzero frequencies, as shown in Fig. S2. In the static case, the contribution of charge flow overtakes that of the dipole only when the number of non-hydrogen atoms in the TS42 database exceeds 5. For small molecules, most notably HF, HCl, and HBr, the isotropic dipole-only descriptor, $s_{1(2)}[\alpha(0)]$, is close to 1, while other contributions remain negligible. This is likely due to the limited number of non-hydrogen atoms in these molecules, which restricts charge exchange between atoms. Molecules with longer chains (e.g., C_6H_{14}, C_7H_{16}, and C_8H_{18}) or π-conjugated systems (e.g., C_6H_6) have the largest charge-flow contributions. This can be traced back to the larger number of non-hydrogen atoms in these molecules and the delocalized bonds, which are known to be highly polarizable. These results confirm that charge flow varies with molecular topology and chemical bonding, which is consistent with the use of atom-condensed response kernels for the characterization of chemical bonding.[44]

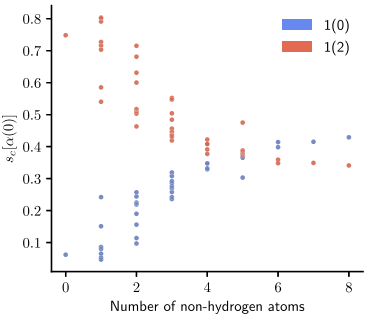

FIG. 4. The distributions of the isotropic descriptor for the static polarizability, $s_c[\alpha(0)]$, for the charge-flow $[c = 1(0)]$ and dipole-only $[c = 1(2)]$ contributions, grouped by the number of non-hydrogen atoms in the TS42 molecules.

B. Anisotropy of dipole polarizability

Table IV details the $u_c^{\|}[\alpha(0)]$ values of (static) anisotropic polarizability. Tables S13–S24 show analogous results for other frequencies. Figure 5 shows the violin plots of the $u_c^{\|}[\alpha(0)]$ values for different contributions c. Similar violin plots of $u_c^{\|}[\alpha(\omega)]$ at higher frequencies can be found in Fig. S3. In addition, the results of $\|\alpha_c(\omega)\|$ for all frequencies studied are presented in Tables S25–S37.

The average values of $u_0^{\|}[\alpha(0)]$ (0.032) and $u_{1(0)}^{\|}[\alpha(0)]$ (0.034) are close to the reference result $u_{\text{ref}}[\alpha(0)]$ (0.035). Both approaches to isolate the charge-flow contribution are again consistent. The reference is qualitatively reproduced by the charge-flow result, meaning that charge-flow contributions can explain most of the anisotropy of the static dipole polarizability. On average, the charge-dipole and dipole–dipole effects also contribute, but they compensate each other to a large extent.

The descriptor $u_c^{\|}[\alpha]$ is designed to have a meaningful sign that reveals whether contribution c is pointing in the right direction. However, a good correspondence between $u_c^{\|}[\alpha]$ and $u_{\text{ref}}^{\|}[\alpha]$ is only a necessary condition for contribution c to fully explain the reference. Because this descriptor is defined as a scalar product, it is insensitive to contributions orthogonal to the reference. To further support our claim that the anisotropy is qualitatively reproduced by the charge-flow contribution, we verified that the following inequality holds for all molecules and all imaginary frequencies up to $0.386 \times i$:

$$\frac{\|\vec{\alpha}_{1(0)}(\omega) - \vec{\alpha}(\omega)\|^2}{\|\vec{\alpha}(\omega)\|^2 + (\alpha^{\text{iso}}(\omega))^2} \leq 0.02. \tag{26}$$

The term $(\alpha^{\text{iso}}(\omega))^2$ in the denominator is included to avoid (near) division by zero for molecules lacking anisotropy in the reference calculation. For imaginary frequencies with a larger magnitude, the charge flow and other contributions do not vanish as quickly, as mentioned in the previous paragraph, thereby making larger relative errors.

All $u_0^{\|}[\alpha(0)]$ and $u_{1(0)}^{\|}[\alpha(0)]$ values are positive, while all $u_{1(2)}^{\|}[\alpha(0)]$ values are negative, except for NH_3 and H_2S. Similar to other molecules with a single non-hydrogen atom, these two are only weakly anisotropic. Unlike other molecules, the charge-flow and charge-dipole contributions to the anisotropy have the wrong sign. These aberrations could be due to the presence of lone pairs, whose contribution is local within the non-hydrogen atom, such that charge-flow models should not be expected to perform well for these specific cases.

Notably, the charge-flow contribution significantly influences the anisotropic polarizability of molecules with highly polarizable bonds, typically delocalized double or triple bonds For example, these are present in the molecules CS_2, N_2, COS, CO_2, C_6H_6, and C_2H_2. For such molecules, $u_{1(2)}^{\|}[\alpha(0)]$ also contributes significantly, but with the opposite sign. The large contributions with opposite signs may pose challenges when parametrizing an approximate polarizable force field. Due to the cancellation of different effects, small absolute errors on individual contributions would be needed to obtain a small relative error on the combined result.

Figure 6 shows the dependence of $u_{1(0)}^{\|}[\alpha(\omega)]$ and $u_{\text{ref}}^{\|}[\alpha(\omega)]$ on the imaginary frequency ω. It can be observed that with

Published under an exclusive license by AIP Publishing

The Journal of Chemical Physics ARTICLE pubs.aip.org/aip/jcp

TABLE IV. Anisotropic descriptors $u_c^{\|}[\alpha(0)]$ for all molecules in the TS42 database, for each contribution c, as documented in Table II.

Molecule	$u_{\text{ref}}^{\|}[\alpha(0)]$	$u_0^{\|}[\alpha(0)]$	$u_1^{\|}[\alpha(0)]$	$u_{1(0)}^{\|}[\alpha(0)]$	$u_{1(1)}^{\|}[\alpha(0)]$	$u_{1(2)}^{\|}[\alpha(0)]$
CS_2	0.199	0.151	0.176	0.156	0.078	−0.058
N_2O	0.187	0.130	0.173	0.149	0.088	−0.064
CO_2	0.132	0.102	0.128	0.123	0.072	−0.067
COS	0.123	0.101	0.116	0.112	0.060	−0.056
C_6H_6	0.061	0.069	0.064	0.070	0.034	−0.041
C_2H_2	0.067	0.065	0.071	0.067	0.062	−0.058
SO_2	0.070	0.060	0.066	0.066	0.028	−0.028
Cl_2	0.071	0.057	0.059	0.057	0.038	−0.037
C_8H_{18}	0.034	0.051	0.034	0.051	−0.002	−0.015
C_3H_6	0.041	0.045	0.042	0.047	0.018	−0.023
C_7H_{16}	0.029	0.043	0.029	0.043	−0.000	−0.013
C_2H_4	0.042	0.041	0.044	0.042	0.030	−0.028
H_2CO	0.052	0.036	0.052	0.039	0.038	−0.024
C_6H_{14}	0.024	0.036	0.024	0.037	−0.000	−0.012
CH_3CHO	0.033	0.028	0.032	0.031	0.014	−0.014
N_2	0.036	0.027	0.039	0.030	0.038	−0.030
$CH_3CH_2OCH_2CH_3$	0.019	0.028	0.019	0.028	0.000	−0.009
C_5H_{12}	0.018	0.027	0.018	0.027	0.000	−0.010
$C_4H_{10}O$	0.018	0.027	0.018	0.027	0.002	−0.011
CH_3COCH_3	0.022	0.021	0.022	0.022	0.008	−0.009
C_4H_{10}	0.013	0.020	0.013	0.020	0.001	−0.008
$CH_3CH_3CH_3N$	0.014	0.019	0.014	0.019	0.002	−0.007
C_3H_7OH	0.012	0.018	0.012	0.018	0.002	−0.009
H_2	0.043	0.018	0.044	0.018	0.052	−0.027
CO	0.016	0.016	0.019	0.017	0.022	−0.020
CH_3OCH_3	0.010	0.016	0.011	0.016	0.002	−0.008
HF	0.031	0.011	0.027	0.012	0.032	−0.017
CH_3NHCH_3	0.008	0.011	0.008	0.011	0.002	−0.005
C_2H_5OH	0.007	0.010	0.007	0.010	0.002	−0.006
C_3H_8	0.006	0.009	0.006	0.009	0.002	−0.004
CH_3OH	0.005	0.007	0.005	0.007	0.003	−0.005
CH_3NH_2	0.006	0.007	0.006	0.007	0.002	−0.004
C_2H_6	0.005	0.007	0.005	0.007	0.000	−0.003
C_4H_8	0.004	0.006	0.004	0.006	0.000	−0.001
HCl	0.005	0.004	0.005	0.005	0.008	−0.007
HBr	0.003	0.004	0.003	0.004	0.006	−0.007
H_2O	0.002	0.002	0.002	0.002	0.006	−0.006
CH_4	0.000	−0.000	0.000	0.000	0.000	−0.000
CCl_4	0.000	0.000	0.000	−0.000	0.000	0.000
SiH_4	0.000	0.000	−0.000	0.000	0.000	−0.000
H_2S	0.000	−0.001	−0.000	−0.001	−0.000	0.001
NH_3	0.005	−0.003	0.004	−0.003	−0.006	0.013
Min.	0.000	−0.003	−0.000	−0.003	−0.006	−0.067
Max.	0.199	0.151	0.176	0.156	0.088	0.013
Mean	0.035	0.032	0.034	0.034	0.018	−0.018

increasing $|\omega|$, the anisotropy of the TD-DFT reference decreases and becomes very small at high frequencies ($|\omega| \geq 2.308$). Tables S25–S37 show in more detail how the anisotropy disappears at high frequencies for individual molecules. This behavior is reproduced quantitatively by the ACKS2ω model with $\ell_{\max} = 1$. (See Fig. S3.) The charge-flow contribution follows this trend closely but does not drop as sharply to zero at higher frequencies. In this regime, some molecules, e.g., C_2H_2, C_6H_6, and CO_2, have relatively large

Published under an exclusive license by AIP Publishing

The Journal of Chemical Physics ARTICLE pubs.aip.org/aip/jcp

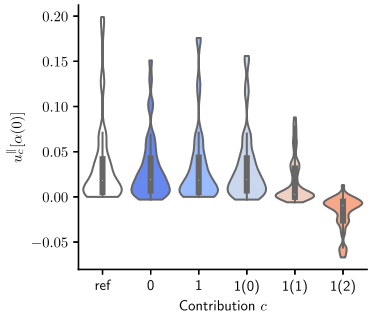

FIG. 5. Violin plots of the anisotropic descriptor of the static dipole polarizability, $u_c^{\parallel}[\alpha(0)]$, for all molecules in TS42, grouped by contribution c, as documented in Table II.

contributions $c = 1(0)$ and $c = 1(2)$, adding up to a much smaller total anisotropy, as shown in Tables S22–S24. In addition, here, quantitative results rely on compensation effects between different terms, which may be challenging to reproduce with more approximate models.

C. C_6 coefficients

Figure 7(a) shows the violin plots of the distribution of $s_c[C_6]$ over all molecular pairs, for each contribution c. In Fig. 3, $s_0[\alpha(\omega)]$ shows a mild dependency on frequency. We can use this weak frequency dependency to approximate $s_0[C_6]$ in terms of $s_0[\alpha(\omega)]$ by rewriting Eq. (20) as follows:

$$s_0^{AB}[C_6] \approx \int_0^{\infty} s_0^{A}[\alpha(iv)]s_0^{B}[\alpha(iv)]dv, \tag{27}$$

where $s_0^{AB}[C_6]$ is the $s_0[C_6]$ value of molecular pair A and B, and $s_0^{A(B)}[\alpha(iv)]$ are the $s_0[\alpha(iv)]$ values for molecule A (B). Our results indicate that charge-flow contributions to C_6 are relatively small, with very similar trends observed for $c = 0$ and $c = 1(00)$. The small magnitude of charge-flow dispersion emerges from the underestimation of the isotropic dipole polarizability across all frequencies by the charge-flow contribution. This underestimation is amplified in the isotropic C_6 coefficient because it scales quadratically with the dipole polarizability. The dipole-only contribution, $c = 1(22)$, is in general the largest, but other contributions involving fluctuating charges and dipoles are also needed to obtain a quantitative reproduction of the reference result. These findings align with previous work.[72]

Figure 8 shows the dependence of the largest $s_{1(00)}[C_6]$ values on the number of non-hydrogen atoms in the molecular dimer. The corresponding detailed data are shown in Table V. Charge-flow effects have an increasing contribution to the isotropic C_6 of larger molecular pairs, in line with our results for the isotropic polarizability.

Figure 7(b) shows violin plots of the distribution of $u_c^{\parallel}[C_6]$ values over all molecular pairs in TS42 for each contribution c. The charge flow contribution to anisotropic dispersion is on average 0.066 for $u_0^{\parallel}[C_6]$ and 0.069 for $u_{1(00)}^{\parallel}[C_6]$. Again, both characterizations of charge flow agree with each other. Whereas charge flow could explain most of the anisotropy of the dipole polarizability, it cannot accomplish the same for dispersion. This can be understood by analyzing Eq. (19): some of the anisotropic dispersion coefficients depend on the isotropic frequency-dependent polarizability of one of the two molecules. As discussed in Sec. IV A, this isotropic contribution is not reproduced qualitatively when only considering charge flow. Nonetheless, $u_0^{\parallel}[C_6]$ remains significant for several molecular pairs, and we list the top 50 in Table VI. The minor discrepancy between the distribution of $u_{\text{ref}}^{\parallel}[C_6]$ and $u_1^{\parallel}[C_6]$ values suggests that anisotropic C_6 coefficients can be accurately represented by combining frequency-dependent fluctuating charges and dipoles.

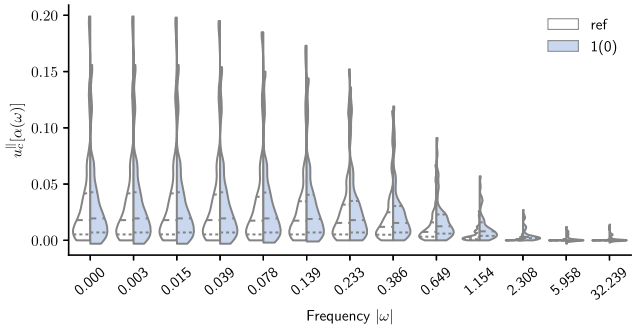

FIG. 6. The dependence on the frequency of the anisotropic descriptor for the polarizability, $u_c^{\parallel}[\alpha(\omega)]$, for the charge-flow contribution [$c = 1(0)$] and the reference [c = ref].

Published under an exclusive license by AIP Publishing

The Journal of Chemical Physics ARTICLE pubs.aip.org/aip/jcp

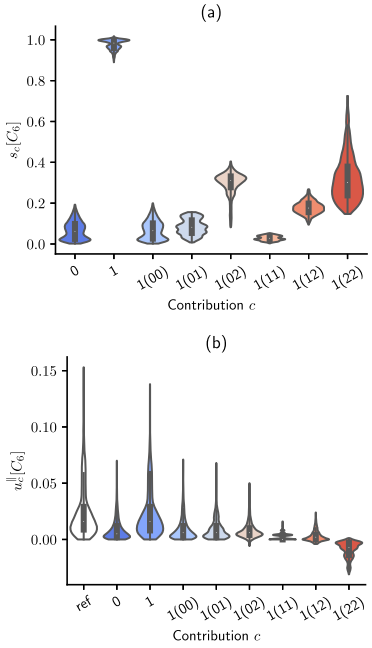

FIG. 7. Violin plots of the isotropic descriptor for dispersion coefficients, $s_c[C_6]$ [panel (a)], and the anisotropic descriptor, $u_c^{\parallel}[C_6]$ [panel (b)], for all molecular pairs from the TS42 database, for each category c, as documented in Table II.

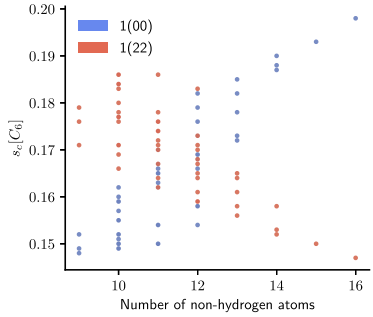

FIG. 8. The dependence on the number of non-hydrogen atoms of the 50 highest charge-flow isotropic descriptors for the C_6 dispersion coefficient, $s_{1(00)}[C_6]$. For the same molecular pairs, the corresponding dipole-only descriptor $[c = 1(22)]$ is also included.

Finally, it is noteworthy that the dipole-only contribution to the anisotropy, $u^{\parallel}_{1(22)}[C_6]$, is negative in general. This suggests that fluctuating dipoles render the dispersion more isotropic, countering the anisotropy from all other contributions.

V. DISCUSSION

While our findings demonstrate the relative importance of fluctuating charges in molecular polarizability and dispersion interactions, we acknowledge that there are alternative methods to accurately describe these phenomena without explicitly relying on charge flow.[88] For example, many interaction models, such as polarizable force fields[38,58,89–91] and dispersion corrections for DFT calculations,[2,7,8,13,14,19,22,24,25,33,35,36] are motivated by a picture of dipole-polarizable atoms without charge flow. Quantitative predictions made by such models imply that effects attributed to charge flow in this work can also be reproduced with a different dipole-only model. This can be understood as follows: The distributed multipole analysis used here is only one way to decompose the molecular response kernel into separate contributions, and different atom-in-molecule partitioning schemes can be employed within this framework.[69,74] Furthermore, response localization schemes can translate charge-flow effects into a dipole-only picture, explaining how dipole-only models can make quantitative predictions.[68] In addition, other approaches exist that can result in a quantitative dipole-only response model, e.g., by constructing complete response basis sets without monopolar terms[92] or by transforming response functions to polarization densities.[93]

One could even go a step further and consider decomposing the molecular electron density into different units than the atoms in molecules. While it is uncommon to partition the density in contributions attributed to bonds, one can anticipate the result of such a hypothetical bond partitioning by treating a diatomic molecule as a single bond unit instead of partitioning it into two atoms. The results in Fig. 1 illustrate this for carbon monoxide. When using atomic partitions, there is a significant charge-flow contribution to the polarizability. When treating this molecule as a single unit, there is no charge transfer to be observed, and the response properties are all attributed to the polarization of the C ≡ O bond unit.

All the ambiguities and choices discussed above will lead to a different perspective on what constitutes charge flow, if any. In the literature, the importance of charge flow is well established for long-range polarization in near-metallic extended systems.[7,39–43,45–48] In addition, our numerical assessment confirms that the charge-flow contribution, as defined in this work, is related to non-local features, such as molecular geometry and chemical bonding, also in smaller molecules, such as those in the TS42 set.[44] Polarizable force fields and dispersion models may build on these relationships to parametrize charge flow explicitly, thereby improving their description of anisotropic response properties. In other words, we show that the charge flow is not only useful for modeling non-standard power laws in type-C dispersion[15] but that it is also helpful for understanding anisotropic dispersion of isolated molecules.

Published under an exclusive license by AIP Publishing

The Journal of Chemical Physics ARTICLE pubs.aip.org/aip/jcp

TABLE V. Isotropic descriptors $s_c[C_6]$ for the 50 molecular pairs from TS42 with the highest $s_{1(00)}[C_6]$ value.

Molecule	$s_0[C_6]$	$s_1[C_6]$	$s_{1(00)}[C_6]$	$s_{1(01)}[C_6]$	$s_{1(02)}[C_6]$	$s_{1(11)}[C_6]$	$s_{1(12)}[C_6]$	$s_{1(22)}[C_6]$
$C_8H_{18}\cdots C_8H_{18}$	0.192	1.002	0.198	0.156	0.340	0.036	0.128	0.147
$C_8H_{18}\cdots C_7H_{16}$	0.187	1.002	0.193	0.154	0.339	0.036	0.132	0.150
$C_8H_{18}\cdots C_6H_6$	0.186	0.995	0.190	0.144	0.346	0.032	0.126	0.158
$C_7H_{16}\cdots C_7H_{16}$	0.182	1.001	0.188	0.152	0.338	0.036	0.132	0.152
$C_8H_{18}\cdots C_6H_{14}$	0.181	1.001	0.187	0.154	0.337	0.036	0.134	0.153
$C_6H_6\cdots C_7H_{16}$	0.182	0.995	0.185	0.144	0.344	0.032	0.128	0.161
$C_7H_{16}\cdots C_6H_{14}$	0.176	1.001	0.182	0.154	0.336	0.036	0.136	0.156
$C_6H_6\cdots C_6H_6$	0.181	0.988	0.182	0.136	0.350	0.028	0.124	0.170
$C_6H_{14}\cdots C_6H_6$	0.175	0.995	0.179	0.142	0.342	0.032	0.134	0.165
$C_5H_{12}\cdots C_8H_{18}$	0.172	1.001	0.178	0.152	0.336	0.036	0.138	0.158
$C_6H_{14}\cdots C_6H_{14}$	0.170	1.001	0.176	0.152	0.334	0.040	0.140	0.159
$C_7H_{16}\cdots C_5H_{12}$	0.168	1.001	0.173	0.152	0.334	0.040	0.142	0.161
$C_8H_{18}\cdots CH_3CH_2OCH_2CH_3$	0.169	1.001	0.173	0.148	0.340	0.036	0.140	0.165
$C_8H_{18}\cdots C_4H_{10}O$	0.167	1.001	0.172	0.150	0.337	0.036	0.140	0.164
$C_6H_6\cdots C_5H_{12}$	0.167	0.995	0.170	0.144	0.340	0.036	0.138	0.170
$CH_3CH_2OCH_2CH_3\cdots C_7H_{16}$	0.164	1.001	0.169	0.146	0.337	0.036	0.142	0.168
$C_4H_8\cdots C_8H_{18}$	0.165	0.999	0.169	0.156	0.330	0.040	0.146	0.159
$C_4H_{10}O\cdots C_7H_{16}$	0.163	1.001	0.168	0.150	0.336	0.036	0.142	0.167
$C_6H_{14}\cdots C_5H_{12}$	0.162	1.001	0.167	0.152	0.331	0.040	0.146	0.164
$C_8H_{18}\cdots C_4H_{10}$	0.161	1.001	0.166	0.152	0.333	0.040	0.146	0.164
$CH_3CH_2OCH_2CH_3\cdots C_6H_6$	0.163	0.994	0.166	0.138	0.343	0.032	0.136	0.178
$C_6H_6\cdots C_4H_{10}O$	0.162	0.995	0.165	0.140	0.341	0.032	0.140	0.176
$C_4H_8\cdots C_7H_{16}$	0.160	0.999	0.165	0.154	0.328	0.040	0.148	0.162
$C_6H_{14}\cdots CH_3CH_2OCH_2CH_3$	0.159	1.001	0.163	0.146	0.335	0.036	0.146	0.172
$C_4H_8\cdots C_6H_6$	0.159	0.993	0.162	0.146	0.333	0.036	0.144	0.171
$C_7H_{16}\cdots C_4H_{10}$	0.157	1.001	0.162	0.152	0.332	0.040	0.148	0.167
$C_4H_{10}O\cdots C_6H_{14}$	0.157	1.001	0.162	0.148	0.332	0.040	0.146	0.171
$C_5H_{12}\cdots C_5H_{12}$	0.155	1.001	0.160	0.152	0.328	0.040	0.152	0.169
$C_4H_8\cdots C_6H_{14}$	0.155	0.999	0.159	0.154	0.326	0.044	0.152	0.166
$C_4H_{10}\cdots C_6H_6$	0.156	0.994	0.159	0.144	0.336	0.036	0.144	0.177
$C_8H_{18}\cdots CH_3CH_3CH_3N$	0.153	1.002	0.158	0.150	0.335	0.040	0.150	0.171
$C_3H_7OH\cdots C_8H_{18}$	0.154	1.001	0.158	0.148	0.336	0.040	0.146	0.173
$C_6H_{14}\cdots C_4H_{10}$	0.152	1.001	0.157	0.150	0.328	0.040	0.152	0.171
$C_5H_{12}\cdots C_4H_{10}O$	0.150	1.001	0.155	0.146	0.329	0.040	0.154	0.176
$C_5H_{12}\cdots CH_3CH_2OCH_2CH_3$	0.151	1.000	0.155	0.146	0.332	0.040	0.150	0.177
$CH_3COCH_3\cdots C_8H_{18}$	0.148	0.997	0.154	0.138	0.345	0.036	0.144	0.183
$CH_3CH_3CH_3N\cdots C_7H_{16}$	0.149	1.002	0.154	0.148	0.332	0.040	0.154	0.174
$C_7H_{16}\cdots C_3H_7OH$	0.150	1.001	0.154	0.146	0.334	0.040	0.150	0.176
$C_3H_7OH\cdots C_6H_6$	0.149	0.994	0.152	0.138	0.338	0.036	0.144	0.186
$CH_3CH_3CH_3N\cdots C_6H_6$	0.149	0.995	0.152	0.140	0.337	0.036	0.148	0.184
$C_5H_{12}\cdots C_4H_8$	0.148	0.999	0.152	0.152	0.322	0.044	0.158	0.171
$CH_3CH_2OCH_2CH_3\cdots CH_3CH_2OCH_2CH_3$	0.148	1.000	0.151	0.140	0.334	0.036	0.152	0.186
$C_4H_{10}O\cdots CH_3CH_2OCH_2CH_3$	0.147	1.000	0.150	0.142	0.333	0.040	0.152	0.184
$C_4H_{10}O\cdots C_4H_{10}O$	0.145	1.000	0.150	0.144	0.330	0.040	0.156	0.183
$C_7H_{16}\cdots CH_3COCH_3$	0.144	0.997	0.150	0.136	0.341	0.036	0.148	0.186
$C_3H_8\cdots C_8H_{18}$	0.145	1.000	0.150	0.150	0.331	0.040	0.154	0.174
$C_6H_{14}\cdots CH_3CH_3CH_3N$	0.144	1.002	0.149	0.148	0.329	0.040	0.158	0.178
$C_6H_{14}\cdots C_3H_7OH$	0.145	1.000	0.149	0.146	0.330	0.040	0.156	0.180
$C_4H_{10}\cdots C_5H_{12}$	0.145	1.000	0.149	0.148	0.325	0.044	0.160	0.176
$CH_3CH_2OCH_2CH_3\cdots C_4H_8$	0.145	0.999	0.148	0.146	0.325	0.044	0.158	0.179
⋯	⋯	⋯	⋯	⋯	⋯	⋯	⋯	⋯
Min.	0.002	0.890	0.002	0.008	0.082	0.004	0.096	0.147
Max.	0.192	1.016	0.198	0.156	0.403	0.052	0.268	0.726
Mean	0.066	0.977	0.069	0.083	0.297	0.028	0.178	0.322

Published under an exclusive license by AIP Publishing

The Journal of Chemical Physics ARTICLE pubs.aip.org/aip/jcp

TABLE VI. Anisotropic descriptors $u_c^{\parallel}[C_6]$ for the 50 molecular pairs from TS42 with the highest $u_{1(00)}^{\parallel}[C_6]$ value.

Molecule	$u_{ref}^{\parallel}[C_6]$	$u_0^{\parallel}[C_6]$	$u_1^{\parallel}[C_6]$	$u_{1(00)}^{\parallel}[C_6]$	$u_{1(01)}^{\parallel}[C_6]$	$u_{1(02)}^{\parallel}[C_6]$	$u_{1(11)}^{\parallel}[C_6]$	$u_{1(12)}^{\parallel}[C_6]$	$u_{1(22)}^{\parallel}[C_6]$
$CS_2\cdots CS_2$	0.153	0.070	0.131	0.071	0.056	0.010	0.012	0.004	−0.023
$N_2O\cdots CS_2$	0.151	0.065	0.134	0.070	0.060	0.009	0.016	0.004	−0.024
$N_2O\cdots N_2O$	0.151	0.061	0.138	0.070	0.068	0.006	0.016	0.004	−0.024
$CO_2\cdots CS_2$	0.121	0.052	0.110	0.059	0.050	0.010	0.012	0.004	−0.025
$CO_2\cdots N_2O$	0.124	0.050	0.115	0.059	0.056	0.008	0.016	0.004	−0.026
$COS\cdots CS_2$	0.119	0.052	0.105	0.056	0.042	0.015	0.008	0.006	−0.024
$N_2O\cdots COS$	0.122	0.050	0.111	0.056	0.048	0.014	0.012	0.006	−0.025
$N_2O\cdots C_6H_6$	0.095	0.050	0.091	0.054	0.046	−0.002	0.012	0.000	−0.018
$CS_2\cdots C_6H_6$	0.090	0.052	0.083	0.052	0.038	0.001	0.008	0.000	−0.017
$CO_2\cdots CO_2$	0.100	0.040	0.094	0.049	0.048	0.010	0.012	0.004	−0.027
$CO_2\cdots COS$	0.097	0.040	0.089	0.047	0.040	0.014	0.008	0.006	−0.026
$N_2O\cdots C_8H_{18}$	0.080	0.042	0.077	0.045	0.032	0.007	0.004	0.002	−0.014
$C_6H_6\cdots CO_2$	0.073	0.040	0.071	0.045	0.038	−0.002	0.008	0.000	−0.018
$CS_2\cdots C_8H_{18}$	0.074	0.043	0.068	0.044	0.026	0.008	0.004	0.000	−0.013
$COS\cdots COS$	0.093	0.039	0.084	0.044	0.032	0.016	0.008	0.008	−0.025
$N_2O\cdots C_7H_{16}$	0.078	0.039	0.074	0.042	0.030	0.008	0.004	0.004	−0.015
$COS\cdots C_6H_6$	0.068	0.039	0.064	0.041	0.032	0.002	0.008	0.002	−0.018
$CS_2\cdots C_7H_{16}$	0.071	0.040	0.066	0.041	0.024	0.009	0.004	0.000	−0.013
$N_2O\cdots C_2H_2$	0.100	0.038	0.095	0.040	0.048	0.012	0.016	0.006	−0.027
$C_2H_2\cdots CS_2$	0.094	0.039	0.087	0.039	0.044	0.013	0.012	0.006	−0.026
$N_2O\cdots C_6H_{14}$	0.076	0.036	0.072	0.039	0.030	0.009	0.004	0.004	−0.015
$CS_2\cdots SO_2$	0.089	0.035	0.079	0.038	0.028	0.022	0.008	0.006	−0.021
$N_2O\cdots SO_2$	0.094	0.034	0.087	0.038	0.032	0.023	0.008	0.010	−0.023
$C_8H_{18}\cdots CO_2$	0.060	0.033	0.058	0.037	0.026	0.005	0.004	0.000	−0.014
$CS_2\cdots C_6H_{14}$	0.069	0.037	0.064	0.037	0.024	0.010	0.004	0.000	−0.013
$C_3H_6\cdots N_2O$	0.081	0.033	0.077	0.036	0.034	0.013	0.008	0.004	−0.019
$CH_3CH_2OCH_2CH_3\cdots N_2O$	0.073	0.032	0.070	0.035	0.026	0.012	0.004	0.006	−0.016
$CS_2\cdots C_3H_6$	0.075	0.034	0.069	0.035	0.028	0.014	0.008	0.002	−0.017
$C_5H_{12}\cdots N_2O$	0.073	0.032	0.069	0.035	0.028	0.011	0.008	0.004	−0.015
$C_6H_6\cdots C_6H_6$	0.045	0.035	0.046	0.035	0.024	−0.006	0.004	−0.004	−0.012
$C_8H_{18}\cdots COS$	0.054	0.032	0.051	0.034	0.020	0.007	0.004	−0.002	−0.012
$CO_2\cdots C_2H_2$	0.077	0.030	0.075	0.034	0.040	0.011	0.012	0.006	−0.028
$N_2O\cdots C_4H_{10}O$	0.073	0.032	0.069	0.034	0.028	0.011	0.008	0.004	−0.016
$CO_2\cdots C_7H_{16}$	0.058	0.031	0.056	0.034	0.024	0.005	0.004	0.002	−0.014
$CS_2\cdots C_4H_{10}O$	0.065	0.032	0.060	0.033	0.024	0.012	0.004	0.000	−0.014
$CS_2\cdots C_5H_{12}$	0.065	0.033	0.060	0.033	0.024	0.012	0.004	0.002	−0.013
$CH_3CH_2OCH_2CH_3\cdots CS_2$	0.066	0.033	0.061	0.033	0.022	0.013	0.004	0.002	−0.014
$C_7H_{16}\cdots COS$	0.052	0.030	0.049	0.032	0.020	0.008	0.004	−0.002	−0.012
$C_6H_{14}\cdots CO_2$	0.056	0.028	0.054	0.032	0.024	0.006	0.004	0.002	−0.014
$CO_2\cdots SO_2$	0.072	0.027	0.068	0.032	0.026	0.019	0.004	0.008	−0.023
$COS\cdots C_2H_2$	0.072	0.030	0.068	0.031	0.034	0.013	0.008	0.008	−0.026
$C_4H_{10}\cdots N_2O$	0.070	0.029	0.067	0.031	0.026	0.013	0.008	0.006	−0.016
$N_2O\cdots C_2H_4$	0.083	0.029	0.079	0.031	0.036	0.017	0.012	0.008	−0.022
$CH_3COCH_3\cdots N_2O$	0.072	0.027	0.069	0.030	0.026	0.016	0.008	0.006	−0.017
$Cl_2\cdots N_2O$	0.093	0.028	0.081	0.030	0.028	0.028	0.008	0.014	−0.027
$N_2O\cdots C_3H_7OH$	0.070	0.027	0.067	0.030	0.026	0.014	0.008	0.006	−0.016
$CH_3CHO\cdots N_2O$	0.077	0.027	0.073	0.030	0.028	0.018	0.008	0.008	−0.019
$CS_2\cdots C_2H_4$	0.077	0.030	0.071	0.030	0.030	0.017	0.008	0.004	−0.020
$COS\cdots SO_2$	0.067	0.027	0.062	0.030	0.020	0.020	0.004	0.006	−0.020
$CS_2\cdots C_4H_{10}$	0.063	0.029	0.058	0.029	0.022	0.013	0.004	0.002	−0.014
⋯	⋯	⋯	⋯	⋯	⋯	⋯	⋯	⋯	⋯
Min.	0.000	0.000	0.000	0.000	0.000	−0.006	0.000	−0.004	−0.031
Max.	0.153	0.070	0.138	0.071	0.068	0.050	0.016	0.024	0.001
Mean	0.024	0.009	0.023	0.009	0.009	0.008	0.002	0.003	−0.009

Published under an exclusive license by AIP Publishing

The Journal of Chemical Physics ARTICLE pubs.aip.org/aip/jcp

VI. CONCLUSIONS

The impact of fluctuating charges on dynamic linear-response properties is investigated and numerically assessed with the TS42 dataset, which comprises both organic and inorganic molecules. The dipole polarizability tensor is recoupled to easily separate isotropic and anisotropic components, which also allows for the definition of anisotropic C_6 dispersion coefficients. The recoupled properties are then used to define two descriptors (isotropic and anisotropic) for the charge-flow contribution to polarizability and dispersion. The molecular frequency-dependent polarizabilities are computed with the ACKS2ω model, either with fluctuating charges only ($\ell_{\max} = 0$) or fluctuating charges and dipoles ($\ell_{\max} = 1$). In the latter case, charge-flow, charge-dipole, and dipole-only effects are easily separated. All ACKS2ω parameters are derived from LDA/Aug-cc-pVDZ wavefunctions, and the response properties at this level of theory are used as a reference. Our tests reveal that the two ways to define the charge-flow contribution ($\ell_{\max} = 0$ or the charge-flow part of $\ell_{\max} = 1$) yield very similar results. In general, the $\ell_{\max} = 1$ model quantitatively reproduces all tested quantities: both isotropic and anisotropic polarizability and dispersion.

The results for the TS42 set show that charge-flow contributions alone significantly underestimate the molecular isotropic dipole polarizability and that the dipole-only contribution is larger. Nevertheless, the charge-flow contribution is, in general, not negligible, and its significance depends strongly on molecular geometry, the presence of polarizable bonds, and the number of non-hydrogen atoms. In long-chain or π-conjugated molecules, the charge-flow contribution can even exceed the dipole-only counterpart. Our results also reveal a weak dependence of the charge-flow contribution on frequency, whereas charge-dipole and dipole-only contributions, respectively, decrease and increase slightly with increasing magnitude of the imaginary frequency.

We also investigate static anisotropic polarizability and its contributions across different frequencies. The results demonstrate that the charge-flow contribution alone reasonably predicts the anisotropy of the polarizability. The overall anisotropy decreases with increasing magnitude of the imaginary frequency and becomes negligible at the highest frequencies ($|\omega| \geq 2.308$). In this limit, polarizability becomes almost perfectly isotropic. Charge-flow and other contributions to the anisotropic polarizability follow the same decreasing trend in magnitude, except that they do not approach zero as closely at higher frequencies. In this limit, their residual contributions cancel each other out.

The analysis also reveals that the isotropic C_6 coefficients are considerably underestimated by charge-flow contributions alone. This discrepancy is the logical consequence of the noticeable underestimation of the isotropic dipole polarizability by charge flow at all the frequencies employed in the C_6 computations. Charge-flow and charge-dipole effects still contribute significantly, but the dipole-only effect is larger.

Unlike anisotropic polarizability, anisotropic dispersion is not fully reproduced by charge-flow contributions alone. The impact of charge flow is not negligible, but other charge-dipole terms are also important. Remarkably, the dipole-only contribution generally reduces the dispersion anisotropy.

In conclusion, this research offers valuable insights into the leading contributors to molecular polarizability and C_6 coefficients, highlighting the significance of fluctuating charges in determining the dynamic linear-response properties of finite systems. Nevertheless, we acknowledge, existing interaction models without charge flow, i.e., which rely exclusively on atomic dipoles, have proven their effectiveness. This contrast remains fascinating as charge-flow contributions correlate with non-local features at a higher length scale than that of local atomic polarizabilities. Future (frequency-dependent) polarizable force fields could improve by including charge-flow effects, and this work shows in which cases such improvements should be expected to be beneficial.

SUPPLEMENTARY MATERIAL

The supplementary material is a PDF document containing:

- Violin plots of the distribution of $s_c[\alpha(\omega)]$ over the TS42 dataset, for all relevant contributions c, and for all imaginary frequencies used in this work.
- Scatter plots showing the dependence of the descriptors $s_{1(0)}[\alpha(\omega)]$ and $s_{1(2)}[\alpha(\omega)]$ on the number of non-hydrogen atoms in molecules for all imaginary frequencies considered in this work.
- Violin plots of the distribution of the descriptor $u_c^{\parallel}[\alpha(\omega)]$ over the TS42 database, for all relevant contributions c and all imaginary frequencies considered in this work.
- Tables with numerical values of $s_c[\alpha(\omega)]$, $\|\vec{\alpha}_c\|$, $u_c^{\parallel}[\alpha(\omega)]$, for all molecules in TS42, for all relevant contributions c, and for all imaginary frequencies used in this work.

ACKNOWLEDGMENTS

Y.C. and T.V. acknowledge the Foundation of Scientific Research–Flanders (FWO, file Grant No. G0A9717N) and the Research Board of Ghent University (BOF) for their financial support. The resources and services used in this work were provided by the VSC (Flemish Supercomputer Center), funded by the Research Foundation–Flanders (FWO) and the Flemish Government. We thank Dr. Jelle Vekeman for helpful comments on the manuscript.

AUTHOR DECLARATIONS

Conflict of Interest

The authors have no conflicts to disclose.

Author Contributions

YingXing Cheng: Conceptualization (lead); Data curation (lead); Formal analysis (lead); Investigation (equal); Methodology (lead); Software (lead); Validation (lead); Visualization (lead); Writing – original draft (lead); Writing – review & editing (equal). **Toon Verstraelen**: Conceptualization (supporting); Data curation (supporting); Formal analysis (supporting); Funding acquisition (lead); Investigation (equal); Methodology (supporting); Project administration (lead); Resources (equal); Supervision (lead); Validation (supporting); Visualization (supporting); Writing – review & editing (equal).

Published under an exclusive license by AIP Publishing

The Journal of Chemical Physics ARTICLE pubs.aip.org/aip/jcp

DATA AVAILABILITY

The data that support the findings of this study are openly available in "TS42 TD-DFT Dipole Polarizabilities as a function of imaginary frequency," at https://doi.org/10.5281/zenodo.8047106, reference number 8047106.

REFERENCES

[1] M. Stöhr, T. Van Voorhis, and A. Tkatchenko, "Theory and practice of modeling van der Waals interactions in electronic-structure calculations," Chem. Soc. Rev. **48**(15), 4118–4154 (2019).

[2] S. Grimme, A. Hansen, J. G. Brandenburg, and C. Bannwarth, "Dispersion-corrected mean-field electronic structure methods," Chem. Rev. **116**(9), 5105–5154 (2016).

[3] S. Grimme and C. Bannwarth, "Ultra-fast computation of electronic spectra for large systems by tight-binding based simplified Tamm-Dancoff approximation (sTDA-xTB)," J. Chem. Phys. **145**(5), 054103 (2016).

[4] J. G. Ángyán, I. C. Gerber, A. Savin, and J. Toulouse, "van der Waals forces in density functional theory: Perturbational long-range electron-interaction corrections," Phys. Rev. A **72**(1), 012510 (2005).

[5] K. Berland, V. R. Cooper, K. Lee, E. Schröder, T. Thonhauser, P. Hyldgaard, and B. I. Lundqvist, "van der Waals forces in density functional theory: A review of the vdW-DF method," Rep. Prog. Phys. **78**(6), 066501 (2015).

[6] A. D. Buckingham, P. W. Fowler, and J. M. Hutson, "Theoretical studies of van der Waals molecules and intermolecular forces," Chem. Rev. **88**(6), 963–988 (1988).

[7] J. Hermann, R. A. DiStasio, Jr., and A. Tkatchenko, "First-principles models for van der Waals interactions in molecules and materials: Concepts, theory, and applications," Chem. Rev. **117**(6), 4714–4758 (2017).

[8] L. M. Woods, D. A. R. Dalvit, A. Tkatchenko, P. Rodriguez-Lopez, A. W. Rodriguez, and R. Podgornik, "Materials perspective on Casimir and van der Waals interactions," Rev. Mod. Phys. **88**(4), 045003 (2016).

[9] P. Xu, M. Alkan, and M. S. Gordon, "Many-body dispersion," Chem. Rev. **120**(22), 12343–12356 (2020).

[10] F. London, "Zur theorie und systematik der molekularkräfte," Z. Phys. **63**(3), 245–279 (1930).

[11] E. Zaremba and W. Kohn, "Van der Waals interaction between an atom and a solid surface," Phys. Rev. B **13**(6), 2270–2285 (1976).

[12] A. D. Becke and E. R. Johnson, "Exchange-hole dipole moment and the dispersion interaction revisited," J. Chem. Phys. **127**(15), 154108 (2007).

[13] A. Tkatchenko and M. Scheffler, "Accurate molecular van der Waals interactions from ground-state electron density and free-atom reference data," Phys. Rev. Lett. **102**(7), 073005 (2009).

[14] S. Grimme, S. Ehrlich, and L. Goerigk, "Effect of the damping function in dispersion corrected density functional theory," J. Comput. Chem. **32**(7), 1456–1465 (2011).

[15] J. F. Dobson, "Beyond pairwise additivity in London dispersion interactions," Int. J. Quantum Chem. **114**(18), 1157–1161 (2014).

[16] T. Gould, S. Lebègue, J. G. Ángyán, and T. Bučko, "A fractionally ionic approach to polarizability and van der Waals many-body dispersion calculations," J. Chem. Theory Comput. **12**(12), 5920–5930 (2016).

[17] A. Otero-de-la-Roza, L. M. LeBlanc, and E. R. Johnson, "What is 'many-body' dispersion and should I worry about it?," Phys. Chem. Chem. Phys. **22**(16), 8266–8276 (2020).

[18] J. F. Dobson, A. Savin, J. G. Ángyán, and R.-F. Liu, "Spooky correlations and unusual van der Waals forces between gapless and near-gapless molecules," J. Chem. Phys. **145**(20), 204107 (2016).

[19] E. Caldeweyher, C. Bannwarth, and S. Grimme, "Extension of the D3 dispersion coefficient model," J. Chem. Phys. **147**(3), 034112 (2017).

[20] M. Elstner, P. Hobza, T. Frauenheim, S. Suhai, and E. Kaxiras, "Hydrogen bonding and stacking interactions of nucleic acid base pairs: A density-functional-theory based treatment," J. Chem. Phys. **114**(12), 5149–5155 (2001).

[21] S. Grimme, "Accurate description of van der Waals complexes by density functional theory including empirical corrections," J. Comput. Chem. **25**(12), 1463–1473 (2004).

[22] S. Grimme, J. Antony, S. Ehrlich, and H. Krieg, "A consistent and accurate *ab initio* parametrization of density functional dispersion correction (DFT-D) for the 94 elements H-Pu," J. Chem. Phys. **132**(15), 154104 (2010).

[23] P. Jurečka, J. Černý, P. Hobza, and D. R. Salahub, "Density functional theory augmented with an empirical dispersion term. Interaction energies and geometries of 80 noncovalent complexes compared with *ab initio* quantum mechanics calculations," J. Comput. Chem. **28**(2), 555–569 (2007).

[24] A. D. Becke and E. R. Johnson, "Exchange-hole dipole moment and the dispersion interaction," J. Chem. Phys. **122**(15), 154104 (2005).

[25] A. D. Becke and E. R. Johnson, "A density-functional model of the dispersion interaction," J. Chem. Phys. **123**(15), 154101 (2005).

[26] Y. Ikabata and H. Nakai, "Local response dispersion method: A density-dependent dispersion correction for density functional theory," Int. J. Quantum Chem. **115**(5), 309–324 (2015).

[27] T. Sato and H. Nakai, "Density functional method including weak interactions: Dispersion coefficients based on the local response approximation," J. Chem. Phys. **131**(22), 224104 (2009).

[28] T. Sato and H. Nakai, "Local response dispersion method. II. Generalized multicenter interactions," J. Chem. Phys. **133**(19), 194101 (2010).

[29] B. M. Axilrod and E. Teller, "Interaction of the van der Waals type between three atoms," J. Chem. Phys. **11**(6), 299–300 (1943).

[30] Y. Muto, "Force between nonpolar molecules," J. Phys. Math. Soc. Jpn **17**, 629–631 (1943).

[31] A. Otero-de-la-Roza, L. M. LeBlanc, and E. R. Johnson, "Asymptotic pairwise dispersion corrections can describe layered materials accurately," J. Phys. Chem. Lett. **11**(6), 2298–2302 (2020).

[32] E. R. Johnson, "Chapter 5 - the exchange-hole dipole moment dispersion model," in *Non-Covalent Interactions in Quantum Chemistry and Physics*, edited by A. Otero de la Roza and G. A. DiLabio (Elsevier, 2017), pp. 169–194.

[33] A. Otero-de-la-Roza and E. R. Johnson, "Many-body dispersion interactions from the exchange-hole dipole moment model," J. Chem. Phys. **138**(5), 054103 (2013).

[34] A. Ambrosetti, A. M. Reilly, R. A. DiStasio, and A. Tkatchenko, "Long-range correlation energy calculated from coupled atomic response functions," J. Chem. Phys. **140**(18), 18A508 (2014).

[35] A. Tkatchenko, R. A. DiStasio, R. Car, and M. Scheffler, "Accurate and efficient method for many-body van der Waals interactions," Phys. Rev. Lett. **108**(23), 236402 (2012).

[36] T. Alexandre, A. Ambrosetti, and R. A. DiStasio, "Interatomic methods for the dispersion energy derived from the adiabatic connection fluctuation-dissipation theorem," J. Chem. Phys. **138**(7), 074106 (2013).

[37] A. Ambrosetti, N. Ferri, R. A. DiStasio, and A. Tkatchenko, "Wavelike charge density fluctuations and van der Waals interactions at the nanoscale," Science **351**(6278), 1171–1176 (2016).

[38] A. Stone, *The Theory of Intermolecular Forces* (Oxford University Press, 2013).

[39] J. F. Dobson, A. White, and A. Rubio, "Asymptotics of the dispersion interaction: Analytic benchmarks for van der Waals energy functionals," Phys. Rev. Lett. **96**(7), 073201 (2006).

[40] J. F. Dobson, "Towards efficient description of type-C London dispersion forces between low-dimensional metallic nanostructures," Electron. Struct. **3**(4), 044001 (2021).

[41] K. Jackson, M. Yang, and J. Jellinek, "Site-specific analysis of dielectric properties of finite systems," J. Phys. Chem. C **111**(48), 17952–17960 (2007).

[42] K. Jackson and J. Jellinek, "Si clusters are more metallic than bulk Si," J. Chem. Phys. **145**(24), 244302 (2016).

[43] J. F. Dobson and T. Gould, "Calculation of dispersion energies," J. Phys.: Condens. Matter **24**(7), 073201 (2012).

[44] N. Sablon, F. D. Proft, P. W. Ayers, and P. Geerlings, "Computing second-order functional derivatives with respect to the external potential," J. Chem. Theory Comput. **6**(12), 3671–3680 (2010).

[45] A. J. Misquitta, J. Spencer, A. J. Stone, and A. Alavi, "Dispersion interactions between semiconducting wires," Phys. Rev. B **82**(7), 075312 (2010).

Published under an exclusive license by AIP Publishing

The Journal of Chemical Physics ARTICLE pubs.aip.org/aip/jcp

[46]A. J. Misquitta, R. Maezono, N. D. Drummond, A. J. Stone, and R. J. Needs, "Anomalous nonadditive dispersion interactions in systems of three one-dimensional wires," Phys. Rev. B **89**(4), 045140 (2014).
[47]J. Tao, J. P. Perdew, and A. Ruzsinszky, "Accurate van der Waals coefficients from density functional theory," Proc. Natl. Acad. Sci. U. S. A. **109**(1), 18–21 (2012).
[48]A. Ruzsinszky, J. P. Perdew, J. Tao, G. I. Csonka, and J. M. Pitarke, "Van der Waals coefficients for nanostructures: Fullerenes defy conventional wisdom," Phys. Rev. Lett. **109**(23), 233203 (2012).
[49]A. Krishtal, P. Senet, M. Yang, and C. Van Alsenoy, "A Hirshfeld partitioning of polarizabilities of water clusters," J. Chem. Phys. **125**(3), 034312 (2006).
[50]B. A. Bauer, T. R. Lucas, A. Krishtal, C. Van Alsenoy, and S. Patel, "Variation of ion polarizability from vacuum to hydration: Insights from Hirshfeld partitioning," J. Phys. Chem. A **114**(34), 8984–8992 (2010).
[51]A. Krishtal, P. Senet, and C. Van Alsenoy, "Influence of structure on the polarizability of hydrated methane sulfonic acid clusters," J. Chem. Theory Comput. **4**(12), 2122–2129 (2008).
[52]A. Krishtal, P. Senet, and C. Van Alsenoy, "Origin of the size-dependence of the polarizability per atom in heterogeneous clusters: The case of AlP clusters," J. Chem. Phys. **133**(15), 154310 (2010).
[53]Y. Mei, A. C. Simmonett, F. C. Pickard IV, R. A. DiStasio, Jr., B. R. Brooks, and Y. Shao, "Numerical study on the partitioning of the molecular polarizability into fluctuating charge and induced atomic dipole contributions," J. Phys. Chem. A **119**(22), 5865–5882 (2015).
[54]M. Galante and A. Tkatchenko, "Anisotropic van der Waals dispersion forces in polymers: Structural symmetry breaking leads to enhanced conformational search," Phys. Rev. Res. **5**, L012028 (2023).
[55]A. J. Stone, "Distributed multipole analysis, or how to describe a molecular charge distribution," Chem. Phys. Lett. **83**(2), 233–239 (1981).
[56]L. Gagliardi, R. Lindh, and G. Karlström, "Local properties of quantum chemical systems: The LoProp approach," J. Chem. Phys. **121**(10), 4494–4500 (2004).
[57]I. Harczuk, B. Nagy, F. Jensen, O. Vahtras, and H. Ågren, "Local decomposition of imaginary polarizabilities and dispersion coefficients," Phys. Chem. Chem. Phys. **19**(30), 20241–20250 (2017).
[58]D. Elking, T. Darden, and R. J. Woods, "Gaussian induced dipole polarization model," J. Comput. Chem. **28**(7), 1261–1274 (2007).
[59]W. C. Lu, C. Z. Wang, M. W. Schmidt, L. Bytautas, K. M. Ho, and K. Ruedenberg, "Molecule intrinsic minimal basis sets. I. Exact resolution of *ab initio* optimized molecular orbitals in terms of deformed atomic minimal-basis orbitals," J. Chem. Phys. **120**(6), 2629–2637 (2004).
[60]G. Knizia, "Intrinsic atomic orbitals: An unbiased bridge between quantum theory and chemical concepts," J. Chem. Theory Comput. **9**(11), 4834–4843 (2013).
[61]A. C. West, M. W. Schmidt, M. S. Gordon, and K. Ruedenberg, "A comprehensive analysis of molecule-intrinsic quasi-atomic, bonding, and correlating orbitals. I. Hartree-Fock wave functions," J. Chem. Phys. **139**(23), 234107 (2013).
[62]T. Janowski, "Near equivalence of intrinsic atomic orbitals and quasiatomic orbitals," J. Chem. Theory Comput. **10**(8), 3085–3091 (2014).
[63]A. J. Misquitta and A. J. Stone, "Distributed polarizabilities obtained using a constrained density-fitting algorithm," J. Chem. Phys. **124**(2), 024111 (2006).
[64]K. E. Laidig and R. F. W. Bader, "Properties of atoms in molecules: Atomic polarizabilities," J. Chem. Phys. **93**(10), 7213–7224 (1990).
[65]P. L. A. Popelier, *Atoms in Molecules: An Introduction* (Prentice Hall, 2000).
[66]F. L. Hirshfeld, "Bonded-atom fragments for describing molecular charge densities," Theor. Chim. Acta **44**(2), 129–138 (1977).
[67]P. Bultinck, C. Van Alsenoy, P. W. Ayers, and R. Carbó-Dorca, "Critical analysis and extension of the Hirshfeld atoms in molecules," J. Chem. Phys. **126**(14), 144111 (2007).
[68]T. C. Lillestolen and R. J. Wheatley, "First-principles calculation of local atomic polarizabilities," J. Phys. Chem. A **111**(43), 11141–11146 (2007).
[69]A. J. Misquitta and A. J. Stone, "ISA-Pol: Distributed polarizabilities and dispersion models from a basis-space implementation of the iterated stockholder atoms procedure," Theor. Chem. Acc. **137**(11), 153 (2018).
[70]T. Verstraelen, P. W. Ayers, V. Van Speybroeck, and M. Waroquier, "ACKS2: Atom-condensed Kohn-Sham DFT approximated to second order," J. Chem. Phys. **138**(7), 074108 (2013).
[71]T. Verstraelen, S. Vandenbrande, and P. W. Ayers, "Direct computation of parameters for accurate polarizable force fields," J. Chem. Phys. **141**(19), 194114 (2014).
[72]Y. Cheng and T. Verstraelen, "A new framework for frequency-dependent polarizable force fields," J. Chem. Phys. **157**(12), 124106 (2022).
[73]T. Verstraelen, S. Vandenbrande, F. Heidar-Zadeh, L. Vanduyfhuys, V. Van Speybroeck, M. Waroquier, and P. W. Ayers, "Minimal basis iterative stockholder: Atoms in molecules for force-field development," J. Chem. Theory Comput. **12**(8), 3894–3912 (2016).
[74]A. J. Stone, "Distributed polarizabilities," Mol. Phys. **56**(5), 1065–1082 (1985).
[75]A. J. Misquitta and A. J. Stone, "Dispersion energies for small organic molecules: First row atoms," Mol. Phys. **106**(12-13), 1631–1643 (2008).
[76]N. Otero, C. Van Alsenoy, C. Pouchan, and P. Karamanis, "Hirshfeld-based intrinsic polarizability density representations as a tool to analyze molecular polarizability," J. Comput. Chem. **36**(24), 1831–1843 (2015).
[77]A. Olasz, K. Vanommeslaeghe, A. Krishtal, T. Veszprémi, C. Van Alsenoy, and P. Geerlings, "The use of atomic intrinsic polarizabilities in the evaluation of the dispersion energy," J. Chem. Phys. **127**(22), 224105 (2007).
[78]A. Krishtal, P. Senet, and C. Van Alsenoy, "Local softness, softness dipole, and polarizabilities of functional groups: Application to the side chains of the 20 amino acids," J. Chem. Phys. **131**(4), 044312 (2009).
[79]D. Geldof, A. Krishtal, P. Geerlings, and C. Van Alsenoy, "Partitioning of higher multipole polarizabilities: Numerical evaluation of transferability," J. Phys. Chem. A **115**(45), 13096–13103 (2011).
[80]G. J. Williams and A. J. Stone, "Distributed dispersion: A new approach," J. Chem. Phys. **119**(9), 4620–4628 (2003).
[81]N. El-Bakali Kassimi and Z. Lin, "Aza-substituted thiophene derivatives: Structures, dipole moments, and polarizabilities," J. Phys. Chem. A **102**(48), 9906–9911 (1998).
[82]J.-F. Truchon, A. Nicholls, R. I. Iftimie, B. Roux, and C. I. Bayly, "Accurate molecular polarizabilities based on continuum electrostatics," J. Chem. Theory Comput. **4**(9), 1480–1493 (2008).
[83]A. J. Stone and R. J. A. Tough, "Spherical tensor theory of long-range intermolecular forces," Chem. Phys. Lett. **110**(2), 123–129 (1984).
[84]W. Kohn and L. J. Sham, "Self-consistent equations including exchange and correlation effects," Phys. Rev. **140**(4A), A1133–A1138 (1965).
[85]R. A. Kendall, T. H. Dunning, and R. J. Harrison, "Electron affinities of the first-row atoms revisited. Systematic basis sets and wave functions," J. Chem. Phys. **96**(9), 6796–6806 (1992).
[86]T. Verstraelen, P. Tecmer, F. Heidar-Zadeh, C. E. González-Espinoza, M. Chan, T. D. Kim, K. Boguslawski, S. Fias, S. Vandenbrande, D. Berrocal, and P. W. Ayers, Horton 2.1.1, 2017, accessed on 7 June 2023.
[87]K. Aidas, C. Angeli, K. L. Bak, V. Bakken, R. Bast, L. Boman, O. Christiansen, R. Cimiraglia, S. Coriani, P. Dahle, E. K. Dalskov, U. Ekström, T. Enevoldsen, J. J. Eriksen, P. Ettenhuber, B. Fernández, L. Ferrighi, H. Fliegl, L. Frediani, K. Hald, A. Halkier, C. Hättig, H. Heiberg, T. Helgaker, A. C. Hennum, H. Hettema, E. Hjertenaes, S. Høst, I.-M. Høyvik, M. F. Iozzi, B. Jansík, H. J. Aa. Jensen, D. Jonsson, P. Jørgensen, J. Kauczor, S. Kirpekar, T. Kjaergaard, W. Klopper, S. Knecht, R. Kobayashi, H. Koch, J. Kongsted, A. Krapp, K. Kristensen, A. Ligabue, O. B. Lutnaes, J. I. Melo, K. V. Mikkelsen, R. H. Myhre, C. Neiss, C. B. Nielsen, P. Norman, J. Olsen, J. M. H. Olsen, A. Osted, M. J. Packer, F. Pawlowski, T. B. Pedersen, P. F. Provasi, S. Reine, Z. Rinkevicius, T. A. Ruden, K. Ruud, V. V. Rybkin, P. Sałek, C. C. M. Samson, A. S. de Merás, T. Saue, S. P. A. Sauer, B. Schimmelpfennig, K. Sneskov, A. H. Steindal, K. O. Sylvester-Hvid, P. R. Taylor, A. M. Teale, E. I. Tellgren, D. P. Tew, A. J. Thorvaldsen, L. Thøgersen, O. Vahtras, M. A. Watson, D. J. D. Wilson, M. Ziolkowski, H. Ågren, and H. Ågren, "The Dalton quantum chemistry program system," Wiley Interdiscip. Rev.: Comput. Mol. Sci. **4**(3), 269–284 (2013).
[88]M. Montilla, J. M. Luis, and P. Salvador, "Origin-independent decomposition of the static polarizability," J. Chem. Theory Comput. **17**(2), 1098–1105 (2021).
[89]B. T. Thole, "Molecular polarizabilities calculated with a modified dipole interaction," Chem. Phys. **59**(3), 341–350 (1981).

Published under an exclusive license by AIP Publishing

The Journal of Chemical Physics ARTICLE pubs.aip.org/aip/jcp

[90]G. Lamoureux, A. D. MacKerell, and B. Roux, "A simple polarizable model of water based on classical Drude oscillators," J. Chem. Phys. **119**(10), 5185–5197 (2003).
[91] P. Ren, C. Wu, and J. W. Ponder, "Polarizable atomic multipole-based molecular mechanics for organic molecules," J. Chem. Theory Comput. **7**(10), 3143–3161 (2011).
[92]Q. Ge, Y. Mao, and M. Head-Gordon, "Energy decomposition analysis for exciplexes using absolutely localized molecular orbitals," J. Chem. Phys. **148**(6), 064105 (2018).
[93]F. F. Summa, G. Monaco, P. Lazzeretti, and R. Zanasi, "Origin-independent densities of static and dynamic molecular polarizabilities," J. Phys. Chem. Lett. **12**(36), 8855–8864 (2021).

Published under an exclusive license by AIP Publishing

Supplementary Material for

The Significance of Fluctuating Charges for Molecular Polarizability and Dispersion Coefficients

YingXing Cheng* and Toon Verstraelen*,#

* Center for Molecular Modeling (CMM), Ghent University, Technologiepark-Zwijnaarde 46, B-9052, Ghent, Belgium

toon.verstraelen@ugent.be

Contents

S1 Additional figures

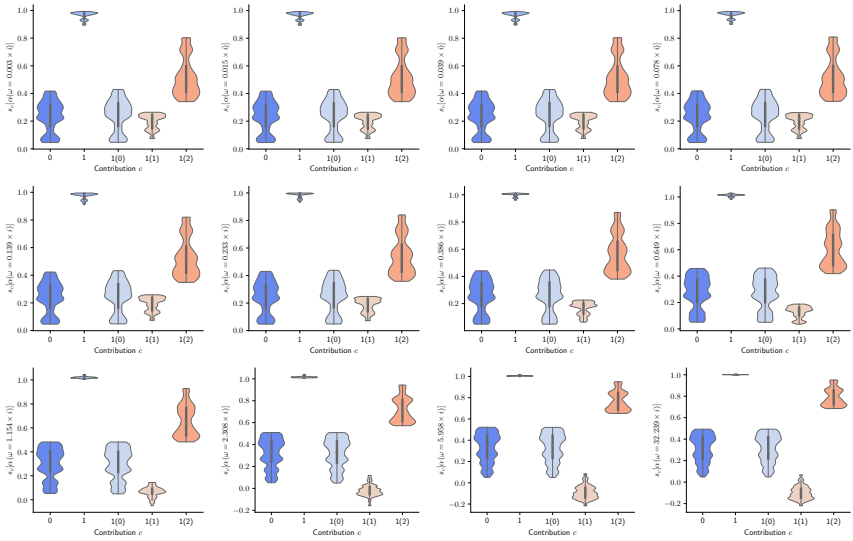

Figure S1: The distribution of the descriptor $s_c[\alpha(\omega)]$ over the TS42 database, for all relevant contributions c, and for all imaginary frequencies considered in this work.

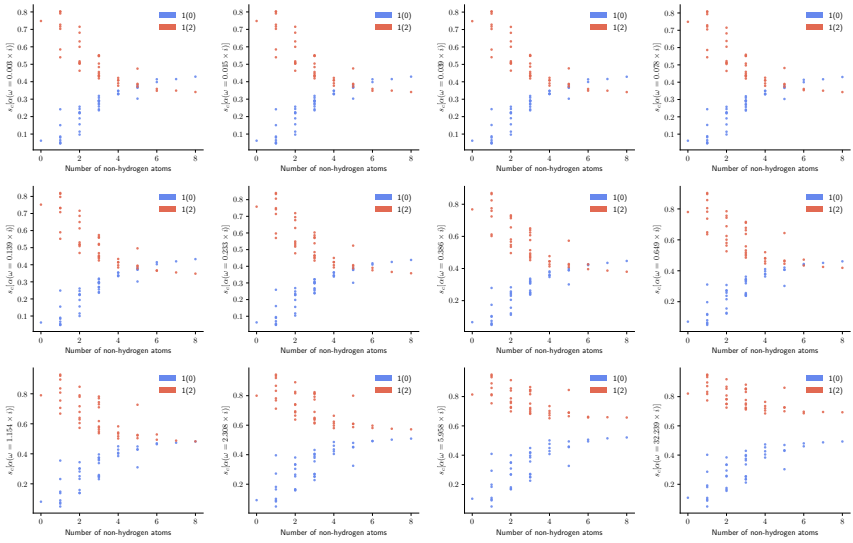

Figure S2: Scatter plots showing the dependence of the descriptors $s_{1(0)}[\alpha(\omega)]$ and $s_{1(2)}[\alpha(\omega)]$ on the number of non-hydrogen atoms, for all imaginary frequencies considered in this work.

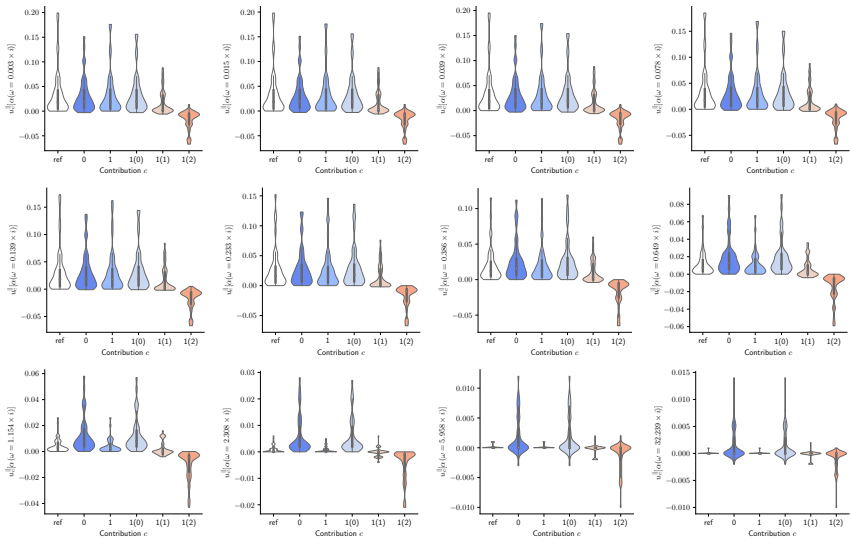

Figure S3: Violin plots of the distribution of the descriptor $u_c^{\parallel}[\alpha(\omega)]$ over the TS42 database, for all relevant contributions c and all imaginary frequencies considered in this work.

S2 Additional tables

S2.1 Tables with $s_c[\alpha(\omega)]$

Table S1: Isotropic descriptors $s_c[\alpha(\omega = 0.003 \times i)]$ for all molecules in the TS42 database, for each contribution c, as documented in Table II in the main text.

Molecule	$s_0[\alpha(\omega)]$	$s_1[\alpha(\omega)]$	$s_{1(0)}[\alpha(\omega)]$	$s_{1(1)}[\alpha(\omega)]$	$s_{1(2)}[\alpha(\omega)]$
C_8H_{18}	0.417	0.988	0.429	0.218	0.341
C_7H_{16}	0.404	0.988	0.415	0.224	0.349
C_6H_6	0.404	0.965	0.414	0.204	0.348
C_6H_{14}	0.387	0.987	0.398	0.230	0.359
C_5H_{12}	0.365	0.986	0.377	0.238	0.372
$CH_3CH_2OCH_2CH_3$	0.358	0.985	0.368	0.230	0.388
$C_4H_{10}O$	0.354	0.983	0.366	0.234	0.384
C_4H_{10}	0.337	0.986	0.348	0.248	0.391
C_4H_8	0.336	0.984	0.347	0.260	0.377
C_3H_7OH	0.322	0.982	0.332	0.242	0.408
$CH_3CH_3CH_3N$	0.318	0.981	0.329	0.244	0.408
CH_3COCH_3	0.312	0.974	0.329	0.222	0.422
C_3H_6	0.309	0.975	0.319	0.222	0.434
C_3H_8	0.299	0.985	0.308	0.258	0.419
CCl_4	0.299	0.905	0.303	0.126	0.475
CH_3OCH_3	0.284	0.982	0.292	0.254	0.437
CH_3CHO	0.273	0.970	0.291	0.224	0.456
CH_3NHCH_3	0.283	0.981	0.291	0.260	0.430
C_2H_5OH	0.278	0.980	0.286	0.248	0.447
CS_2	0.267	0.899	0.276	0.140	0.484
N_2O	0.235	0.934	0.270	0.162	0.504
CO_2	0.214	0.956	0.258	0.152	0.548
C_2H_6	0.249	0.984	0.257	0.264	0.463
C_2H_4	0.236	0.970	0.244	0.220	0.506
COS	0.218	0.922	0.242	0.128	0.552
SiH_4	0.235	0.975	0.242	0.194	0.540
SO_2	0.217	0.923	0.236	0.140	0.547
H_2CO	0.211	0.967	0.225	0.224	0.517
CH_3NH_2	0.215	0.978	0.222	0.254	0.503
CH_3OH	0.212	0.978	0.219	0.248	0.510
C_2H_2	0.183	0.966	0.190	0.176	0.600
Cl_2	0.156	0.894	0.156	0.108	0.631
CH_4	0.148	0.983	0.151	0.246	0.585
N_2	0.104	0.941	0.114	0.148	0.681
CO	0.090	0.932	0.097	0.120	0.715
H_2S	0.083	0.932	0.086	0.130	0.716
NH_3	0.078	0.972	0.080	0.190	0.703
H_2O	0.063	0.971	0.065	0.178	0.727
H_2	0.061	0.993	0.062	0.184	0.748
HBr	0.051	0.930	0.053	0.074	0.803
HCl	0.046	0.926	0.047	0.078	0.801
HF	0.045	0.973	0.047	0.134	0.791
Min.	0.045	0.894	0.047	0.074	0.341
Max.	0.417	0.993	0.429	0.264	0.803
Mean	0.237	0.963	0.247	0.197	0.520

Table S2: Isotropic descriptors $s_c[\alpha(\omega = 0.015 \times i)]$ for all molecules in the TS42 database, for each contribution c, as documented in Table II in the main text.

Molecule	$s_0[\alpha(\omega)]$	$s_1[\alpha(\omega)]$	$s_{1(0)}[\alpha(\omega)]$	$s_{1(1)}[\alpha(\omega)]$	$s_{1(2)}[\alpha(\omega)]$
C_8H_{18}	0.417	0.988	0.429	0.218	0.341
C_7H_{16}	0.404	0.988	0.415	0.224	0.349
C_6H_6	0.404	0.966	0.414	0.204	0.348
C_6H_{14}	0.387	0.987	0.398	0.230	0.359
C_5H_{12}	0.365	0.986	0.377	0.238	0.372
$CH_3CH_2OCH_2CH_3$	0.359	0.985	0.368	0.230	0.388
$C_4H_{10}O$	0.354	0.984	0.366	0.234	0.384
C_4H_{10}	0.337	0.986	0.348	0.248	0.391
C_4H_8	0.337	0.984	0.348	0.260	0.377
C_3H_7OH	0.322	0.982	0.332	0.242	0.408
$CH_3CH_3CH_3N$	0.318	0.982	0.329	0.244	0.408
CH_3COCH_3	0.312	0.974	0.329	0.222	0.422
C_3H_6	0.309	0.975	0.319	0.222	0.434
C_3H_8	0.299	0.985	0.308	0.258	0.419
CCl_4	0.299	0.905	0.303	0.126	0.476
CH_3OCH_3	0.284	0.982	0.292	0.254	0.437
CH_3CHO	0.274	0.970	0.291	0.222	0.456
CH_3NHCH_3	0.283	0.981	0.291	0.260	0.430
C_2H_5OH	0.278	0.980	0.286	0.246	0.447
CS_2	0.267	0.899	0.276	0.140	0.484
N_2O	0.235	0.934	0.270	0.162	0.504
CO_2	0.214	0.957	0.258	0.152	0.548
C_2H_6	0.249	0.984	0.257	0.264	0.463
C_2H_4	0.236	0.970	0.244	0.220	0.506
COS	0.218	0.922	0.242	0.128	0.552
SiH_4	0.235	0.975	0.242	0.194	0.540
SO_2	0.217	0.924	0.236	0.140	0.548
H_2CO	0.211	0.967	0.225	0.224	0.517
CH_3NH_2	0.216	0.979	0.222	0.254	0.503
CH_3OH	0.212	0.978	0.219	0.248	0.510
C_2H_2	0.183	0.966	0.190	0.176	0.600
Cl_2	0.156	0.894	0.156	0.108	0.631
CH_4	0.148	0.983	0.151	0.246	0.585
N_2	0.104	0.941	0.114	0.146	0.681
CO	0.090	0.932	0.097	0.120	0.715
H_2S	0.083	0.933	0.086	0.130	0.716
NH_3	0.078	0.972	0.080	0.190	0.703
H_2O	0.063	0.971	0.065	0.178	0.727
H_2	0.061	0.994	0.062	0.184	0.748
HBr	0.051	0.930	0.053	0.074	0.803
HCl	0.046	0.926	0.047	0.078	0.801
HF	0.045	0.973	0.047	0.134	0.791
Min.	0.045	0.894	0.047	0.074	0.341
Max.	0.417	0.994	0.429	0.264	0.803
Mean	0.237	0.964	0.247	0.197	0.520

Table S3: Isotropic descriptors $s_c[\alpha(\omega = 0.039 \times i)]$ for all molecules in the TS42 database, for each contribution c, as documented in Table II in the main text.

Molecule	$s_0[\alpha(\omega)]$	$s_1[\alpha(\omega)]$	$s_{1(0)}[\alpha(\omega)]$	$s_{1(1)}[\alpha(\omega)]$	$s_{1(2)}[\alpha(\omega)]$
C_8H_{18}	0.418	0.988	0.429	0.218	0.341
C_7H_{16}	0.404	0.988	0.416	0.224	0.349
C_6H_6	0.404	0.967	0.414	0.204	0.349
C_6H_{14}	0.388	0.988	0.399	0.230	0.359
C_5H_{12}	0.366	0.987	0.377	0.238	0.373
$CH_3CH_2OCH_2CH_3$	0.359	0.985	0.368	0.228	0.388
$C_4H_{10}O$	0.355	0.984	0.366	0.234	0.385
C_4H_{10}	0.338	0.986	0.348	0.246	0.391
C_4H_8	0.337	0.984	0.348	0.258	0.378
C_3H_7OH	0.323	0.982	0.333	0.242	0.408
$CH_3CH_3CH_3N$	0.319	0.982	0.330	0.244	0.409
CH_3COCH_3	0.313	0.975	0.330	0.222	0.423
C_3H_6	0.309	0.975	0.319	0.222	0.435
C_3H_8	0.299	0.985	0.309	0.258	0.419
CCl_4	0.299	0.907	0.303	0.126	0.477
CH_3CHO	0.274	0.971	0.292	0.222	0.457
CH_3OCH_3	0.285	0.982	0.292	0.252	0.437
CH_3NHCH_3	0.284	0.982	0.292	0.258	0.431
C_2H_5OH	0.278	0.981	0.287	0.246	0.447
CS_2	0.267	0.901	0.275	0.138	0.487
N_2O	0.236	0.935	0.270	0.160	0.505
CO_2	0.214	0.957	0.257	0.150	0.549
C_2H_6	0.250	0.984	0.257	0.264	0.464
C_2H_4	0.237	0.971	0.244	0.220	0.507
SiH_4	0.236	0.975	0.243	0.192	0.541
COS	0.218	0.923	0.242	0.128	0.554
SO_2	0.217	0.925	0.236	0.140	0.549
H_2CO	0.211	0.967	0.225	0.224	0.518
CH_3NH_2	0.216	0.979	0.222	0.254	0.504
CH_3OH	0.213	0.978	0.219	0.248	0.511
C_2H_2	0.183	0.967	0.191	0.174	0.601
Cl_2	0.156	0.896	0.156	0.108	0.632
CH_4	0.148	0.983	0.152	0.246	0.585
N_2	0.104	0.942	0.114	0.146	0.681
CO	0.090	0.933	0.097	0.120	0.715
H_2S	0.083	0.934	0.087	0.130	0.717
NH_3	0.078	0.973	0.080	0.190	0.703
H_2O	0.063	0.972	0.065	0.180	0.728
H_2	0.061	0.994	0.062	0.184	0.748
HBr	0.051	0.931	0.053	0.074	0.804
HCl	0.046	0.927	0.047	0.078	0.802
HF	0.045	0.973	0.047	0.134	0.791
Min.	0.045	0.896	0.047	0.074	0.341
Max.	0.418	0.994	0.429	0.264	0.804
Mean	0.238	0.964	0.247	0.197	0.520

Table S4: Isotropic descriptors $s_c[\alpha(\omega = 0.078 \times i)]$ for all molecules in the TS42 database, for each contribution c, as documented in Table II in the main text.

Molecule	$s_0[\alpha(\omega)]$	$s_1[\alpha(\omega)]$	$s_{1(0)}[\alpha(\omega)]$	$s_{1(1)}[\alpha(\omega)]$	$s_{1(2)}[\alpha(\omega)]$
C_8H_{18}	0.419	0.990	0.430	0.216	0.343
C_7H_{16}	0.406	0.989	0.417	0.222	0.351
C_6H_6	0.405	0.970	0.414	0.202	0.354
C_6H_{14}	0.389	0.989	0.400	0.228	0.361
C_5H_{12}	0.368	0.988	0.378	0.236	0.374
$CH_3CH_2OCH_2CH_3$	0.361	0.987	0.370	0.226	0.390
$C_4H_{10}O$	0.357	0.986	0.367	0.232	0.386
C_4H_{10}	0.340	0.987	0.350	0.244	0.393
C_4H_8	0.339	0.986	0.350	0.256	0.379
C_3H_7OH	0.324	0.984	0.334	0.240	0.410
$CH_3CH_3CH_3N$	0.321	0.984	0.331	0.242	0.411
CH_3COCH_3	0.314	0.977	0.330	0.220	0.426
C_3H_6	0.310	0.978	0.319	0.220	0.438
C_3H_8	0.301	0.987	0.310	0.256	0.421
CCl_4	0.299	0.912	0.303	0.126	0.482
CH_3OCH_3	0.287	0.983	0.294	0.250	0.439
CH_3NHCH_3	0.286	0.984	0.294	0.258	0.433
CH_3CHO	0.276	0.973	0.293	0.220	0.460
C_2H_5OH	0.280	0.982	0.288	0.246	0.449
CS_2	0.266	0.907	0.274	0.136	0.497
N_2O	0.236	0.937	0.269	0.160	0.508
C_2H_6	0.251	0.985	0.258	0.262	0.465
CO_2	0.214	0.958	0.257	0.150	0.551
C_2H_4	0.238	0.973	0.245	0.218	0.511
SiH_4	0.238	0.977	0.244	0.190	0.544
COS	0.218	0.927	0.242	0.126	0.559
SO_2	0.217	0.928	0.236	0.140	0.553
H_2CO	0.212	0.969	0.226	0.222	0.522
CH_3NH_2	0.218	0.982	0.224	0.252	0.505
CH_3OH	0.214	0.980	0.220	0.248	0.513
C_2H_2	0.185	0.970	0.191	0.174	0.605
Cl_2	0.156	0.900	0.156	0.106	0.638
CH_4	0.149	0.985	0.153	0.246	0.586
N_2	0.104	0.943	0.114	0.146	0.682
CO	0.091	0.934	0.098	0.120	0.715
H_2S	0.084	0.939	0.088	0.130	0.721
NH_3	0.079	0.977	0.082	0.190	0.705
H_2O	0.063	0.974	0.065	0.180	0.729
H_2	0.062	0.994	0.062	0.182	0.749
HBr	0.051	0.936	0.053	0.074	0.809
HCl	0.046	0.932	0.048	0.078	0.806
HF	0.045	0.975	0.047	0.134	0.793
Min.	0.045	0.900	0.047	0.074	0.343
Max.	0.419	0.994	0.430	0.262	0.809
Mean	0.239	0.967	0.248	0.195	0.523

Table S5: Isotropic descriptors $s_c[\alpha(\omega = 0.139 \times i)]$ for all molecules in the TS42 database, for each contribution c, as documented in Table II in the main text.

Molecule	$s_0[\alpha(\omega)]$	$s_1[\alpha(\omega)]$	$s_{1(0)}[\alpha(\omega)]$	$s_{1(1)}[\alpha(\omega)]$	$s_{1(2)}[\alpha(\omega)]$
C_8H_{18}	0.423	0.993	0.433	0.212	0.348
C_7H_{16}	0.410	0.993	0.420	0.218	0.355
C_6H_6	0.408	0.978	0.415	0.196	0.367
C_6H_{14}	0.393	0.992	0.403	0.224	0.365
C_5H_{12}	0.372	0.992	0.382	0.232	0.379
$CH_3CH_2OCH_2CH_3$	0.365	0.991	0.373	0.222	0.395
$C_4H_{10}O$	0.361	0.989	0.371	0.228	0.391
C_4H_{10}	0.344	0.991	0.354	0.240	0.397
C_4H_8	0.345	0.989	0.354	0.252	0.384
C_3H_7OH	0.329	0.988	0.338	0.236	0.414
$CH_3CH_3CH_3N$	0.326	0.990	0.336	0.238	0.415
CH_3COCH_3	0.318	0.982	0.333	0.216	0.434
C_3H_6	0.312	0.983	0.319	0.216	0.448
C_3H_8	0.306	0.990	0.314	0.252	0.425
CCl_4	0.299	0.924	0.302	0.126	0.496
CH_3NHCH_3	0.292	0.989	0.298	0.252	0.437
CH_3OCH_3	0.291	0.987	0.297	0.246	0.444
CH_3CHO	0.279	0.979	0.295	0.216	0.468
C_2H_5OH	0.284	0.987	0.291	0.242	0.454
CS_2	0.265	0.921	0.270	0.128	0.522
N_2O	0.239	0.943	0.269	0.156	0.517
C_2H_6	0.255	0.989	0.261	0.258	0.469
CO_2	0.216	0.961	0.256	0.146	0.558
SiH_4	0.243	0.982	0.249	0.180	0.552
C_2H_4	0.241	0.980	0.246	0.214	0.520
COS	0.220	0.935	0.241	0.120	0.574
SO_2	0.219	0.937	0.236	0.138	0.563
CH_3NH_2	0.223	0.987	0.227	0.250	0.509
H_2CO	0.215	0.972	0.226	0.216	0.531
CH_3OH	0.218	0.984	0.223	0.244	0.517
C_2H_2	0.189	0.977	0.194	0.170	0.613
Cl_2	0.156	0.911	0.156	0.104	0.650
CH_4	0.152	0.988	0.155	0.242	0.590
N_2	0.106	0.947	0.115	0.146	0.686
CO	0.094	0.937	0.100	0.122	0.716
H_2S	0.086	0.951	0.090	0.130	0.731
NH_3	0.082	0.985	0.084	0.192	0.708
H_2O	0.065	0.981	0.067	0.180	0.733
H_2	0.062	0.995	0.062	0.180	0.752
HBr	0.052	0.947	0.054	0.074	0.820
HCl	0.047	0.941	0.048	0.078	0.815
HF	0.046	0.979	0.048	0.136	0.797
Min.	0.046	0.911	0.048	0.074	0.348
Max.	0.423	0.995	0.433	0.258	0.820
Mean	0.242	0.972	0.250	0.192	0.530

Table S6: Isotropic descriptors $s_c[\alpha(\omega = 0.233 \times i)]$ for all molecules in the TS42 database, for each contribution c, as documented in Table II in the main text.

Molecule	$s_0[\alpha(\omega)]$	$s_1[\alpha(\omega)]$	$s_{1(0)}[\alpha(\omega)]$	$s_{1(1)}[\alpha(\omega)]$	$s_{1(2)}[\alpha(\omega)]$
C_8H_{18}	0.430	0.999	0.438	0.202	0.358
C_7H_{16}	0.417	0.999	0.426	0.208	0.366
C_6H_6	0.415	0.992	0.418	0.184	0.391
C_6H_{14}	0.402	0.998	0.410	0.214	0.376
C_5H_{12}	0.381	0.998	0.389	0.220	0.388
$CH_3CH_2OCH_2CH_3$	0.374	0.997	0.380	0.212	0.407
$C_4H_{10}O$	0.370	0.997	0.378	0.218	0.401
C_4H_8	0.357	0.996	0.364	0.238	0.393
C_4H_{10}	0.354	0.998	0.361	0.230	0.407
$CH_3CH_3CH_3N$	0.337	0.999	0.345	0.230	0.425
C_3H_7OH	0.338	0.996	0.345	0.226	0.425
CH_3COCH_3	0.326	0.992	0.338	0.204	0.450
C_3H_8	0.316	0.997	0.322	0.240	0.434
C_3H_6	0.318	0.993	0.321	0.206	0.465
CH_3NHCH_3	0.303	0.997	0.307	0.242	0.448
CH_3OCH_3	0.300	0.994	0.304	0.236	0.454
CCl_4	0.300	0.946	0.301	0.120	0.524
CH_3CHO	0.287	0.989	0.299	0.206	0.485
C_2H_5OH	0.293	0.995	0.298	0.232	0.464
C_2H_6	0.264	0.995	0.269	0.248	0.478
N_2O	0.243	0.954	0.268	0.150	0.538
CS_2	0.261	0.945	0.262	0.112	0.570
SiH_4	0.254	0.990	0.259	0.162	0.570
CO_2	0.220	0.968	0.254	0.140	0.574
C_2H_4	0.247	0.991	0.249	0.204	0.539
COS	0.223	0.952	0.239	0.110	0.603
SO_2	0.223	0.954	0.238	0.130	0.586
CH_3NH_2	0.232	0.997	0.235	0.244	0.518
CH_3OH	0.225	0.992	0.229	0.236	0.528
H_2CO	0.220	0.980	0.227	0.204	0.549
C_2H_2	0.196	0.989	0.198	0.162	0.630
CH_4	0.159	0.994	0.161	0.236	0.597
Cl_2	0.157	0.932	0.156	0.098	0.677
N_2	0.109	0.955	0.117	0.144	0.695
CO	0.099	0.944	0.104	0.120	0.719
H_2S	0.091	0.970	0.095	0.126	0.749
NH_3	0.088	0.997	0.090	0.194	0.714
H_2O	0.068	0.994	0.070	0.182	0.742
H_2	0.064	0.998	0.063	0.176	0.758
HBr	0.054	0.967	0.056	0.072	0.840
HCl	0.048	0.960	0.050	0.076	0.834
HF	0.047	0.989	0.048	0.134	0.806
Min.	0.047	0.932	0.048	0.072	0.358
Max.	0.430	0.999	0.438	0.248	0.840
Mean	0.248	0.983	0.254	0.184	0.545

Table S7: Isotropic descriptors $s_c[\alpha(\omega = 0.386 \times i)]$ for all molecules in the TS42 database, for each contribution c, as documented in Table II in the main text.

Molecule	$s_0[\alpha(\omega)]$	$s_1[\alpha(\omega)]$	$s_{1(0)}[\alpha(\omega)]$	$s_{1(1)}[\alpha(\omega)]$	$s_{1(2)}[\alpha(\omega)]$
C_8H_{18}	0.441	1.007	0.447	0.180	0.380
C_7H_{16}	0.430	1.007	0.435	0.184	0.387
C_6H_6	0.429	1.010	0.426	0.158	0.426
C_6H_{14}	0.416	1.007	0.421	0.190	0.396
C_5H_{12}	0.397	1.007	0.402	0.196	0.409
$CH_3CH_2OCH_2CH_3$	0.388	1.006	0.390	0.188	0.428
$C_4H_{10}O$	0.385	1.007	0.389	0.196	0.422
C_4H_8	0.379	1.005	0.382	0.210	0.413
C_4H_{10}	0.371	1.007	0.375	0.206	0.426
$CH_3CH_3CH_3N$	0.355	1.010	0.359	0.208	0.444
C_3H_7OH	0.354	1.007	0.358	0.204	0.445
CH_3COCH_3	0.340	1.005	0.347	0.180	0.477
C_3H_8	0.334	1.006	0.337	0.216	0.452
C_3H_6	0.329	1.007	0.329	0.184	0.494
CH_3NHCH_3	0.320	1.008	0.321	0.222	0.466
CH_3OCH_3	0.316	1.004	0.317	0.214	0.474
C_2H_5OH	0.309	1.007	0.311	0.212	0.484
CH_3CHO	0.300	1.003	0.306	0.182	0.514
CCl_4	0.302	0.977	0.301	0.102	0.573
C_2H_6	0.281	1.005	0.283	0.226	0.496
SiH_4	0.276	1.001	0.279	0.120	0.602
N_2O	0.249	0.973	0.263	0.132	0.577
C_2H_4	0.259	1.007	0.257	0.184	0.567
CS_2	0.256	0.974	0.252	0.082	0.639
CH_3NH_2	0.248	1.010	0.248	0.226	0.535
CO_2	0.226	0.980	0.248	0.126	0.607
SO_2	0.233	0.979	0.242	0.114	0.624
CH_3OH	0.239	1.005	0.240	0.218	0.547
COS	0.229	0.975	0.237	0.088	0.650
H_2CO	0.229	0.993	0.230	0.182	0.581
C_2H_2	0.208	1.005	0.205	0.144	0.656
CH_4	0.173	1.004	0.174	0.218	0.612
Cl_2	0.157	0.963	0.156	0.084	0.723
N_2	0.116	0.970	0.121	0.136	0.713
CO	0.108	0.960	0.112	0.116	0.731
H_2S	0.100	0.993	0.104	0.114	0.775
NH_3	0.098	1.013	0.100	0.190	0.724
H_2O	0.073	1.012	0.074	0.178	0.759
H_2	0.067	1.003	0.066	0.170	0.768
HBr	0.057	0.994	0.059	0.064	0.870
HCl	0.051	0.987	0.053	0.070	0.863
HF	0.049	1.005	0.049	0.132	0.824
Min.	0.049	0.960	0.049	0.064	0.380
Max.	0.441	1.013	0.447	0.226	0.870
Mean	0.259	0.998	0.262	0.165	0.570

Table S8: Isotropic descriptors $s_c[\alpha(\omega = 0.649 \times i)]$ for all molecules in the TS42 database, for each contribution c, as documented in Table II in the main text.

Molecule	$s_0[\alpha(\omega)]$	$s_1[\alpha(\omega)]$	$s_{1(0)}[\alpha(\omega)]$	$s_{1(1)}[\alpha(\omega)]$	$s_{1(2)}[\alpha(\omega)]$
C_8H_{18}	0.458	1.014	0.461	0.134	0.419
C_7H_{16}	0.448	1.014	0.451	0.138	0.425
C_6H_6	0.452	1.025	0.444	0.108	0.472
C_6H_{14}	0.436	1.014	0.438	0.142	0.434
C_5H_{12}	0.420	1.014	0.421	0.148	0.445
C_4H_8	0.413	1.013	0.411	0.156	0.447
$CH_3CH_2OCH_2CH_3$	0.408	1.015	0.407	0.142	0.466
$C_4H_{10}O$	0.406	1.017	0.406	0.150	0.461
C_4H_{10}	0.397	1.015	0.397	0.156	0.461
$CH_3CH_3CH_3N$	0.380	1.020	0.380	0.162	0.479
C_3H_7OH	0.377	1.017	0.377	0.158	0.482
CH_3COCH_3	0.362	1.017	0.363	0.134	0.520
C_3H_8	0.362	1.015	0.362	0.168	0.485
C_3H_6	0.349	1.018	0.346	0.140	0.532
CH_3NHCH_3	0.346	1.018	0.344	0.178	0.498
CH_3OCH_3	0.339	1.014	0.337	0.170	0.508
C_2H_5OH	0.333	1.019	0.331	0.168	0.519
CH_3CHO	0.320	1.017	0.319	0.140	0.558
SiH_4	0.312	1.009	0.311	0.050	0.649
C_2H_6	0.309	1.015	0.308	0.180	0.526
CCl_4	0.307	1.004	0.302	0.058	0.644
C_2H_4	0.279	1.020	0.274	0.144	0.601
CH_3NH_2	0.273	1.022	0.270	0.188	0.563
CH_3OH	0.260	1.018	0.258	0.180	0.580
N_2O	0.254	0.995	0.256	0.100	0.638
SO_2	0.247	1.003	0.249	0.076	0.678
CS_2	0.254	0.999	0.246	0.036	0.716
CO_2	0.233	0.998	0.240	0.098	0.662
COS	0.239	0.998	0.238	0.050	0.710
H_2CO	0.243	1.010	0.238	0.146	0.625
C_2H_2	0.224	1.019	0.216	0.116	0.688
CH_4	0.197	1.015	0.197	0.182	0.636
Cl_2	0.158	0.994	0.156	0.052	0.785
N_2	0.126	0.991	0.128	0.120	0.743
CO	0.122	0.982	0.123	0.104	0.756
H_2S	0.117	1.010	0.120	0.086	0.805
NH_3	0.114	1.026	0.115	0.174	0.737
H_2O	0.081	1.030	0.080	0.168	0.782
H_2	0.073	1.010	0.071	0.160	0.780
HBr	0.064	1.016	0.065	0.048	0.903
HCl	0.057	1.010	0.058	0.056	0.896
HF	0.051	1.027	0.050	0.122	0.857
Min.	0.051	0.982	0.050	0.036	0.419
Max.	0.458	1.030	0.461	0.188	0.903
Mean	0.276	1.012	0.275	0.128	0.609

Table S9: Isotropic descriptors $s_c[\alpha(\omega = 1.154 \times i)]$ for all molecules in the TS42 database, for each contribution c, as documented in Table II in the main text.

Molecule	$s_0[\alpha(\omega)]$	$s_1[\alpha(\omega)]$	$s_{1(0)}[\alpha(\omega)]$	$s_{1(1)}[\alpha(\omega)]$	$s_{1(2)}[\alpha(\omega)]$
C_8H_{18}	0.482	1.015	0.482	0.050	0.483
C_7H_{16}	0.474	1.016	0.474	0.054	0.488
C_6H_6	0.479	1.028	0.470	0.028	0.529
C_6H_{14}	0.464	1.016	0.464	0.058	0.494
C_4H_8	0.454	1.016	0.450	0.064	0.502
C_5H_{12}	0.450	1.016	0.449	0.064	0.504
$CH_3CH_2OCH_2CH_3$	0.433	1.018	0.430	0.062	0.526
$C_4H_{10}O$	0.430	1.020	0.428	0.070	0.522
C_4H_{10}	0.430	1.017	0.428	0.072	0.517
$CH_3CH_3CH_3N$	0.410	1.022	0.407	0.080	0.534
C_3H_7OH	0.404	1.022	0.401	0.080	0.542
C_3H_8	0.399	1.018	0.396	0.084	0.537
CH_3COCH_3	0.389	1.022	0.385	0.054	0.583
CH_3NHCH_3	0.379	1.022	0.375	0.100	0.547
C_3H_6	0.379	1.022	0.374	0.066	0.582
CH_3OCH_3	0.369	1.019	0.364	0.094	0.561
C_2H_5OH	0.361	1.024	0.357	0.092	0.574
SiH_4	0.358	1.010	0.355	-0.050	0.706
C_2H_6	0.347	1.018	0.344	0.100	0.573
CH_3CHO	0.343	1.024	0.338	0.068	0.618
CCl_4	0.316	1.015	0.310	-0.022	0.727
C_2H_4	0.309	1.024	0.303	0.080	0.640
CH_3NH_2	0.305	1.026	0.301	0.120	0.605
CH_3OH	0.286	1.026	0.282	0.114	0.629
SO_2	0.263	1.017	0.259	0.014	0.744
CS_2	0.262	1.011	0.253	-0.024	0.782
H_2CO	0.259	1.022	0.251	0.092	0.679
N_2O	0.258	1.013	0.250	0.052	0.710
COS	0.251	1.012	0.244	-0.002	0.770
C_2H_2	0.242	1.025	0.233	0.074	0.717
CH_4	0.234	1.019	0.232	0.118	0.668
CO_2	0.237	1.015	0.231	0.054	0.730
Cl_2	0.162	1.010	0.159	0.004	0.847
H_2S	0.146	1.015	0.148	0.030	0.836
N_2	0.144	1.010	0.140	0.088	0.780
CO	0.141	1.003	0.138	0.074	0.790
NH_3	0.138	1.029	0.138	0.136	0.755
H_2O	0.091	1.039	0.090	0.140	0.808
H_2	0.083	1.014	0.081	0.144	0.790
HBr	0.075	1.022	0.076	0.018	0.928
HCl	0.068	1.018	0.068	0.030	0.920
HF	0.052	1.044	0.049	0.100	0.895
Min.	0.052	1.003	0.049	-0.050	0.483
Max.	0.482	1.044	0.482	0.144	0.928
Mean	0.299	1.019	0.295	0.065	0.659

Table S10: Isotropic descriptors $s_c[\alpha(\omega = 2.308 \times i)]$ for all molecules in the TS42 database, for each contribution c, as documented in Table II in the main text.

Molecule	$s_0[\alpha(\omega)]$	$s_1[\alpha(\omega)]$	$s_{1(0)}[\alpha(\omega)]$	$s_{1(1)}[\alpha(\omega)]$	$s_{1(2)}[\alpha(\omega)]$
C_8H_{18}	0.510	1.010	0.509	-0.072	0.572
C_7H_{16}	0.503	1.011	0.502	-0.068	0.576
C_6H_{14}	0.494	1.011	0.493	-0.062	0.581
C_6H_6	0.498	1.018	0.492	-0.070	0.597
C_4H_8	0.489	1.011	0.486	-0.054	0.580
C_5H_{12}	0.481	1.011	0.480	-0.056	0.587
C_4H_{10}	0.463	1.012	0.461	-0.046	0.597
$CH_3CH_2OCH_2CH_3$	0.455	1.013	0.453	-0.048	0.609
$C_4H_{10}O$	0.451	1.015	0.450	-0.044	0.609
$CH_3CH_3CH_3N$	0.438	1.015	0.436	-0.034	0.612
C_3H_8	0.434	1.012	0.432	-0.032	0.612
C_3H_7OH	0.425	1.016	0.423	-0.030	0.624
CH_3NHCH_3	0.409	1.015	0.406	-0.010	0.618
CH_3COCH_3	0.409	1.017	0.405	-0.052	0.664
C_3H_6	0.407	1.015	0.403	-0.032	0.644
SiH_4	0.398	1.006	0.396	-0.158	0.768
CH_3OCH_3	0.393	1.016	0.390	-0.010	0.637
C_2H_6	0.384	1.013	0.381	-0.008	0.638
C_2H_5OH	0.382	1.018	0.379	-0.010	0.650
CH_3CHO	0.360	1.019	0.355	-0.026	0.690
C_2H_4	0.339	1.016	0.335	-0.006	0.687
CH_3NH_2	0.335	1.018	0.332	0.022	0.665
CCl_4	0.329	1.010	0.325	-0.116	0.800
CH_3OH	0.307	1.021	0.304	0.024	0.694
CH_4	0.273	1.013	0.272	0.030	0.712
CS_2	0.275	1.009	0.269	-0.084	0.824
SO_2	0.273	1.017	0.269	-0.064	0.812
H_2CO	0.272	1.020	0.265	0.016	0.738
C_2H_2	0.259	1.017	0.253	0.022	0.742
COS	0.259	1.014	0.253	-0.056	0.816
N_2O	0.259	1.019	0.251	-0.006	0.774
CO_2	0.237	1.021	0.228	0.000	0.793
H_2S	0.181	1.009	0.182	-0.040	0.867
Cl_2	0.168	1.008	0.166	-0.048	0.891
NH_3	0.165	1.021	0.165	0.074	0.782
N_2	0.167	1.016	0.162	0.038	0.816
CO	0.162	1.013	0.158	0.028	0.826
H_2O	0.102	1.031	0.101	0.096	0.833
H_2	0.094	1.010	0.092	0.118	0.800
HBr	0.090	1.013	0.090	-0.020	0.943
HCl	0.083	1.011	0.083	-0.006	0.934
HF	0.052	1.038	0.049	0.068	0.920
Min.	0.052	1.006	0.049	-0.158	0.572
Max.	0.510	1.038	0.509	0.118	0.943
Mean	0.321	1.015	0.318	-0.020	0.717

Table S11: Isotropic descriptors $s_c[\alpha(\omega = 5.958 \times i)]$ for all molecules in the TS42 database, for each contribution c, as documented in Table II in the main text.

Molecule	$s_0[\alpha(\omega)]$	$s_1[\alpha(\omega)]$	$s_{1(0)}[\alpha(\omega)]$	$s_{1(1)}[\alpha(\omega)]$	$s_{1(2)}[\alpha(\omega)]$
C_8H_{18}	0.522	1.003	0.521	-0.174	0.657
C_7H_{16}	0.515	1.003	0.515	-0.170	0.659
C_6H_{14}	0.506	1.004	0.506	-0.164	0.662
C_4H_8	0.502	1.004	0.501	-0.150	0.652
C_5H_{12}	0.495	1.004	0.494	-0.156	0.666
C_6H_6	0.495	1.006	0.494	-0.144	0.657
C_4H_{10}	0.477	1.004	0.477	-0.146	0.672
$CH_3CH_2OCH_2CH_3$	0.460	1.005	0.459	-0.144	0.691
$C_4H_{10}O$	0.456	1.006	0.455	-0.140	0.690
$CH_3CH_3CH_3N$	0.449	1.005	0.449	-0.132	0.687
C_3H_8	0.450	1.004	0.449	-0.128	0.682
C_3H_7OH	0.429	1.006	0.428	-0.124	0.702
CH_3NHCH_3	0.421	1.005	0.420	-0.104	0.688
C_3H_6	0.416	1.005	0.415	-0.110	0.700
SiH_4	0.409	1.002	0.409	-0.216	0.809
CH_3COCH_3	0.409	1.006	0.408	-0.136	0.735
C_2H_6	0.401	1.004	0.400	-0.094	0.699
CH_3OCH_3	0.398	1.006	0.397	-0.102	0.712
C_2H_5OH	0.386	1.007	0.385	-0.100	0.722
CH_3CHO	0.359	1.007	0.357	-0.102	0.752
C_2H_4	0.352	1.005	0.351	-0.074	0.729
CH_3NH_2	0.348	1.006	0.348	-0.064	0.723
CCl_4	0.328	1.003	0.327	-0.168	0.845
CH_3OH	0.310	1.008	0.309	-0.056	0.756
CH_4	0.295	1.004	0.294	-0.044	0.754
CS_2	0.273	1.003	0.272	-0.114	0.845
H_2CO	0.271	1.009	0.269	-0.048	0.788
SO_2	0.269	1.008	0.268	-0.124	0.865
C_2H_2	0.270	1.005	0.268	-0.028	0.765
COS	0.254	1.006	0.252	-0.090	0.845
N_2O	0.252	1.009	0.249	-0.056	0.816
CO_2	0.229	1.010	0.226	-0.050	0.835
H_2S	0.199	1.003	0.199	-0.086	0.890
NH_3	0.184	1.007	0.184	0.008	0.815
N_2	0.183	1.007	0.181	-0.016	0.841
CO	0.172	1.008	0.171	-0.020	0.856
Cl_2	0.167	1.003	0.167	-0.076	0.912
H_2O	0.109	1.012	0.109	0.044	0.859
H_2	0.104	1.003	0.103	0.084	0.814
HBr	0.098	1.004	0.098	-0.044	0.950
HCl	0.092	1.003	0.092	-0.030	0.942
HF	0.051	1.017	0.050	0.036	0.932
Min.	0.051	1.002	0.050	-0.216	0.652
Max.	0.522	1.017	0.521	0.084	0.950
Mean	0.328	1.006	0.327	-0.089	0.768

Table S12: Isotropic descriptors $s_c[\alpha(\omega = 32.239 \times i)]$ for all molecules in the TS42 database, for each contribution c, as documented in Table II in the main text.

Molecule	$s_0[\alpha(\omega)]$	$s_1[\alpha(\omega)]$	$s_{1(0)}[\alpha(\omega)]$	$s_{1(1)}[\alpha(\omega)]$	$s_{1(2)}[\alpha(\omega)]$
C_8H_{18}	0.493	1.001	0.493	-0.186	0.693
C_7H_{16}	0.487	1.000	0.487	-0.182	0.695
C_6H_{14}	0.480	1.001	0.480	-0.176	0.697
C_4H_8	0.473	1.001	0.473	-0.158	0.685
C_5H_{12}	0.469	1.001	0.469	-0.168	0.700
C_6H_6	0.460	1.001	0.460	-0.146	0.686
C_4H_{10}	0.453	1.000	0.453	-0.158	0.705
$CH_3CH_2OCH_2CH_3$	0.433	1.001	0.433	-0.160	0.727
C_3H_8	0.429	1.001	0.429	-0.140	0.712
$C_4H_{10}O$	0.429	1.001	0.429	-0.154	0.725
$CH_3CH_3CH_3N$	0.426	1.000	0.426	-0.146	0.720
C_3H_7OH	0.404	1.001	0.404	-0.140	0.736
SiH_4	0.402	1.000	0.402	-0.220	0.818
CH_3NHCH_3	0.400	1.001	0.400	-0.118	0.719
C_3H_6	0.394	1.001	0.394	-0.118	0.725
C_2H_6	0.384	1.001	0.384	-0.108	0.725
CH_3COCH_3	0.383	1.001	0.383	-0.146	0.764
CH_3OCH_3	0.375	1.001	0.375	-0.120	0.745
C_2H_5OH	0.364	1.001	0.364	-0.116	0.753
CH_3CHO	0.336	1.001	0.336	-0.112	0.777
C_2H_4	0.335	1.001	0.335	-0.084	0.750
CH_3NH_2	0.333	1.001	0.333	-0.082	0.750
CCl_4	0.303	1.000	0.303	-0.164	0.861
CH_3OH	0.294	1.001	0.294	-0.076	0.783
CH_4	0.286	1.001	0.286	-0.058	0.774
C_2H_2	0.258	1.001	0.258	-0.038	0.781
CS_2	0.255	1.000	0.255	-0.108	0.853
H_2CO	0.254	1.001	0.254	-0.062	0.808
SO_2	0.252	1.001	0.252	-0.134	0.882
COS	0.235	1.001	0.235	-0.090	0.855
N_2O	0.234	1.001	0.234	-0.066	0.832
CO_2	0.212	1.001	0.212	-0.062	0.850
H_2S	0.192	1.000	0.192	-0.090	0.897
NH_3	0.181	1.001	0.181	-0.014	0.833
N_2	0.175	1.001	0.175	-0.028	0.854
CO	0.164	1.001	0.164	-0.032	0.868
Cl_2	0.155	1.000	0.155	-0.074	0.919
H_2	0.108	1.000	0.108	0.068	0.821
H_2O	0.107	1.001	0.107	0.022	0.872
HBr	0.096	1.001	0.096	-0.048	0.951
HCl	0.088	1.000	0.088	-0.034	0.946
HF	0.048	1.001	0.048	0.018	0.934
Min.	0.048	1.000	0.048	-0.220	0.685
Max.	0.493	1.001	0.493	0.068	0.951
Mean	0.310	1.001	0.310	-0.100	0.790

Table S13: Anisotropy $\|\vec{\alpha}_c(\omega = 0)\|$ for all molecules in the TS42 database, for each contribution c, as documented in Table II in the main text.

Molecule	$\|\vec{\alpha}_{\text{ref}}(\omega)\|$	$\|\vec{\alpha}_0(\omega)\|$	$\|\vec{\alpha}_1(\omega)\|$	$\|\vec{\alpha}_{1(0)}(\omega)\|$	$\|\vec{\alpha}_{1(1)}(\omega)\|$	$\|\vec{\alpha}_{1(2)}(\omega)\|$
C_8H_{18}	20.760	31.283	21.102	31.300	1.038	9.312
C_7H_{16}	16.713	25.346	16.983	25.399	0.640	7.883
CS_2	27.413	20.777	24.298	21.447	10.840	7.988
C_6H_6	18.237	20.347	19.020	20.852	10.292	12.124
C_6H_{14}	13.170	20.030	13.374	20.120	0.386	6.633
C_5H_{12}	9.456	14.471	9.594	14.563	0.230	5.141
$CH_3CH_2OCH_2CH_3$	8.829	13.150	8.960	13.321	0.448	4.455
$C_4H_{10}O$	8.364	12.551	8.468	12.735	1.122	5.177
COS	12.734	10.473	11.998	11.652	6.156	5.810
C_3H_6	8.830	9.840	9.077	10.171	4.515	5.503
C_4H_{10}	6.564	9.985	6.652	10.078	0.534	3.953
$CH_3CH_3CH_3N$	6.444	8.937	6.356	9.102	1.196	3.942
C_3H_7OH	5.436	8.049	5.443	8.202	1.241	3.877
N_2O	9.361	6.502	8.668	7.450	4.450	3.233
CH_3COCH_3	6.769	6.749	6.724	7.050	2.484	2.668
SO_2	7.369	6.272	6.897	6.927	3.018	2.923
Cl_2	8.268	6.615	6.864	6.619	4.552	4.308
C_2H_2	6.318	6.089	6.734	6.344	5.844	5.453
CO_2	6.712	5.209	6.539	6.282	3.686	3.430
C_2H_4	5.983	5.956	6.287	6.163	4.736	4.911
CH_3NHCH_3	3.733	5.855	3.775	5.973	1.058	3.640
CH_3CHO	5.996	5.452	5.896	5.972	2.888	2.593
CH_3OCH_3	3.752	5.615	3.860	5.730	0.938	2.814
C_3H_8	3.466	5.173	3.503	5.229	0.572	2.312
C_4H_8	3.394	4.388	3.351	4.399	0.014	1.060
C_2H_5OH	2.954	4.240	2.997	4.348	1.251	2.501
H_2CO	4.334	3.022	4.377	3.307	3.126	2.049
C_2H_6	2.069	2.963	2.081	2.997	0.452	1.367
CH_3NH_2	2.158	2.808	2.115	2.866	1.349	2.561
CH_3OH	1.643	2.064	1.584	2.140	1.081	1.584
N_2	2.346	1.778	2.524	1.948	2.518	1.942
CO	1.729	1.711	1.974	1.838	2.294	2.157
HBr	1.238	1.637	1.274	1.708	2.396	2.830
H_2S	0.245	1.511	0.238	1.600	2.304	3.740
HCl	1.156	1.087	1.158	1.124	1.866	1.832
NH_3	1.088	0.632	0.897	0.650	1.172	2.721
H_2O	0.399	0.580	0.453	0.598	1.398	1.596
H_2	1.240	0.507	1.264	0.514	1.518	0.768
HF	0.962	0.341	0.857	0.360	1.028	0.532
CCl_4	0.000	0.000	0.000	0.000	0.000	0.000
CH_4	0.000	0.000	0.000	0.000	0.000	0.000
SiH_4	0.000	0.000	0.000	0.000	0.000	0.001
Min.	0.000	0.000	0.000	0.000	0.000	0.000
Max.	27.413	31.283	24.298	31.300	10.840	12.124
Mean	6.134	7.143	6.053	7.359	2.301	3.555

S2.2 Tables with $\|\vec{\alpha}_c(\omega)\|$

Table S14: Anisotropy $\|\vec{\alpha}_c(\omega = 0.003 \times i)\|$ for all molecules in the TS42 database, for each contribution c, as documented in Table II in the main text.

Molecule	$\|\vec{\alpha}_{\mathrm{ref}}(\omega)\|$	$\|\vec{\alpha}_0(\omega)\|$	$\|\vec{\alpha}_1(\omega)\|$	$\|\vec{\alpha}_{1(0)}(\omega)\|$	$\|\vec{\alpha}_{1(1)}(\omega)\|$	$\|\vec{\alpha}_{1(2)}(\omega)\|$
C_8H_{18}	20.759	31.281	21.099	31.297	1.038	9.311
C_7H_{16}	16.713	25.345	16.982	25.398	0.642	7.883
CS_2	27.409	20.776	24.295	21.445	10.838	7.988
C_6H_6	18.235	20.346	19.018	20.852	10.292	12.125
C_6H_{14}	13.170	20.030	13.373	20.119	0.386	6.632
C_5H_{12}	9.456	14.470	9.594	14.562	0.230	5.141
$CH_3CH_2OCH_2CH_3$	8.828	13.149	8.960	13.322	0.448	4.456
$C_4H_{10}O$	8.364	12.551	8.467	12.733	1.121	5.176
COS	12.733	10.472	11.997	11.651	6.156	5.809
C_3H_6	8.829	9.839	9.076	10.171	4.515	5.503
C_4H_{10}	6.564	9.984	6.652	10.078	0.534	3.953
$CH_3CH_3CH_3N$	6.444	8.936	6.357	9.103	1.195	3.942
C_3H_7OH	5.436	8.048	5.443	8.201	1.241	3.877
N_2O	9.360	6.502	8.666	7.449	4.450	3.234
CH_3COCH_3	6.769	6.749	6.724	7.050	2.484	2.667
SO_2	7.368	6.272	6.897	6.927	3.018	2.923
Cl_2	8.267	6.615	6.864	6.619	4.552	4.308
C_2H_2	6.318	6.089	6.734	6.344	5.844	5.453
CO_2	6.712	5.209	6.536	6.281	3.686	3.431
C_2H_4	5.982	5.956	6.287	6.162	4.736	4.911
CH_3NHCH_3	3.733	5.855	3.776	5.973	1.058	3.640
CH_3CHO	5.995	5.452	5.896	5.972	2.888	2.593
CH_3OCH_3	3.751	5.616	3.859	5.730	0.938	2.814
C_3H_8	3.465	5.173	3.503	5.228	0.572	2.312
C_4H_8	3.394	4.388	3.351	4.399	0.012	1.060
C_2H_5OH	2.953	4.240	2.997	4.347	1.251	2.501
H_2CO	4.334	3.022	4.377	3.307	3.126	2.049
C_2H_6	2.069	2.963	2.080	2.997	0.450	1.367
CH_3NH_2	2.158	2.808	2.114	2.866	1.348	2.560
CH_3OH	1.643	2.064	1.583	2.140	1.081	1.583
N_2	2.346	1.778	2.523	1.948	2.518	1.942
CO	1.729	1.711	1.974	1.838	2.294	2.157
HBr	1.238	1.637	1.274	1.708	2.396	2.830
H_2S	0.245	1.511	0.238	1.600	2.304	3.740
HCl	1.156	1.087	1.158	1.125	1.866	1.833
NH_3	1.087	0.632	0.897	0.651	1.172	2.720
H_2O	0.399	0.580	0.452	0.598	1.398	1.595
H_2	1.240	0.507	1.264	0.514	1.518	0.768
HF	0.962	0.341	0.857	0.360	1.028	0.532
CCl_4	0.000	0.000	0.000	0.000	0.000	0.000
CH_4	0.000	0.000	0.000	0.000	0.000	0.000
SiH_4	0.000	0.000	0.000	0.000	0.000	0.000
Min.	0.000	0.000	0.000	0.000	0.000	0.000
Max.	27.409	31.281	24.295	31.297	10.838	12.125
Mean	6.134	7.142	6.052	7.359	2.301	3.555

Table S15: Anisotropy $\|\vec{\alpha}_c(\omega = 0.015 \times i)\|$ for all molecules in the TS42 database, for each contribution c, as documented in Table II in the main text.

Molecule	$\|\vec{\alpha}_{\text{ref}}(\omega)\|$	$\|\vec{\alpha}_0(\omega)\|$	$\|\vec{\alpha}_1(\omega)\|$	$\|\vec{\alpha}_{1(0)}(\omega)\|$	$\|\vec{\alpha}_{1(1)}(\omega)\|$	$\|\vec{\alpha}_{1(2)}(\omega)\|$
C_8H_{18}	20.731	31.247	21.070	31.262	1.040	9.301
C_7H_{16}	16.691	25.318	16.959	25.370	0.644	7.875
CS_2	27.312	20.735	24.222	21.400	10.808	7.986
C_6H_6	18.191	20.318	18.972	20.821	10.270	12.119
C_6H_{14}	13.152	20.010	13.355	20.097	0.385	6.625
C_5H_{12}	9.444	14.456	9.582	14.547	0.228	5.136
$CH_3CH_2OCH_2CH_3$	8.820	13.136	8.951	13.308	0.446	4.450
$C_4H_{10}O$	8.355	12.540	8.457	12.721	1.118	5.171
COS	12.708	10.462	11.974	11.637	6.144	5.806
C_3H_6	8.806	9.825	9.052	10.153	4.504	5.499
C_4H_{10}	6.555	9.975	6.643	10.068	0.530	3.949
$CH_3CH_3CH_3N$	6.433	8.927	6.347	9.093	1.193	3.937
C_3H_7OH	5.431	8.042	5.438	8.195	1.239	3.873
N_2O	9.348	6.498	8.655	7.443	4.444	3.233
CH_3COCH_3	6.753	6.742	6.710	7.042	2.478	2.667
SO_2	7.356	6.265	6.888	6.919	3.014	2.919
Cl_2	8.255	6.609	6.854	6.613	4.548	4.306
C_2H_2	6.308	6.084	6.722	6.338	5.834	5.450
CO_2	6.705	5.206	6.529	6.276	3.682	3.430
C_2H_4	5.968	5.948	6.271	6.153	4.728	4.907
CH_3NHCH_3	3.727	5.850	3.771	5.968	1.056	3.632
CH_3CHO	5.982	5.446	5.884	5.965	2.883	2.591
CH_3OCH_3	3.750	5.611	3.857	5.725	0.938	2.810
C_3H_8	3.461	5.169	3.498	5.224	0.570	2.310
C_4H_8	3.388	4.385	3.346	4.394	0.010	1.059
C_2H_5OH	2.952	4.237	2.995	4.344	1.251	2.498
H_2CO	4.326	3.020	4.369	3.304	3.122	2.049
C_2H_6	2.066	2.961	2.078	2.994	0.450	1.366
CH_3NH_2	2.153	2.806	2.110	2.864	1.346	2.556
CH_3OH	1.641	2.063	1.582	2.138	1.080	1.582
N_2	2.344	1.778	2.521	1.947	2.516	1.942
CO	1.729	1.710	1.974	1.837	2.292	2.155
HBr	1.240	1.636	1.273	1.707	2.394	2.828
H_2S	0.237	1.510	0.239	1.599	2.300	3.734
HCl	1.157	1.087	1.157	1.124	1.864	1.831
NH_3	1.076	0.632	0.889	0.650	1.172	2.711
H_2O	0.402	0.580	0.454	0.597	1.398	1.592
H_2	1.238	0.507	1.262	0.514	1.518	0.769
HF	0.962	0.341	0.857	0.360	1.028	0.531
CCl_4	0.000	0.000	0.000	0.000	0.000	0.000
CH_4	0.000	0.000	0.000	0.000	0.000	0.000
SiH_4	0.000	0.000	0.000	0.000	0.000	0.000
Min.	0.000	0.000	0.000	0.000	0.000	0.000
Max.	27.312	31.247	24.222	31.262	10.808	12.119
Mean	6.123	7.135	6.042	7.350	2.297	3.552

Table S16: Anisotropy $\|\vec{\alpha}_c(\omega = 0.039 \times i)\|$ for all molecules in the TS42 database, for each contribution c, as documented in Table II in the main text.

Molecule	$\|\vec{\alpha}_{\mathrm{ref}}(\omega)\|$	$\|\vec{\alpha}_0(\omega)\|$	$\|\vec{\alpha}_1(\omega)\|$	$\|\vec{\alpha}_{1(0)}(\omega)\|$	$\|\vec{\alpha}_{1(1)}(\omega)\|$	$\|\vec{\alpha}_{1(2)}(\omega)\|$
C_8H_{18}	20.571	31.048	20.901	31.054	1.053	9.242
C_7H_{16}	16.563	25.162	16.825	25.206	0.656	7.825
CS_2	26.754	20.503	23.801	21.140	10.634	7.973
C_6H_6	17.936	20.159	18.710	20.643	10.154	12.086
C_6H_{14}	13.052	19.890	13.251	19.971	0.385	6.584
C_5H_{12}	9.372	14.374	9.508	14.459	0.214	5.104
$CH_3CH_2OCH_2CH_3$	8.769	13.061	8.898	13.229	0.442	4.418
$C_4H_{10}O$	8.306	12.474	8.403	12.652	1.101	5.139
COS	12.560	10.398	11.843	11.553	6.078	5.788
C_3H_6	8.671	9.740	8.912	10.054	4.446	5.476
C_4H_{10}	6.505	9.922	6.592	10.011	0.513	3.925
$CH_3CH_3CH_3N$	6.369	8.877	6.292	9.037	1.180	3.907
C_3H_7OH	5.404	8.004	5.409	8.155	1.225	3.850
N_2O	9.273	6.474	8.596	7.408	4.416	3.227
CH_3COCH_3	6.662	6.702	6.632	6.995	2.448	2.665
SO_2	7.280	6.226	6.838	6.871	2.992	2.901
Cl_2	8.184	6.577	6.800	6.581	4.514	4.296
C_2H_2	6.253	6.059	6.652	6.304	5.784	5.435
CO_2	6.665	5.192	6.489	6.251	3.662	3.423
C_2H_4	5.885	5.906	6.178	6.102	4.676	4.887
CH_3NHCH_3	3.692	5.819	3.742	5.934	1.045	3.589
CH_3CHO	5.906	5.414	5.818	5.924	2.852	2.584
CH_3OCH_3	3.740	5.585	3.846	5.696	0.934	2.789
C_3H_8	3.433	5.144	3.471	5.196	0.558	2.297
C_4H_8	3.355	4.364	3.315	4.371	0.004	1.052
C_2H_5OH	2.942	4.219	2.981	4.325	1.240	2.483
H_2CO	4.280	3.008	4.324	3.287	3.096	2.050
C_2H_6	2.048	2.949	2.061	2.981	0.440	1.359
CH_3NH_2	2.123	2.795	2.085	2.850	1.331	2.531
CH_3OH	1.635	2.057	1.577	2.131	1.075	1.573
N_2	2.331	1.774	2.510	1.941	2.506	1.938
CO	1.729	1.706	1.974	1.832	2.280	2.139
HBr	1.250	1.630	1.269	1.700	2.380	2.811
H_2S	0.191	1.504	0.244	1.593	2.284	3.699
HCl	1.160	1.083	1.152	1.121	1.854	1.824
NH_3	1.011	0.630	0.844	0.648	1.168	2.661
H_2O	0.417	0.579	0.461	0.596	1.392	1.574
H_2	1.226	0.505	1.249	0.511	1.508	0.770
HF	0.961	0.341	0.856	0.359	1.026	0.528
CCl_4	0.000	0.000	0.000	0.000	0.000	0.000
CH_4	0.000	0.000	0.000	0.000	0.000	0.000
SiH_4	0.000	0.000	0.000	0.000	0.000	0.000
Min.	0.000	0.000	0.000	0.000	0.000	0.000
Max.	26.754	31.048	23.801	31.054	10.634	12.086
Mean	6.059	7.092	5.984	7.302	2.275	3.533

Table S17: Anisotropy $\|\vec{\alpha}_c(\omega = 0.078 \times i)\|$ for all molecules in the TS42 database, for each contribution c, as documented in Table II in the main text.

Molecule	$\|\vec{\alpha}_{\text{ref}}(\omega)\|$	$\|\vec{\alpha}_0(\omega)\|$	$\|\vec{\alpha}_1(\omega)\|$	$\|\vec{\alpha}_{1(0)}(\omega)\|$	$\|\vec{\alpha}_{1(1)}(\omega)\|$	$\|\vec{\alpha}_{1(2)}(\omega)\|$
C_8H_{18}	20.021	30.368	20.323	30.348	1.098	9.043
C_7H_{16}	16.126	24.626	16.366	24.645	0.702	7.656
CS_2	24.958	19.740	22.428	20.288	10.062	7.923
C_6H_6	17.107	19.632	17.849	20.057	9.764	11.972
C_6H_{14}	12.708	19.483	12.892	19.540	0.394	6.443
C_5H_{12}	9.128	14.092	9.256	14.158	0.168	4.995
$CH_3CH_2OCH_2CH_3$	8.589	12.804	8.709	12.956	0.424	4.310
$C_4H_{10}O$	8.136	12.249	8.217	12.412	1.043	5.034
COS	12.067	10.183	11.402	11.270	5.856	5.725
C_4H_{10}	6.332	9.741	6.417	9.815	0.452	3.844
C_3H_6	8.232	9.458	8.454	9.727	4.256	5.396
$CH_3CH_3CH_3N$	6.158	8.708	6.106	8.847	1.134	3.810
C_3H_7OH	5.308	7.877	5.307	8.018	1.179	3.774
N_2O	9.018	6.393	8.394	7.286	4.316	3.208
CH_3COCH_3	6.366	6.567	6.375	6.837	2.348	2.655
SO_2	7.027	6.097	6.659	6.715	2.912	2.849
Cl_2	7.936	6.465	6.612	6.468	4.404	4.260
C_2H_2	6.064	5.970	6.416	6.189	5.610	5.383
CO_2	6.526	5.141	6.353	6.163	3.590	3.400
C_2H_4	5.613	5.765	5.872	5.931	4.508	4.818
CH_3NHCH_3	3.583	5.714	3.645	5.820	1.006	3.455
CH_3CHO	5.658	5.305	5.599	5.786	2.751	2.560
CH_3OCH_3	3.701	5.495	3.799	5.598	0.920	2.719
C_3H_8	3.340	5.058	3.380	5.102	0.516	2.252
C_4H_8	3.244	4.294	3.213	4.289	0.048	1.028
C_2H_5OH	2.905	4.158	2.934	4.259	1.204	2.433
H_2CO	4.129	2.968	4.176	3.229	3.008	2.053
C_2H_6	1.989	2.907	2.004	2.933	0.408	1.337
CH_3NH_2	2.029	2.756	2.007	2.806	1.282	2.451
CH_3OH	1.611	2.035	1.556	2.106	1.056	1.544
N_2	2.288	1.761	2.469	1.923	2.470	1.924
CO	1.727	1.693	1.971	1.814	2.244	2.087
HBr	1.278	1.609	1.251	1.677	2.328	2.756
H_2S	0.095	1.483	0.259	1.571	2.226	3.586
HCl	1.169	1.072	1.132	1.109	1.822	1.797
NH_3	0.811	0.624	0.707	0.642	1.154	2.503
H_2O	0.465	0.573	0.485	0.589	1.372	1.517
H_2	1.185	0.498	1.206	0.503	1.476	0.773
HF	0.958	0.338	0.852	0.356	1.014	0.518
CCl_4	0.000	0.000	0.000	0.000	0.000	0.000
CH_4	0.000	0.000	0.000	0.000	0.000	0.000
SiH_4	0.000	0.000	0.000	0.000	0.000	0.000
Min.	0.000	0.000	0.000	0.000	0.000	0.000
Max.	24.958	30.368	22.428	30.348	10.062	11.972
Mean	5.847	6.945	5.787	7.138	2.203	3.471

Table S18: Anisotropy $\|\vec{\alpha}_c(\omega = 0.139 \times i)\|$ for all molecules in the TS42 database, for each contribution c, as documented in Table II in the main text.

Molecule	$\|\vec{\alpha}_{\mathrm{ref}}(\omega)\|$	$\|\vec{\alpha}_0(\omega)\|$	$\|\vec{\alpha}_1(\omega)\|$	$\|\vec{\alpha}_{1(0)}(\omega)\|$	$\|\vec{\alpha}_{1(1)}(\omega)\|$	$\|\vec{\alpha}_{1(2)}(\omega)\|$
C_8H_{18}	18.572	28.589	18.807	28.505	1.237	8.532
C_7H_{16}	14.974	23.221	15.162	23.181	0.840	7.224
C_6H_6	15.183	18.359	15.820	18.653	8.822	11.654
C_6H_{14}	11.801	18.412	11.951	18.414	0.474	6.082
CS_2	20.917	17.923	19.231	18.279	8.712	7.759
C_5H_{12}	8.485	13.351	8.593	13.371	0.136	4.717
$CH_3CH_2OCH_2CH_3$	8.076	12.131	8.180	12.243	0.384	4.049
$C_4H_{10}O$	7.667	11.655	7.714	11.783	0.895	4.769
COS	10.844	9.632	10.299	10.554	5.298	5.553
C_4H_{10}	5.878	9.263	5.957	9.300	0.298	3.636
C_3H_6	7.209	8.768	7.381	8.941	3.802	5.187
$CH_3CH_3CH_3N$	5.633	8.269	5.630	8.360	1.021	3.580
C_3H_7OH	5.038	7.537	5.024	7.655	1.058	3.583
N_2O	8.361	6.173	7.862	6.963	4.056	3.157
CH_3COCH_3	5.679	6.228	5.763	6.447	2.110	2.616
SO_2	6.399	5.789	6.180	6.336	2.706	2.748
Cl_2	7.274	6.173	6.119	6.173	4.112	4.167
CO_2	6.156	5.001	5.989	5.925	3.400	3.337
C_2H_2	5.574	5.734	5.816	5.889	5.170	5.242
CH_3NHCH_3	3.334	5.439	3.402	5.522	0.907	3.167
C_2H_4	4.967	5.413	5.144	5.514	4.098	4.637
CH_3CHO	5.071	5.029	5.071	5.441	2.512	2.498
CH_3OCH_3	3.558	5.254	3.641	5.336	0.868	2.554
C_3H_8	3.097	4.829	3.139	4.854	0.410	2.136
C_2H_5OH	2.790	3.995	2.795	4.082	1.112	2.308
C_4H_8	2.966	4.107	2.953	4.078	0.158	0.966
H_2CO	3.760	2.862	3.815	3.080	2.794	2.050
C_2H_6	1.836	2.793	1.858	2.808	0.326	1.277
CH_3NH_2	1.829	2.654	1.825	2.690	1.165	2.274
CH_3OH	1.547	1.976	1.497	2.038	1.005	1.473
N_2	2.172	1.724	2.357	1.872	2.370	1.885
CO	1.709	1.657	1.946	1.767	2.142	1.962
HBr	1.315	1.552	1.193	1.617	2.192	2.616
H_2S	0.288	1.429	0.292	1.512	2.078	3.317
HCl	1.174	1.041	1.076	1.076	1.732	1.731
NH_3	0.418	0.608	0.432	0.623	1.112	2.167
H_2O	0.562	0.559	0.530	0.573	1.318	1.389
H_2	1.079	0.479	1.095	0.481	1.392	0.778
HF	0.946	0.332	0.836	0.347	0.982	0.493
CCl_4	0.000	0.000	0.000	0.000	0.000	0.000
CH_4	0.000	0.000	0.000	0.000	0.000	0.000
SiH_4	0.000	0.000	0.000	0.000	0.000	0.000
Min.	0.000	0.000	0.000	0.000	0.000	0.000
Max.	20.917	28.589	19.231	28.505	8.822	11.654
Mean	5.337	6.570	5.295	6.721	2.029	3.316

Table S19: Anisotropy $\|\vec{\alpha}_c(\omega = 0.233 \times i)\|$ for all molecules in the TS42 database, for each contribution c, as documented in Table II in the main text.

Molecule	$\|\vec{\alpha}_{\text{ref}}(\omega)\|$	$\|\vec{\alpha}_0(\omega)\|$	$\|\vec{\alpha}_1(\omega)\|$	$\|\vec{\alpha}_{1(0)}(\omega)\|$	$\|\vec{\alpha}_{1(1)}(\omega)\|$	$\|\vec{\alpha}_{1(2)}(\omega)\|$
C_8H_{18}	15.478	24.796	15.593	24.614	1.570	7.480
C_7H_{16}	12.505	20.213	12.602	20.081	1.164	6.334
C_6H_6	11.933	16.010	12.302	16.109	7.080	10.887
C_6H_{14}	9.864	16.107	9.950	16.020	0.762	5.336
CS_2	14.548	14.700	13.860	14.781	6.352	7.273
C_5H_{12}	7.109	11.744	7.177	11.690	0.390	4.140
$CH_3CH_2OCH_2CH_3$	6.889	10.687	6.964	10.728	0.372	3.551
$C_4H_{10}O$	6.600	10.359	6.591	10.421	0.606	4.230
COS	8.528	8.508	8.173	9.130	4.192	5.148
C_4H_{10}	4.917	8.217	4.979	8.191	0.061	3.198
C_3H_6	5.482	7.478	5.549	7.517	2.995	4.723
$CH_3CH_3CH_3N$	4.612	7.334	4.662	7.343	0.825	3.142
C_3H_7OH	4.396	6.784	4.364	6.855	0.799	3.197
N_2O	7.005	5.677	6.720	6.259	3.492	3.031
CH_3COCH_3	4.487	5.541	4.653	5.674	1.688	2.485
SO_2	5.217	5.209	5.193	5.617	2.264	2.579
Cl_2	5.912	5.545	5.075	5.538	3.478	3.941
CO_2	5.339	4.672	5.185	5.391	2.976	3.182
C_2H_2	4.565	5.209	4.631	5.254	4.282	4.906
CH_3NHCH_3	2.847	4.851	2.886	4.890	0.700	2.706
CH_3CHO	4.028	4.476	4.102	4.764	2.079	2.357
CH_3OCH_3	3.142	4.720	3.201	4.762	0.714	2.253
C_2H_4	3.844	4.725	3.877	4.735	3.336	4.238
C_3H_8	2.587	4.325	2.629	4.314	0.196	1.888
C_2H_5OH	2.485	3.630	2.456	3.691	0.917	2.065
C_4H_8	2.421	3.699	2.434	3.627	0.364	0.830
H_2CO	3.072	2.632	3.137	2.773	2.374	2.005
C_2H_6	1.523	2.537	1.551	2.530	0.162	1.141
CH_3NH_2	1.516	2.430	1.506	2.442	0.947	1.976
CH_3OH	1.396	1.839	1.350	1.883	0.890	1.337
N_2	1.914	1.635	2.102	1.754	2.144	1.794
CO	1.610	1.569	1.827	1.656	1.914	1.742
HBr	1.267	1.425	1.033	1.481	1.888	2.335
H_2S	0.561	1.310	0.315	1.382	1.756	2.820
HCl	1.109	0.970	0.932	1.001	1.528	1.596
NH_3	0.043	0.570	0.094	0.582	1.000	1.676
H_2O	0.660	0.524	0.563	0.534	1.194	1.186
H_2	0.867	0.436	0.872	0.434	1.210	0.771
HF	0.897	0.317	0.785	0.327	0.910	0.451
CCl_4	0.000	0.000	0.000	0.000	0.000	0.000
CH_4	0.000	0.000	0.000	0.000	0.000	0.000
SiH_4	0.000	0.000	0.000	0.000	0.000	0.000
Min.	0.000	0.000	0.000	0.000	0.000	0.000
Max.	15.478	24.796	15.593	24.614	7.080	10.887
Mean	4.361	5.795	4.330	5.876	1.704	2.998

Table S20: Anisotropy $\|\vec{\alpha}_c(\omega = 0.386 \times i)\|$ for all molecules in the TS42 database, for each contribution c, as documented in Table II in the main text.

Molecule	$\|\vec{\alpha}_{\mathrm{ref}}(\omega)\|$	$\|\vec{\alpha}_0(\omega)\|$	$\|\vec{\alpha}_1(\omega)\|$	$\|\vec{\alpha}_{1(0)}(\omega)\|$	$\|\vec{\alpha}_{1(1)}(\omega)\|$	$\|\vec{\alpha}_{1(2)}(\omega)\|$
C_8H_{18}	10.432	18.441	10.405	18.190	2.058	5.745
C_7H_{16}	8.462	15.131	8.446	14.927	1.632	4.864
C_6H_6	7.928	12.622	7.887	12.545	4.630	9.287
C_6H_{14}	6.694	12.170	6.695	12.007	1.231	4.098
CS_2	7.762	10.482	7.633	10.338	3.404	6.108
C_5H_{12}	4.847	8.965	4.857	8.844	0.820	3.180
$CH_3CH_2OCH_2CH_3$	4.841	8.225	4.864	8.189	0.580	2.780
$C_4H_{10}O$	4.711	8.079	4.642	8.062	0.348	3.345
COS	5.364	6.705	5.182	6.953	2.562	4.334
C_4H_{10}	3.356	6.374	3.382	6.287	0.457	2.460
$CH_3CH_3CH_3N$	3.097	5.723	3.160	5.649	0.694	2.442
C_3H_6	3.421	5.639	3.355	5.579	1.936	3.868
C_3H_7OH	3.211	5.421	3.158	5.429	0.392	2.559
N_2O	4.878	4.751	4.809	5.034	2.534	2.758
SO_2	3.542	4.293	3.643	4.504	1.526	2.281
CH_3COCH_3	2.958	4.421	3.132	4.455	1.132	2.158
Cl_2	3.836	4.457	3.376	4.435	2.376	3.434
CO_2	3.911	4.012	3.779	4.407	2.220	2.848
C_2H_2	3.036	4.254	2.934	4.187	2.938	4.191
CH_3NHCH_3	2.038	3.837	2.020	3.830	0.393	2.090
CH_3OCH_3	2.310	3.765	2.332	3.761	0.416	1.801
CH_3CHO	2.663	3.594	2.766	3.727	1.475	2.060
C_2H_4	2.459	3.690	2.342	3.631	2.272	3.495
C_3H_8	1.768	3.416	1.795	3.369	0.128	1.462
C_2H_5OH	1.873	2.961	1.812	2.982	0.602	1.675
C_4H_8	1.616	2.966	1.645	2.857	0.614	0.597
H_2CO	2.100	2.217	2.162	2.265	1.722	1.825
C_2H_6	1.034	2.060	1.061	2.029	0.076	0.892
CH_3NH_2	1.101	2.019	1.057	2.002	0.627	1.548
CH_3OH	1.095	1.571	1.050	1.590	0.678	1.118
N_2	1.448	1.448	1.620	1.516	1.710	1.605
CO	1.311	1.387	1.478	1.434	1.494	1.450
HBr	0.966	1.188	0.704	1.229	1.338	1.864
H_2S	0.579	1.094	0.259	1.146	1.210	2.083
HCl	0.852	0.832	0.644	0.856	1.144	1.355
NH_3	0.295	0.496	0.119	0.502	0.776	1.158
H_2O	0.624	0.456	0.490	0.460	0.962	0.948
H_2	0.558	0.356	0.549	0.348	0.902	0.701
HF	0.750	0.285	0.647	0.286	0.764	0.404
CCl_4	0.000	0.000	0.000	0.000	0.000	0.000
CH_4	0.000	0.000	0.000	0.000	0.000	0.000
SiH_4	0.000	0.000	0.000	0.000	0.000	0.000
Min.	0.000	0.000	0.000	0.000	0.000	0.000
Max.	10.432	18.441	10.405	18.190	4.630	9.287
Mean	2.946	4.519	2.902	4.520	1.257	2.449

Table S21: Anisotropy $\|\vec{\alpha}_c(\omega = 0.649 \times i)\|$ for all molecules in the TS42 database, for each contribution c, as documented in Table II in the main text.

Molecule	$\|\vec{\alpha}_{\text{ref}}(\omega)\|$	$\|\vec{\alpha}_0(\omega)\|$	$\|\vec{\alpha}_1(\omega)\|$	$\|\vec{\alpha}_{1(0)}(\omega)\|$	$\|\vec{\alpha}_{1(1)}(\omega)\|$	$\|\vec{\alpha}_{1(2)}(\omega)\|$
C_8H_{18}	4.888	10.731	4.778	10.524	2.239	3.528
C_7H_{16}	3.987	8.883	3.902	8.709	1.840	2.985
C_6H_6	4.139	8.561	3.837	8.421	2.050	6.635
C_6H_{14}	3.172	7.240	3.113	7.093	1.484	2.511
CS_2	2.925	6.278	2.868	6.084	0.896	4.113
C_5H_{12}	2.314	5.411	2.279	5.297	1.084	1.946
$CH_3CH_2OCH_2CH_3$	2.460	5.091	2.424	5.034	0.808	1.810
$C_4H_{10}O$	2.417	5.061	2.317	5.010	0.563	2.182
COS	2.444	4.462	2.340	4.449	0.926	3.035
C_4H_{10}	1.613	3.943	1.602	3.852	0.757	1.505
C_3H_6	1.643	3.593	1.516	3.519	0.928	2.621
$CH_3CH_3CH_3N$	1.502	3.604	1.525	3.510	0.731	1.536
C_3H_7OH	1.709	3.533	1.642	3.503	0.221	1.705
N_2O	2.537	3.397	2.541	3.422	1.350	2.231
SO_2	1.798	3.047	1.876	3.084	0.656	1.754
CO_2	2.143	2.953	2.033	3.035	1.230	2.232
Cl_2	1.679	2.991	1.481	2.954	1.000	2.474
CH_3COCH_3	1.508	2.970	1.596	2.942	0.646	1.583
C_2H_2	1.490	2.912	1.339	2.811	1.498	2.969
CH_3CHO	1.362	2.464	1.418	2.477	0.840	1.539
CH_3NHCH_3	1.069	2.493	1.015	2.466	0.247	1.352
CH_3OCH_3	1.241	2.465	1.224	2.442	0.160	1.225
C_2H_4	1.224	2.467	1.066	2.401	1.152	2.390
C_3H_8	0.856	2.174	0.859	2.120	0.372	0.898
C_2H_5OH	1.045	2.003	0.974	1.996	0.280	1.156
C_4H_8	0.776	1.943	0.800	1.842	0.720	0.321
H_2CO	1.103	1.616	1.134	1.598	0.950	1.415
CH_3NH_2	0.615	1.412	0.556	1.381	0.301	1.010
C_2H_6	0.502	1.368	0.514	1.332	0.270	0.548
CH_3OH	0.653	1.150	0.611	1.147	0.395	0.812
N_2	0.840	1.126	0.946	1.137	1.074	1.266
CO	0.804	1.077	0.890	1.083	0.910	1.102
HBr	0.470	0.846	0.302	0.867	0.634	1.199
H_2S	0.326	0.786	0.128	0.811	0.558	1.225
HCl	0.428	0.618	0.282	0.632	0.612	0.962
NH_3	0.252	0.375	0.133	0.376	0.460	0.703
H_2O	0.402	0.346	0.288	0.345	0.626	0.692
H_2	0.264	0.241	0.249	0.234	0.524	0.509
HF	0.472	0.228	0.395	0.220	0.538	0.363
CCl_4	0.000	0.000	0.000	0.000	0.000	0.000
CH_4	0.000	0.000	0.000	0.000	0.000	0.000
SiH_4	0.000	0.000	0.000	0.000	0.000	0.000
Min.	0.000	0.000	0.000	0.000	0.000	0.000
Max.	4.888	10.731	4.778	10.524	2.239	6.635
Mean	1.454	2.901	1.400	2.861	0.775	1.668

Table S22: Anisotropy $\|\vec{\alpha}_c(\omega = 1.154 \times i)\|$ for all molecules in the TS42 database, for each contribution c, as documented in Table II in the main text.

Molecule	$\|\vec{\alpha}_{\mathrm{ref}}(\omega)\|$	$\|\vec{\alpha}_0(\omega)\|$	$\|\vec{\alpha}_1(\omega)\|$	$\|\vec{\alpha}_{1(0)}(\omega)\|$	$\|\vec{\alpha}_{1(1)}(\omega)\|$	$\|\vec{\alpha}_{1(2)}(\omega)\|$
C_6H_6	1.444	4.530	1.216	4.446	0.272	3.502
C_8H_{18}	1.316	4.479	1.235	4.388	1.652	1.517
C_7H_{16}	1.079	3.738	1.014	3.662	1.380	1.281
C_6H_{14}	0.864	3.088	0.815	3.023	1.142	1.077
CS_2	0.695	2.967	0.644	2.869	0.278	1.947
C_5H_{12}	0.636	2.342	0.603	2.291	0.864	0.832
$CH_3CH_2OCH_2CH_3$	0.759	2.319	0.712	2.291	0.698	0.883
$C_4H_{10}O$	0.739	2.312	0.668	2.282	0.580	1.046
COS	0.722	2.319	0.664	2.257	0.018	1.575
N_2O	0.864	1.915	0.841	1.856	0.390	1.406
C_3H_6	0.529	1.785	0.448	1.749	0.332	1.309
C_4H_{10}	0.448	1.751	0.429	1.710	0.644	0.643
C_3H_7OH	0.549	1.698	0.499	1.675	0.342	0.844
SO_2	0.574	1.683	0.587	1.658	0.182	1.006
CO_2	0.763	1.699	0.690	1.654	0.390	1.353
$CH_3CH_3CH_3N$	0.434	1.649	0.426	1.601	0.602	0.696
CH_3COCH_3	0.519	1.537	0.527	1.507	0.372	0.876
Cl_2	0.373	1.522	0.307	1.495	0.036	1.225
C_2H_2	0.491	1.535	0.404	1.479	0.472	1.547
CH_3CHO	0.474	1.317	0.475	1.294	0.377	0.870
C_2H_4	0.417	1.304	0.329	1.271	0.342	1.204
CH_3OCH_3	0.408	1.210	0.381	1.198	0.200	0.640
CH_3NHCH_3	0.340	1.205	0.298	1.191	0.274	0.649
C_2H_5OH	0.359	1.013	0.311	1.004	0.153	0.609
C_3H_8	0.241	0.996	0.234	0.971	0.356	0.385
H_2CO	0.397	0.934	0.394	0.905	0.314	0.826
C_4H_8	0.219	0.917	0.227	0.869	0.520	0.122
CH_3NH_2	0.212	0.742	0.176	0.723	0.164	0.490
N_2	0.327	0.706	0.350	0.690	0.438	0.777
CO	0.325	0.673	0.342	0.662	0.356	0.676
CH_3OH	0.241	0.648	0.212	0.640	0.179	0.458
C_2H_6	0.143	0.658	0.143	0.640	0.264	0.234
HBr	0.117	0.474	0.061	0.480	0.108	0.527
H_2S	0.089	0.446	0.029	0.452	0.104	0.507
HCl	0.109	0.366	0.056	0.370	0.162	0.475
NH_3	0.102	0.224	0.056	0.223	0.172	0.340
H_2O	0.150	0.209	0.093	0.208	0.288	0.402
HF	0.174	0.147	0.135	0.138	0.278	0.283
H_2	0.084	0.125	0.075	0.121	0.216	0.263
CH_4	0.000	0.000	0.000	0.000	0.000	0.000
CCl_4	0.000	0.000	0.000	0.000	0.000	0.000
SiH_4	0.000	0.000	0.000	0.000	0.000	0.000
Min.	0.000	0.000	0.000	0.000	0.000	0.000
Max.	1.444	4.530	1.235	4.446	1.652	3.502
Mean	0.446	1.409	0.407	1.380	0.379	0.841

Table S23: Anisotropy $\|\vec{\alpha}_c(\omega = 2.308 \times i)\|$ for all molecules in the TS42 database, for each contribution c, as documented in Table II in the main text.

Molecule	$\|\vec{\alpha}_{\mathrm{ref}}(\omega)\|$	$\|\vec{\alpha}_0(\omega)\|$	$\|\vec{\alpha}_1(\omega)\|$	$\|\vec{\alpha}_{1(0)}(\omega)\|$	$\|\vec{\alpha}_{1(1)}(\omega)\|$	$\|\vec{\alpha}_{1(2)}(\omega)\|$
C_6H_6	0.256	1.600	0.200	1.582	0.228	1.154
C_8H_{18}	0.157	1.234	0.135	1.217	0.699	0.387
C_7H_{16}	0.129	1.035	0.112	1.021	0.588	0.326
CS_2	0.087	0.973	0.076	0.955	0.300	0.579
C_6H_{14}	0.103	0.862	0.090	0.850	0.488	0.275
COS	0.116	0.822	0.101	0.803	0.176	0.527
N_2O	0.156	0.737	0.139	0.713	0.016	0.557
$CH_3CH_2OCH_2CH_3$	0.107	0.705	0.090	0.699	0.338	0.273
$C_4H_{10}O$	0.102	0.697	0.081	0.691	0.302	0.310
C_5H_{12}	0.076	0.660	0.067	0.651	0.374	0.212
CO_2	0.144	0.662	0.122	0.638	0.000	0.517
SO_2	0.090	0.620	0.087	0.610	0.190	0.341
C_3H_6	0.088	0.602	0.069	0.595	0.147	0.413
C_2H_2	0.090	0.553	0.070	0.541	0.048	0.517
C_3H_7OH	0.079	0.536	0.063	0.531	0.210	0.260
CH_3COCH_3	0.094	0.536	0.088	0.527	0.186	0.305
Cl_2	0.017	0.512	0.006	0.506	0.148	0.351
C_4H_{10}	0.054	0.501	0.048	0.494	0.282	0.166
$CH_3CH_3CH_3N$	0.055	0.487	0.049	0.478	0.271	0.199
CH_3CHO	0.088	0.473	0.082	0.464	0.144	0.309
C_2H_4	0.075	0.468	0.056	0.461	0.058	0.383
CH_3OCH_3	0.061	0.398	0.050	0.396	0.136	0.213
CH_3NHCH_3	0.048	0.384	0.036	0.382	0.156	0.196
H_2CO	0.078	0.366	0.072	0.356	0.020	0.301
C_2H_5OH	0.056	0.338	0.042	0.335	0.098	0.201
N_2	0.070	0.307	0.066	0.299	0.070	0.302
C_3H_8	0.029	0.291	0.026	0.287	0.162	0.099
CO	0.073	0.290	0.072	0.284	0.052	0.264
C_4H_8	0.026	0.264	0.027	0.256	0.192	0.037
CH_3NH_2	0.032	0.251	0.022	0.248	0.092	0.151
CH_3OH	0.039	0.239	0.030	0.237	0.084	0.161
C_2H_6	0.017	0.198	0.016	0.195	0.116	0.062
HBr	0.009	0.178	0.001	0.179	0.040	0.138
H_2S	0.007	0.169	0.002	0.170	0.042	0.131
HCl	0.007	0.146	0.001	0.146	0.010	0.136
NH_3	0.017	0.089	0.009	0.088	0.028	0.108
H_2O	0.025	0.086	0.012	0.086	0.074	0.146
HF	0.022	0.064	0.013	0.061	0.086	0.133
H_2	0.012	0.044	0.010	0.043	0.056	0.088
CH_4	0.000	0.000	0.000	0.000	0.000	0.000
CCl_4	0.000	0.000	0.000	0.000	0.000	0.000
SiH_4	0.000	0.000	0.000	0.000	0.000	0.000
Min.	0.000	0.000	0.000	0.000	0.000	0.000
Max.	0.256	1.600	0.200	1.582	0.699	1.154
Mean	0.066	0.461	0.056	0.454	0.160	0.267

Table S24: Anisotropy $\|\vec{\alpha}_c(\omega = 5.958 \times i)\|$ for all molecules in the TS42 database, for each contribution c, as documented in Table II in the main text.

Molecule	$\|\vec{\alpha}_{\mathrm{ref}}(\omega)\|$	$\|\vec{\alpha}_0(\omega)\|$	$\|\vec{\alpha}_1(\omega)\|$	$\|\vec{\alpha}_{1(0)}(\omega)\|$	$\|\vec{\alpha}_{1(1)}(\omega)\|$	$\|\vec{\alpha}_{1(2)}(\omega)\|$
C_6H_6	0.020	0.285	0.018	0.284	0.084	0.183
C_8H_{18}	0.005	0.186	0.004	0.185	0.132	0.050
CS_2	0.006	0.167	0.005	0.166	0.070	0.091
C_7H_{16}	0.004	0.156	0.003	0.156	0.110	0.042
COS	0.008	0.149	0.007	0.148	0.054	0.088
N_2O	0.009	0.141	0.008	0.140	0.032	0.101
C_6H_{14}	0.003	0.130	0.002	0.130	0.092	0.036
CO_2	0.010	0.128	0.009	0.127	0.028	0.090
$CH_3CH_2OCH_2CH_3$	0.004	0.115	0.002	0.115	0.074	0.039
SO_2	0.006	0.115	0.005	0.114	0.058	0.051
$C_4H_{10}O$	0.003	0.113	0.002	0.112	0.066	0.044
C_3H_6	0.007	0.105	0.006	0.105	0.036	0.064
C_2H_2	0.008	0.103	0.007	0.102	0.010	0.084
C_5H_{12}	0.002	0.100	0.002	0.100	0.070	0.028
CH_3COCH_3	0.007	0.096	0.006	0.095	0.046	0.049
C_3H_7OH	0.002	0.089	0.001	0.089	0.050	0.038
Cl_2	0.004	0.088	0.004	0.087	0.040	0.052
CH_3CHO	0.006	0.086	0.006	0.086	0.034	0.050
C_2H_4	0.006	0.085	0.006	0.084	0.020	0.060
C_4H_{10}	0.002	0.076	0.001	0.076	0.052	0.023
$CH_3CH_3CH_3N$	0.001	0.076	0.001	0.075	0.052	0.030
H_2CO	0.006	0.070	0.006	0.070	0.014	0.050
CH_3OCH_3	0.002	0.069	0.001	0.069	0.036	0.032
N_2	0.006	0.064	0.005	0.064	0.006	0.053
CH_3NHCH_3	0.001	0.064	0.001	0.064	0.034	0.029
CO	0.007	0.060	0.007	0.060	0.006	0.047
C_2H_5OH	0.002	0.058	0.001	0.058	0.028	0.030
CH_3OH	0.001	0.044	0.000	0.044	0.022	0.025
C_3H_8	0.001	0.045	0.001	0.044	0.030	0.014
CH_3NH_2	0.001	0.043	0.000	0.043	0.021	0.023
C_4H_8	0.000	0.038	0.000	0.037	0.030	0.008
HBr	0.001	0.033	0.001	0.033	0.014	0.019
H_2S	0.001	0.031	0.001	0.031	0.014	0.018
C_2H_6	0.000	0.030	0.000	0.030	0.020	0.009
HCl	0.001	0.028	0.001	0.028	0.010	0.020
H_2O	0.001	0.017	0.000	0.017	0.006	0.023
NH_3	0.001	0.017	0.000	0.017	0.000	0.017
HF	0.000	0.014	0.001	0.013	0.010	0.024
H_2	0.000	0.008	0.000	0.008	0.006	0.014
CH_4	0.000	0.000	0.000	0.000	0.000	0.000
CCl_4	0.000	0.000	0.000	0.000	0.000	0.000
SiH_4	0.000	0.000	0.000	0.000	0.000	0.000
Min.	0.000	0.000	0.000	0.000	0.000	0.000
Max.	0.020	0.285	0.018	0.284	0.132	0.183
Mean	0.004	0.079	0.003	0.079	0.036	0.042

Table S25: Anisotropy $\|\vec{\alpha}_c(\omega = 32.239 \times i)\|$ for all molecules in the TS42 database, for each contribution c, as documented in Table II in the main text.

Molecule	$\|\vec{\alpha}_{\mathrm{ref}}(\omega)\|$	$\|\vec{\alpha}_0(\omega)\|$	$\|\vec{\alpha}_1(\omega)\|$	$\|\vec{\alpha}_{1(0)}(\omega)\|$	$\|\vec{\alpha}_{1(1)}(\omega)\|$	$\|\vec{\alpha}_{1(2)}(\omega)\|$
C_6H_6	0.001	0.010	0.001	0.010	0.004	0.006
CS_2	0.000	0.006	0.000	0.006	0.002	0.003
C_8H_{18}	0.000	0.006	0.000	0.006	0.004	0.002
C_7H_{16}	0.000	0.005	0.000	0.005	0.004	0.001
COS	0.000	0.005	0.000	0.005	0.002	0.003
CO_2	0.000	0.005	0.000	0.005	0.002	0.003
N_2O	0.000	0.005	0.000	0.005	0.002	0.003
C_2H_2	0.000	0.004	0.000	0.004	0.000	0.003
$C_4H_{10}O$	0.000	0.004	0.000	0.004	0.002	0.001
SO_2	0.000	0.004	0.000	0.004	0.002	0.002
C_6H_{14}	0.000	0.004	0.000	0.004	0.004	0.001
C_3H_6	0.000	0.004	0.000	0.004	0.002	0.002
$CH_3CH_2OCH_2CH_3$	0.000	0.004	0.000	0.004	0.002	0.001
$CH_3CH_3CH_3N$	0.000	0.003	0.000	0.003	0.002	0.001
C_2H_4	0.000	0.003	0.000	0.003	0.000	0.002
CH_3COCH_3	0.000	0.003	0.000	0.003	0.002	0.002
CH_3CHO	0.000	0.003	0.000	0.003	0.002	0.002
Cl_2	0.000	0.003	0.000	0.003	0.002	0.002
C_4H_{10}	0.000	0.003	0.000	0.003	0.002	0.001
C_3H_7OH	0.000	0.003	0.000	0.003	0.002	0.001
C_5H_{12}	0.000	0.003	0.000	0.003	0.002	0.001
H_2CO	0.000	0.003	0.000	0.003	0.000	0.002
CO	0.000	0.002	0.000	0.002	0.000	0.002
N_2	0.000	0.002	0.000	0.002	0.000	0.002
CH_3NHCH_3	0.000	0.002	0.000	0.002	0.002	0.001
CH_3OCH_3	0.000	0.002	0.000	0.002	0.002	0.001
CH_3NH_2	0.000	0.002	0.000	0.002	0.000	0.001
C_2H_5OH	0.000	0.002	0.000	0.002	0.002	0.001
CH_3OH	0.000	0.002	0.000	0.002	0.000	0.001
C_3H_8	0.000	0.002	0.000	0.002	0.002	0.000
H_2S	0.000	0.001	0.000	0.001	0.000	0.001
C_2H_6	0.000	0.001	0.000	0.001	0.000	0.000
NH_3	0.000	0.001	0.000	0.001	0.000	0.001
C_4H_8	0.000	0.001	0.000	0.001	0.000	0.000
H_2O	0.000	0.001	0.000	0.001	0.000	0.001
HBr	0.000	0.001	0.000	0.001	0.000	0.001
HCl	0.000	0.001	0.000	0.001	0.000	0.001
HF	0.000	0.001	0.000	0.001	0.000	0.001
CH_4	0.000	0.000	0.000	0.000	0.000	0.000
H_2	0.000	0.000	0.000	0.000	0.000	0.000
CCl_4	0.000	0.000	0.000	0.000	0.000	0.000
SiH_4	0.000	0.000	0.000	0.000	0.000	0.000
Min.	0.000	0.000	0.000	0.000	0.000	0.000
Max.	0.001	0.010	0.001	0.010	0.004	0.006
Mean	0.000	0.003	0.000	0.003	0.001	0.001

Table S26: Anisotropic descriptors $u_c^{\parallel}[\alpha(\omega = 0.003 \times i)]$ for all molecules in the TS42 database, for each contribution c, as documented in Table II in the main text.

Molecule	$u_{\text{ref}}^{\parallel}[\alpha(\omega)]$	$u_0^{\parallel}[\alpha(\omega)]$	$u_1^{\parallel}[\alpha(\omega)]$	$u_{1(0)}^{\parallel}[\alpha(\omega)]$	$u_{1(1)}^{\parallel}[\alpha(\omega)]$	$u_{1(2)}^{\parallel}[\alpha(\omega)]$
CS_2	0.199	0.151	0.176	0.156	0.078	-0.058
N_2O	0.187	0.130	0.173	0.149	0.088	-0.065
CO_2	0.132	0.102	0.128	0.123	0.072	-0.067
COS	0.123	0.101	0.116	0.112	0.060	-0.056
C_6H_6	0.061	0.069	0.064	0.070	0.034	-0.041
C_2H_2	0.067	0.065	0.071	0.067	0.062	-0.058
SO_2	0.070	0.060	0.066	0.066	0.028	-0.028
Cl_2	0.071	0.057	0.059	0.057	0.038	-0.037
C_8H_{18}	0.034	0.051	0.034	0.051	-0.002	-0.015
C_3H_6	0.041	0.045	0.042	0.047	0.018	-0.023
C_7H_{16}	0.029	0.043	0.029	0.043	-0.000	-0.013
C_2H_4	0.042	0.041	0.044	0.042	0.030	-0.028
H_2CO	0.052	0.036	0.052	0.039	0.038	-0.024
C_6H_{14}	0.024	0.036	0.024	0.037	-0.000	-0.012
CH_3CHO	0.033	0.028	0.032	0.031	0.014	-0.014
N_2	0.036	0.027	0.039	0.030	0.038	-0.030
$CH_3CH_2OCH_2CH_3$	0.019	0.028	0.019	0.028	0.000	-0.009
C_5H_{12}	0.018	0.027	0.018	0.027	0.000	-0.010
$C_4H_{10}O$	0.018	0.027	0.018	0.027	0.002	-0.011
CH_3COCH_3	0.022	0.021	0.022	0.022	0.008	-0.009
C_4H_{10}	0.013	0.020	0.013	0.020	0.001	-0.008
$CH_3CH_3CH_3N$	0.014	0.019	0.014	0.019	0.002	-0.007
C_3H_7OH	0.012	0.018	0.012	0.018	0.002	-0.009
H_2	0.043	0.018	0.044	0.018	0.052	-0.027
CO	0.016	0.016	0.019	0.017	0.022	-0.020
CH_3OCH_3	0.010	0.016	0.011	0.016	0.002	-0.008
HF	0.031	0.011	0.027	0.012	0.032	-0.017
CH_3NHCH_3	0.008	0.011	0.008	0.011	0.002	-0.005
C_2H_5OH	0.007	0.010	0.007	0.010	0.002	-0.006
C_3H_8	0.006	0.009	0.006	0.009	0.002	-0.004
CH_3OH	0.005	0.007	0.005	0.007	0.003	-0.005
CH_3NH_2	0.006	0.007	0.006	0.007	0.002	-0.004
C_2H_6	0.005	0.007	0.005	0.007	0.000	-0.003
C_4H_8	0.004	0.006	0.004	0.006	0.000	-0.001
HCl	0.005	0.004	0.005	0.005	0.008	-0.007
HBr	0.003	0.004	0.003	0.004	0.006	-0.007
H_2O	0.002	0.002	0.002	0.002	0.006	-0.006
CH_4	0.000	0.000	0.000	0.000	0.000	-0.000
CCl_4	0.000	0.000	-0.000	-0.000	-0.000	0.000
SiH_4	0.000	0.000	0.000	0.000	0.000	0.000
H_2S	0.000	-0.000	-0.000	-0.001	-0.000	0.001
NH_3	0.005	-0.003	0.004	-0.003	-0.006	0.013
Min.	0.000	-0.003	-0.000	-0.003	-0.006	-0.067
Max.	0.199	0.151	0.176	0.156	0.088	0.013
Mean	0.035	0.032	0.034	0.034	0.018	-0.018

S2.3 Tables with $u_c^{\parallel}[\alpha(\omega)]$

Table S27: Anisotropic descriptors $u_c^{\parallel}[\alpha(\omega = 0.015 \times i)]$ for all molecules in the TS42 database, for each contribution c, as documented in Table II in the main text.

Molecule	$u_{\text{ref}}^{\parallel}[\alpha(\omega)]$	$u_0^{\parallel}[\alpha(\omega)]$	$u_1^{\parallel}[\alpha(\omega)]$	$u_{1(0)}^{\parallel}[\alpha(\omega)]$	$u_{1(1)}^{\parallel}[\alpha(\omega)]$	$u_{1(2)}^{\parallel}[\alpha(\omega)]$
CS_2	0.198	0.151	0.176	0.156	0.078	-0.058
N_2O	0.187	0.130	0.173	0.149	0.088	-0.065
CO_2	0.131	0.102	0.128	0.123	0.072	-0.067
COS	0.123	0.101	0.115	0.112	0.060	-0.056
C_6H_6	0.061	0.068	0.064	0.070	0.034	-0.041
C_2H_2	0.067	0.065	0.071	0.067	0.062	-0.058
SO_2	0.070	0.060	0.066	0.066	0.028	-0.028
Cl_2	0.071	0.057	0.059	0.057	0.038	-0.037
C_8H_{18}	0.034	0.051	0.034	0.051	-0.002	-0.015
C_3H_6	0.041	0.045	0.042	0.047	0.018	-0.023
C_7H_{16}	0.029	0.043	0.029	0.043	-0.000	-0.013
C_2H_4	0.042	0.041	0.044	0.042	0.030	-0.028
H_2CO	0.052	0.036	0.052	0.039	0.038	-0.024
C_6H_{14}	0.024	0.036	0.024	0.037	-0.000	-0.012
CH_3CHO	0.032	0.028	0.032	0.031	0.014	-0.014
N_2	0.036	0.027	0.039	0.030	0.038	-0.030
$CH_3CH_2OCH_2CH_3$	0.019	0.028	0.019	0.028	0.000	-0.009
C_5H_{12}	0.018	0.027	0.018	0.027	0.000	-0.010
$C_4H_{10}O$	0.018	0.027	0.018	0.027	0.002	-0.011
CH_3COCH_3	0.022	0.021	0.022	0.022	0.008	-0.009
C_4H_{10}	0.013	0.020	0.013	0.020	0.001	-0.008
$CH_3CH_3CH_3N$	0.014	0.019	0.014	0.019	0.002	-0.007
C_3H_7OH	0.012	0.018	0.012	0.018	0.002	-0.009
H_2	0.043	0.018	0.044	0.018	0.052	-0.027
CO	0.016	0.016	0.019	0.017	0.022	-0.020
CH_3OCH_3	0.010	0.016	0.011	0.016	0.002	-0.008
HF	0.031	0.011	0.027	0.012	0.032	-0.017
CH_3NHCH_3	0.008	0.011	0.008	0.011	0.002	-0.005
C_2H_5OH	0.007	0.010	0.007	0.010	0.002	-0.006
C_3H_8	0.006	0.009	0.006	0.009	0.002	-0.004
CH_3OH	0.005	0.007	0.005	0.007	0.003	-0.005
CH_3NH_2	0.006	0.007	0.006	0.007	0.002	-0.004
C_2H_6	0.005	0.007	0.005	0.007	0.000	-0.003
C_4H_8	0.004	0.006	0.004	0.006	0.000	-0.001
HCl	0.005	0.004	0.005	0.005	0.008	-0.007
HBr	0.003	0.004	0.003	0.004	0.006	-0.007
H_2O	0.002	0.002	0.002	0.002	0.006	-0.006
CH_4	0.000	0.000	0.000	0.000	0.000	-0.000
CCl_4	0.000	0.000	-0.000	-0.000	-0.000	0.000
H_2S	0.000	-0.000	-0.000	-0.000	-0.000	0.001
SiH_4	0.000	0.000	0.000	0.000	0.000	-0.000
NH_3	0.005	-0.003	0.004	-0.003	-0.006	0.013
Min.	0.000	-0.003	-0.000	-0.003	-0.006	-0.067
Max.	0.198	0.151	0.176	0.156	0.088	0.013
Mean	0.035	0.032	0.034	0.034	0.018	-0.018

Table S28: Anisotropic descriptors $u_c^{\parallel}[\alpha(\omega = 0.039 \times i)]$ for all molecules in the TS42 database, for each contribution c, as documented in Table II in the main text.

Molecule	$u_{\text{ref}}^{\parallel}[\alpha(\omega)]$	$u_0^{\parallel}[\alpha(\omega)]$	$u_1^{\parallel}[\alpha(\omega)]$	$u_{1(0)}^{\parallel}[\alpha(\omega)]$	$u_{1(1)}^{\parallel}[\alpha(\omega)]$	$u_{1(2)}^{\parallel}[\alpha(\omega)]$
CS_2	0.195	0.150	0.174	0.154	0.078	-0.058
N_2O	0.186	0.130	0.172	0.148	0.088	-0.065
CO_2	0.131	0.102	0.127	0.123	0.072	-0.067
COS	0.122	0.101	0.115	0.112	0.058	-0.056
C_6H_6	0.061	0.068	0.063	0.070	0.034	-0.041
C_2H_2	0.067	0.065	0.071	0.067	0.062	-0.058
SO_2	0.070	0.060	0.065	0.066	0.028	-0.028
Cl_2	0.070	0.056	0.058	0.056	0.038	-0.037
C_8H_{18}	0.034	0.051	0.034	0.051	-0.002	-0.015
C_3H_6	0.040	0.045	0.041	0.046	0.018	-0.023
C_7H_{16}	0.028	0.043	0.029	0.043	-0.000	-0.013
C_2H_4	0.041	0.041	0.043	0.042	0.028	-0.028
H_2CO	0.051	0.036	0.052	0.039	0.036	-0.024
C_6H_{14}	0.024	0.036	0.024	0.037	-0.000	-0.012
CH_3CHO	0.032	0.028	0.032	0.031	0.014	-0.014
N_2	0.036	0.027	0.039	0.030	0.038	-0.030
$CH_3CH_2OCH_2CH_3$	0.019	0.028	0.019	0.028	0.000	-0.009
C_5H_{12}	0.018	0.027	0.018	0.027	0.000	-0.010
$C_4H_{10}O$	0.018	0.027	0.018	0.027	0.002	-0.011
CH_3COCH_3	0.021	0.021	0.021	0.022	0.008	-0.009
C_4H_{10}	0.013	0.020	0.013	0.020	0.001	-0.008
$CH_3CH_3CH_3N$	0.014	0.019	0.014	0.019	0.002	-0.007
C_3H_7OH	0.012	0.018	0.012	0.018	0.002	-0.009
H_2	0.042	0.017	0.043	0.018	0.052	-0.027
CO	0.016	0.016	0.019	0.017	0.022	-0.020
CH_3OCH_3	0.010	0.016	0.011	0.016	0.002	-0.008
HF	0.031	0.011	0.028	0.012	0.032	-0.017
CH_3NHCH_3	0.008	0.011	0.008	0.011	0.002	-0.005
C_2H_5OH	0.007	0.010	0.007	0.010	0.002	-0.006
C_3H_8	0.006	0.009	0.006	0.009	0.002	-0.004
CH_3OH	0.005	0.007	0.005	0.007	0.003	-0.005
CH_3NH_2	0.006	0.007	0.006	0.007	0.002	-0.004
C_2H_6	0.005	0.007	0.005	0.007	0.000	-0.003
C_4H_8	0.004	0.006	0.004	0.006	-0.000	-0.001
HCl	0.005	0.004	0.005	0.005	0.008	-0.007
HBr	0.003	0.004	0.003	0.004	0.006	-0.007
H_2O	0.002	0.002	0.002	0.003	0.006	-0.006
CH_4	0.000	0.000	0.000	0.000	0.000	-0.000
CCl_4	0.000	0.000	-0.000	-0.000	-0.000	0.000
H_2S	0.000	-0.000	-0.000	-0.000	-0.000	0.001
SiH_4	0.000	0.000	0.000	0.000	0.000	0.000
NH_3	0.005	-0.003	0.004	-0.003	-0.006	0.012
Min.	0.000	-0.003	-0.000	-0.003	-0.006	-0.067
Max.	0.195	0.150	0.174	0.154	0.088	0.012
Mean	0.035	0.032	0.034	0.033	0.018	-0.018

Table S29: Anisotropic descriptors $u_c^{\parallel}[\alpha(\omega = 0.078 \times i)]$ for all molecules in the TS42 database, for each contribution c, as documented in Table II in the main text.

Molecule	$u_{\text{ref}}^{\parallel}[\alpha(\omega)]$	$u_0^{\parallel}[\alpha(\omega)]$	$u_1^{\parallel}[\alpha(\omega)]$	$u_{1(0)}^{\parallel}[\alpha(\omega)]$	$u_{1(1)}^{\parallel}[\alpha(\omega)]$	$u_{1(2)}^{\parallel}[\alpha(\omega)]$
CS_2	0.185	0.146	0.166	0.150	0.074	-0.059
N_2O	0.182	0.129	0.169	0.147	0.088	-0.065
CO_2	0.129	0.102	0.126	0.122	0.072	-0.067
COS	0.118	0.100	0.112	0.110	0.058	-0.056
C_6H_6	0.059	0.067	0.061	0.069	0.034	-0.041
C_2H_2	0.066	0.065	0.070	0.067	0.060	-0.058
SO_2	0.068	0.059	0.064	0.065	0.028	-0.027
Cl_2	0.069	0.056	0.057	0.056	0.038	-0.037
C_8H_{18}	0.033	0.050	0.034	0.050	-0.002	-0.015
C_3H_6	0.038	0.044	0.039	0.045	0.018	-0.023
C_7H_{16}	0.028	0.043	0.028	0.043	-0.002	-0.013
C_2H_4	0.039	0.040	0.041	0.041	0.028	-0.028
H_2CO	0.050	0.036	0.050	0.039	0.036	-0.025
C_6H_{14}	0.024	0.036	0.024	0.036	-0.000	-0.012
CH_3CHO	0.031	0.028	0.030	0.030	0.014	-0.014
N_2	0.036	0.027	0.038	0.030	0.038	-0.030
$CH_3CH_2OCH_2CH_3$	0.019	0.028	0.019	0.028	0.000	-0.009
C_5H_{12}	0.017	0.027	0.018	0.027	0.000	-0.009
$C_4H_{10}O$	0.018	0.027	0.018	0.027	0.002	-0.011
CH_3COCH_3	0.020	0.020	0.020	0.022	0.008	-0.008
C_4H_{10}	0.013	0.020	0.013	0.020	0.000	-0.008
$CH_3CH_3CH_3N$	0.013	0.019	0.013	0.019	0.002	-0.007
C_3H_7OH	0.012	0.018	0.012	0.018	0.002	-0.009
CO	0.017	0.017	0.019	0.018	0.022	-0.021
H_2	0.041	0.017	0.042	0.017	0.052	-0.027
CH_3OCH_3	0.011	0.016	0.011	0.016	0.002	-0.008
HF	0.031	0.011	0.028	0.012	0.034	-0.017
CH_3NHCH_3	0.008	0.011	0.008	0.012	0.002	-0.006
C_2H_5OH	0.007	0.010	0.007	0.010	0.002	-0.006
C_3H_8	0.006	0.009	0.006	0.009	0.000	-0.004
CH_3OH	0.005	0.007	0.005	0.007	0.004	-0.005
CH_3NH_2	0.006	0.007	0.006	0.007	0.002	-0.004
C_2H_6	0.004	0.006	0.004	0.007	0.000	-0.003
C_4H_8	0.004	0.006	0.004	0.006	-0.000	-0.001
HCl	0.005	0.005	0.005	0.005	0.008	-0.008
HBr	0.003	0.004	0.003	0.004	0.006	-0.007
H_2O	0.002	0.003	0.002	0.003	0.006	-0.007
CH_4	0.000	0.000	0.000	0.000	0.000	-0.000
CCl_4	0.000	0.000	-0.000	-0.000	-0.000	0.000
H_2S	0.000	0.000	0.000	0.000	-0.000	0.000
SiH_4	0.000	0.000	0.000	0.000	0.000	0.000
NH_3	0.003	-0.002	0.003	-0.002	-0.004	0.010
Min.	0.000	-0.002	-0.000	-0.002	-0.004	-0.067
Max.	0.185	0.146	0.169	0.150	0.088	0.010
Mean	0.034	0.031	0.033	0.033	0.017	-0.018

Table S30: Anisotropic descriptors $u_c^{\parallel}[\alpha(\omega = 0.139 \times i)]$ for all molecules in the TS42 database, for each contribution c, as documented in Table II in the main text.

Molecule	$u_{\text{ref}}^{\parallel}[\alpha(\omega)]$	$u_0^{\parallel}[\alpha(\omega)]$	$u_1^{\parallel}[\alpha(\omega)]$	$u_{1(0)}^{\parallel}[\alpha(\omega)]$	$u_{1(1)}^{\parallel}[\alpha(\omega)]$	$u_{1(2)}^{\parallel}[\alpha(\omega)]$
N_2O	0.173	0.127	0.162	0.144	0.084	-0.065
CS_2	0.160	0.137	0.147	0.140	0.066	-0.059
CO_2	0.124	0.101	0.121	0.119	0.068	-0.067
COS	0.109	0.097	0.104	0.106	0.054	-0.056
C_2H_2	0.063	0.065	0.066	0.067	0.058	-0.059
C_6H_6	0.054	0.065	0.056	0.066	0.032	-0.041
SO_2	0.063	0.057	0.061	0.062	0.026	-0.027
Cl_2	0.064	0.054	0.054	0.054	0.036	-0.036
C_8H_{18}	0.032	0.049	0.032	0.048	-0.002	-0.014
C_7H_{16}	0.027	0.042	0.027	0.042	-0.002	-0.013
C_3H_6	0.033	0.040	0.034	0.041	0.016	-0.022
C_2H_4	0.035	0.038	0.036	0.039	0.026	-0.028
H_2CO	0.046	0.035	0.047	0.038	0.034	-0.025
C_6H_{14}	0.023	0.035	0.023	0.035	-0.000	-0.012
N_2	0.034	0.027	0.037	0.030	0.038	-0.030
CH_3CHO	0.028	0.026	0.028	0.029	0.012	-0.013
$CH_3CH_2OCH_2CH_3$	0.018	0.028	0.019	0.028	-0.000	-0.009
$C_4H_{10}O$	0.017	0.026	0.017	0.027	0.002	-0.011
C_5H_{12}	0.017	0.026	0.017	0.026	-0.000	-0.009
CH_3COCH_3	0.018	0.019	0.018	0.020	0.006	-0.008
$CH_3CH_3CH_3N$	0.013	0.018	0.013	0.019	0.001	-0.007
C_4H_{10}	0.012	0.019	0.012	0.019	0.000	-0.007
CO	0.018	0.018	0.021	0.019	0.022	-0.021
C_3H_7OH	0.012	0.018	0.012	0.018	0.002	-0.009
H_2	0.038	0.017	0.038	0.017	0.048	-0.027
CH_3OCH_3	0.011	0.016	0.011	0.016	0.002	-0.008
HF	0.033	0.011	0.029	0.012	0.034	-0.017
CH_3NHCH_3	0.008	0.012	0.008	0.012	0.002	-0.006
C_2H_5OH	0.007	0.010	0.007	0.010	0.002	-0.006
C_3H_8	0.006	0.009	0.006	0.009	0.000	-0.004
CH_3OH	0.005	0.007	0.005	0.007	0.004	-0.005
CH_3NH_2	0.005	0.007	0.005	0.007	0.002	-0.005
C_2H_6	0.004	0.006	0.004	0.006	0.000	-0.003
HBr	0.004	0.005	0.004	0.005	0.006	-0.008
HCl	0.006	0.005	0.005	0.005	0.008	-0.008
C_4H_8	0.004	0.005	0.004	0.005	-0.000	-0.001
H_2O	0.004	0.004	0.003	0.004	0.008	-0.009
H_2S	0.000	0.001	0.000	0.001	0.002	-0.002
CH_4	0.000	0.000	0.000	0.000	0.000	-0.000
CCl_4	0.000	-0.000	-0.000	-0.000	0.000	0.000
SiH_4	0.000	0.000	0.000	0.000	0.000	0.000
NH_3	0.001	-0.001	0.001	-0.001	-0.002	0.005
Min.	0.000	-0.001	-0.000	-0.001	-0.002	-0.067
Max.	0.173	0.137	0.162	0.144	0.084	0.005
Mean	0.032	0.031	0.031	0.032	0.017	-0.018

Table S31: Anisotropic descriptors $u_c^{\parallel}[\alpha(\omega = 0.233 \times i)]$ for all molecules in the TS42 database, for each contribution c, as documented in Table II in the main text.

Molecule	$u_{\text{ref}}^{\parallel}[\alpha(\omega)]$	$u_0^{\parallel}[\alpha(\omega)]$	$u_1^{\parallel}[\alpha(\omega)]$	$u_{1(0)}^{\parallel}[\alpha(\omega)]$	$u_{1(1)}^{\parallel}[\alpha(\omega)]$	$u_{1(2)}^{\parallel}[\alpha(\omega)]$
N_2O	0.152	0.123	0.146	0.136	0.076	-0.066
CS_2	0.118	0.119	0.112	0.119	0.052	-0.059
CO_2	0.112	0.098	0.109	0.113	0.062	-0.067
COS	0.091	0.091	0.087	0.097	0.044	-0.055
C_2H_2	0.056	0.064	0.057	0.064	0.052	-0.060
C_6H_6	0.046	0.061	0.047	0.062	0.028	-0.042
SO_2	0.054	0.053	0.053	0.057	0.022	-0.026
Cl_2	0.053	0.050	0.045	0.050	0.032	-0.035
C_8H_{18}	0.028	0.045	0.028	0.045	-0.002	-0.013
C_7H_{16}	0.024	0.038	0.024	0.038	-0.002	-0.012
H_2CO	0.039	0.033	0.040	0.035	0.030	-0.025
C_3H_6	0.026	0.035	0.026	0.035	0.012	-0.021
C_2H_4	0.028	0.034	0.028	0.034	0.022	-0.028
C_6H_{14}	0.020	0.033	0.020	0.033	-0.002	-0.011
N_2	0.032	0.027	0.035	0.029	0.036	-0.030
$CH_3CH_2OCH_2CH_3$	0.017	0.026	0.017	0.027	-0.000	-0.009
CH_3CHO	0.023	0.024	0.023	0.026	0.010	-0.013
$C_4H_{10}O$	0.016	0.025	0.016	0.026	0.001	-0.010
C_5H_{12}	0.015	0.024	0.015	0.024	-0.000	-0.009
CO	0.020	0.020	0.023	0.021	0.024	-0.022
CH_3COCH_3	0.015	0.017	0.015	0.018	0.006	-0.008
C_4H_{10}	0.011	0.018	0.011	0.018	-0.000	-0.007
C_3H_7OH	0.012	0.018	0.012	0.018	0.002	-0.008
$CH_3CH_3CH_3N$	0.011	0.017	0.011	0.017	0.000	-0.007
H_2	0.031	0.016	0.031	0.016	0.044	-0.028
CH_3OCH_3	0.011	0.016	0.011	0.016	0.002	-0.008
HF	0.034	0.012	0.030	0.012	0.034	-0.017
CH_3NHCH_3	0.007	0.012	0.007	0.012	0.002	-0.006
C_2H_5OH	0.007	0.010	0.007	0.010	0.002	-0.006
C_3H_8	0.005	0.008	0.005	0.008	0.000	-0.004
CH_3OH	0.005	0.007	0.005	0.007	0.003	-0.005
CH_3NH_2	0.004	0.007	0.004	0.007	0.002	-0.005
C_2H_6	0.004	0.006	0.004	0.006	0.000	-0.003
H_2O	0.006	0.005	0.005	0.005	0.012	-0.011
HBr	0.005	0.005	0.004	0.005	0.006	-0.008
HCl	0.006	0.005	0.005	0.005	0.008	-0.009
C_4H_8	0.003	0.005	0.003	0.005	-0.000	-0.001
H_2S	0.001	0.002	0.000	0.002	0.002	-0.004
CH_4	0.000	0.000	0.000	0.000	0.000	-0.000
CCl_4	0.000	-0.000	-0.000	0.000	0.000	-0.000
NH_3	0.000	0.000	-0.000	0.000	0.000	-0.000
SiH_4	0.000	0.000	0.000	0.000	0.000	0.000
Min.	0.000	-0.000	-0.000	0.000	-0.002	-0.067
Max.	0.152	0.123	0.146	0.136	0.076	0.000
Mean	0.027	0.029	0.027	0.030	0.015	-0.018

Table S32: Anisotropic descriptors $u_c^{\parallel}[\alpha(\omega = 0.386 \times i)]$ for all molecules in the TS42 database, for each contribution c, as documented in Table II in the main text.

Molecule	$u^{\parallel}_{\text{ref}}[\alpha(\omega)]$	$u^{\parallel}_{0}[\alpha(\omega)]$	$u^{\parallel}_{1}[\alpha(\omega)]$	$u^{\parallel}_{1(0)}[\alpha(\omega)]$	$u^{\parallel}_{1(1)}[\alpha(\omega)]$	$u^{\parallel}_{1(2)}[\alpha(\omega)]$
N_2O	0.115	0.112	0.114	0.119	0.060	-0.065
CO_2	0.089	0.091	0.086	0.100	0.050	-0.064
CS_2	0.067	0.090	0.066	0.089	0.030	-0.053
COS	0.063	0.079	0.061	0.081	0.030	-0.051
C_2H_2	0.042	0.059	0.041	0.058	0.042	-0.059
C_6H_6	0.035	0.056	0.035	0.055	0.020	-0.041
SO_2	0.039	0.047	0.040	0.049	0.016	-0.025
Cl_2	0.035	0.041	0.031	0.041	0.022	-0.032
C_8H_{18}	0.021	0.037	0.021	0.036	-0.004	-0.011
C_7H_{16}	0.018	0.032	0.018	0.031	-0.004	-0.010
H_2CO	0.029	0.030	0.029	0.031	0.024	-0.025
C_2H_4	0.019	0.029	0.018	0.029	0.016	-0.027
C_3H_6	0.017	0.028	0.017	0.028	0.008	-0.019
N_2	0.026	0.026	0.029	0.027	0.030	-0.029
C_6H_{14}	0.015	0.027	0.015	0.027	-0.002	-0.009
$CH_3CH_2OCH_2CH_3$	0.014	0.023	0.014	0.023	-0.002	-0.008
CH_3CHO	0.016	0.021	0.017	0.022	0.008	-0.012
$C_4H_{10}O$	0.013	0.022	0.013	0.022	-0.000	-0.009
CO	0.021	0.022	0.023	0.022	0.024	-0.023
C_5H_{12}	0.011	0.021	0.011	0.020	-0.002	-0.007
C_3H_7OH	0.010	0.016	0.010	0.016	0.001	-0.008
CH_3COCH_3	0.010	0.015	0.011	0.015	0.004	-0.007
CH_3OCH_3	0.009	0.015	0.009	0.015	0.002	-0.007
C_4H_{10}	0.008	0.015	0.008	0.015	-0.002	-0.006
$CH_3CH_3CH_3N$	0.008	0.014	0.008	0.014	-0.000	-0.006
H_2	0.022	0.014	0.021	0.013	0.034	-0.027
HF	0.032	0.012	0.028	0.012	0.032	-0.017
CH_3NHCH_3	0.006	0.011	0.006	0.011	0.000	-0.006
C_2H_5OH	0.006	0.010	0.006	0.010	0.002	-0.005
CH_3OH	0.005	0.007	0.005	0.007	0.002	-0.005
CH_3NH_2	0.004	0.007	0.004	0.007	0.002	-0.005
C_3H_8	0.004	0.007	0.004	0.007	-0.000	-0.003
H_2O	0.008	0.006	0.006	0.006	0.012	-0.012
HCl	0.005	0.005	0.004	0.006	0.008	-0.009
HBr	0.004	0.005	0.003	0.005	0.006	-0.008
C_2H_6	0.003	0.005	0.003	0.005	-0.000	-0.002
C_4H_8	0.002	0.004	0.002	0.004	-0.000	-0.001
H_2S	0.002	0.003	0.001	0.003	0.004	-0.005
NH_3	0.001	0.002	0.000	0.002	0.002	-0.004
CH_4	0.000	0.000	0.000	0.000	0.000	-0.000
CCl_4	0.000	0.000	-0.000	0.000	0.000	-0.000
SiH_4	0.000	0.000	0.000	-0.000	-0.000	0.000
Min.	0.000	0.000	-0.000	-0.000	-0.004	-0.065
Max.	0.115	0.112	0.114	0.119	0.060	0.000
Mean	0.020	0.025	0.020	0.026	0.011	-0.017

Table S33: Anisotropic descriptors $u_c^{\parallel}[\alpha(\omega = 0.649 \times i)]$ for all molecules in the TS42 database, for each contribution c, as documented in Table II in the main text.

Molecule	$u_{\text{ref}}^{\parallel}[\alpha(\omega)]$	$u_0^{\parallel}[\alpha(\omega)]$	$u_1^{\parallel}[\alpha(\omega)]$	$u_{1(0)}^{\parallel}[\alpha(\omega)]$	$u_{1(1)}^{\parallel}[\alpha(\omega)]$	$u_{1(2)}^{\parallel}[\alpha(\omega)]$
N_2O	0.067	0.090	0.067	0.091	0.036	-0.059
CO_2	0.054	0.075	0.051	0.077	0.032	-0.056
COS	0.033	0.060	0.032	0.060	0.012	-0.041
CS_2	0.027	0.059	0.027	0.057	0.008	-0.038
C_2H_2	0.026	0.050	0.023	0.048	0.026	-0.051
C_6H_6	0.023	0.048	0.022	0.047	0.012	-0.037
SO_2	0.022	0.037	0.023	0.037	0.006	-0.021
Cl_2	0.016	0.028	0.014	0.027	0.010	-0.023
H_2CO	0.017	0.025	0.018	0.025	0.014	-0.022
N_2	0.017	0.023	0.020	0.024	0.022	-0.026
C_2H_4	0.012	0.024	0.010	0.023	0.010	-0.023
C_8H_{18}	0.011	0.024	0.011	0.023	-0.004	-0.008
CO	0.016	0.022	0.018	0.022	0.018	-0.022
C_7H_{16}	0.009	0.021	0.009	0.020	-0.004	-0.007
C_3H_6	0.010	0.021	0.009	0.020	0.004	-0.015
C_6H_{14}	0.008	0.018	0.008	0.018	-0.004	-0.006
CH_3CHO	0.010	0.017	0.010	0.017	0.004	-0.011
$CH_3CH_2OCH_2CH_3$	0.008	0.017	0.008	0.017	-0.002	-0.006
$C_4H_{10}O$	0.008	0.017	0.008	0.016	-0.002	-0.007
C_5H_{12}	0.006	0.014	0.006	0.014	-0.002	-0.005
C_3H_7OH	0.006	0.013	0.006	0.013	-0.000	-0.006
CH_3OCH_3	0.006	0.012	0.006	0.012	0.000	-0.006
CH_3COCH_3	0.006	0.012	0.006	0.011	0.002	-0.006
H_2	0.013	0.012	0.012	0.011	0.026	-0.025
$CH_3CH_3CH_3N$	0.004	0.010	0.004	0.010	-0.002	-0.004
HF	0.022	0.011	0.019	0.010	0.026	-0.017
C_4H_{10}	0.004	0.011	0.004	0.010	-0.002	-0.004
CH_3NHCH_3	0.004	0.009	0.004	0.009	-0.000	-0.005
C_2H_5OH	0.004	0.008	0.004	0.008	0.000	-0.005
CH_3OH	0.004	0.007	0.004	0.007	0.002	-0.005
CH_3NH_2	0.003	0.006	0.002	0.006	0.000	-0.004
H_2O	0.007	0.006	0.005	0.006	0.010	-0.012
HBr	0.002	0.004	0.002	0.005	0.004	-0.006
HCl	0.003	0.004	0.002	0.005	0.004	-0.007
C_3H_8	0.002	0.005	0.002	0.005	-0.000	-0.002
C_2H_6	0.001	0.004	0.001	0.004	-0.000	-0.002
H_2S	0.001	0.003	0.000	0.003	0.002	-0.005
C_4H_8	0.001	0.003	0.001	0.003	-0.002	-0.001
NH_3	0.002	0.002	0.001	0.002	0.002	-0.004
CH_4	0.000	0.000	0.000	0.000	0.000	0.000
CCl_4	0.000	-0.000	0.000	-0.000	0.000	-0.000
SiH_4	0.000	0.000	0.000	-0.000	-0.000	0.000
Min.	0.000	-0.000	0.000	-0.000	-0.004	-0.059
Max.	0.067	0.090	0.067	0.091	0.036	0.000
Mean	0.012	0.020	0.011	0.020	0.006	-0.015

Table S34: Anisotropic descriptors $u_c^{\parallel}[\alpha(\omega = 1.154 \times i)]$ for all molecules in the TS42 database, for each contribution c, as documented in Table II in the main text.

Molecule	$u_{\text{ref}}^{\parallel}[\alpha(\omega)]$	$u_0^{\parallel}[\alpha(\omega)]$	$u_1^{\parallel}[\alpha(\omega)]$	$u_{1(0)}^{\parallel}[\alpha(\omega)]$	$u_{1(1)}^{\parallel}[\alpha(\omega)]$	$u_{1(2)}^{\parallel}[\alpha(\omega)]$
N_2O	0.026	0.058	0.026	0.057	0.012	-0.043
CO_2	0.022	0.049	0.020	0.048	0.012	-0.039
COS	0.012	0.039	0.011	0.038	-0.000	-0.026
C_2H_2	0.012	0.037	0.010	0.036	0.012	-0.037
C_6H_6	0.012	0.036	0.010	0.035	0.002	-0.028
CS_2	0.007	0.032	0.007	0.031	-0.002	-0.021
SO_2	0.008	0.023	0.008	0.023	-0.000	-0.014
CO	0.009	0.019	0.010	0.019	0.010	-0.019
N_2	0.009	0.019	0.009	0.018	0.012	-0.021
H_2CO	0.008	0.019	0.008	0.018	0.006	-0.016
C_2H_4	0.006	0.018	0.004	0.017	0.004	-0.016
Cl_2	0.003	0.013	0.003	0.013	0.000	-0.010
C_3H_6	0.004	0.014	0.003	0.013	0.000	-0.010
CH_3CHO	0.004	0.012	0.004	0.012	0.000	-0.008
C_8H_{18}	0.003	0.011	0.003	0.011	-0.004	-0.004
C_7H_{16}	0.003	0.010	0.003	0.009	-0.004	-0.003
H_2	0.006	0.009	0.005	0.009	0.016	-0.019
$CH_3CH_2OCH_2CH_3$	0.003	0.009	0.003	0.009	-0.002	-0.004
$C_4H_{10}O$	0.003	0.009	0.003	0.009	-0.002	-0.004
C_3H_7OH	0.002	0.008	0.002	0.008	-0.002	-0.004
C_6H_{14}	0.002	0.009	0.002	0.008	-0.004	-0.003
CH_3COCH_3	0.003	0.008	0.003	0.008	-0.000	-0.005
C_5H_{12}	0.002	0.007	0.002	0.007	-0.002	-0.002
CH_3OCH_3	0.002	0.007	0.002	0.007	-0.002	-0.004
HF	0.008	0.006	0.006	0.006	0.012	-0.012
CH_3NHCH_3	0.001	0.005	0.001	0.005	-0.002	-0.003
CH_3OH	0.002	0.005	0.002	0.005	0.000	-0.004
$CH_3CH_3CH_3N$	0.001	0.005	0.001	0.005	-0.002	-0.002
C_4H_{10}	0.001	0.005	0.001	0.005	-0.002	-0.002
C_2H_5OH	0.002	0.005	0.002	0.005	-0.000	-0.003
CH_3NH_2	0.001	0.004	0.001	0.004	-0.000	-0.003
H_2O	0.003	0.004	0.002	0.004	0.006	-0.008
HBr	0.001	0.003	0.000	0.003	0.000	-0.003
HCl	0.001	0.003	0.000	0.003	0.002	-0.004
C_3H_8	0.001	0.003	0.001	0.003	-0.000	-0.001
C_4H_8	0.000	0.002	0.000	0.002	-0.000	-0.000
H_2S	0.000	0.002	0.000	0.002	0.000	-0.003
C_2H_6	0.000	0.002	0.000	0.002	-0.000	-0.001
NH_3	0.001	0.002	0.001	0.002	0.002	-0.003
CH_4	0.000	0.000	0.000	0.000	0.000	0.000
CCl_4	0.000	-0.000	0.000	-0.000	0.000	-0.000
SiH_4	0.000	0.000	0.000	0.000	-0.000	0.000
Min.	0.000	-0.000	0.000	-0.000	-0.004	-0.043
Max.	0.026	0.058	0.026	0.057	0.016	0.000
Mean	0.005	0.013	0.004	0.012	0.002	-0.010

Table S35: Anisotropic descriptors $u_c^{\parallel}[\alpha(\omega = 2.308 \times i)]$ for all molecules in the TS42 database, for each contribution c, as documented in Table II in the main text.

Molecule	$u_{\text{ref}}^{\parallel}[\alpha(\omega)]$	$u_0^{\parallel}[\alpha(\omega)]$	$u_1^{\parallel}[\alpha(\omega)]$	$u_{1(0)}^{\parallel}[\alpha(\omega)]$	$u_{1(1)}^{\parallel}[\alpha(\omega)]$	$u_{1(2)}^{\parallel}[\alpha(\omega)]$
N_2O	0.006	0.028	0.005	0.027	-0.000	-0.021
CO_2	0.005	0.024	0.004	0.023	0.000	-0.019
C_2H_2	0.004	0.022	0.003	0.021	0.002	-0.020
C_6H_6	0.003	0.020	0.002	0.020	-0.002	-0.014
COS	0.003	0.019	0.002	0.019	-0.004	-0.012
CS_2	0.001	0.014	0.001	0.013	-0.004	-0.008
CO	0.003	0.013	0.003	0.013	0.002	-0.012
N_2	0.003	0.013	0.003	0.012	0.002	-0.012
H_2CO	0.002	0.011	0.002	0.011	0.000	-0.009
C_2H_4	0.002	0.010	0.001	0.010	-0.000	-0.008
SO_2	0.001	0.010	0.001	0.010	-0.002	-0.005
C_3H_6	0.001	0.007	0.001	0.007	-0.002	-0.005
CH_3CHO	0.001	0.006	0.001	0.006	-0.000	-0.004
H_2	0.001	0.005	0.001	0.005	0.006	-0.010
CH_3COCH_3	0.001	0.004	0.001	0.004	-0.000	-0.002
C_6H_{14}	0.000	0.003	0.000	0.003	-0.002	-0.001
C_7H_{16}	0.000	0.003	0.000	0.003	-0.002	-0.001
$CH_3CH_2OCH_2CH_3$	0.001	0.003	0.000	0.003	-0.002	-0.001
$C_4H_{10}O$	0.000	0.003	0.000	0.003	-0.002	-0.001
CH_3OCH_3	0.000	0.003	0.000	0.003	-0.000	-0.002
C_3H_7OH	0.000	0.003	0.000	0.003	-0.002	-0.001
C_8H_{18}	0.000	0.003	0.000	0.003	-0.002	-0.001
H_2O	0.001	0.002	0.000	0.002	0.002	-0.003
Cl_2	0.000	0.002	0.000	0.002	-0.000	-0.001
HF	0.001	0.002	0.000	0.002	0.002	-0.004
CH_3NHCH_3	0.000	0.002	0.000	0.002	-0.000	-0.001
CH_3OH	0.000	0.002	0.000	0.002	-0.000	-0.002
CH_3NH_2	0.000	0.002	0.000	0.002	-0.000	-0.001
$CH_3CH_3CH_3N$	0.000	0.002	0.000	0.002	-0.000	-0.001
C_5H_{12}	0.000	0.002	0.000	0.002	-0.002	-0.001
C_4H_{10}	0.000	0.002	0.000	0.002	-0.000	-0.001
C_2H_5OH	0.000	0.002	0.000	0.002	-0.000	-0.001
H_2S	0.000	0.001	-0.000	0.001	-0.000	-0.001
HBr	0.000	0.001	0.000	0.001	-0.000	-0.001
HCl	0.000	0.001	-0.000	0.001	-0.000	-0.001
C_3H_8	0.000	0.001	0.000	0.001	-0.000	-0.000
C_2H_6	0.000	0.001	0.000	0.001	-0.000	-0.000
NH_3	0.000	0.001	0.000	0.001	0.000	-0.001
CH_4	0.000	0.000	0.000	-0.000	-0.000	0.000
CCl_4	0.000	-0.000	0.000	-0.000	0.000	0.000
C_4H_8	0.000	0.001	0.000	0.000	-0.000	-0.000
SiH_4	0.000	0.000	0.000	-0.000	-0.000	0.000
Min.	0.000	-0.000	-0.000	-0.000	-0.004	-0.021
Max.	0.006	0.028	0.005	0.027	0.006	0.000
Mean	0.001	0.006	0.001	0.006	-0.000	-0.004

Table S36: Anisotropic descriptors $u_c^{\parallel}[\alpha(\omega = 5.958 \times i)]$ for all molecules in the TS42 database, for each contribution c, as documented in Table II in the main text.

Molecule	$u_{\text{ref}}^{\parallel}[\alpha(\omega)]$	$u_0^{\parallel}[\alpha(\omega)]$	$u_1^{\parallel}[\alpha(\omega)]$	$u_{1(0)}^{\parallel}[\alpha(\omega)]$	$u_{1(1)}^{\parallel}[\alpha(\omega)]$	$u_{1(2)}^{\parallel}[\alpha(\omega)]$
C_2H_2	0.001	0.012	0.001	0.012	-0.002	-0.010
C_6H_6	0.001	0.009	0.001	0.009	-0.002	-0.006
N_2O	0.001	0.008	0.000	0.008	-0.002	-0.006
CO_2	0.001	0.008	0.001	0.008	-0.002	-0.006
COS	0.000	0.007	0.000	0.007	-0.002	-0.004
CO	0.001	0.007	0.001	0.007	-0.000	-0.005
N_2	0.001	0.006	0.000	0.006	-0.000	-0.005
CS_2	0.000	0.005	0.000	0.005	-0.002	-0.003
C_2H_4	0.000	0.005	0.000	0.005	-0.002	-0.004
H_2CO	0.000	0.005	0.000	0.005	-0.000	-0.003
C_3H_6	0.000	0.003	0.000	0.003	-0.000	-0.002
SO_2	0.000	0.003	0.000	0.003	-0.002	-0.001
CH_3CHO	0.000	0.002	0.000	0.002	-0.000	-0.001
CH_3COCH_3	0.000	0.002	0.000	0.002	-0.000	-0.001
H_2	0.000	0.001	0.000	0.001	0.000	-0.002
$CH_3CH_2OCH_2CH_3$	0.000	0.001	0.000	0.001	-0.000	-0.000
C_8H_{18}	0.000	0.001	0.000	0.001	-0.000	-0.000
H_2O	0.000	0.000	0.000	0.000	0.000	-0.001
CH_4	0.000	0.000	-0.000	-0.000	-0.000	0.000
HF	0.000	-0.000	0.000	-0.000	-0.000	0.000
H_2S	0.000	-0.000	0.000	-0.000	0.000	0.000
NH_3	0.000	0.000	0.000	0.000	0.000	-0.000
HBr	0.000	-0.000	0.000	-0.000	0.000	0.000
CH_3NHCH_3	0.000	0.000	0.000	0.000	-0.000	-0.000
CH_3OH	0.000	0.000	0.000	0.000	-0.000	-0.000
CH_3OCH_3	0.000	0.000	0.000	0.000	-0.000	-0.000
C_2H_5OH	0.000	0.000	0.000	0.000	-0.000	-0.000
C_2H_6	0.000	0.000	0.000	0.000	-0.000	-0.000
C_3H_7OH	0.000	0.000	0.000	0.000	-0.000	-0.000
C_3H_8	0.000	0.000	0.000	0.000	-0.000	-0.000
C_4H_{10}	0.000	0.000	0.000	0.000	-0.000	-0.000
$C_4H_{10}O$	0.000	0.000	0.000	0.000	-0.000	-0.000
C_4H_8	0.000	0.000	0.000	0.000	-0.000	-0.000
C_5H_{12}	0.000	0.000	0.000	0.000	-0.000	-0.000
C_6H_{14}	0.000	0.000	0.000	0.000	-0.000	-0.000
C_7H_{16}	0.000	0.000	0.000	0.000	-0.000	-0.000
CCl_4	0.000	0.000	-0.000	-0.000	-0.000	-0.000
$CH_3CH_3CH_3N$	0.000	0.000	0.000	0.000	-0.000	-0.000
CH_3NH_2	0.000	0.000	0.000	0.000	-0.000	-0.000
SiH_4	0.000	0.000	0.000	-0.000	0.000	0.000
HCl	0.000	-0.001	0.000	-0.001	0.000	0.000
Cl_2	0.000	-0.003	0.000	-0.003	0.002	0.002
Min.	0.000	-0.003	-0.000	-0.003	-0.002	-0.010
Max.	0.001	0.012	0.001	0.012	0.002	0.002
Mean	0.000	0.002	0.000	0.002	-0.000	-0.001

Table S37: Anisotropic descriptors $u_c^{\parallel}[\alpha(\omega = 32.239 \times i)]$ for all molecules in the TS42 database, for each contribution c, as documented in Table II in the main text.

Molecule	$u_{\text{ref}}^{\parallel}[\alpha(\omega)]$	$u_0^{\parallel}[\alpha(\omega)]$	$u_1^{\parallel}[\alpha(\omega)]$	$u_{1(0)}^{\parallel}[\alpha(\omega)]$	$u_{1(1)}^{\parallel}[\alpha(\omega)]$	$u_{1(2)}^{\parallel}[\alpha(\omega)]$
C_2H_2	0.001	0.014	0.001	0.014	-0.002	-0.010
C_6H_6	0.001	0.008	0.001	0.008	-0.002	-0.005
N_2O	0.000	0.006	0.000	0.006	-0.002	-0.004
CO_2	0.000	0.006	0.000	0.006	-0.002	-0.004
CS_2	0.000	0.005	0.000	0.005	-0.002	-0.002
C_2H_4	0.001	0.005	0.001	0.005	-0.002	-0.004
CO	0.000	0.005	0.000	0.005	-0.000	-0.004
COS	0.000	0.005	0.000	0.005	-0.002	-0.003
N_2	0.000	0.004	0.000	0.004	-0.000	-0.003
C_3H_6	0.000	0.003	0.000	0.003	-0.000	-0.002
H_2CO	0.000	0.003	0.000	0.003	-0.000	-0.002
SO_2	0.000	0.002	0.000	0.002	-0.000	-0.001
CH_3CHO	0.000	0.002	0.000	0.002	-0.000	-0.001
CH_3COCH_3	0.000	0.001	0.000	0.001	-0.000	-0.000
H_2O	0.000	0.001	0.000	0.001	0.000	-0.001
H_2	0.000	-0.000	0.000	-0.000	-0.000	0.000
CH_3OH	0.000	0.000	0.000	0.000	-0.000	-0.000
H_2S	0.000	0.000	0.000	0.000	-0.000	0.000
HBr	0.000	-0.000	0.000	-0.000	0.000	0.000
HCl	0.000	-0.000	0.000	-0.000	0.000	0.000
HF	0.000	-0.000	0.000	-0.000	-0.000	0.000
NH_3	0.000	0.000	0.000	0.000	-0.000	-0.000
CH_4	0.000	-0.000	0.000	-0.000	-0.000	0.000
CH_3NHCH_3	0.000	0.000	0.000	0.000	-0.000	-0.000
CH_3OCH_3	0.000	0.000	0.000	0.000	-0.000	-0.000
CH_3NH_2	0.000	0.000	0.000	0.000	-0.000	-0.000
C_2H_5OH	0.000	0.000	0.000	0.000	-0.000	-0.000
C_2H_6	0.000	-0.000	0.000	-0.000	0.000	0.000
C_3H_7OH	0.000	-0.000	0.000	-0.000	0.000	0.000
C_3H_8	0.000	-0.000	0.000	-0.000	0.000	0.000
C_4H_{10}	0.000	-0.000	0.000	-0.000	0.000	0.000
$C_4H_{10}O$	0.000	-0.000	0.000	-0.000	0.000	0.000
C_4H_8	0.000	-0.000	0.000	-0.000	0.000	0.000
C_5H_{12}	0.000	-0.000	0.000	-0.000	0.000	0.000
C_6H_{14}	0.000	-0.000	0.000	-0.000	0.000	0.000
C_7H_{16}	0.000	-0.000	0.000	-0.000	0.000	0.000
C_8H_{18}	0.000	-0.000	0.000	-0.000	0.000	0.000
CCl_4	0.000	-0.000	-0.000	-0.000	0.000	-0.000
$CH_3CH_2OCH_2CH_3$	0.000	0.000	0.000	0.000	-0.000	-0.000
$CH_3CH_3CH_3N$	0.000	-0.000	0.000	-0.000	0.000	0.000
SiH_4	0.000	0.000	0.000	0.000	0.000	-0.000
Cl_2	0.000	-0.002	0.000	-0.002	0.002	0.001
Min.	0.000	-0.002	-0.000	-0.002	-0.002	-0.010
Max.	0.001	0.014	0.001	0.014	0.002	0.001
Mean	0.000	0.002	0.000	0.002	-0.000	-0.001

5

Conclusions and perspectives

There will come a time when you believe everything is finished.
That will be the beginning
Louis L'Amour (1908-1988)

5.1 Conclusions

This thesis consists of two parts. The first part focuses on the development of a frequency-dependent extension of the ACKS2 model, i.e., ACKS2ω. ACKS2ω facilitates theoretical predictions of dynamic response properties of finite systems via partitioning the frequency-dependent molecular response function. We also found that ACKS2ω amalgamates the benefits of a quantum-mechanical description of frequency-dependent response with the computational efficiency of force-field models. The strength of the ACKS2ω model lies in its low computational demand for calculations involving response kernels, achieving a complexity comparable to conventional polarizable force fields, post-parameterization. Nevertheless, the parameterization proved computationally demanding to accomplish accurate predictions, substantiating the ability of ACKS2ω to reproduce its TDDFT reference.

Figure 5.1 summarizes the derivation workflow of traditional PFFs, ACKS2 and ACKS2ω models.

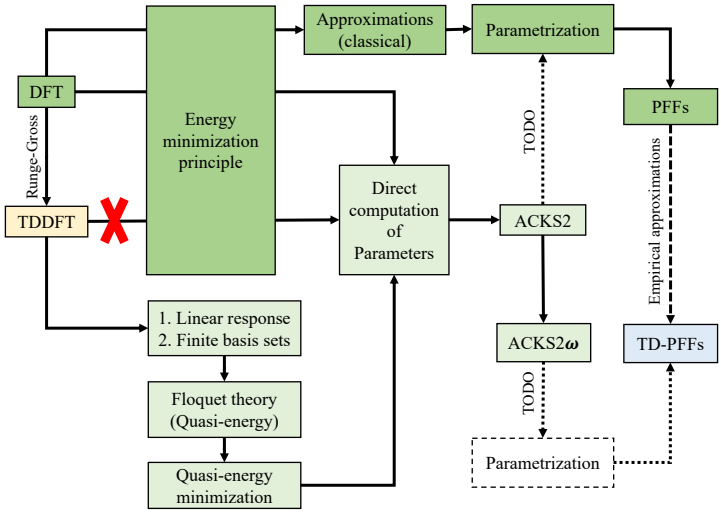

Figure 5.1: A summary of the derivation workflow for polarizable force fields (PFFs), emphasizing the ACKS2 and ACKS2ω models. The workflow transitions from quantum mechanical methods, such as DFT, to classical approximations, leading to the development of PFFs. Different line styles are used to distinguish between various processes: solid lines represent direct derivations, dotted lines indicate tasks that need to be addressed (TODO), and dashed lines signify indirect derivations, such as empirical approximations. Traditional elements of PFF development are highlighted in deep green and light blue (for the time-dependent case), while newer components associated with ACKS2 and ACKS2ω are depicted in light green.

The second part of this thesis focuses on the applications of the ACKS2ω model. We applied the ACKS2ω model to examine the influence of fluctuating charges, also known as charge flow, on the dynamic linear-response properties of finite systems, including frequency-dependent dipole polarizability and molecular C_6 dispersion coefficients. The analysis encompasses 42 organic and inorganic molecules for dipole polarizability, and 903 molecular dimers for C_6 dispersion coefficients. An overview of the charge-flow contribution is summarized as follows:

- We studied the charge-flow contribution to isotropic dipole polarizability, finding that it is smaller than the dipole-only contribution but not negligible. This contribution is influenced by molecular topology, including geometry, polarizable bonds, and non-hydrogen atoms. It

has a weak dependence on the modulus of imaginary frequencies.

- Our analysis of the charge-flow contribution to anisotropic dipole polarizability suggested that it can predict anisotropy of polarizability, with its contribution decreasing as the modulus increases, eventually approaching zero at higher frequencies. We further highlight that charge-flow and charge-dipole responses are key contributors to molecular polarizability anisotropy in both static and frequency-dependent scenarios. In contrast, dipole-only interactions have a significant, but opposing, impact on anisotropic dipole polarizability.

- In terms of isotropic C_6 coefficients, the charge-flow contribution significantly underestimates the isotropic C_6 coefficients. However, it could be more important than the dipole-only contribution in larger systems with a greater number of non-hydrogen atoms.

- The study of the charge-flow contribution to anisotropic C_6 coefficients shows that unlike anisotropic dipole polarizability, the anisotropic C_6 coefficients are not fully reproduced by the charge-flow contributions. This discrepancy is due to the definition of anisotropic C_6 coefficients. Generally, dipole-only contributions tend to reduce dispersion anisotropy.

5.2 Perspectives

For the development of ACKS2ω, future efforts will focus on simpler force-field-like parameterizations to circumvent the computational limitations of the current parameterization, which will likely aid in calculations of long-range correlation energies of extended systems where DFT may be unfeasible.

However, there are several limitations in ACKS2ω that need to be considered and addressed first. Firstly, in our current papers, the ACKS2 or ACKS2ω parameters are non-robust, sensitive to nuclear coordinates, due to the numerical limitations of the pseudo-inverse used to construct density basis functions.[157] Addressing the issue of robustness is therefore a priority. This may require abandoning biorthogonal basis sets; however, this would result in non-zero overlap elements between density and potential basis functions, which would, to some extent, introduce additional computational costs. Recently, Gütlein *et al.* implemented ACKS2 using Gaussian functions for both potential and density basis functions.[160, 161] While most of the ACKS2 parameters can be determined analytically thanks to the introduction of Gaussian basis functions, and observables, induced moments, and polarization energy

agree well due to error cancellations, there are significant differences between the induced density obtained from ACKS2 and the corresponding DFT counterparts. One significant issue is that ACKS2 with Gaussian basis functions is not suitable for interacting distributed polarizabilities calculations, which are important for developing novel dispersion models in the future. One possible solution is to add more Gaussian basis functions instead of using minimal basis sets, but this will inevitably introduce more computational costs. Once the issue of parameter robustness has been addressed, machine learning techniques can be employed to explore the relationship between molecular geometry and Kohn-Sham response matrix and atomic hardness matrix. This has the potential to provide a computationally efficient way to compute interacting response matrices.

Secondly, ACKS2 and ACKS2ω models can theoretically be applied to wavefunctions obtained by DFT with any XC functional. However, the current validation of the model is limited to local and semi-local XC functionals, and the performance with hybrid XC functionals is an open question. This raises several concerns:

- How should we compute the contribution of the Hartree exchange functional? Should it be included in the implicit or explicit functional? Since the ACKS2 model is derived with this term included in the implicit functional, it would result in an additional contribution to the response matrix, which is then no longer the Kohn-Sham response matrix.
- Another open question is how to compute this non-local term using a set of atom-condensed potential basis functions. An alternative could be to include the Hartree exchange functional in the explicit functional and compute the hardness with density basis functions, analogous to the TDDFT case. However, in TDDFT, this is usually done with a product space of occupied and virtual orbitals. One potential approach is to expand the density basis functions in this product space and compute the atomic hardness from two-electron four-center repulsion integrals. However, this could be computationally infeasible.

Thirdly, the current implementation is solely for closed-shell finite systems; extending it to open-shell or periodic systems would also be intriguing. One might also anticipate that ACKS2ω could compute triplet excitation properties. Furthermore, is it possible for ACKS2ω to be utilized for double, triple, or even higher-order excitation calculations? This would likely require a frequency-dependent atomic hardness rather than the frequency-independent version currently in use. Additionally, the current work con-

siders only ground-state structures; however, exploring non-optimized structures would be an interesting avenue for future research.

Another important point from this thesis is the importance of fluctuating charges in determining the dynamic linear-response properties of finite systems, which suggests potential avenues for future research in developing more accurate polarizable force fields.

For example, incorporating charge-flow effects into the MBD model to address type-C dispersion interactions has recently been proposed by Dobson *et al.*[162] This enhanced method is named MBD+C and improves the accuracy of dispersion interaction predictions across a range of separations. The MBD+C model has been validated through various tests, including those on metallic chains, lithium-doped graphene, and carbon nanotubes, demonstrating its potential for applications in chemistry and materials science, particularly for large systems where computational efficiency is paramount. It integrates a near-neighbor interaction model that relies on the metallic band structure, highlighting its sophisticated approach to theoretical dispersion energy calculations. However, the MBD+C method is not yet user-friendly or fully automatic ("black box") because it requires users to possess a certain level of understanding of the band structure of the metal being studied. One potential application of ACKS2ω is to generate parameters for the MBD+C model.

Next, I will discuss some perspectives on combining ACKS2ω and ACFD theory to develop a novel dispersion model that includes charge-flow and dipoles. The basic idea is to rewrite the ACFD model using ACKS2 or AKCS2ω parameters. Specifically, the correlation energy from ACFD is based on the following expression:[43]

$$E_c = -\frac{1}{2\pi}\int_0^\infty du \int_0^1 d\lambda \int\int d\boldsymbol{r}_1 d\boldsymbol{r}_2 \frac{\chi_\lambda(\boldsymbol{r}_1,\boldsymbol{r}_2,iu) - \chi_0(\boldsymbol{r}_1,\boldsymbol{r}_2,iu)}{|\boldsymbol{r}_1-\boldsymbol{r}_2|} \tag{5.1}$$

where $\chi_\lambda(\boldsymbol{r}_1,\boldsymbol{r}_2,iu)$ is the density response function at imaginary frequency iu of a system whose electrons interact with a scaled Coulomb interaction $\frac{\lambda}{|\boldsymbol{r}_1-\boldsymbol{r}_2|}$. χ_1 and χ_0 correspond to the response functions in fully interacting and Kohn-Sham non-interacting systems, respectively.

For $\lambda > 0$, the interacting density response function $\chi_\lambda(iu)$ can be related to the non-interacting one via a Dyson equation obtained from TDDFT:

$$\chi_\lambda(iu) = \chi_0(iu) + \chi_0(iu)[\lambda v_c + f_{xc}^\lambda(iu)]\chi_\lambda(iu) \tag{5.2}$$

where $f_{xc}^\lambda(iu)$ is the scaled frequency-dependent XC kernel. Spatial coordinates dependence is implicit in the matrix notation.

With the adiabatic approximation, $f_{xc}^{\lambda}(iu)$ becomes $f_{xc}^{\lambda}(0)$. Moreover, if $f_{xc}^{\lambda}(0) \approx f_{xc}^{0}(0)$, then $\chi_{\lambda}(iu)$ can be easily reproduced using ACKS2ω parameters, i.e., $\chi_0(iu)$ and $f_{xc}^{0}(0)$. Furthermore, when RPA methods are used, the correlation energy becomes:

$$E_{c,\mathrm{RPA}} = -\frac{1}{2\pi}\int_0^{\infty} du \sum_{n=2}^{\infty} \frac{1}{n}\mathrm{Tr}[(\chi_0(iu)v)^n]. \tag{5.3}$$

In this case, only the ACKS2 model is required. It should be noted that this approach has been employed in the MBD model for dispersion energy calculations,[25, 26] whereas in our case, the charge-flow contribution is also included instead of relying solely on dipoles. However, one concern is that some long-range correlation energy may have already been accounted for in the XC functional, resulting in double counting in ACFD. To address this issue, range-separated DFT can be used, where the short-range correlation energy is treated by DFT, while the long-range correlation energy is treated by wavefunction-based methods such as CI and CC. Alternatively, ACFD can be used to compute the long-range correlation energy. The difficulty lies in addressing the contribution from the Hartree exchange functional to atomic hardness.

Once the limitations discussed above are properly addressed, this innovative dispersion model could be applied in both dispersion-corrected DFT calculations and force fields derived from quantum-mechanical methods, particularly for systems such as low-dimensional nanostructures and metallic systems. In these systems, type-C non-additive dispersion interactions play a significant role due to long-range fluctuating charges, resulting in dispersion interactions that follow a non-standard power law characterized by a small magnitude of the exponent R.

Part II

Appendix

A

List of Publications

A.1 Publications in international peer–reviewed journals

1. **The significance of fluctuating charges for molecular polarizability and dispersion coefficients**
   YingXing Cheng, Toon Verstraelen
   J. Chem. Phys., **2023**, 159, 094111

2. **A new framework for frequency-dependent polarizable force fields**
   YingXing Cheng, Toon Verstraelen
   J. Chem. Phys., **2022**, 157, 124106

A.2 Conference contributions

1. **A new frequency-dependent polarizable force field: ACKS2ω**
   YingXing Cheng and Toon Verstraelen
   19th International Conference on Density Functional Theory and its Applications, Brussels, Belgium, August 28 – September 2, 2022

B

List of Software Packages

In the context of this Ph.D. dissertation, various software packages have been developed. Below, an overview of these software packages is provided.

1. **Pydisp**
   Pure Python implementation for various dispersion models using distributed polarizabilities generated by the ACKS2ω model.
   Website: https://github.com/yingxingcheng/pydisp

2. **ACKS2-omega**
   Pure Python implementation for the ACKS2ω model.
   Website: https://github.com/yingxingcheng/acks2-omega

3. **Horton2-wrapper**
   A Horton2 wrapper for generating input files for the ACKS2ω model.
   Website: https://github.com/yingxingcheng/horton2-wrapper

4. **Horton-Part**
   A Python library offering a variety of partitioning methods based on the Horton program.
   Website: https://github.com/yingxingcheng/horton-part

5. **LRC-CD**
   This package calculates long-range correlation energy, taking into account charges and dipoles. It includes implementations for all ACKS2ω variants, as well as *ab-initio* implementations such as HFsrDFT and various RPA energy models. Although the package is not currently open-source, it can be made available upon request.
   Website: https://github.com/yingxingcheng/LRC-CD

6. **Libsrxc**
   A Python library designed for short-range DFT exchange-correlation functional.
   Website:
   https://github.com/yingxingcheng/short-range-xc-functionals

7. **PyDIRAC**
   A Python wrapper for the DIRAC program, used for high-precision quantum chemical calculations. This wrapper provides a user-friendly interface for performing complex calculations and analyzing results.
   Website: https://github.com/yingxingcheng/pydirac

Bibliography

[1] M. Stöhr, T. V. Voorhis, and A. Tkatchenko, "Theory and practice of modeling van der Waals interactions in electronic-structure calculations," *Chem. Soc. Rev.*, vol. 48, no. 15, pp. 4118–4154, 2019.

[2] F. London, "Zur Theorie und Systematik der Molekularkräfte," *Z. Physik*, vol. 63, no. 3, pp. 245–279, 1930.

[3] E. Zaremba and W. Kohn, "Van der Waals interaction between an atom and a solid surface," *Phys. Rev. B*, vol. 13, no. 6, pp. 2270–2285, 1976.

[4] S. Grimme, S. Ehrlich, and L. Goerigk, "Effect of the damping function in dispersion corrected density functional theory," *J. Comput. Chem.*, vol. 32, no. 7, pp. 1456–1465, 2011.

[5] J. F. Dobson, "Beyond pairwise additivity in London dispersion interactions," *Int. J. Quantum Chem.*, vol. 114, no. 18, pp. 1157–1161, 2014.

[6] A. Otero-de-la-Roza, L. M. LeBlanc, and E. R. Johnson, "What is "many-body" dispersion and should I worry about it?," *Phys. Chem. Chem. Phys.*, vol. 22, no. 16, pp. 8266–8276, 2020.

[7] E. Caldeweyher, C. Bannwarth, and S. Grimme, "Extension of the D3 dispersion coefficient model," *J. Chem. Phys.*, vol. 147, no. 3, p. 034112, 2017.

[8] M. Elstner, P. Hobza, T. Frauenheim, S. Suhai, and E. Kaxiras, "Hydrogen bonding and stacking interactions of nucleic acid base pairs: A density-functional-theory based treatment," *J. Chem. Phys.*, vol. 114, no. 12, pp. 5149–5155, 2001.

[9] S. Grimme, "Accurate description of van der Waals complexes by density functional theory including empirical corrections," *J. Comput. Chem.*, vol. 25, no. 12, pp. 1463–1473, 2004.

[10] S. Grimme, J. Antony, S. Ehrlich, and H. Krieg, "A consistent and accurate ab initio parametrization of density functional dispersion correction (DFT-D) for the 94 elements H-Pu," *J. Chem. Phys.*, vol. 132, no. 15, p. 154104, 2010.

[11] P. Jurečka, J. Černý, P. Hobza, and D. R. Salahub, "Density functional theory augmented with an empirical dispersion term. Interaction energies and geometries of 80 noncovalent complexes compared with ab initio quantum mechanics calculations," *J. Comput. Chem.*, vol. 28, no. 2, pp. 555–569, 2007.

[12] A. Tkatchenko and M. Scheffler, "Accurate Molecular Van Der Waals Interactions from Ground-State Electron Density and Free-Atom Reference Data," *Phys. Rev. Lett.*, vol. 102, no. 7, p. 073005, 2009.

[13] A. D. Becke and E. R. Johnson, "Exchange-hole dipole moment and the dispersion interaction," *J. Chem. Phys.*, vol. 122, no. 15, p. 154104, 2005.

[14] A. D. Becke and E. R. Johnson, "A density-functional model of the dispersion interaction," *J. Chem. Phys.*, vol. 123, no. 15, p. 154101, 2005.

[15] A. D. Becke and E. R. Johnson, "Exchange-hole dipole moment and the dispersion interaction revisited," *J. Chem. Phys.*, vol. 127, no. 15, p. 154108, 2007.

[16] Y. Ikabata and H. Nakai, "Local response dispersion method: A density-dependent dispersion correction for density functional theory," *Int. J. Quantum Chem.*, vol. 115, no. 5, pp. 309–324, 2015.

[17] T. Sato and H. Nakai, "Density functional method including weak interactions: Dispersion coefficients based on the local response approximation," *J. Chem. Phys.*, vol. 131, no. 22, p. 224104, 2009.

[18] T. Sato and H. Nakai, "Local response dispersion method. II. Generalized multicenter interactions," *J. Chem. Phys.*, vol. 133, no. 19, p. 194101, 2010.

[19] B. M. Axilrod and E. Teller, "Interaction of the van der Waals Type Between Three Atoms," *J. Chem. Phys.*, vol. 11, no. 6, pp. 299–300, 1943.

[20] Y. Muto, "Force between nonpolar molecules," *J. Phys. Math. Soc. Jpn*, vol. 17, pp. 629–631, 1943.

[21] A. Otero-de-la-Roza, L. M. LeBlanc, and E. R. Johnson, "Asymptotic Pairwise Dispersion Corrections Can Describe Layered Materials Accurately," *J. Phys. Chem. Lett.*, vol. 11, no. 6, pp. 2298–2302, 2020.

[22] E. R. Johnson, "Chapter 5 - The Exchange-Hole Dipole Moment Dispersion Model," in *Non-Covalent Interactions in Quantum Chemistry and Physics* (A. Otero de la Roza and G. A. DiLabio, eds.), pp. 169–194, Elsevier, January 2017.

[23] A. Otero-de-la-Roza and E. R. Johnson, "Many-body dispersion interactions from the exchange-hole dipole moment model," *J. Chem. Phys.*, vol. 138, no. 5, p. 054103, 2013.

[24] A. Ambrosetti, A. M. Reilly, R. A. DiStasio, and A. Tkatchenko, "Long-range correlation energy calculated from coupled atomic response functions," *J. Chem. Phys.*, vol. 140, no. 18, p. 18A508, 2014.

[25] A. Tkatchenko, R. A. DiStasio, R. Car, and M. Scheffler, "Accurate and Efficient Method for Many-Body van der Waals Interactions," *Phys. Rev. Lett.*, vol. 108, no. 23, p. 236402, 2012.

[26] A. Tkatchenko, A. Ambrosetti, and R. A. DiStasio, "Interatomic methods for the dispersion energy derived from the adiabatic connection fluctuation-dissipation theorem," *J. Chem. Phys.*, vol. 138, no. 7, p. 074106, 2013.

[27] A. Stone, *The Theory of Intermolecular Forces*. Oxford University Press, January 2013.

[28] J. F. Dobson, A. White, and A. Rubio, "Asymptotics of the Dispersion Interaction: Analytic Benchmarks for van der Waals Energy Functionals," *Phys. Rev. Lett.*, vol. 96, no. 7, p. 073201, 2006.

[29] J. Hermann, R. A. J. DiStasio, and A. Tkatchenko, "First-Principles Models for van der Waals Interactions in Molecules and Materials: Concepts, Theory, and Applications," *Chem. Rev.*, vol. 117, no. 6, pp. 4714–4758, 2017.

[30] J. F. Dobson, "Towards efficient description of type-C London dispersion forces between low-dimensional metallic nanostructures," *Electron. Struct.*, vol. 3, no. 4, p. 044001, 2021.

[31] K. Jackson, M. Yang, and J. Jellinek, "Site-Specific Analysis of Dielectric Properties of Finite Systems," *J. Phys. Chem. C*, vol. 111, no. 48, pp. 17952–17960, 2007.

[32] K. Jackson and J. Jellinek, "Si clusters are more metallic than bulk Si," *J. Chem. Phys.*, vol. 145, no. 24, p. 244302, 2016.

[33] J. F. Dobson and T. Gould, "Calculation of dispersion energies," *J. Phys. Condens. Matter*, vol. 24, no. 7, p. 073201, 2012.

[34] N. Sablon, F. D. Proft, P. W. Ayers, and P. Geerlings, "Computing Second-Order Functional Derivatives with Respect to the External Potential," *J. Chem. Theory Comput.*, vol. 6, no. 12, pp. 3671–3680, 2010.

[35] A. J. Misquitta, J. Spencer, A. J. Stone, and A. Alavi, "Dispersion interactions between semiconducting wires," *Phys. Rev. B*, vol. 82, no. 7, p. 075312, 2010.

[36] A. J. Misquitta, R. Maezono, N. D. Drummond, A. J. Stone, and R. J. Needs, "Anomalous nonadditive dispersion interactions in systems of three one-dimensional wires," *Phys. Rev. B*, vol. 89, no. 4, p. 045140, 2014.

[37] J. Tao, J. P. Perdew, and A. Ruzsinszky, "Accurate van der Waals coefficients from density functional theory," *Proc. Natl. Acad. Sci.*, vol. 109, no. 1, pp. 18–21, 2012.

[38] A. Ruzsinszky, J. P. Perdew, J. Tao, G. I. Csonka, and J. M. Pitarke, "Van der Waals Coefficients for Nanostructures: Fullerenes Defy Conventional Wisdom," *Phys. Rev. Lett.*, vol. 109, no. 23, p. 233203, 2012.

[39] P. Hohenberg and W. Kohn, "Inhomogeneous Electron Gas," *Phys. Rev.*, vol. 136, no. 3B, pp. B864–B871, 1964.

[40] W. Kohn and L. J. Sham, "Self-Consistent Equations Including Exchange and Correlation Effects," *Phys. Rev.*, vol. 140, no. 4A, pp. A1133–A1138, 1965.

[41] E. Runge and E. K. U. Gross, "Density-Functional Theory for Time-Dependent Systems," *Physical Rev. Lett.*, vol. 52, no. 12, pp. 997–1000, 1984.

[42] C. A. Ullrich, *Time-dependent density-functional theory: concepts and applications.* OUP Oxford, 2011.

[43] M. A. Marques, N. T. Maitra, F. M. Nogueira, E. K. Gross, and A. Rubio, *Fundamentals of time-dependent density functional theory*, vol. 837. Springer, 2012.

[44] M. E. Casida, "Time-Dependent Density Functional Response Theory for Molecules," in *Recent Advances in Density Functional Methods* (D. P. Chong, ed.), pp. 155–192, World Scientific, 1995.

[45] J. H. Shirley, "Solution of the schrödinger equation with a hamiltonian periodic in time," *Phys. Rev.*, vol. 138, pp. B979–B987, May 1965.

[46] N. T. Maitra and K. Burke, "On the floquet formulation of time-dependent density functional theory," *Chem. Phys. Lett.*, vol. 359, no. 3-4, pp. 237–240, 2002.

[47] P. Salek, T. Helgaker, and T. Saue, "Linear response at the 4-component relativistic density-functional level: Application to the frequency-dependent dipole polarizability of Hg, AuH and PtH2," *Chem. Phys.*, vol. 311, no. 1-2 SPEC.ISS., pp. 187–201, 2005.

[48] P. Samal and M. K. Harbola, "Analysis of Floquet formulation of time-dependent density-functional theory," *Chem. Phys. Lett.*, vol. 433, no. 1-3, pp. 204–210, 2006.

[49] N. T. Maitra and K. Burke, "Comment on "Analysis of Floquet formulation of time-dependent density-functional theory"[Chem. Phys. Lett. 433 (2006) 204]," *Chem. Phys. Lett.*, vol. 441, no. 1-3, pp. 167–169, 2007.

[50] V. Kapoor, M. Ruggenthaler, and D. Bauer, "Periodicity of the time-dependent Kohn-Sham equation and the Floquet theorem," *Phys. Rev. A*, vol. 87, no. 4, pp. 1–7, 2013.

[51] P. W. Langhoff, S. T. Epstein, and M. Karplus, "Aspects of time-dependent perturbation theory," *Rev. Mod. Phys.*, vol. 44, no. 3, pp. 602–644, 1972.

[52] C. M. Baker, "Polarizable force fields for molecular dynamics simulations of biomolecules," *WIREs Comput. Mol. Sci.*, vol. 5, no. 2, pp. 241–254, 2015.

[53] B. R. Brooks, R. E. Bruccoleri, B. D. Olafson, D. J. States, S. Swaminathan, and M. Karplus, "CHARMM: A program for macromolecular energy, minimization, and dynamics calculations," *J. Comput. Chem.*, vol. 4, no. 2, pp. 187–217, 1983.

[54] P. Cieplak, F.-Y. Dupradeau, Y. Duan, and J. Wang, "Polarization effects in molecular mechanical force fields," *J. Phys. Condens. Matter*, vol. 21, no. 33, p. 333102, 2009.

[55] G. A. Cisneros, M. Karttunen, P. Ren, and C. Sagui, "Classical Electrostatics for Biomolecular Simulations," *Chem. Rev.*, vol. 114, no. 1, pp. 779–814, 2014.

[56] W. D. Cornell, P. Cieplak, C. I. Bayly, I. R. Gould, K. M. Merz, D. M. Ferguson, D. C. Spellmeyer, T. Fox, J. W. Caldwell, and P. A. Kollman, "A Second Generation Force Field for the Simulation of Proteins, Nucleic Acids, and Organic Molecules," *J. Am. Chem. Soc.*, vol. 117, no. 19, pp. 5179–5197, 1995.

[57] M. A. González, "Force fields and molecular dynamics simulations," *Éc. Thématique Société Fr. Neutron.*, vol. 12, pp. 169–200, 2011.

[58] T. A. Halgren and W. Damm, "Polarizable force fields," *Curr. Opin. Struct. Biol.*, vol. 11, no. 2, pp. 236–242, 2001.

[59] X. He, B. Walker, V. H. Man, P. Ren, and J. Wang, "Recent progress in general force fields of small molecules," *Curr. Opin. Struct. Biol.*, vol. 72, pp. 187–193, 2022.

[60] V. S. Inakollu, D. P. Geerke, C. N. Rowley, and H. Yu, "Polarisable force fields: What do they add in biomolecular simulations?," *Curr. Opin. Struct. Biol.*, vol. 61, pp. 182–190, 2020.

[61] Z. Jing, C. Liu, S. Y. Cheng, R. Qi, B. D. Walker, J.-P. Piquemal, and P. Ren, "Polarizable Force Fields for Biomolecular Simulations: Recent Advances and Applications," *Annu. Rev. Biophys.*, vol. 48, no. 1, pp. 371–394, 2019.

[62] J. A. Lemkul, J. Huang, B. Roux, and A. D. J. MacKerell, "An Empirical Polarizable Force Field Based on the Classical Drude Oscillator Model: Development History and Recent Applications," *Chem. Rev.*, vol. 116, no. 9, pp. 4983–5013, 2016.

[63] P. S. Nerenberg and T. Head-Gordon, "New developments in force fields for biomolecular simulations," *Curr. Opin. Struct. Biol.*, vol. 49, pp. 129–138, 2018.

[64] S. Patel and C. L. Brooks III, "CHARMM fluctuating charge force field for proteins: I parameterization and application to bulk organic liquid simulations," *J. Comput. Chem.*, vol. 25, no. 1, pp. 1–16, 2004.

[65] J. W. Ponder, C. Wu, P. Ren, V. S. Pande, J. D. Chodera, M. J. Schnieders, I. Haque, D. L. Mobley, D. S. Lambrecht, R. A. Distasio, M. Head-Gordon, G. N. Clark, M. E. Johnson, and T. Head-Gordon, "Current status of the AMOEBA polarizable force field," *J. Phys. Chem. B*, vol. 114, no. 8, pp. 2549–2564, 2010.

[66] P. Ren, J. Chun, D. G. Thomas, M. J. Schnieders, M. Marucho, J. Zhang, and N. A. Baker, "Biomolecular electrostatics and solvation: A computational perspective," *Q. Rev. Biophys.*, vol. 45, no. 4, pp. 427–491, 2012.

[67] R. Salomon-Ferrer, A. W. Götz, D. Poole, S. Le Grand, and R. C. Walker, "Routine Microsecond Molecular Dynamics Simulations with AMBER on GPUs. 2. Explicit Solvent Particle Mesh Ewald," *J. Chem. Theory Comput.*, vol. 9, no. 9, pp. 3878–3888, 2013.

[68] T. P. Senftle, S. Hong, M. M. Islam, S. B. Kylasa, Y. Zheng, Y. K. Shin, C. Junkermeier, R. Engel-Herbert, M. J. Janik, H. M. Aktulga, T. Verstraelen, A. Grama, and A. C. T. van Duin, "The ReaxFF reactive force-field: Development, applications and future directions," *Npj Comput. Mater.*, vol. 2, no. 1, pp. 1–14, 2016.

[69] K. Vanommeslaeghe and A. D. MacKerell, "CHARMM additive and polarizable force fields for biophysics and computer-aided drug design," *Biochim. Biophys. Acta (BBA) - Gen. Subj.*, vol. 1850, no. 5, pp. 861–871, 2015.

[70] X. Zhu, P. E. M. Lopes, and A. D. MacKerell Jr, "Recent developments and applications of the CHARMM force fields," *WIREs Comput. Mol. Sci.*, vol. 2, no. 1, pp. 167–185, 2012.

[71] A. C. Van Duin, S. Dasgupta, F. Lorant, and W. A. Goddard, "ReaxFF: A reactive force field for hydrocarbons," *J. Phys. Chem. A*, vol. 105, no. 41, pp. 9396–9409, 2001.

[72] A. C. T. Van Duin, A. Strachan, S. Stewman, Q. Zhang, X. Xu, and W. A. Goddard, "ReaxFFSiO reactive force field for silicon and silicon oxide systems," *J. Phys. Chem. A*, vol. 107, no. 19, pp. 3803–3811, 2003.

[73] M. M. Islam, G. Kolesov, T. Verstraelen, E. Kaxiras, and A. C. T. van Duin, "eReaxFF: A Pseudoclassical Treatment of Explicit Electrons within Reactive Force Field Simulations," *J. Chem. Theory Comput.*, vol. 12, no. 8, pp. 3463–3472, 2016.

[74] S. Grimme, "A General Quantum Mechanically Derived Force Field (QMDFF) for Molecules and Condensed Phase Simulations," *J. Chem. Theory Comput.*, vol. 10, no. 10, pp. 4497–4514, 2014.

[75] S. Vandenbrande, M. Waroquier, V. V. Speybroeck, and T. Verstraelen, "The Monomer Electron Density Force Field (MEDFF): A Physically Inspired Model for Noncovalent Interactions," *J. Chem. Theory Comput.*, vol. 13, no. 1, pp. 161–179, 2017.

[76] P. Xu, E. B. Guidez, C. Bertoni, and M. S. Gordon, "Perspective: Ab initio force field methods derived from quantum mechanics," *J. Chem. Phys.*, vol. 148, no. 9, p. 090901, 2018.

[77] B. Anderson, T. S. Hy, and R. Kondor, "Cormorant: Covariant Molecular Neural Networks," 2019.

[78] I. Batatia, D. P. Kovacs, G. Simm, C. Ortner, and G. Csanyi, "MACE: Higher order equivariant message passing neural networks for fast and accurate force fields," 2022.

[79] S. Batzner, A. Musaelian, L. Sun, M. Geiger, J. P. Mailoa, M. Kornbluth, N. Molinari, T. E. Smidt, and B. Kozinsky, "E(3)-equivariant graph neural networks for data-efficient and accurate interatomic potentials," *Nat. Commun.*, vol. 13, no. 1, p. 2453, 2022.

[80] M. Cools-Ceuppens, J. Dambre, and T. Verstraelen, "Modeling Electronic Response Properties with an Explicit-Electron Machine Learning Potential," *J. Chem. Theory Comput.*, vol. 18, no. 3, pp. 1672–1691, 2022.

[81] J. Gasteiger, J. Groß, and S. Günnemann, "Directional Message Passing for Molecular Graphs," 2022.

[82] J. Gilmer, S. S. Schoenholz, P. F. Riley, O. Vinyals, and G. E. Dahl, "Neural Message Passing for Quantum Chemistry," 2017.

[83] D. P. Metcalf, A. Jiang, S. A. Spronk, D. L. Cheney, and C. D. Sherrill, "Electron-Passing Neural Networks for Atomic Charge Prediction in Systems with Arbitrary Molecular Charge," *J. Chem. Inf. Model.*, vol. 61, no. 1, pp. 115–122, 2021.

[84] K. T. Schütt, F. Arbabzadah, S. Chmiela, K. R. Müller, and A. Tkatchenko, "Quantum-chemical insights from deep tensor neural networks," *Nat. Commun.*, vol. 8, no. 1, p. 13890, 2017.

[85] K. T. Schütt, H. E. Sauceda, P.-J. Kindermans, A. Tkatchenko, and K.-R. Müller, "SchNet – A deep learning architecture for molecules and materials," *J. Chem. Phys.*, vol. 148, no. 24, p. 241722, 2018.

[86] S. Vandenhaute, M. Cools-Ceuppens, S. DeKeyser, T. Verstraelen, and V. Van Speybroeck, "Machine learning potentials for metal-organic frameworks using an incremental learning approach," *Npj Comput. Mater.*, vol. 9, no. 1, pp. 1–8, 2023.

[87] X. Xie, K. A. Persson, and D. W. Small, "Incorporating Electronic Information into Machine Learning Potential Energy Surfaces via Approaching the Ground-State Electronic Energy as a Function of Atom-Based Electronic Populations," *J. Chem. Theory Comput.*, vol. 16, no. 7, pp. 4256–4270, 2020.

[88] R. Zubatyuk, J. S. Smith, B. T. Nebgen, S. Tretiak, and O. Isayev, "Teaching a neural network to attach and detach electrons from molecules," *Nat. Commun.*, vol. 12, no. 1, p. 4870, 2021.

[89] D. A. Case, T. E. Cheatham III, T. Darden, H. Gohlke, R. Luo, K. M. Merz Jr., A. Onufriev, C. Simmerling, B. Wang, and R. J. Woods, "The Amber biomolecular simulation programs," *J. Comput. Chem.*, vol. 26, no. 16, pp. 1668–1688, 2005.

[90] R. Salomon-Ferrer, D. A. Case, and R. C. Walker, "An overview of the Amber biomolecular simulation package," *WIREs Comput. Mol. Sci.*, vol. 3, no. 2, pp. 198–210, 2013.

[91] B. R. Brooks, C. L. Brooks III, A. D. Mackerell Jr., L. Nilsson, R. J. Petrella, B. Roux, Y. Won, G. Archontis, C. Bartels, S. Boresch, A. Caflisch, L. Caves, Q. Cui, A. R. Dinner, M. Feig, S. Fischer, J. Gao, M. Hodoscek, W. Im, K. Kuczera, T. Lazaridis, J. Ma, V. Ovchinnikov, E. Paci, R. W. Pastor, C. B. Post, J. Z. Pu, M. Schaefer, B. Tidor, R. M. Venable, H. L. Woodcock, X. Wu, W. Yang, D. M. York, and M. Karplus, "CHARMM: The biomolecular simulation program," *J. Comput. Chem.*, vol. 30, no. 10, pp. 1545–1614, 2009.

[92] S. Patel, A. D. Mackerell Jr., and C. L. Brooks III, "CHARMM fluctuating charge force field for proteins: II Protein/solvent properties from molecular dynamics simulations using a nonadditive electrostatic model," *J. Comput. Chem.*, vol. 25, no. 12, pp. 1504–1514, 2004.

[93] E. Harder, W. Damm, J. Maple, C. Wu, M. Reboul, J. Y. Xiang, L. Wang, D. Lupyan, M. K. Dahlgren, J. L. Knight, J. W. Kaus, D. S. Cerutti, G. Krilov, W. L. Jorgensen, R. Abel, and R. A. Friesner, "OPLS3: A Force Field Providing Broad Coverage of Drug-like Small Molecules and Proteins," *J. Chem. Theory Comput.*, vol. 12, no. 1, pp. 281–296, 2016.

[94] W. L. Jorgensen, D. S. Maxwell, and J. Tirado-Rives, "Development and Testing of the OPLS All-Atom Force Field on Conformational Energetics and Properties of Organic Liquids," *J. Am. Chem. Soc.*, vol. 118, no. 45, pp. 11225–11236, 1996.

[95] H. J. C. Berendsen, D. van der Spoel, and R. van Drunen, "GROMACS: A message-passing parallel molecular dynamics implementation," *Comput. Phys. Commun.*, vol. 91, no. 1, pp. 43–56, 1995.

[96] S. Pronk, S. Páll, R. Schulz, P. Larsson, P. Bjelkmar, R. Apostolov, M. R. Shirts, J. C. Smith, P. M. Kasson, D. van der Spoel, B. Hess, and E. Lindahl, "GROMACS 4.5: A high-throughput and highly parallel open source molecular simulation toolkit," *Bioinformatics*, vol. 29, no. 7, pp. 845–854, 2013.

[97] D. Van Der Spoel, E. Lindahl, B. Hess, G. Groenhof, A. E. Mark, and H. J. C. Berendsen, "GROMACS: Fast, flexible, and free," *J. Comput. Chem.*, vol. 26, no. 16, pp. 1701–1718, 2005.

[98] J. C. Phillips, R. Braun, W. Wang, J. Gumbart, E. Tajkhorshid, E. Villa, C. Chipot, R. D. Skeel, L. Kalé, and K. Schulten, "Scalable molecular dynamics with NAMD," *J. Comput. Chem.*, vol. 26, no. 16, pp. 1781–1802, 2005.

[99] S. S. Zimmerman, M. S. Pottle, G. Némethy, and H. A. Scheraga, "Conformational Analysis of the 20 Naturally Occurring Amino Acid Residues Using ECEPP," *Macromolecules*, vol. 10, no. 1, pp. 1–9, 1977.

[100] T. A. Halgren, "The representation of van der Waals (vdW) interactions in molecular mechanics force fields: Potential form, combination rules, and vdW parameters," *J. Am. Chem. Soc.*, vol. 114, no. 20, pp. 7827–7843, 1992.

[101] M. J. Hwang, T. P. Stockfisch, and A. T. Hagler, "Derivation of Class II Force Fields. 2. Derivation and Characterization of a Class II Force Field, CFF93, for the Alkyl Functional Group and Alkane Molecules," *J. Am. Chem. Soc.*, vol. 116, no. 6, pp. 2515–2525, 1994.

[102] D. Hofmann, L. Fritz, J. Ulbrich, C. Schepers, and M. Böhning, "Detailed-atomistic molecular modeling of small molecule diffusion and solution processes in polymeric membrane materials," *Macromol. Theory Simul.*, vol. 9, no. 6, pp. 293–327, 2000.

[103] N. L. Allinger, "Conformational analysis. 130. MM2. A hydrocarbon force field utilizing V1 and V2 torsional terms," *J. Am. Chem. Soc.*, vol. 99, no. 25, pp. 8127–8134, 1977.

[104] A. D. Buckingham, P. W. Fowler, and J. M. Hutson, "Theoretical studies of van der Waals molecules and intermolecular forces," *Chem. Rev.*, vol. 88, no. 6, pp. 963–988, 1988.

[105] J. H. Lii and N. L. Allinger, "Molecular mechanics. The MM3 force field for hydrocarbons. 3. The van der Waals' potentials and crystal data for aliphatic and aromatic hydrocarbons," *J. Am. Chem. Soc.*, vol. 111, no. 23, pp. 8576–8582, 1989.

[106] A. K. Rappe, C. J. Casewit, K. S. Colwell, W. A. I. Goddard, and W. M. Skiff, "UFF, a full periodic table force field for molecular mechanics and molecular dynamics simulations," *J. Am. Chem. Soc.*, vol. 114, no. 25, pp. 10024–10035, 1992.

[107] Y. Shi, Z. Xia, J. Zhang, R. Best, C. Wu, J. W. Ponder, and P. Ren, "Polarizable Atomic Multipole-Based AMOEBA Force Field for Proteins," *J. Chem. Theory Comput.*, vol. 9, no. 9, pp. 4046–4063, 2013.

[108] N. L. Allinger, Y. H. Yuh, and J. H. Lii, "Molecular mechanics. The MM3 force field for hydrocarbons. 1," *J. Am. Chem. Soc.*, vol. 111, no. 23, pp. 8551–8566, 1989.

[109] N. L. Allinger, K.-H. Chen, J.-H. Lii, and K. A. Durkin, "Alcohols, ethers, carbohydrates, and related compounds. I. The MM4 force field for simple compounds," *J. Comput. Chem.*, vol. 24, no. 12, pp. 1447–1472, 2003.

[110] T. A. Halgren, "Merck molecular force field. I. Basis, form, scope, parameterization, and performance of MMFF94," *J. Comput. Chem.*, vol. 17, no. 5-6, pp. 490–519, 1996.

[111] T. A. Halgren, "MMFF VII. Characterization of MMFF94, MMFF94s, and other widely available force fields for conformational energies and for intermolecular-interaction energies and geometries," *J. Comput. Chem.*, vol. 20, no. 7, pp. 730–748, 1999.

[112] A. T. Hagler and C. S. Ewig, "On the use of quantum energy surfaces in the derivation of molecular force fields," *Comput. Phys. Commun.*, vol. 84, no. 1, pp. 131–155, 1994.

[113] M.-J. Hwang, X. Ni, M. Waldman, C. S. Ewig, and A. T. Hagler, "Derivation of class II force fields. VI. Carbohydrate compounds and anomeric effects," *Biopolymers*, vol. 45, no. 6, pp. 435–468, 1998.

[114] J. Maple, M.-J. Hwang, T. Stockfisch, and A. Hagler, "Derivation of Class II Force Fields. III. Characterization of a Quantum Force Field for Alkanes," *Isr. J. Chem.*, vol. 34, no. 2, pp. 195–231, 1994.

[115] J. R. Maple, M.-J. Hwang, T. P. Stockfisch, U. Dinur, M. Waldman, C. S. Ewig, and A. T. Hagler, "Derivation of class II force fields. I. Methodology and quantum force field for the alkyl functional group and alkane molecules," *J. Comput. Chem.*, vol. 15, no. 2, pp. 162–182, 1994.

[116] J. R. Maple, M.-J. Hwang, K. J. Jalkanen, T. P. Stockfisch, and A. T. Hagler, "Derivation of class II force fields: V. Quantum force field for amides, peptides, and related compounds," *J. Comput. Chem.*, vol. 19, no. 4, pp. 430–458, 1998.

[117] C. J. Casewit, K. S. Colwell, and A. K. Rappe, "Application of a universal force field to organic molecules," *J. Am. Chem. Soc.*, vol. 114, no. 25, pp. 10035–10046, 1992.

[118] S. Lifson and A. Warshel, "Consistent Force Field for Calculations of Conformations, Vibrational Spectra, and Enthalpies of Cycloalkane and n-Alkane Molecules," *J. Chem. Phys.*, vol. 49, no. 11, pp. 5116–5129, 1968.

[119] A. Warshel and S. Lifson, "Consistent Force Field Calculations. II. Crystal Structures, Sublimation Energies, Molecular and Lattice Vibrations, Molecular Conformations, and Enthalpies of Alkanes," *J. Chem. Phys.*, vol. 53, no. 2, pp. 582–594, 1970.

[120] A. T. Hagler, P. S. Stern, S. Lifson, and S. Ariel, "Urey-Bradley force field, valence force field, and ab initio study of intramolecular forces in tri-tert-butylmethane and isobutane," *J. Am. Chem. Soc.*, vol. 101, no. 4, pp. 813–819, 1979.

[121] A. Warshel and M. Levitt, "Theoretical studies of enzymic reactions: Dielectric, electrostatic and steric stabilization of the carbonium ion in the reaction of lysozyme," *J. Mol. Biol.*, vol. 103, no. 2, pp. 227–249, 1976.

[122] G. A. Kaminski, H. A. Stern, B. J. Berne, R. A. Friesner, Y. X. Cao, R. B. Murphy, R. Zhou, and T. A. Halgren, "Development of a polarizable force field for proteins via ab initio quantum chemistry: First generation model and gas phase tests," *J. Comput. Chem.*, vol. 23, no. 16, pp. 1515–1531, 2002.

[123] P. Ren and J. W. Ponder, "Consistent treatment of inter- and intramolecular polarization in molecular mechanics calculations," *J. Comput. Chem.*, vol. 23, no. 16, pp. 1497–1506, 2002.

[124] W. L. Jorgensen, K. P. Jensen, and A. N. Alexandrova, "Polarization Effects for Hydrogen-Bonded Complexes of Substituted Phenols with Water and Chloride Ion," *J. Chem. Theory Comput.*, vol. 3, no. 6, pp. 1987–1992, 2007.

[125] G. Lamoureux and B. Roux, "Modeling induced polarization with classical Drude oscillators: Theory and molecular dynamics simulation algorithm," *J. Chem. Phys.*, vol. 119, no. 6, pp. 3025–3039, 2003.

[126] H. Yu, T. Hansson, and W. F. van Gunsteren, "Development of a simple, self-consistent polarizable model for liquid water," *J. Chem. Phys.*, vol. 118, no. 1, pp. 221–234, 2003.

[127] A.-P. E. Kunz and W. F. van Gunsteren, "Development of a Nonlinear Classical Polarization Model for Liquid Water and Aqueous Solutions: COS/D," *J. Phys. Chem. A*, vol. 113, no. 43, pp. 11570–11579, 2009.

[128] W. J. Mortier, K. Van Genechten, and J. Gasteiger, "Electronegativity equalization: Application and parametrization," *J. Am. Chem. Soc.*, vol. 107, no. 4, pp. 829–835, 1985.

[129] W. J. Mortier, S. K. Ghosh, and S. Shankar, "Electronegativity-equalization method for the calculation of atomic charges in molecules," *J. Am. Chem. Soc.*, vol. 108, no. 15, pp. 4315–4320, 1986.

[130] S. Kale and J. Herzfeld, "Pairwise Long-Range Compensation for Strongly Ionic Systems," *J. Chem. Theory Comput.*, vol. 7, no. 11, pp. 3620–3624, 2011.

[131] S. Kale, J. Herzfeld, S. Dai, and M. Blank, "Lewis-inspired representation of dissociable water in clusters and Grotthuss chains," *J. Biol. Phys.*, vol. 38, no. 1, pp. 49–59, 2012.

[132] S. Kale and J. Herzfeld, "Natural polarizability and flexibility via explicit valency: The case of water," *J. Chem. Phys.*, vol. 136, no. 8, p. 084109, 2012.

[133] C. Bai, S. Kale, and J. Herzfeld, "Chemistry with semi-classical electrons: Reaction trajectories auto-generated by sub-atomistic force fields," *Chem. Sci.*, vol. 8, no. 6, pp. 4203–4210, 2017.

[134] S. W. Rick, S. J. Stuart, and B. J. Berne, "Dynamical fluctuating charge force fields: Application to liquid water," *J. Chem. Phys.*, vol. 101, no. 7, pp. 6141–6156, 1994.

[135] S. W. Rick and B. J. Berne, "Dynamical Fluctuating Charge Force Fields: The Aqueous Solvation of Amides," *J. Am. Chem. Soc.*, vol. 118, no. 3, pp. 672–679, 1996.

[136] H. A. Stern, F. Rittner, B. J. Berne, and R. A. Friesner, "Combined fluctuating charge and polarizable dipole models: Application to a five-site water potential function," *J. Chem. Phys.*, vol. 115, no. 5, pp. 2237–2251, 2001.

[137] A. K. Rappe and W. A. I. Goddard, "Charge equilibration for molecular dynamics simulations," *J. Phys. Chem.*, vol. 95, no. 8, pp. 3358–3363, 1991.

[138] Y. Zhong and S. Patel, "Nonadditive Empirical Force Fields for Short-Chain Linear Alcohols: Methanol to Butanol. Hydration Free Energetics and Kirkwood-Buff Analysis Using Charge Equilibration Models," *J. Phys. Chem. B*, vol. 114, no. 34, pp. 11076–11092, 2010.

[139] D. M. York and W. Yang, "A chemical potential equalization method for molecular simulations," *J. Chem. Phys.*, vol. 104, no. 1, pp. 159–172, 1996.

[140] H. S. Antila and E. Salonen, "Polarizable Force Fields," in *Biomolecular Simulations: Methods and Protocols* (L. Monticelli and E. Salonen, eds.), pp. 215–241, Totowa, NJ: Humana Press, 2013.

[141] P. Bultinck, C. Van Alsenoy, P. W. Ayers, and R. Carbó-Dorca, "Critical analysis and extension of the Hirshfeld atoms in molecules," *J. Chem. Phys.*, vol. 126, no. 14, p. 144111, 2007.

[142] M. Devereux, M. Pezzella, S. Raghunathan, and M. Meuwly, "Polarizable Multipolar Molecular Dynamics Using Distributed Point Charges," *J. Chem. Theory Comput.*, vol. 16, no. 12, pp. 7267–7280, 2020.

[143] T. Verstraelen, E. Pauwels, F. De Proft, V. Van Speybroeck, P. Geerlings, and M. Waroquier, "Assessment of Atomic Charge Models for Gas-Phase Computations on Polypeptides," *J. Chem. Theory Comput.*, vol. 8, no. 2, pp. 661–676, 2012.

[144] O. T. Unke, M. Devereux, and M. Meuwly, "Minimal distributed charges: Multipolar quality at the cost of point charge electrostatics," *J. Chem. Phys.*, vol. 147, no. 16, p. 161712, 2017.

[145] R. Chelli, P. Procacci, R. Righini, and S. Califano, "Electrical response in chemical potential equalization schemes," *J. Chem. Phys.*, vol. 111, no. 18, pp. 8569–8575, 1999.

[146] R. A. Nistor, J. G. Polihronov, M. H. Müser, and N. J. Mosey, "A generalization of the charge equilibration method for nonmetallic materials," *J. Chem. Phys.*, vol. 125, no. 9, p. 094108, 2006.

[147] G. Lee Warren, J. E. Davis, and S. Patel, "Origin and control of superlinear polarizability scaling in chemical potential equalization methods," *J. Chem. Phys.*, vol. 128, no. 14, p. 144110, 2008.

[148] R. Chelli, M. Pagliai, P. Procacci, G. Cardini, and V. Schettino, "Polarization response of water and methanol investigated by a polarizable force field and density functional theory calculations: Implications for charge transfer," *J. Chem. Phys.*, vol. 122, no. 7, p. 074504, 2005.

[149] J. Chen and T. J. Martínez, "QTPIE: Charge transfer with polarization current equalization. A fluctuating charge model with correct asymptotics," *Chem. Phys. Lett.*, vol. 438, no. 4, pp. 315–320, 2007.

[150] R. A. Nistor and M. H. Müser, "Dielectric properties of solids in the regular and split-charge equilibration formalisms," *Phys. Rev. B*, vol. 79, no. 10, p. 104303, 2009.

[151] A. Morita and S. Kato, "Molecular dynamics simulation with the charge response kernel: Diffusion dynamics of pyrazine and pyrazinyl radical in methanol," *J. Chem. Phys.*, vol. 108, no. 16, pp. 6809–6818, 1998.

[152] H. Nakano, T. Yamamoto, and S. Kato, "A wave-function based approach for polarizable charge model: Systematic comparison of polarization effects on protic, aprotic, and ionic liquids," *J. Chem. Phys.*, vol. 132, no. 4, p. 044106, 2010.

[153] J. Cioslowski and M. Martinov, "The atomic softness matrix," *J. Chem. Phys.*, vol. 101, no. 1, pp. 366–370, 1994.

[154] A. Holt, G. Karlström, and R. Lindh, "The charge capacity of the chemical bond," *Chem. Phys. Lett.*, vol. 436, no. 1, pp. 297–301, 2007.

[155] F. Jensen, "Unifying Charge-Flow Polarization Models," *J. Chem. Theory Comput.*, vol. 19, no. 13, pp. 4047–4073, 2023.

[156] T. Verstraelen, P. W. Ayers, V. Van Speybroeck, and M. Waroquier, "ACKS2: Atom-condensed Kohn-Sham DFT approximated to second order," *J. Chem. Phys.*, vol. 138, no. 7, p. 074108, 2013.

[157] T. Verstraelen, S. Vandenbrande, and P. W. Ayers, "Direct computation of parameters for accurate polarizable force fields," *J. Chem. Phys.*, vol. 141, no. 19, p. 194114, 2014.

[158] M. F. Russo and A. C. T. van Duin, "Atomistic-scale simulations of chemical reactions: Bridging from quantum chemistry to engineering," *Nucl. Instrum. Methods Phys. Res. B: Beam Interact. Mater. At.*, vol. 269, no. 14, pp. 1549–1554, 2011.

[159] J. P. Koski, S. G. Moore, R. C. Clay, K. A. O'Hearn, H. M. Aktulga, M. A. Wilson, J. A. Rackers, J. M. D. Lane, and N. A. Modine, "Water in an External Electric Field: Comparing Charge Distribution Methods Using ReaxFF Simulations," *J. Chem. Theory Comput.*, vol. 18, no. 1, pp. 580–594, 2022.

[160] P. Gütlein, L. Lang, K. Reuter, J. Blumberger, and H. Oberhofer, "Toward First-Principles-Level Polarization Energies in Force Fields: A Gaussian Basis for the Atom-Condensed Kohn-Sham Method," *J. Chem. Theory Comput.*, vol. 15, no. 8, pp. 4516–4525, 2019.

[161] P. Gütlein, J. Blumberger, and H. Oberhofer, "An Iterative Fragment Scheme for the ACKS2 Electronic Polarization Model: Application to Molecular Dimers and Chains," *J. Chem. Theory Comput.*, vol. 16, no. 9, pp. 5723–5735, 2020.

[162] J. F. Dobson and A. Ambrosetti, "MBD + C: How to Incorporate Metallic Character into Atom-Based Dispersion Energy Schemes," *J. Chem. Theory Comput.*, vol. 19, no. 18, pp. 6434–6451, 2023.

This research was supported by the Foundation of Scientific Research - Flanders (FWO, file number G0A9717N) and the Research Board of Ghent University (BOF).

The computational resources (Stevin Supercomputer Infrastructure) and services used in this work were provided by the VSC (Flemish Supercomputer Center), funded by Ghent University, and FWO.